INJECTABLE ANTIMICROBIAL AGENT-LOADED *IN SITU* FORMING
EUDRAGIT L, NITROCELLULOSE AND ZEIN-BASED SOLVENT REMOVAL
PHASE-INVERSION MATRICES FOR PERIODONTITIS TREATMENT

By
Mr. Setthapong SENARAT

A Thesis Submitted in Partial Fulfillment of the Requirements
for Doctor of Philosophy PHARMACEUTICAL ENGINEERING
(INTERNATIONAL PROGRAM)
Silpakorn University
Academic Year 2023
Copyright of Silpakorn University

เมทริกซ์ก่อตัวในแหล่งกำเนิดชนิดกลับวัฏภาคจากการกำจัดตัวทำละลายของยูดราจิต แอล ไนโตรเซลลูโลส และเซอินชนิดฉีดบรรจุยาต้านจุลชีพสำหรับรักษาโรคปริทันต์อักเสบ

โดย
Mr.Setthapong Senarat

INJECTABLE ANTIMICROBIAL AGENT-LOADED *IN SITU*
FORMING EUDRAGIT L, NITROCELLULOSE AND ZEIN-BASED
SOLVENT REMOVAL PHASE-INVERSION MATRICES FOR
PERIODONTITIS TREATMENT

By

Mr. Setthapong SENARAT

A Thesis Submitted in Partial Fulfillment of the Requirements
for Doctor of Philosophy PHARMACEUTICAL ENGINEERING
(INTERNATIONAL PROGRAM)
Silpakorn University
Academic Year 2023
Copyright of Silpakorn University

Title	Injectable antimicrobial agent-loaded *in situ* forming eudragit L, nitrocellulose and zein-based solvent removal phase-inversion matrices for periodontitis treatment
By	Mr. Setthapong SENARAT
Field of Study	PHARMACEUTICAL ENGINEERING (INTERNATIONAL PROGRAM)
Advisor	Professor Thawatchai Phaechamud, Ph.D.
Co advisor	Associate Professor Pornsarp Pornsawad, Ph.D.

Faculty of Pharmacy, Silpakorn University in Partial Fulfillment of the Requirements for the Doctor of Philosophy

.... Dean of Faculty of Pharmacy

(Professor Pornsak Sriamornsak, Ph.D.)

Approved by

.... Chair person

(Associate Professor Wiwat Pichayakorn, Ph.D.)

.... Advisor

(Professor Thawatchai Phaechamud, Ph.D.)

.... Co advisor

(Associate Professor Pornsarp Pornsawad, Ph.D.)

.... Committee

(Associate Professor Chutima Limmatvapirat, Ph.D.)

.... Committee

(Assistant Professor Vipaluk Patomchaiviwat, Ph.D.)

.... Committee

(Professor Sontaya Limmatvapirat, Ph.D.)

620830006 : Major PHARMACEUTICAL ENGINEERING (INTERNATIONAL PROGRAM)
Keyword : In situ matrix; Zein; Nitrocellulose; Eudragit L; solvent removal; Numerical

Mr. Setthapong SENARAT : Injectable antimicrobial agent-loaded *in situ* forming eudragit L, nitrocellulose and zein-based solvent removal phase-inversion matrices for periodontitis treatment Thesis advisor : Professor Thawatchai Phaechamud, Ph.D.

The *in-situ* forming matrix (ISM) established through solvent removal phase-inversion, emerges as a promising method for treating periodontitis by administering it to the periodontal pocket. This innovative drug delivery system entails dissolving the therapeutic agent within polymer solution using a biocompatible solvent. Subsequent water exposure facilitates solvent removal, causing insoluble polymer to solidify into a gel matrix. In the pursuit of an effective ISM formulation for periodontitis, three matrix-forming agents-zein, Eudragit L, and nitrocellulose (Nc)-were selected, and using various solvents. The objective of this research were to comprehensively characterize the physical properties of these formulations, investigate their drug release kinetics, and assess their antimicrobial efficacy. The ISM based on 20% zein loaded with levofloxacin HCl (Lv) and formulated using glycerol formal (GF) as the solvent exhibited favorable attributes. This included appropriate viscosity, consistent Newtonian flow, satisfactory matrix formation, and injectability. Additionally, this formulation demonstrated prolonged Lv release over a span of 7 days, effectively combating various microorganisms responsible for periodontal infections. Similarly encouraging results were observed with the ISM containing 1% Lv and 15% Eudragit L, dissolved in monopropylene glycol, showing appropriate viscosity (3674.54 ± 188.03 cP), Newtonian flow, gel formation, injectability (21.08 ± 1.38 N), prolonged release, and antimicrobial activity against microorganisms. Conversely, Nc-based ISMs, incorporating moxifloxacin HCl (Mx) with dimethyl sulfoxide (DMSO) and *N*-methyl pyrrolidone (NMP) solvents, exhibited advantageous properties. The viscosity and injection force of the Nc ISMs varied depending on the solvent used, with GF resulting in higher values of 4631.41 ± 52.81 cPs and 4.34 ± 0.42 N, respectively. All Nc-based ISMs exhibited Newtonian flow and transformed into a matrix state upon exposure to the aqueous phase. Nc-based ISM formulations demonstrated low viscosity, ease of injectability, swift gel transformation upon water exposure, and sustained drug release against bacterial pathogens. UV-vis imaging revealed matrix formation and solvent diffusion, insights into the impact of solvents. Mathematical modeling and experiments enhance our understanding of zein-based ISMs, aiding the development of future drug delivery strategies. This holistic approach connects observations and simulations, deepening our knowledge of drug release mechanisms in zein-based ISMs for potential applications in periodontitis treatment. Nc is the most interesting to use as a matrix-forming agent because of its sustainable drug release. Moreover, it is noteworthy that this study presents the pioneering use of Nc-based ISM formulations, clinical trials are needed to establish safety and efficacy.

ACKNOWLEDGEMENTS

Setthapong SENARAT

TABLE OF CONTENTS

LIST OF TABLES

LIST OF FIGURES

LIST OF ABBREVIATIONS

%	percentage (s)
%v/v	percent volume by volume
%w/w	percent weight by weight
°C	degree Celsius
cm^{-1}	per centimeter
α	alpha
β	beta
γ	gamma
δ	delta
<	less than
>	more than
±	plus-minus sign
r^2	coefficient of determination
μg	microgram (s)
μg/mL	microgram per milliliter
μL	microliter (s)
μm	micrometer (s)
k	release rate
n	solvent release exponent value
2θ	two theta
3-D	three-dimension
β-lap	β-lapachone
μCT	X-ray computed microtomography
Abs	absorbance
ATCC	American Type Culture Collection
ANOVA	analysis of variance
CAS No.	Chemical abstracts service registry number

cm	centimeter (s)
CO., LTD.	Company Limited
cPs	centipoise
DH	Doxycycline hyclate
DMEM	dulbecco's Modified Eagle's Medium
DMST	Department of Medical Sciences Thailand
DMSO	dimethyl sulfoxide
DNA	deoxyribonucleic acid
DOE	design of experiments
e.g. (Latin);	for example
et al.	and others
EC	Ethyl cellulose
Eq.	Equation
FBS	fetal bovine serum
FDA	Food and Drug Administration
FT-IR	Fourier-transform infrared
G (needle)	gauge
g	gram (s)
GF	glycerol formal
GRAS	generally regarded as safe
GV	gigavolt
h	hour (s)
HCl	hydrochloride
HIV	human immunodeficiency virus infection
HPMC	hydroxypropyl methylcellulose
ICH	The International Council for Harmonisation of Technical Requirements for Pharmaceuticals for Human Use
IC	inhibition concentration
IM	Imatinib mesylate

ISG	*in situ* forming gel
ISM	*in situ* forming matrix
kDa	kilodaltons
kV	kilovolts
KH_2PO_4	potassium dihydrogen phosphate
L	liter (s)
LD_{50}	median lethal dose
Lv	levofloxacin HCl
mA	milliampere
MP	monopropylene glycol
min	minute (s)
mg	milligram (s)
mm	millimeter (s)
mm Hg	millimetre (s) of mercury
MIC	minimum inhibition concentration
min	minute (s)
mL	milliliter (s)
MOFs	metal-organic frameworks
MRSA	methicillin-resistant *Staphylococcus aureus*
MSC	model selection criterion
MW	molecular weight
mV	millivolt(s)
Mx	moxifloxacin hydrochloride
m^2/s	cubic meter per second
N	newton
n	flow behavior index
Nc	Nitrocellulose
ND	not determined
nm	nanometer (s)

NMP	*N*-methyl pyrrolidone
No.	number
NR	nile red
PBS	phosphate buffer saline
PEG	polyethylene glycol
pH	potentia hydrogenii (Latin); power of hydrogen
PLA	Poly (lactide)
PLGA	Poly (D, L-lactide-co-glycolide)
PSSA	pseudo-steady state approximation
PYR	2 -pyrrolidone
r^2	coefficient of detrmination
rpm	revolutions per minute
SAIB	sucrose acetate isobutyrate
sec	second (s)
SEM	scanning electron microscopy
SF	sodium fluorescein
S.D.	standard deviation
SLRI	Synchrotron Light Research Institute
SPSS	statistical package for social science
t	time
UV	ultraviolet
UV -vis	Ultraviolet - visible
UK	United Kingdom
USA	United States of America
US-FDA	United States Food and Drug Administration
V	volt(s)
Vis	visible
XTM	X-ray tomographic microscopy
ZOI	zone of inhibition

CHAPTER 1

INTRODUCTION

RATIONAL AND PROBLEM STATEMENT:

Normally, health of oral cavity is a key indicator of overall health, well-being and quality of life. Nowadays, periodontal diseases influence about 20-50% of global population. Periodontal diseases are group of conditions, including gingivitis and periodontitis, which affect the supporting structures of the teeth (periodontium) such as gums, periodontal ligaments, alveolar bone and dental cementum. The microflora found in periodontal disease is complex and composed mainly of Gram-negative anaerobic bacteria such as *Porphyromonas gingivalis, Prevotella intermedia, Aggregatibacter actinomycetemcomitans* and *Fusobacterium nucleatum.* Thus, the periodontal treatment is necessary to remove or inhibit the growth of bacteria on tooth surface and in crevicular pocket by mechanical scaling, root planning and medications. Antimicrobial agents are typically used in periodontal treatment for infection elimination. Many active compounds such as chlorhexidine, tetracyclines (tetracycline, doxycycline, and minocycline), metronidazole, ciprofloxacin, vancomycin, and other antimicrobial drugs have been clinically utilized for their anti-microbiological effectiveness in periodontal diseases. Periodontitis is currently treated microbiologically using either the systemic antibiotics or the localized delivery systems incorporating a recommended antibiotic. Nevertheless, large doses of systemic antibiotic must be given in order to achieve the appropriate concentrations in the gingival crevicular fluid of periodontal pocket, in which potentially associated with side effects of antibiotics and other problems regarding mainly about antibiotic resistance. These limitations have attracted the attention of investigators for developing local drug delivery systems for the treatment of periodontal diseases. Therefore, applying a controlled release system to give antimicrobial administration directly into the crevicular pocket is a more satisfying strategy. Local drug delivery limits the drug to its target site, with little or no systemic uptake; thus, a much smaller dose is required for effective therapy and harmful side effects can be reduced or eliminated. It's important to note that the choice of antibiotic depends on the specific infection, its causative agent, and local resistance patterns. Lv and Mx are valuable options, especially when dealing with antibiotic-resistant infections or when other antibiotics are contraindicated. In the present study, levofloxacin HCl (Lv) and moxifloxacin HCl (Mx) are applied as the model drugs for local drug administration with solvent removal phase-inversion matrices for periodontitis treatment.

Lv could be one alternative, as it is effective against a broad range of Gram-positive, Gram-negative, and atypical bacteria. It is a well-established treatment option for respiratory and urinary tract infections, and is active against some penicillin- and macrolide resistant species. Lv has been used due to its activity against

facultative anaerobic periodontopathic bacteria and widely used for the treatment of periodontal diseases. Lv has shown advantages over ciprofloxacin in terms of clinical efficacy and disease recurrence, with a low rate of adverse events for the treatment of chronic bacterial prostatitis.

Mx is a broad-spectrum fourth generation fluoroquinolone antibiotic. Mx shows bactericidal, concentration dependent, anti-infective. It interferes with bacterial survival by binding to DNA gyrase (topoisomerase II) and topoisomerase IV, essential bacterial enzymes involved in the replication, translation, repair and recombination of deoxyribonucleic acid. Mx has improved activity against Gram-positives and anaerobes. *In vitro* studies showed good activity against planktonic microorganisms as well as bacteria located within a biofilm or intracellularly. Mx has been used as an adjunctive antibiotic in the treatment of periodontitis. Moreover, some studys revealed that Mx preserved its antibacterial effectiveness against selected *Staphylococcus aureus* and *Escherichia coli* when produced as an *in situ* forming matrix delivery method for periodontal disease. Thus, theses medication possesses the desired properties for use as an active compound in periodontal drug delivery systems.

The beneficial usages of antibiotic drugs with local drug delivery are side effect minimization, less potential antibiotic resistance and adequate/effective concentration at the target site. *In situ* forming systems are recognized as the one of useful pharmaceutical delivery systems due to their self-transformation into an expected state such as gel, solid, and microparticle after administrating into the target site for controlling drug liberation. Solvent removal phase-inversion matrix or solvent-exchange induced *in situ* forming gel (ISG) is one of the various types of these systems. Drug-loaded solvent removal phase-inversion-induced *in situ* forming matrices (ISMs) are prepared by dissolving that active compound with water-insoluble polymers such as poly (D, L-lactide-co-glycolide) (PLGA), ethyl cellulose (EC) and Eudragit® RS in the biocompatible solvents such as *N*-methyl-pyrrolidone (NMP) or dimethyl sulfoxide (DMSO). The prepared drug-loaded polymeric solutions convert into a solid-like matrix after being exposed to an aqueous physiological environment owing to the inward diffusion of the aqueous fluid from the target site and the outward solvent diffusion from the delivery system inducing phase inversion of water-insoluble material. The key substance of *in situ* forming system is matrix forming agent which should be a water insoluble matter with biocompatible, biodegradable, safety (non-toxic) characters and it should be miscible with solvent and drug. The hydrophobic property seems to be a crucial factor to the designing of this system. Thus, another aqueous insoluble material such as Eudragit® L, zein and Nitrocellulose (Nc) are interest for using as a matrix former of the solvent removal phase-inversion-induced ISMs.

Eudragit®L is an anionic copolymer based on methacrylic acid and methacrylate (1:1) which has been widely employed as pharmaceutical excipient in

drug delivery systems. The polymer is insoluble in acid medium, hence when used in a coating layer of drug formulation it will protect the acid-unstable drug from degradation once it reaches the stomach. Therefore, Eudragit® L in enteric-coated tablet formulation is very helpful in formulating a bioequivalent drug product. In addition, Eudragit®L/DMSO ISMs exhibited as a potential periodontal pocket drug delivery system based on solvent removal mechanism with modulating the doxycycline hyclate (DH) release longer than 3 days. Nevertheless, the application of Eudragit®L dissolve in monopropylene glycol (MP) as the ISM has not been reported.

Zein is a major storage protein which comprises about 45-50% of the total protein in corn. The molecular structure of zein is helical wheel conformation in which nine homologous repeating units are arranged in an antiparallel form stabilized by hydrogen bonds. It has been mainly used as biodegradable films. Zein is generally regarded as safe ('GRAS') as food material and is being used as water and moisture barrier in tablet coatings since long back. Zein was also used for preparation of microspheres which exhibited a constant release of drugs. Earlier study demonstrated that zein was a promising biomaterial with good biocompatibility for the development of tissue engineering. The zein-based ISM had been designed for intra-tumoral injection described here was suitable for use as a sustained-release. Zein is interesting for use as matrix forming agent in a solvent removal phase inversion-based ISM system loaded with antimicrobial for periodontitis treatment. This developed drug delivery system has not been reported previously.

Nc is a nitrated ester of cellulose that is prepared by using a mixture of sulfuric and nitric acids for cellulose treatment. It is also known as pyroxylin, gun cotton, or collodion. It is a solid polymer which has no odor nor taste with a white appearance looks like that of cotton. Nc was non-toxic to rats and dogs; however, mortality was seen in mice, which was attributed to the relatively large size of the fibers relative to the size of the murine intestinal lumen rather than to chemical toxicity. Nc has proven itself being greatly beneficial including skin coverings to prevent wounds from contamination, cosmetic preparations, film, inert support for chromatographic separations in research, and components used in the production of lacquers, and artificial leathers, adhesives, and other products. However, the Nc-based ISM has not been addressed previously. Owing to its longed term use with safety, apparent low aqueous solubility, these materials may serve as a matrix forming agent of ISM for this research.

A limitation of this ISM model is that it assumes a very rapid (seconds to minutes) implant phase inversion. This assumption is likely true with the formation of a thin, flat implant membrane whereas most *in vitro* and *in vivo* ISMs produce the spherical or globular forms and phase inversion over a longer time scales (h to days). The rate of implant phase inversion has a significant effect on the drug release kinetics. Therefore, a different model is needed to describe the drug release kinetics from more realistic globular implants that phase inverts on a slower time scale.

Mechanistic model of phase inversion and drug release from an ISM should be developed to predict the effect of implant composition and characteristics on drug release kinetics.

The field of drug delivery has witnessed significant advancements with the emergence of innovative techniques, and one such promising approach is the utilization of UV-vis imaging for ISMs. ISMs represent a versatile class of drug delivery systems that transform from a liquid to a matrix-like state upon administration, offering controlled and localized drug release. UV-vis imaging, a powerful analytical tool, has gained traction as a non-invasive and real-time visualization technique to monitor various processes within ISMs.

The aims of this study are to develop ISM formulation by using Eudragit® L, Nc and zein as the matrix formers of *in situ* forming solvent removal phase-inversion matrices for periodontitis treatment. To achieve the formulation development, understanding matrix forming behavior of these matrix forming agents are needed. Thus, the influence of matrix concentrations is studied and discussed in terms of physicochemical properties, matrix forming behavior and the antimicrobial activities of developed ISMs. The physicochemical characters of prepared Lv and Mx-loaded ISM formulations are investigated via the issue of viscosity, rheology behavior, injectability, matrix formation behavior, morphology of matrix, interface interaction, drug release and antimicrobial activities. Modified experiments in this study such as model substance permeation and fluorescent tracking are undertaken to support an understanding and address the phase inversion phenomenon and matrix formation. Moreover, a numerical simulation based on mathematical model is performed to predict the drug release pattern from rate of species transport from the polymer matrix and exterior phase which might be linked with matrix forming behavior characteristics of injectable antimicrobial agent-loaded *in situ* forming zein-based solvent removal phase-inversion matrices.

OBJECTIVES:

1. To investigate the physicochemical properties and matrix forming behavior of Eudragit® L, Nc and zein-based solvent removal phase-inversion ISM formulations

2. To develop and evaluate Lv-loaded Eudragit® L-based solvent removal phase-inversion ISM for periodontitis treatment

3. To develop and evaluate Lv-loaded zein-based solvent removal phase-inversion ISM for periodontitis treatment

4. To develop and evaluate Mx-loaded Nc-based solvent removal phase-inversion ISM for periodontitis treatment

5. To develop mechanistic mathematical model to describe drug release from rate of species transport from the polymer matrix phase and exterior phase of zein-based solvent removal phase-inversion ISMs

6. To investigate the relationship between drug release patterns and rate of species transport from the polymer matrix phase and exterior phase of zein-based solvent removal phase-inversion ISMs using numerical technique applied to the mathematical model.

HYPOTHESIS:

1. The concentration of matrix forming agent significantly affects the physicochemical properties and matrix forming behavior of Eudragit® L, Nc and zein-based solvent removal phase-inversion ISMs.

2. The concentration of matrix forming agent is a key factor influencing the release pattern of antimicrobial agent-loaded Eudragit® L, Nc and zein-based solvent removal phase-inversion ISMs.

3. The choice of solvent type plays a crucial role in determining the release pattern of antimicrobial agent-loaded Eudragit® L, Nc and zein-based solvent removal phase-inversion ISMs.

4. The matrix forming agent concentration, solvent type and incorporated-drugs influence on mechanistic phase inversion and the antimicrobial activities of antimicrobial agent-loaded Eudragit® L, Nc and zein-based solvent removal phase-inversion ISMs.

5. The utilization of numerical techniques and simulations from experimental data is a viable approach for elucidating the relationship between drug release patterns and rate of species transport from the polymer matrix phase to exterior phase of antimicrobial agent-loaded zein-based solvent removal phase-inversion ISMs.

6. Numerical simulations will provide insights into the dynamic coupling between drug release profiles and the kinetics of species transport from the polymer matrix phase to the exterior phase within antimicrobial agent-loaded zein-based solvent removal phase-inversion ISMs.

CHAPTER 2

REVIEW LITERATURES

In situ forming matrix (ISM)

Over the past few decades, the aspect of personalized medicine has been appreciated to play a crucial role in the healthcare sector and also in pharmaceutical field. Personalized medicine adapts the current conventional dosage forms corresponded to the needs of the patient. Based on this provoked concept, the appropriate treatment options are achieved for a particular individual patient for better therapeutic outcomes and decreased adverse drug reaction and adverse effect. Thus, over the last few decades, drug delivery systems have progressed from conventional tablets to innovative systems and bioengineered systems (1). Parenteral sustained drug delivery systems have gained popularity in recent decades due to several advantages over other typical systems, including reduced drug delivery frequency due to controlled drug release manner for several days to months, minimizing side effects by achieving an intravenous infusion type profile and reducing peak valley plasma fluctuations, achieving good patient compliance, providing delivery system flexibility, improving bioavailability, and achieving improved bioavailability (2, 3). *In situ* forming matrix (ISM) systems have increased in popularity over the years because of a number of benefits, including site-specification, less invasive application, longer drug release, reduced side effects associated with systemic administration, and improved patient compliance and comfort (4, 5). The mechanism of phase transformation for *in-situ* forming systems can be classified into different types such as phase separation systems (*via* thermo-responsive, solvent exchange and pH change), crosslinked systems (*via* photo-initiated, chemical and physical) and solidifying organo-gels (*via* solubility change) (6). Solvent exchange-based or anti-solvent induced ISM systems have caught the interest of pharmaceutical corporations all over the globe, leading to the development of commercial therapeutic solutions for a wide range of clinical uses (7, 8).

Drug delivery systems based on solvent-exchange or solvent removal ISM consist in either solubilizing the drug within an organic solution of a bioresorbable polymer using a biocompatible organic solvent. Upon contact with an aqueous medium, the solvent diffuses out and the polymer, designed to be insoluble in water, gradually or rapidly solidifies and transforms into the solid-like matrix. The process of severely quenching a single-phase homogeneous solution, producing separation into two phases, is known as "phase inversion" or "phase separation" after solvent removal with solvent exchange. The drug is then released by diffusion and progressive degradation of the polymers (Figure 1) (6-9). Depending on the kind of solvent employed during preparation, two types of *in situ* forming systems are generated. Slow inverting systems are formed when a water-immiscible solvent, such as triacetin, is used. Unless the system is pre-emulsified or warmed to 37 °C, the viscosity of this solution system generally makes injection difficult (10). Furthermore,

the matrix structure is characterized as uniformly packed with a small number of pores (5). In contrast, rapid inverting systems are formed using solvents that are strong and hydrophilic in nature (e.g. NMP, DMSO, benzyl alcohol), resulting in formation of a thin membrane with an inner porous matrix structure. This system is of a lower viscosity and it requires lower force of injection (10-12).

As an alternative to microparticles or *in situ* implants systems, a novel system has been also developed (13). This drug delivery system consists of an internal phase (drug dissolved/dispersed in polymer solution) that is emulsified with an external phase (usually oil). Upon exposure this emulsion with aqueous fluids, the droplets of internal polymeric phase solidify and form microparticles spontaneously (14) . *In vivo* studies with *in situ* microparticles were carried out in rats indicating its less myotoxicity. Again, an advantage of the *in situ* microparticles system compared to *in situ* forming implants was the significantly reduced burst drug release effect (15) since the external oil phase from emulsion and the polymer precipitation significantly retarded a solvent exchange and drug diffusion compared to *in situ* implants. The particle surface was highly influenced by the rate of polymer precipitation. A slower solvent release into the aqueous medium resulted in less porous microparticles, thus explaining the reduced initial drug release from ISM systems compared to the *in situ* forming implants (16).

Solvent removal phase inversion *in situ* forming systems or solvent exchange-induced or first developed by Dunn et al (17), have been approved for use in the treatment of prostate cancer as a delivery system for large peptide molecules such as Luteinizing hormone-releasing hormone (LH-RH) and is also utilized for delivering medications like Eligard®, which is used in prostate cancer treatment (18). These formulations usually comprised of a biodegradable polymer such as PLGA or poly(ε-caprolactone) dissolved in a water-miscible solvent such as NMP, triacetin, or ethyl benzoate (12). Most attracting feature of ISM systems is its applicability to a wide range of clinical indications such as Atridox® containing DH for treatment of a chronic periodontal disease, Sandostatin® containing octreotide for acromegaly treatment and Relday™ containing risperidone for schizophrenia and bipolar disorder treatments (7). Atridox®, has been introduced in the 1 9 9 0 s and received Food and Drug Administration (FDA) approval in late 1998. DH is the active component, while the matrix forming agent is poly (D, L-lactide) (PLA) dissolved in NMP. It is approved for the treatment of a chronic periodontal disease by injecting into the periodontal pocket while the polymeric solution remains in a liquid state. Its transformed matrix controls the release of DH (19). Atridox® provides for local periodontitis treatment with direct antibiotic administration, with no need for removal due to the biodegradable system. Clinical trials indicated that administering DH locally increased the clinical attachment while also lowering probing depths (20). For the most ISM formulations, matrix-forming agents are required as a key substance of this system. The matrix-forming agents should be a water insoluble, biocompatible, biodegradable, safety (non-toxic) and miscible with solvent and drugs (6).
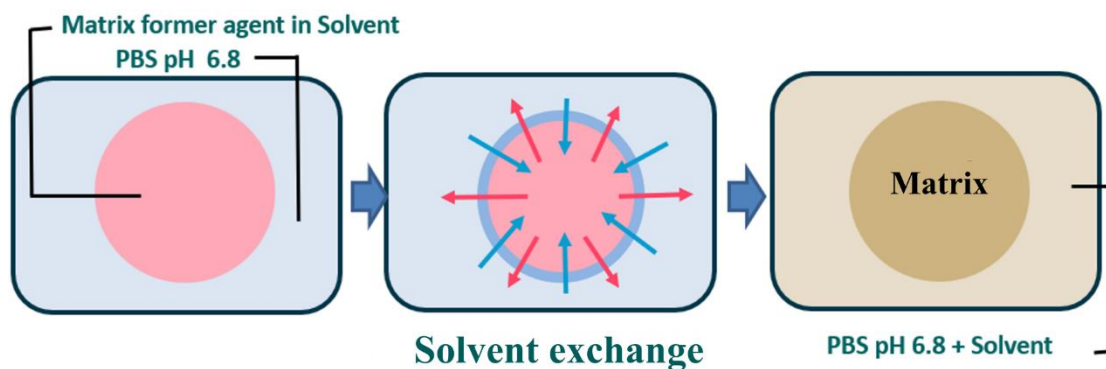
Figure 1. Schematic diagram of drug-free ISM transformation after exposure to phosphate buffer saline (PBS) (pH 6.8) (21).

Periodontitis

Health of oral cavity is a key indicator of overall health, well-being and quality of life. It encompasses a range of diseases and conditions that include dental caries, periodontal (gum) disease, tooth loss, oral cancer, oral manifestations of HIV infection, oro-dental trauma, noma and birth defects such as cleft lip and palate (22). A chronic disease, such as arthritis, heart disease or stroke, diabetes, emphysema, hepatitis C, a liver condition, or obesity, can increase a person's risk of missing teeth and having poor oral health (23). Most oral health conditions are largely preventable and can be treated in their early stages (24). Nowadays, periodontal diseases affect about 20-50% of global population (25). Approximately 25.9% of adults and 36.3% of older individuals in Thailand experience health issues related to periodontitis with a periodontal pocket depth of 4-5 mm. Moreover, over 19.8% of adults and 12.2% of older individuals suffer from severe periodontitis, characterized by a periodontal pocket depth exceeding 6 mm. This condition poses an increased risk of infection, inflammation, tooth loss, and a diminished quality of life (26, 27). The amount of tissue destruction is generally commensurate with dental plaque levels, host defenses and related risk factors (28). Gingivitis is the inflammation of gum caused by bacteria which does not include any loss of bone and tissue. However, it can advance to periodontitis which is a serious gum inflammation and more aggressive than gingivitis. Periodontitis damages the periodontal tissue and destroys the bone that supports the teeth resulting in various size of periodontal pocket which eases for bacteria accumulation resulting in more aggressive condition (Figure 2) (29, 30). Most of the pathogens of this disease are Gram-negative bacteria and some of them are anaerobe bacteria, for example, *Aggregatibacter actinomycetemcomitans, P. gingivalis, Bacteroides forsythus, P. intermedia, Campylobacter rectus, Eubacterium nodatum, Streptococcus intermedius* and *Treponema denticola* (31-33). This bacterial infection can cause the periodontium (gingiva, periodontal ligament, dental cementum, and alveolar bone) damages by the bacterial by-product and immune activation (34). Some of microbes is related to the inflammation and tissue loss including enterobacteria (such as *E. coli*, *Pseudomonas aeruginosa* and *Klebsiella pneumoniae*, *Candida albicans*, *Neisseria* spp., *Olsenella uli*, *Hafnia alvei*, *Serratia*

marcescens and *Filifactor* (35). In addition, *S. aureus* could be found in periodontal pocket (36). In general, the pH of the normal oral cavity of a human is maintained near neutrality (~7.06) by saliva, whereas the average pH of the normal oral cavity of a patient with chronic periodontitis is 6.85, indicating slight acidaemia (37).

For periodontal treatment, the dentist performs on the elimination or inhibition of the growth of bacteria on tooth surface and in periodontal pocket by mechanical scaling, root planning and medications (34, 38). The non-surgery (scaling, root planning) is aimed for removal of subgingival biofilm and calculus, which together with the patient's oral hygiene practices will prevent bacterial recolonization and formation of supragingival biofilms (Figure 3) (39). Several antimicrobial agents have been evaluated for their clinical and microbiological efficacy in periodontal diseases such as chlorhexidine, tetracyclines (tetracycline, doxycycline and minocycline), metronidazole, ciprofloxacin, vancomycin and etc. (29, 32, 33). However, they have some limitations such as serious side effect, antibiotic resistance, local irritation, undesired burst active compound release (40-43). The irregular shape and various size of periodontal pocket seems to be the problem for mentioned local drug delivery systems. Those of them could not be fitted or well fitted with the various periodontal pockets. Moreover, it is difficult to insert the solid or semisolid into the tiny pocket. Thus, *in situ* forming drug delivery system, the liquid form at first, demonstrates a beneficial manner over those drug delivery systems due to the goodness of fitting to pocket, ease of use and acceptable clinical effectiveness (44). The local antibiotics delivery systems are interesting to keep a high and effective drug concentration at the target site with minimizing the side effect (42). The films (45), gel (46), strip (47), and *in situ* forming systems (14, 48) have been developed or reported for carrying antibiotics as the local drug delivery systems for periodontitis treatment. It has been reported for DH-loaded bleached shellac ISM using olive oil containing glyceryl monostearate as the external phase and 2-pyrrolidone (PYR) as a solvent was a suitable formulation for periodontitis treatment (14). Moreover, 40% beta-cyclodextrin ISM in DMSO as the internal phase and camellia oil comprising 5% glyceryl monostearate as the external phase is a potential local meloxicam-controlled release system of anti-inflammatory drug for periodontitis treatment with extended the drug release to 7 days (49). ISM is interesting dosage form for the local treatment of periodontitis to provides the drug release at a controlled rate by way of directly accessing to the target site which reduces side effects, thus improving patient compliance.
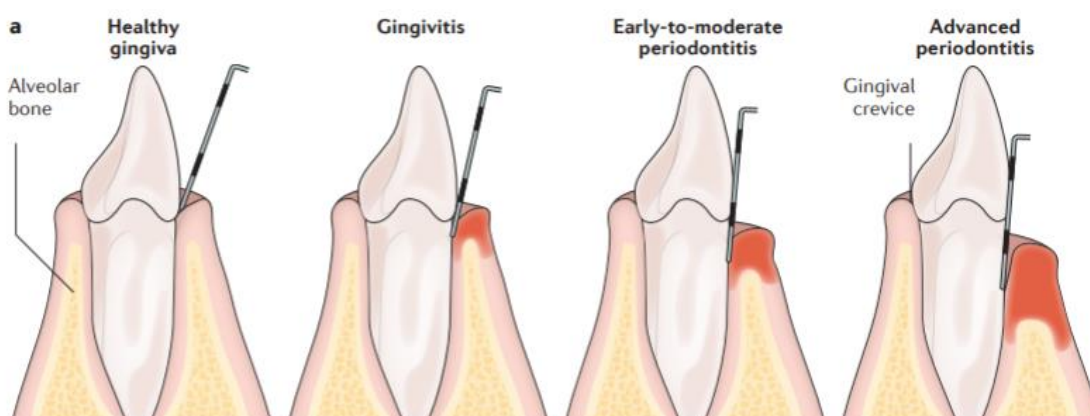
Figure 2. The main stages of periodontal disease; schematics of healthy gingiva, gingivitis, early-to-moderate periodontitis and advanced periodontitis (29).
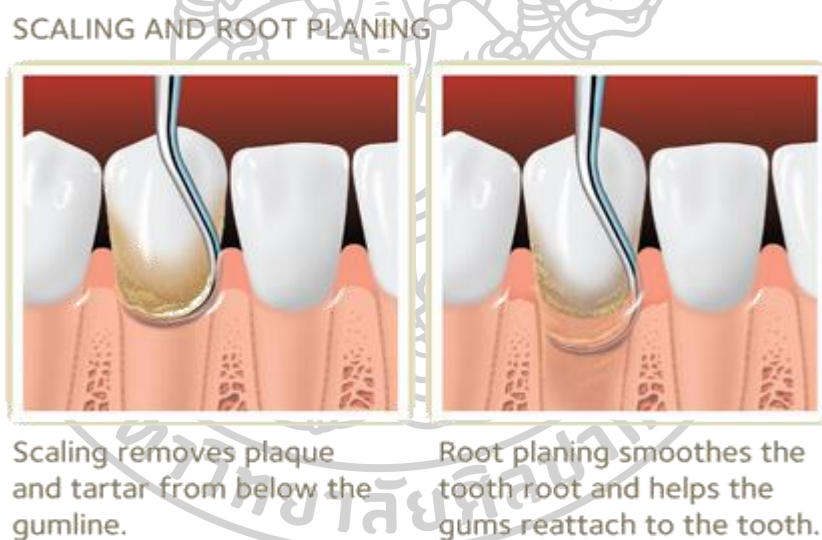
Figure 3. Scaling and root planning (50).

Eudragit® L & S

      Eudragit® L and S are the anionic copolymers of methyl methacrylic acid and meth-acrylic acid with ratio of approximately 1:1 and 1:2, respectively. Both polymers have such a molecular weight of 1,25,000 g/mol, a glass transition temperature of above 150 °C, and an acid value of 315 mg KOH/g of polymer (51). Eudragit® L and S are a pH dependent solubility polymer, which is insoluble in acid medium but dissolves at pH above 6 (52, 53). Eudragit® S demonstrates solubility at pH levels of 7 or higher, a distinctive attribute that defines the Eudragit® series. This property becomes pivotal in enabling controlled drug release that responds to diverse

pH conditions (54). The structure of Eudragit® L and S are shown in Figure 4. They are employed for coatings that dissolve rapidly in the upper intestine, granulation of pharmacological substances in powder form for controlled release, and site-specific drug delivery in the intestines, among other things. A current review on Eudragit® L 100 exhibits that it has been used in formulations microspheres, micro-sponges, nanoparticles, liposomes, lipotomes, tablets for different applications such as enteric coating, sustained release, insulin permeation enhancement, bioavailability enhancement (55-58). Eudragits® are generally regarded as nontoxic and nonirritant materials. A daily intake of 2 mg/kg body-weight of polymethacrylates in humans is regarded as essentially safe. Eudragit® is included in the FDA Inactive Ingredients Guide (52). It has been reported for the DH-loaded Eudragit®RS/NMP solvent removal phase-inversion-based ISM for periodontitis treatment (21). Moreover, Eudragit®L/DMSO ISMs exhibited as a potential periodontal pocket drug delivery system based on solvent removal mechanism with modulating the DH release longer than 3 days (59). Nevertheless, the application of Eudragit®L and S and MP as the ISM have not been reported. Eudragit®L and S are dissolve at pH above 6, that might be easy to handle with providing a degradable matrix to release drug that without the need for clinical removal.
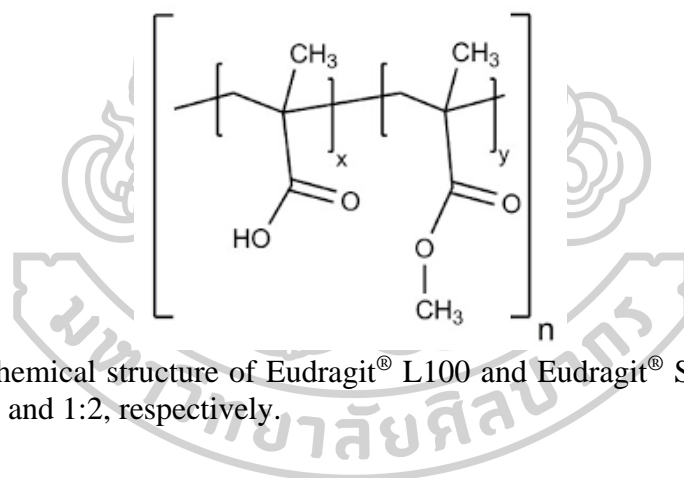
Figure 4. Chemical structure of Eudragit® L100 and Eudragit® S100, where the ratio of x:y is 1:1 and 1:2, respectively.

Zein

Zein is the main storage protein in corn, providing for 45-50% of the protein content. It was found in 1897 due to its solubility in aqueous alcohol or alkaline solutions (pH ≥ 11) (60). Its large abundance (>50%) of nonpolar amino acids including leucine, proline, alanine, and phenylalanine; thus, zein is water insoluble (61, 62). Moreover, it has strongly defined hydrophobic and hydrophilic regions on its surface and can self-assemble into a wide range of meso-structures. Owing to its high glass transition temperature, the hydration of zein requires a rather high temperature to function as a visco-elastic polymer (63, 64). Table 1 highlights some of main physicochemical characteristics of zein (65). Zein is a prolamin with a molecular weight of around 40 kDa (66). The four major varieties of zein (denoted α, β, γ and δ) are categorized based on their solubility, molecular weight, composition and structure. The α-zeins have significant hydrophobic properties (67-69). The major component of

commercially accessible zein is α -zein. The structure of α-zein is made up of homologous repeat units that are arranged in a helical wheel (α-helix) shape.

Figure 5 shows a three-dimensional network aligned in two different ways: cylindrical and ribbon-like models, in which the hydrophobic helices are arranged edgewise and the hydrophilic glutamine bridges connect the top and bottom surfaces of the repeat units (70). It is employed as a coating material because of its substantial hydrophobic interior core, which serves as an excellent water barrier (60). Zein may contain fewer xanthophyll pigments, which therefore leads to its yellow color. Zein is commercially available in two varieties: yellow zein and white zein (71, 72).

In 1985, the US-FDA (United States Food and Drug Administration) approved zein as a GRAS excipient to be a safe substance for use focused mostly on its industrial and consumer applications, such as plastics, inks, molded products, gum, printing film, paper, and food coatings (62, 73). Extensive research has shown that zein is an efficient excipient for the controlled delivery of essential oils, dyes, antimicrobial agents, anticancer agents, macrophage targeting, oral drug delivery with stomach protection, and gene delivery as micro/nanoparticles (74-77). Zein has good degradation property and may be researched for use in implants (78). Zein, being a protein, is degraded by numerous enzymes, including pepsin and pancreatic enzymes, depending on the place of application. Zein is digested in the oral cavity by protein degrading enzymes such as collagenase and trypsin-like enzymes found in saliva and gingival crevicular fluid (79, 80). Moreover zein has been reported that is a favorable biomaterial with good biocompatibility for tissue engineering (81).

Zein can be produced into a strong, glossy coating with antibacterial activity and is thus commonly used in the food and pharmaceutical industries (77, 82). In the pharmaceutical field, zein is an excellent skeleton material to support sustained-release implants. Zein exhibits the mucoadhesive properties and ability to sustain the drug in the gastrointestinal environment, making it suitable for mucosal drug administration (83). Zein tablet had been reported the swelling behavior of zein matrices both alone and in combination with additives is clearly different from that of typical hydrophilic and insoluble polymers, such as hydroxypropyl methylcellulose (HPMC) and EC, respectively. Interestingly, the addition of microcrystalline cellulose to zein matrix could provide a more constant drug release compared to pure zein matrix, thus offering a great advantage for designing efficient controlled drug delivery devices (84). Gao et al. prepared a zein-based ISG containing pingyangmycin, a water-soluble glycopetide drug by dissolved 1.2 g zein in 5 mL of GF, which was left overnight to form a clear solution then the drug was added and the prepared system was employed to treat the venous malformations with an effectively prolonged drug liberation up to 7 days *in vitro* and 4 days *in vivo* (85). The interstitial chemotherapy using a doxorubicin-loaded zein-based ISG has been mentioned by Cao et al. (86). The 15-25 % zein was dissolved by mixing with GF and 70% ethanol-water (3:7, v/v). It was left overnight at room temperature to form a clear solution then the drug was added and dissolved by stirring. The gel demonstrated a superior effectiveness and regulated a drug release over time after intra-tumoral injection than plain doxorubicin

drug solution (87). In periodontitis treatment, a solvent casting/particulate leaching procedure was used to create a zein porous scaffold. The scaffold was suitable for the growth of periodontal ligament cells because it was biocompatible and interconnected well. Zein might utilize to heal periodontal tissue defects as a scaffold (88). Zein was loaded in collagen sponges containing tetracycline loaded-PLGA microparticles designed for *in situ* application within the periodontal pocket. The drug release was more sustained in the formulations containing higher amounts of zein in their composition. Furthermore, the sponges were homogenous, easy to handle, and wettable, with collagen content providing a biodegradable matrix to release tetracycline without the need for clinical removal at a one-visit insertion (89). The present research conceptual framework interests for applying zein as matrix forming agent for solvent removal phase inversion-based ISM system loaded with antimicrobial for periodontitis treatment. This developed drug delivery system has not been reported previously. Zein might be used as a matrix forming agent of ISM for crevicular pocket targeting due to its long-term use with safety and apparent water insolubility but miscible in organic solvent.

Table 1. Properties of zein, a corn protein (65).

Property	Characteristics
Bulking value, l/kg	0.805
Color	Light cream
Dielectric constant (500 V, 60 cycles, 25-90 °C)	4.9-5.0
Diffusion coefficient	3.7×10^{-14} m^2/s
Einstein viscosity coefficient	25
Glass transition temperature	165 °C
Molecular weight	35 kDa (varies 9.6 to 44 kDa)
Partial specific volume	0.771
Physical form	Amorphous powder
Sedimentation coefficient	1.5 s
Specific gravity, at 25 °C	1.25
Thermal degradation point	320 °C

(a) cylindrical model   (b)   ribbon-like
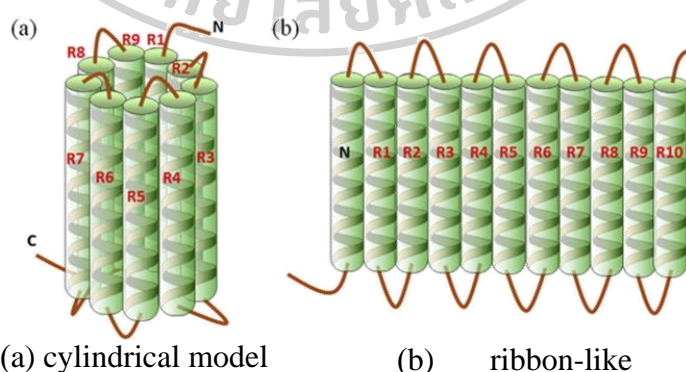
Figure 5. Proposed 3-D structural models of α-zein. (a) cylindrical model; (b) ribbon-like model (22 kDa) (90).

Nitrocellulose (Nc)

Nc (CAS number 9004-70-0) is a white, fibrous, pulp-like substance which has no odor nor taste with the formula $C_{12}H_{16}N_4O_{18}$. Nc is also known as pyroxylin, gun cotton, or collodion, but the latter. Properties of Nc are show in Table 2, it is well notorious for spontaneously igniting when the temperature is increased to 160-170°C and above (91, 92). The FT-IR spectra of isolated Nc were found in the bands of 1000 – 12 00 cm^{-1} (attributed to the valence vibrations of the glucopyranose cycle), and 690 -750 cm^{-1} (assigned to the vibrations of the nitrate group) (93).

Nc is a nitrated ester of cellulose that is prepared by using a mixture of sulfuric and nitric acids for cellulose treatment. This reaction replaces the hydroxyl groups with nitro groups as shown in Figure 6. Because of the compound's explosive instability when dry, Nc is normally maintained wet using water or an organic solvent such as isopropyl alcohol, esters, ketones, or ethers of glycol (91). Nc can be classified based on many properties and made upon the nitrogen content, for A (SS grade) (alcohol) grade it has nitrogen content: 10.7 % - 11.3 % soluble in ethanol and showed thermoplastic behavior, used in printing inks and plastic foils, flexographic inks application. For E grade (RS grade) (ester soluble), it shows the excellent mechanical properties; thus, it is used in forming hard films and military applications and explosives propellants. For AM grade (Alcohol Medium-soluble), it is partially soluble in ethanol and it exhibits the mixed characteristics from that of the A and E grades that is in the middle of thermoplastic and thermoset behavior, used in staple coatings or the cellulose films coating. Nc is fundamental properties change somewhat depending on its nitrogen level (94). Moreover, nitrogen content affects the polymer solubility and viscosity since the solubility decreases when the nitrogen content of Nc decreases (93, 95). Whereas, the density of Nc increases with the increase of its nitrogen content (96). Additional, the higher the increase in intrinsic viscosity with increasing nitration observed (97).

In chronic, sub-chronic, and multigeneration studies Nc was non-toxic to rats and dogs; however, mortality was seen in mice, which was attributed to the relatively large size of the fibers relative to the size of the murine intestinal lumen rather than to chemical toxicity (91, 92). Nc has proven itself versatile and beneficial in many other fields; including skin coverings to prevent wounds from contamination, cosmetic preparations, film, inert support for chromatographic separations in research, and components used in the production of lacquers, and artificial leathers, adhesives, and other products (91, 92, 98, 99). Nc was used as membrane filter impregnated with silver nanoparticles used to purify drinking water (100). In the medical application, with its excellent biological and physiochemical qualities, Nc membrane, which is a paper-like matrix with microscale porous pores has been utilized. Nc membrane is frequently employed to immobilize nucleic acids in southern and northern blots, as well as immobilize proteins in western blots (99, 101, 102). Moreover, Nc bandages can be effective in wound healing especially hard-to-cover wounds, and thus Nc liquid bandages were produced with nanopores to be used in hard-to-cover wounds. Its porosity in nano-size showed an enhanced antibacterial effect, an increased time of

healing, and non-toxicity on the wound itself (103). Nc has shown to be a critical substance with unique features that exhibit potentially used in a variety of sectors. However, the Nc-based *in situ* forming depot has not been addressed previously; thus, it is interesting for developing as the drug delivery system for periodontitis treatment.

Table 2. Properties of Nc (91).

Property	Characteristics
Bulking value, l/kg	1.67-2.00
Specific gravity, at 25 °C	1.4 (solvent damped)
	1.66 (dried chip)
Partition coefficients	Log Pow < 0
Melting point	160-170 ˚C (ignites)
Vapor pressure at 25 ˚C	1×10^{-5} mm Hg
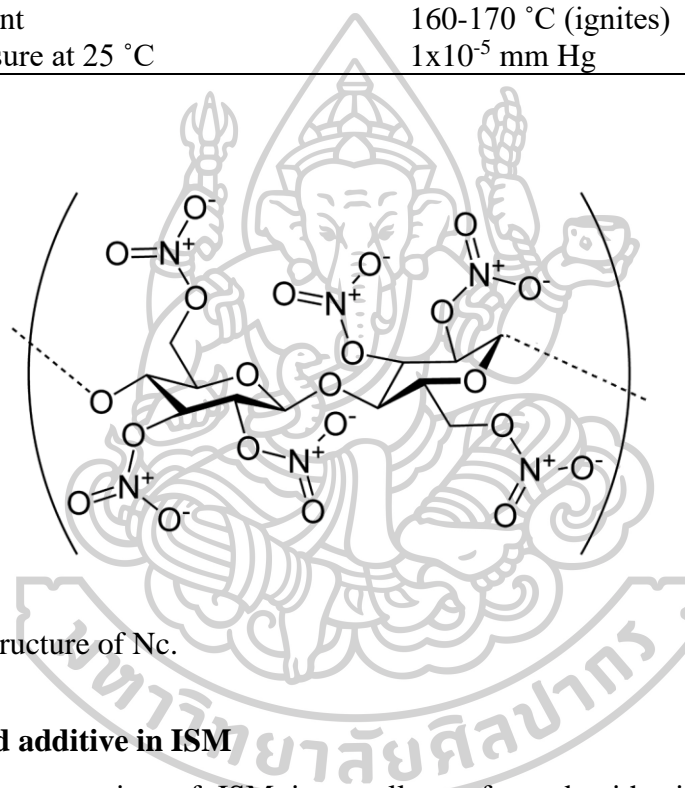
Figure 6. Structure of Nc.

Solvent and additive in ISM

The preparation of ISM is usually performed with simple mixing of the pharmaceutical solution dosage form; therefore, the suitable solvent or vehicle to dissolve the ingredients is necessary. Practically, the solvents or vehicles of the ISM system are water miscible, biocompatible and organic in nature. Importantly, solvents should efficiently dissolve the matrix forming material and active compound, and be miscible with water and bodily fluids. Polarity of the solvent should be such that at least 10% should be soluble in water (7, 17). The viscosity of solvent should be within the range that is injectable. Solvent strength and its affinity for water directly influence the nature of phase inversion and matrix formation. For example, solvents having a high-water affinity such as NMP and DMSO provoke a fast-forming phase inversion (104). Whereas, the hydrophobic solvents such as triacetin and ethyl benzoate promote a slow forming phase inversion (105). Solvents that possess a water solubility of below 7% w/w have been shown to result in a slower drug release due to a reduction in water uptake (106).

Nowadays, ISM systems most commonly consist of DMSO, NMP, and PYR as the solvents preferentially due to their pharmaceutical precedence over other solvents (7). NMP (Figure 7a), molecular weight of 99.13, is a very strong solubilizing agent with low viscosity. It has known as a solubilizing excipient used in parenteral and oral medications. Many commercial pharmaceutical products containing NMP are currently available in the market. The European Commission Scientific Committee on Consumer Safety concluded that NMP has low acute toxicity by oral, dermal, and inhalation routes of administration (107-109). DMSO (Figure 7b), molecular weight of 78.13 is a non-aqueous dipolar aprotic solvent with colorless, oyster-like odor and relatively low toxicity (LD_{50}: 2.5 to 8.9 g/kg) (110, 111). It is safe if used less than 100 mg/day (111). It is miscible with most common solvents such as alcohol, ether, aromatics and water (112). It readily penetrates into the cellular membranes; thus, it has been employed as a skin penetration enhancer (110, 113, 114). It is approved by US-FDA to treat the interstitial cystitis (113). In addition, it shows various pharmacological actions including analgesic, antioxidant and anti-inflammatory activities (114, 115). In results of many studies found that DMSO is vary soluble in water which can breaks down the water structure and forms the strong hydrogen bond complexes with water molecules due to stronger interaction between DMSO-water (110, 113). PYR (Figure 7c), has a molecular weight of 85.12, melting point 25.57 °C, boiling point 245 °C and refractive index: 1.482-1.490. It is a colorless liquid that is miscible with water, alcohol, ether, acetone, ethyl acetate, chloroform, benzene /lipophilic vehicle. PYR itself and various derivatives made from it have a variety of industrial uses (116). PYR has been used as the solvents for an ISM because of biocompatible and low toxic characters (LD_{50} Rat oral 6.5 g/kg) (117, 118) and has been reported as a plasticizer to improve a mechanical properties and reduced a drug burst release of spider silk films (119). It has been shown that when DMSO, NMP, or PYR were used in *in situ* forming implants made with PLA/PLGA or PLA the initial drug release decreased in the rank order DMSO > NMP > PYR (13). Moreover, glycerol formal (GF) molecular weight of 104.10 g/mol (Figure 7d), is used to solubilize water-insoluble compounds for subsequent aqueous dilution. Although GF has little toxicity, the amount used in the ISM was well below the established adverse effects level (85). Limited number of studies also showed use of GF in ISM systems, these solvents have earlier history of using in veterinary formulations (7). GF has been reported as solvents for Doxorubicin-loaded zein ISG for interstitial chemotherapy of colorectal cancer (86) and Pingyangmycin hydrochloride-loaded zein/zein-sucrose acetate isobutyrate (SAIB) ISGs to treat venous malformations (85). MP is also called as propylene glycol. The chemical formula of MP is $C_3H_8O_2$ and the structure is given in Figure 7e. The molecular weight is 76.095 (120). MP is a colorless, odorless, water-soluble liquid. It FDA approved for use in food, tobacco, and pharmaceutical products as an inert ingredient (121). MP was selected as a cosolvent in preparation of ISM formulations of mitiglinide calcium for simultaneous extended delivery and enhanced bioavailability (122). Moreover, MP has been reported as co-surfactant of an *in situ* microemulsion-gel in bio-adhesive HPMC films for transdermal administration of zidovudine (123).
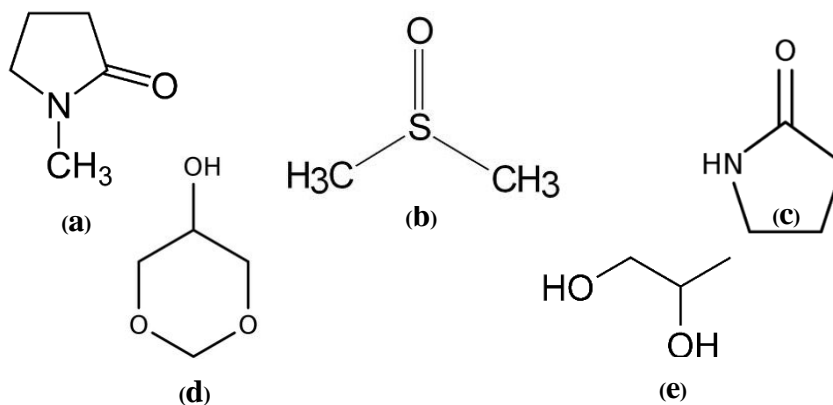
Figure 7. Chemical structure of N-methyl-2-pyrrolidone; NMP (a), dimethyl sulfoxide; DMSO (b), 2-pyrrolidone; PYR (c), glycerol formal; GF (d) and monopropylene glycol; MP (e).

Levofloxacin HCl (Lv)

Lv ($C_{18}H_{20}FN_3O_4 \cdot HCl$), the L-enantiomer of ofloxacin, is a fluoroquinolone antibacterial agent (Figure 8) (124). The molecular weight is 397.8 and it is freely soluble in water. It is a broad-spectrum, third-generation fluoroquinolone antibiotic that diffuses through the bacterial cell wall and acts by inhibiting DNA gyrase and topoisomerase IV, an enzyme required for DNA replication. It demonstrates little inhibition of human, host enzymes and has an excellent safety record. Levofloxacin was approved for use in the USA in 1996 and remains in wide use (125). Lv is active against a wide range of aerobic Gram-positive and Gram-negative organisms and demonstrates a moderate activity against anaerobes (126). Lv is used for mild-to-moderate infections, the usual dose being 250 to 750 mg once daily depending upon the indication and severity of the infection. It is a well-established treatment option for respiratory and urinary tract infections, and is active against some penicillin- and macrolide- resistant species (127). Some studies have shown good results with the adjunctive use of fluoroquinolones, such as ciprofloxacin, ofloxacin, in periodontitis (128, 129). Lv has been effective in the treatment of patients with gynecologic, skin and skin-structure, and bone infections involving anaerobic pathogens. Unique animal bite wound isolates such as *Porphyromonas macaccae* and *P. gingivalis* and *Prevotella heparinolytica* are usually susceptible to 0.25 and 0.5 µg/mL of Lv, respectively (130). Lv with a combination drug ISG-forming nasal delivery system on repairing nasal mucosa damage has been reported since it could prevent a stenosis of new ostia, significant reduce of a chronic inflammation, and actively support a wound healing (131). Chitosan and poloxamer ISG containing Lv and metronidazole has been developed. Poloxamer is a thermoreversible polymer that make the system undergo *in situ* gelation with increasing environmental temperature. The formulation showed an initial burst drug release where about 60-70% Lv released within 6-7 h followed by sustained release upto 48 h (132). In addition, the medicated ISG showed better clinical outcomes as compared to scaling and root planing alone, which could be attributed to the presence of chitosan that is not only effective in treatment of

periodontitis but also acts as a good carrier to deliver drug into periodontal pocket (133). Thus, Lv was selected as an antimicrobial drug for treatment of periodontitis due to its broad spectrum and good activity against selective anaerobic bacteria.
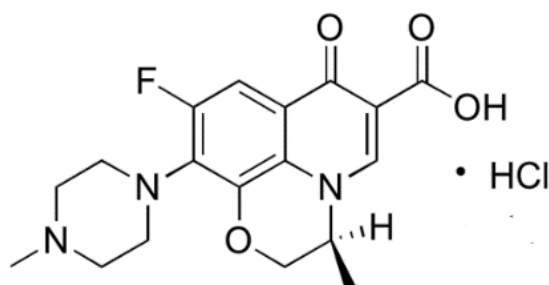
Figure 8. Structure of Lv

Moxifloxacin HCl (Mx)

Mx ($C_{21}H_{24}FN_3O_4$•HCl) is a slightly yellow to yellow crystalline substance with a molecular weight of 437.9 and sparingly soluble in water (24 mg/ml) (Figure 9)(41). It is a fourth-generation flouoroquinolone with activity against a broad spectrum of Gram-positive, Gram-negative and anaerobic bacteria pathogens (134). Mx is a broad-spectrum fluoroquinolone antibiotic. Mx inhibits the bacterial enzymes DNA gyrase (topoisomerase II) and topoisomerase IV, resulting in inhibition of DNA replication, and cell death in sensitive bacterial species (48). Mx recently received approval from the US-FDA for the treatment of complicated skin or skin-structure infections and complicated intra-abdominal infections (135). The eyedrops for ocular treatments, Mx-loaded PLGA microparticles encapsulated in a chondroitin sulfate-based, two-component bio-adhesive to localize drug release by ISG may potentially integrate an antibiotic prophylaxis and a wound healing in the eye (136). Mx was used in ISGs for the treatment of periodontitis using temperature sensitive (poloxamer 407), ion sensitive (gellan gum) and pH sensitive (carbopol 934P) polymers (48). In addition Mx was loaded in ISG eye drops using sodium alginate as a gelling agent in combination with HPMC as a viscosity enhancing agent for treatment of ocular infections successfully (137). The antimicrobial studies indicated that Mx retained its antimicrobial activity when formulated as ISM for periodontal system against selected *S. aureus* and *E. coli*. This drug exhibits the desired characteristics for developing as active compound in periodontal drug delivery systems (136, 137). Moreover, Mx dental implants were fabricated by solvent casting technique using EC and other co-polymers (HPMC-K100M or Eudragit® RL100) as the polymers dissolved in chloroform: methanol. The formula demonstrate a significant *in vitro* antibacterial activity against *Streptococcus mutans* for 6 days with retained antibacterial activity (48).
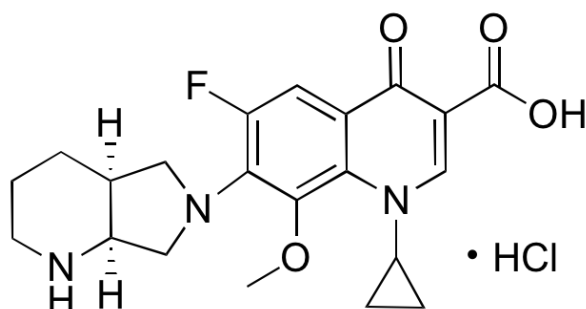
Figure 9. Structure of Mx.

Tracking of fluorescence dye movement

Nile red (NR) (Figure 10a) is employed as a fluorescent dye in this study since it is a popular fluorescent agent used as a model of hydrophobic substance (138). It is applied in neutral lipids, cholesterol, phospholipids in cellular cytoplasmic droplets and lysosomes, foam cells lipid loaded macrophages (139). An excitation and emission wavelengths of NR are 450-550 nm and 525-600 nm, respectively (140, 141). Whereas, sodium fluorescein (SF) (Figure 10b) is widely used as a fluorescent tracer representing as hydrophilic substance due to its high aqueous solubility (142). It absorbs most light in the blue part of the spectrum but most of its emitted light is in the yellow part of the spectrum and some in the green (143). Its major excitation peak is between 465 and 490 nm and the fluorescence emission band is from 510 to 530 nm (144). Thus, SF and NR are chosen as the model compounds of hydrophilic and lipophilic substances, respectively, for the study of drug movement during phase inversion.
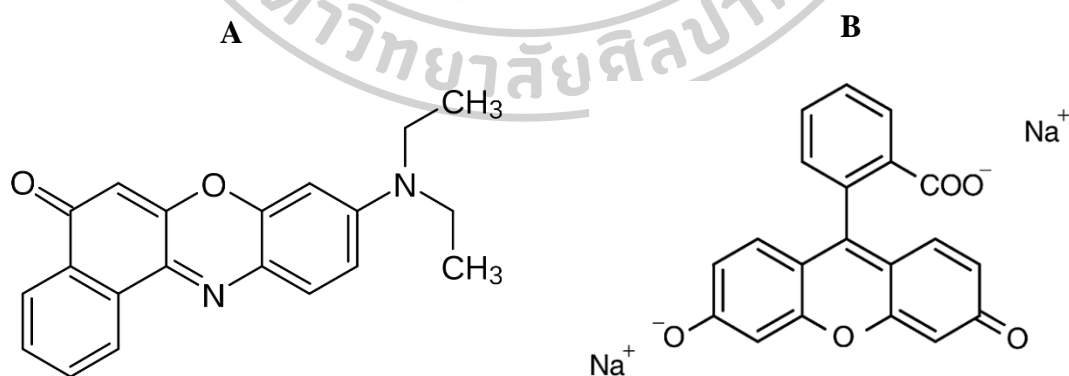
Figure 10. Structure of (A) NR and (B) SF

UV-Vis imaging

The field of drug delivery has been revolutionized by the development of innovative strategies, among which ISM have emerged as promising platforms (145). ISMs are dynamic formulations that undergo a transition from a liquid to a matrix-like state upon administration, offering controlled and sustained drug release over time. In this context, UV-vis imaging has garnered significant attention as a valuable analytical technique for characterizing various aspects of ISM behavior (146). UV-vis imaging leverages the principles of absorption and scattering of light in the ultraviolet (UV) and visible (Vis) regions of the electromagnetic spectrum to visualize and quantify changes in molecular composition, concentration, and distribution within complex systems (147).

The integration of UV-vis imaging into ISM research facilitates real-time monitoring and visualization of critical processes such as gelation, drug solubilization, drug dispersion, and drug release kinetics (148). By offering spatial and temporal information, UV-vis imaging enables researchers to comprehend the dynamic behavior of ISMs and their interactions with physiological environments. A significant advantage of this technique is its non-destructive nature, eliminating the need for extensive sample preparation (149). With the utilization of UV-vis imaging, various aspects of ISMs, such as matrix formation and drug distribution, can be explored (146, 148, 150). This non-invasive and quantitative imaging approach holds the potential to provide insightful information, contributing to a better understanding of the performance and behavior of ISMs. Consequently, it aids in the refinement and enhancement of drug delivery strategies.

In summary, UV-vis imaging represents a versatile tool that enhances our understanding of the intricate dynamics of ISMs. Its ability to provide real-time insights into the behavior of these complex formulations holds great promise for optimizing their design, improving therapeutic efficacy, and advancing drug delivery strategies. As the field continues to evolve, the integration of UV-vis imaging is expected to play a pivotal role in shaping the future of ISM-based drug delivery systems.

Mechanistic model of ISM drug release

A multitude of variables influence the drug release kinetics from controlled release implants, including polymer swelling, polymer erosion or degradation, implant shape or surface area, drug dissolution, and water inflow rate (151). To design drug-delivery devices, all of these parameters should be included in a mathematical model with prediction accuracy. Various release models are investigated for understanding the process of drug release from established and fabricated drug delivery systems and to predict the amount of a drug liberation over duration. The burst drug release effect refers to a large amount of drug release with no retarding effect from the system. For many controlled systems, the burst drug release is often displayed first, followed by the sustained release. To represent the release behavior of any controlled release system, the release kinetics are employed to fit with the release data or profile (152,

153). One of the simplest empirical drug-release models is a zero-order drug release (154):

$$Q_t = Q_0 + k_0 t$$

where Q_t is the total amount of drug release at given time (t), Q_0 is initial drug release, k_0 is the release rate constant, and t is given time. Zero order release is an ideal model for controlled release system in which the release rate is constant.

The Higuchi model assumes that drug release from polymer matrix systems is solely diffusion-controlled and that the drug is uniformly distributed in non-degradable planar systems. The Higuchi's model is given by (155):

$$Q_t = k\sqrt{t}$$

where Q_t is the total amount of drug release at given time (t), k is the release rate constant, and t is given time.

The other main release kinetic including first order and power-law have been developed to describe resultant drug dissolution kinetics well known (153, 154). The degree of curve fitting is indicated by the coefficient of determination (r^2) in which a high r^2 value indicated a high degree of fit. According to the Korsmeyer- Peppas model, the diffusion exponent (n) from the power-law model indicates the drug transport mechanism (156).

While empirical models may be simple, they fail to take into account the dynamic responses of "real" drug delivery devices. Therefore, they cannot be used to accurately simulate the effects of device design variables on drug release. Such simulations can be obtained with mechanistic models that account for mass transport and chemical phenomena such as polymer swelling, water influx, drug dissolution, creation of matrix void space, matrix degradation, and convective processes. Consequently, these models can predict the drug release kinetics from a particular drug delivery device. Models including non-linear differential equations with numerous variables and parameters that need numerical solutions may be used to depict the kinetics of complicated drug delivery systems (155).

Wang et al. (157), has reported a controlled drug release of a poorly water-soluble anti-cancer agent, β-lapachone (β-lap), from cylindrical pre-formed polymer millirod implants with a mechanistic model. This model depicted water influx and pore creation, excipient-drug complex formation, crystalline drug dissolution, and diffusion in solid and liquid phases, among other chemical and mass transport processes. The model was verified by comparing model outputs to experimental data after obtaining optimal parameter estimates. This validated model could predict how the enhanced solubility of β-lap affecting drug release kinetics by simulating the impact of different excipients or drug loading dosages on drug release kinetics (153). Moreover, Raman et al. presented the release kinetics of a protein medicine (lysozyme) from a fast phase inverting ISM in one such mechanistic model. To represent drug dissolution, water input, solvent efflux, and drug diffusion, this model

applied the 1-D diffusion reaction equations. A polymer-rich phase with solvent, water, and drug disseminated within the polymer matrix, and a water-rich phase with solvent and dissolved drug, made up the model implant geometry. Water diffused into the polymer rich phase to dissolve scattered drug particles, while the dissolved drug and solvent from the polymer-rich phase diffused into the water rich phase and subsequently out to the external solution in this model. Model simulations showed a variety of drug release kinetics varying from zero-order to massive first burst drug release by varying model parameters (10).

For ISM the model has a flaw in that it assumes a really fast implant phase inversion (seconds to minutes). While this is certainly true when a thin, flat implant membrane is formed, most ISM *in vitro* and *in vivo* creates the spherical or globular forms that phase inversion occurs over longer time scales (h to days) (158, 159). The rate of implant phase inversion has a significant effect on the drug release kinetics (11). Therefore, a different model is needed to describe the drug release kinetics from more realistic globular implants that phase invert on a slower time scale. In a regulated *in vitro* situation, such computer models may simulate a drug release from very thin *in situ* forming membranes. They are inefficient for characterizing drug release using an ISM that has a significantly smaller surface area to volume ratio, such as those are employed in other *in vitro* or *in vivo* studies (159-161). In addition, mathematical modeling of drug delivery from matrix-type vaginal ring with torus-shaped single-layer devices based on the pseudo-steady state approximation (PSSA) by computational software (MATLAB®) was reported. The reliability and usefulness of the model are ascertained by comparison of the simulation results with matrix-type vaginal ring experimental release data reported in the literature (162).

Based on previous study, a mathematical model presents the tracking of mass concentration dynamics of solvent, polymer, drug, and water through the matrix precipitation and phase inversion process (163, 164). The phase-inversion process of an *in situ* forming implant begins after injection of a liquid implant solution with solvent, polymer, and excipient into an aqueous solution and produces an initial burst release of drug. A thin spherical shell of polymer matrix with continuous void space forms almost instantaneously and surrounds an interior core of (non-phase inverted) implant solution as presented in Figure 11. Solvent and drug diffuse from the inside to the outside through the porous matrix, whereas water diffuses from the exterior to the interior in the void fraction. When the water concentration reaches a threshold level, the polymer precipitates at the array solution interface, increasing the formation of polymer matrix. The volume of the matrix phase rises with time due to the creation of empty space. As water diffuses into the inner (non-phase inverted) zone, it will swell. Eventually, the polymer completely precipitates and forms matrix surrounding an interior filled with water.
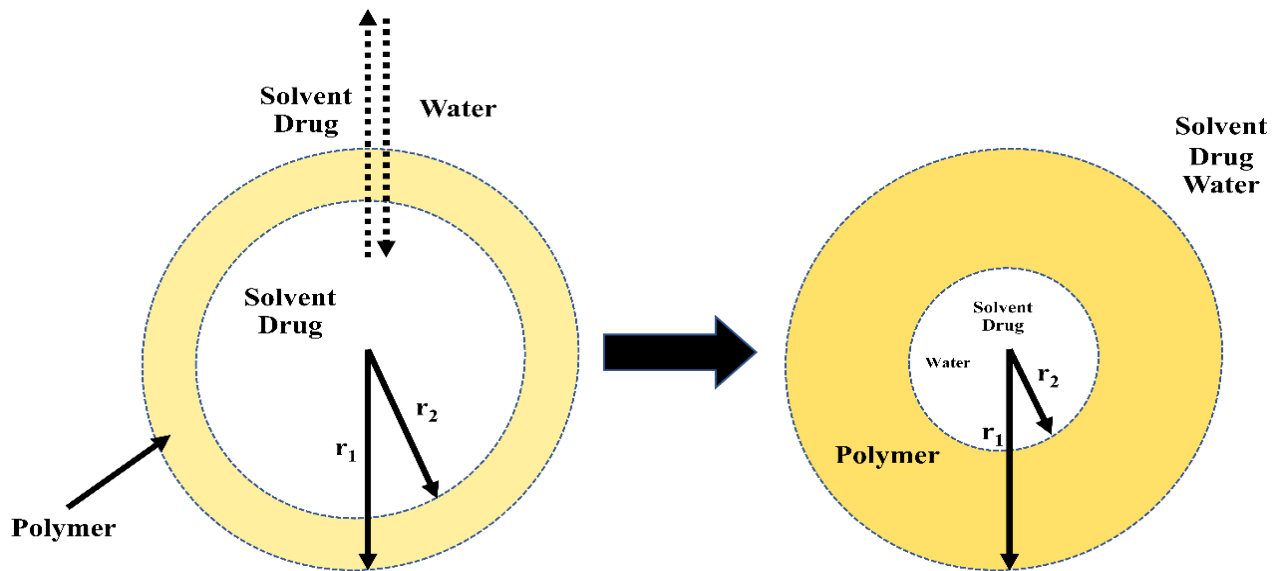
Figure 11. Schematic of implant phase inversion

SCOPE OF RESEARCH WORK

Various concentrations of matrix forming agent and various types of solvent are attempted to solvent removal induced phase inversion-based ISM for loading antimicrobial for periodontitis treatment. Furthermore, antimicrobial properties of Lv and Mx-loaded solvent removal induced phase inversion Eudragit®L, zein and Nc-based ISMs for periodontitis treatment are investigated profoundly. Moreover, novel modified experiments are employed for studying morphology of ISM precipitates. Innovative UV-vis imaging techniques offer visual insights into matrix formation and solvent diffusion, complementing traditional experimentation. Furthermore, numerical simulations, guided by a mechanistic model, employ this model to estimates model parameters by minimizing the difference between model output and experimental data. The model is also utilized to predict the effect of drug release on various formulation design variables, contributing to our understanding of the mechanistic phase inversion of polymer-based solvent removal phase-inversion ISM.

CHAPTER 3

MATERIALS AND METHODS

EQUIPMENT AND INSTRUMENT

1. Anaerobic incubator (Forma Anaerobic System, Thermo Scientific, Ohio, USA)
2. Analytical balance (CP224S, Sartorius, Germany)
3. Analytical balance (PA4102, Ohaus, USA)
4. Desiccators (Biologix Research Company, USA)
5. Freeze dryer (FreeZone 2.5 liter plus benchtop freeze dry system, Labconco, Missouri, USA)
6. Glass slide
7. GNU Octave 6.4.0 for Windows-64
8. Goniometer (FTA 1000, First Ten Angstroms, USA)
9. High-speed camera (Photron, FASTCAM-APX RS, Chiyodaku, Japan)
10. Incubator (BPH-9042, Shenzhen Kingdak, China)
11. Inverted stereomicroscope (TE2000S, Nikon Instruments Inc., New York, USA)
12. Magnetic stirrer (C-MAG-HS7, IKA, Germany)
13. Microbiological safety cabinet class II (safe 2010, Holten, EU)
14. Micropipette 2-20 µl, 20-200 µl, 100-1000 µl and micropipette tip
15. Microplate reader (Victor Nivo, Perkin Elmer, USA)
16. Needle (18, 27 guage)
17. Petri dish glass (9 cm, 15cm) & petri dish plastic (15 cm)
18. pH meter (Seven compact, Mettler Toledo, Japan)
19. Plastic syringe (1 mL, 3 mL, 5 ml, 10 mL)
20. Pycnometer (Densito™ 30PX, Mettler Toledo, Japan) Brookfield rheometer (HADV-III U CP, Brookfield Engineering, USA)
21. Quartz cuvette
22. Scanning Electron Microscope, SEM (TESCAN MIRA3, Czech Republic)
23. Shaking incubator (NB-205, N-Biotek, Korea)
24. Stainless cylinder cup (6 mm)
25. Stereo-microscope (SZX10, Olympus corp., Japan)
26. Surgical blade & surgical scissors
27. Texture analyzer (TA.XT plus, Stable Micro Systems, UK)
28. UV-Visible spectrophotometer (Cary 60 UV-Vis G6860A, Agilent Technologies, Malaysia)
29. Viscometer cone-plate RM 100 CP2000 plus (Lamy Rheology Instruments Company, Champagne-au-Mont-d'Or, France).
30. Vortex mixer (KMC-1300V, Vision scientific, Korea)
31. X-ray tomographic microscopy beamline (BL1.2W: XTM) of the Siam Photon Source (SPS), Synchrotron Light Research Institute (SLRI), Nakhon Ratchasima, Thailand.)

MATERIALS

1. PYR (lot no. BCBP7338V, Fluka Analytical, Germany)
2. Agarose (lot H7014714, Vivantis, Malaysia)
3. *A. actinomycetemcomitans* ATCC 29522 (MicroBiologics Inc., USA)
4. Brain heart infusion (BHI) (lot no. 0270845, Bacto, USA)
5. Brain heart infusion agar (BHA) (lot no. 0298038, Bacto, USA)
6. *C. albicans* ATCC 17110, *C. krusei* TISTR 5259, *C. lusitaniae* TISTR 5156 and *C. tropicalis* TISTR 5306 (Department of Medical Sciences, Ministry of Public Health, Nonthaburi, Thailand)
7. Chocolate agar (Department of medical science, Ministry of public health, Thailand)
8. Dibasic potassium phosphate (Lot no. 0711005, Ajax Finechem, Australia)
9. DMSO (lot no. 1862992, Fisher Chemical, UK)
10. *E. coli* ATCC 8739, *E. coli* ATCC 25922 (Department of Medical Sciences, Ministry of Public Health, Nonthaburi, Thailand)
11. Ethanol, AR grade (lot no. 195125-1223, QReC, New Zealand)
12. Eudragit® L (lot no. B160503007, EVONIK Röhm GmbH, Germany)
13. Eudragit® S (lot no. B180705205, EVONIK Röhm GmbH, Germany)
14. Fully refined paraffin wax (lot no. 7119K18, Nippon Seiro, Japan)
15. GF (lot no BCBR2384V, Sigma, USA)
16. Lv (lot no L, Siam pharmaceutical Co., Thailand)
17. methicillin-resistant *S. aureus* (MRSA) ATCC 43300,
18. MP (lot no. 3625910107, Namsiang Co., Thailand)
19. Mx (lot no MN00000845, Siam pharmaceutical Co., Thailand)
20. NR (lot no. BCBP8959V, Sigma, USA)
21. Nc (lot. no. 200906/09018, Nitro chemical industry LTD, Thailand)
22. NMP (lot no. 144560-118, QReC, New Zealand)
23. *P. gingivalis* ATCC 33277 (MicroBiologics Inc., USA)
24. Potassium dihydrogen orthophosphate (lot no. E23W60, Ajax Finechem, Australia)
25. Sabouraud dextrose agar (SDA) (lot no. 7312647, Difco, USA)
26. Sabouraud dextrose broth (SDB) (lot no. 6345690, Difco, USA)
27. Sheep blood agar (Department of medical science, Ministry of public health, Thailand)
28. SF (lot no. SHBL6563, Sigma, USA)
29. Sodium hydroxide (lot no. AF310204, Ajax Finechem, Australia)
30. *S. aureus* ATCC 25923, *S. aureus* ATCC 6923 and *S. aureus* ATCC 6538 (Department of Medical Sciences, Ministry of Public Health, Nonthaburi, Thailand)
31. Tryptic soy agar (TSA) (lot no. 7341698, Difco, USA),
32. Tryptic soy broth (TSB) (lot no. 8091999, Difco, USA),
33. Zein (lot. no. 9010-66-6, Qingdao Sigma chemical Co., China)

Experimental set-up

3.1. The study of polymer-based ISM

3.1.1. Preparation of formulations

The decision to design these matrix-forming agents was well-considered, as their properties, including water-insolubility, compatibility, and safety, make them suitable candidates for serving as matrix-forming agents. Furthermore, their application in Lv and Mx-loaded ISMs for the treatment of periodontitis is innovative and unprecedented. ISMs comprising various concentrations of different polymeric matrix forming were fabricated, incorporating various concentrations of distinct polymeric matrix-forming agents, including Eudragit® L, Eudragit® S, zein, and Nc solutions ranging from 5% to 30% w/w, dissolved in a mixture of NMP, PYR, MP, DMSO, and GF. The preparation of these ISMs involved continuous mixing for 24 h using a magnetic stirrer (C-MAG-HS7, IKA, Germany) until achieving clear solutions. In the case of zein, the dissolution process was facilitated through heating at 95°C for a duration of 30 minutes. The composition of the formulations is detailed in Table 3.

Table 3. Composition of Eudragit®-based matrix formulations (A), composition of zein-based matrix formulations (B), composition of Nc-based matrix formulations (C).

Formula	Amount (% w/w)		
	L	S	MP
LM5	5	95	-
LM10	10	90	-
LM15	15	85	-
LM20	20	80	-
LM25	25	75	-
LM30	30	70	-
SM5	5	-	95
SM10	10	-	90
SM15	15	-	85
SM20	20	-	80
SM25	25	-	75
SM30	30	-	70

(A)

Formula	Amount (% w/w)				
	Zein	NMP	PYR	DMSO	GF
5ZN	5	95	-	-	-
10ZN	10	90	-	-	-
15ZN	15	85	-	-	-
20ZN	20	80	-	-	-
25ZN	25	75	-	-	-
30ZN	30	70	-	-	-
5ZP	5	-	95	-	-
10ZP	10	-	90	-	-
15ZP	15	-	85	-	-
20ZP	20	-	80	-	-
25ZP	25	-	75	-	-
30ZP	30	-	70	-	-
5ZD	5	-	-	95	-
10ZD	10	-	-	90	-
15ZD	15	-	-	85	-
20ZD	20	-	-	80	-
25ZD	25	-	-	75	-
30ZD	30	-	-	70	-
5ZG	5	-	-	-	95
10ZG	10	-	-	-	90
15ZG	15	-	-	-	85
20ZG	20	-	-	-	80
25ZG	25	-	-	-	75
30ZG	30	-	-	-	70

(B)

Table 3. Composition of Eudragit® L-based matrix formulations (A), composition of zein-based matrix formulations (B), composition of Nc-based matrix formulations (C) (continued).

Formula	Amount (% w/w)					
	Nc	NMP	PYR	DMSO	GF	
5NcN	5	95	-	-	-	
10NcN	10	90	-	-	-	
15NcN	15	85	-	-	-	
20NcN	20	80	-	-	-	
25NcN	25	75	-	-	-	
30NcN	30	70	-	-	-	
5NcP	5	-	95	-	-	
10NcP	10	-	90	-	-	
15NcP	15	-	85	-	-	
20NcP	20	-	80	-	-	
25NcP	25	-	75	-	-	
30NcP	30	-	70	-	-	**(C)**
5NcD	5	-	-	95	-	
10NcD	10	-	-	90	-	
15NcD	15	-	-	85	-	
20NcD	20	-	-	80	-	
25NcD	25	-	-	75	-	
30NcD	30	-	-	70	-	
5NcG	5	-	-	-	95	
10NcG	10	-	-	-	90	
15NcG	15	-	-	-	85	
20NcG	20	-	-	-	80	
25NcG	25	-	-	-	75	
30NcG	30	-	-	-	70	

Abbreviation: L= Eudragit® L; S = Eudragit® S; Z=Zein; Nc=Nitrocellulose; N=*N*-methyl-2-pyrrolidone (NMP); M= monopropylene glycol (MP); P= 2-pyrrolidone (PYR); D=Dimethyl sulfoxide (DMSO); G=Glycerol formal (GF).

3.1.2. Physicochemical characterization of ISM-solutions

3.1.2.1. Appearance of prepared formulation

The appearances of formulations, such as clarity, homogeneity, and precipitation, were observed by visual observation.

3.1.2.2. Apparent viscosity and rheological behavior

Viscosity measurements were conducted by recording viscosity values at various shear rates with an equilibration time of 15 seconds using a cone-plate viscometer (Lamy Rheology Instruments Company, Champagne-au-Mont-d'Or, France). This instrument was also employed to gather rheological data. The sample's shear stress was evaluated at different shear rates under room temperature conditions.

3.1.2.3. Contact angle

The contact angle can indicate the wettability or spreadability of a liquid on a given surface. In our study, contact angles of the formulated substance on glass slides covered with paraffin and agarose gel (0.6% agarose in PBS pH 6.8) were measured employing a goniometer (FTA 1000, First Ten Angstroms, USA) at a pump-out rate of 1.9 µL/s. The contact angle at a time point of 5 seconds was captured and assessed from the initial automated droplet image (n=3).

3.1.2.4. Injectability

An injectability test was conducted to assess the ease of injection. The compression mode of a texture analyzer (TA.XT plus, Stable Micro Systems, UK) was employed to determine the expelling force of the formulation from a 1 mL plastic syringe equipped with an 18-gauge needle. In this procedure, the upper probe of the instrument exerted a constant force of 0.1 N at a speed of 1.0 mm/s until the base of the syringe barrel was reached. The maximum expelling force, which measures the force required for injecting the sample fluid from the syringe through the needle, was recorded. Additionally, the energy expended for expelling was calculated based on the force-displacement profiles.

3.1.3. Characterization of matrix forming behavior

3.1.3.1. Matrix formation after injection

A 1 mL aliquot of the ISM formulation was injected directly through an 18-gauge stainless needle into 5 mL of PBS (pH 6.8) in a glass test tube to investigate matrix formation over time. Photographs were taken at various time points (0, 1, 5, 10, 20, and 30 minutes) to document the progression of matrix formation.

3.1.3.2. Morphology of matrix formation in an artificial crevicular pocket

A 0.6% agarose solution, prepared by dissolving in PBS (pH 6.8), was poured onto petri dishes to create agarose gel with a height of 1 cm. Following gel setting, a cylindrical cup was used to create a 300 µL hole (diameter of 7 mm) at the center of the petri dish. This agarose gel serves as an artificial representation of a crevicular pocket in a human (165). A 150 µL aliquot of the ISM formulation was introduced into the cylindrical hole or well within the aforementioned agarose gel. Upon contact with the aqueous phase from the agarose gel, the formulation induced solvent removal, leading to a transformation into an opaque solid-like matrix via a phase inversion mechanism. The process of matrix formation was captured through photography using a stereomicroscope (SZX10, Olympus corp., Japan) at intervals of 1, 3, 5, 10, 15, 20, and 30 minutes. The determination

of matrix formation was facilitated using the SZX10 Series software under a stereoscope. Furthermore, the interaction at the interface between the formulation and the agarose gel was observed to investigate phase transition. A 2 mm thick agarose gel was created by pouring it onto a glass slide using the same method as described earlier. This gel was subsequently cut with a smooth edge situated 2 cm away from one edge of the glass slide. Placed in proximity to a 20 µL sample, near the incision's edge, this gel was exposed to the formulations in PBS. Morphological alterations due to phase inversion at the interface were captured using an inverted stereomicroscope (SZX10, Olympus Corp., Japan) at various time intervals.

3.1.3.3. Interfacial interaction of ISM formulations and aqueous

To explore the phase transition occurring at the interface between the formulation and the agarose gel, an investigation was conducted. A 0.6% agarose gel was meticulously prepared by dissolving it in PBS (pH 6.8). To monitor the diffusion of both the aqueous and solvent components during the phase transformation process, fluorescent dyes such as sodium fluorescein (150 µg/ml) were introduced into the agarose gel. This gel was subsequently poured onto a glass slide, forming a 2 mm thick layer. To facilitate the observation of the phase transition, the gel was then cut along a straight edge, positioned 2 cm away from one edge of the glass slide. Adjacent to the incision's edge, a 20 µL sample solution was placed in proximity to the agarose gel. Upon exposing the formulations to PBS within the agarose gel, any morphological changes stemming from phase inversion at the interface were captured through photography. These images were captured using an inverted microscope (TE2000S, Nikon Instruments Inc., New York, USA) at various time intervals. The migration of fluorescence color, indicative of the aqueous phase, was documented in a time-lapse manner using the same inverted microscope at a 10x magnification. This enabled the visualization and tracking of the dynamic movement of the fluorescent components during the phase transition process.

To gain a deeper understanding of the interface mentioned above during phase inversion, an examination of the diffusion behavior of fluorescent dyes was conducted. Furthermore, the interfacial interaction of SF (150 µg/ml) and NR (100 µg/ml)-loaded ISM solutions with agarose gel, as well as sodium fluorescein-loaded agarose gel, was also evaluated using the previously described methodology.

3.1.3.4. Mechanical properties

The mechanical properties of the resulting matrix following complete solvent exchange were assessed using the same instrument. Similarly, the preparation of the agarose gel and the use of a cylindrical cup were conducted following the procedure outlined above in section 3.1.3.2. Morphology of matrix formation in an artificial crevicular pocket. A 150 μL aliquot of the sample was deposited into the prepared agarose hole and left for a period of 3 days to ensure full phase inversion and matrix formation. Using a stainless spherical probe with a diameter of 5 mm, integrated with the texture analyzer (TA.XT plus, Stable Micro Systems, UK), gradual penetration was carried out into the obtained matrix at a consistent speed of 0.5 mm/s. Upon achieving a penetration depth of 1.5 mm, the probe was held stationary for a duration of 60 seconds and then subsequently retracted at a speed of 10 mm/s. The force measured at the maximum probe penetration into the sample was denoted as the maximum deformation force (also referred to as "hardness"), and the probe's upward movement between the sample's surface and the probe was recorded as the adhesion force (166). All formulations underwent this analysis in triplicate, and the tests were conducted under room temperature conditions.

3.1.3.5. Antimicrobial activities

The standard strains used in this experiment are *S. aureus* ATCC 25923, *S. aureus* ATCC 6923, methicillin-resistant *S. aureus* (MRSA) ATCC 43300, *E. coli* ATCC 8739, *C. albicans* ATCC 17110, *A. actinomycetemcomitans* ATCC 29522 and *P. gingivalis* ATCC 33277. In the context of periodontitis, *P. gingivalis* is one of the microorganisms frequently found. The antimicrobial activities of the ISM formulation are undertaken using the cylinder plate method. This technique is based on the diffusion of the formulation from a stainless-steel cylinder cup (inside diameter of 6 mm and height of 10 mm) through agar gel inoculated with the test microorganism. The bacterial and fungal inocula approximately closed to the 0.5 McFarland turbidity standard are spread on TSA and SDA, respectively. A 100 μL aliquot of each formulation is dropped into the cylinder cap, which is placed on the surface of an inoculated medium plate. For *P. gingivalis* and *A. actinomycetemcomitans*, the bacterial inocula approximately closed to the 0.5 McFarland turbidity standard are spread on sheep blood agar and chocolate agar, respectively. The test is undertaken in an anaerobic incubator (Forma Anaerobic System, Thermo Scientific, Ohio, USA). After incubation at 37 °C for 18 h, the diameter of inhibition zone against the tested organism is measured using a vernier caliper (n=3).

3.1.4. Characterization of dried ISM

3.1.4.1. Preparation of dried ISM

The ISM formulations are prepared by mixing continuously for 24 h with a magnetic stirrer until clear solutions are obtained. The excess water is adding into each formulation for phase inversion and causing opaque solid-like matrix. Then the matrix is washed several times with distilled water. The ISM systems are dried using a freeze dryer (FreeZone 2.5 liter plus benchtop freeze dry system, Labconco, Missouri, USA) and kept them in a desiccator for one week to avoid the melting and collapse of their structures.

3.1.4.2. Topography by scanning electron microscope (SEM)

The dried ISMs are coated with gold before being examined by field-emission SEM (TESCAN MIRA3, Czech Republic) at an accelerating voltage of 15 kV.

3.2. Study of drug-loaded ISM

The determination of the dosage for Lv and Mx added to the formulation is not primarily contingent on their inhibition zones but is grounded in well-established conventions within the field. Prior to selecting the drug concentrations of 0.5% or 1% for Lv and 0.5% for Mx in ISMs, an exhaustive literature review was conducted to ensure alignment with prevailing practices. These concentrations have garnered widespread usage, notably the 0.5% concentration for Mx in ophthalmic ISMs (48). Furthermore, these concentrations fall within the effective range of the minimum inhibitory concentration (MIC) for the relevant pathogens (167-169). While higher concentrations were explored, they proved to be insoluble or unsuitable in some instances, rendering the selected percentages the most suitable for our intended purposes.

3.2.1. Preparation of drug-loaded formulations

The addition of Lv was carried out at a concentration of 1 % w/w into the selected zein and Eudragit® L formulations. Similarly, a concentration of 0.5% w/w Mx was added into Nc formulations. The preparation of these formulations followed the same methodology as described earlier. The control formulations encompassed 1% w/w Lv dissolved in MP, DMSO, and GF, as well as 0.5% w/w Mx dissolved in NMP, PYR, DMSO, and GF. The composition of these formulations is detailed in Table 4.

Table 4. Composition of Lv-loaded Eudragit® L-based matrix formulations (A). Composition of Lv-loaded zein-based matrix formulations (B), Composition of Mx-loaded Nc-based matrix formulations (C).

(A)

Formula	Amount (% w/w)		
	Lv	L	MP
LLM10	0.5	10	89.5
LLM15	0.5	15	84.5
LLM20	0.5	20	79.5
LVM	0.5	-	99.5

(B)

Formula	Amount (% w/w)			
	Lv	Zein	DMSO	Glycerol formal (GF)
LvG	1	-	99	-
LvD	1	-	99	-
Lv20ZD	1	20	79	-
Lv25ZD	1	25	74	-
Lv20ZG	1	20	-	79
Lv25ZG	1	25	-	74

(C)

Formula	Amount (% w/w)					
	Mx	Nc	NMP	PYR	DMSO	GF
0.5MxN	0.5	-	99.5	-	-	-
0.5MxPy	0.5	-	-	99.5	-	-
0.5MxGf	0.5	-	-	-	99.5	-
0.5MxD	0.5	-	-	-	-	99.5
0.5Mx15NcN	0.5	15	84.5	-	-	-
0.5Mx15NcPy	0.5	15	-	84.5	-	-
0.5Mx15NcGf	0.5	15	-	-	84.5	-
0.5Mx15NcD	0.5	15	-	-	-	84.5

Abbreviation: L= Eudragit® L; Z=Zein; Nc=Nc; *N*=*N*-methyl-2-pyrrolidone (NMP); M= monopropylene glycol (MP); P= 2-pyrrolidone (PYR); D=Dimethyl sulfoxide (DMSO); Gf=Glycerol formal (GF); Lv= levofloxacin HCl; Mx=moxifloxacin HCl.

3.2.2. Physicochemical characterization of drug-loaded ISM-solutions

Physicochemical properties of these formulations are evaluated using the same method as mentioned above (topic number 3.1.2.1 - 3.1.2.4) for their appearance, viscosity, rheological behavior, contact angles, surface tension, injectability and mechanical properties.

3.2.3. Characterization of drug-loaded matrix forming behavior

The matrix-forming behavior of these formulations are evaluated using the same method as mentioned above (3.1.3.1. Matrix formation after injection-3.1.3.4. Mechanical properties) for their matrix formation after injection, interfacial interaction and morphology of matrix formation in an artificial crevicular pocket.

3.2.4. Efficiency of drug-loaded ISM

3.2.4.1. *In vitro* drug release

3.2.4.1.1. Calibration curve of drugs

Standard stock solutions were meticulously prepared by precisely weighing the drugs and subsequently dissolving them in phosphate buffer (pH 6.8). These stock solutions were then diluted to encompass various concentrations that spanned the range relevant to the drug release samples. To establish the optimal concentration range for UV detection, a plot was generated by correlating concentration against absorbance/mAU. This was executed using a UV-visible spectrophotometer (Cary 60 UV-Vis, Model G6860A, Agilent, Malaysia). The resulting plot yielded an r² value between 0.9990 and 1.000, facilitating the identification of the suitable concentration range for UV detection.

The drug release amount is analyzed using UV-vis spectroscopy. For the test that using UV-spectrophotometer, samples were examined at wavelengths of 287 nm and 288 nm, for Lv and Mx, respectively. The eluent was detected using a UV-detector at the specific wavelength for each drug (n = 3). The detected values were then converted into drug quantities using standard drug curves. The cumulative mean drug release, along with its standard deviation (S.D.), was calculated as a percentage (n = 3). This comprehensive analysis allowed for the quantification and representation of the drug release behavior.

3.2.4.1.2. Drug release test with membrane-less method

The drug release was subjected to testing and subsequently compared with a control formulation where the antimicrobial drug was dissolved in a solvent. This comparison aimed to evaluate the drug-entrapped properties of the matrix-forming agent. For this evaluation, a cylindrical porcelain cup with dimensions of 1 cm in diameter and 1.2 cm in height was utilized. Each cup was filled with 0.4 g of the formulation. Subsequently, these cups were immersed in 50 mL of PBS (pH 6.8) at a temperature of 37°C. The rotational shaker was set to operate at a speed of 50 rpm, simulating the drug release behavior that would occur from a crevicular pocket. The release medium was sampled (5 mL) and replaced with 5 mL of fresh PBS. The concentration of drug release was determined with a UV-Visible spectrophotometer (Cary 60

UV-Vis, Model G6860A, Agilent, Malaysia). The cumulative percentage of drug release was calculated from the standard calibration curve (3.2.4.1.1. Calibration curve of drugs)

3.2.4.1.3. Analysis of drug release data

The release data are analyzed by DDSolver (170) was a menu-driven add-in program for Microsoft Excel written in Visual Basic for Applications. DDSolver was used to analyze the data of *in vitro* drug release. Different mathematical release equations were used to fit the cumulative percentage of drug release profiles in the range of 10%-80%. The data were fit with zero-order, first-order, Higuchi, Korsmeyer-Peppas, Hixson-Crowell, Hopfenberg, and Peppas-Sahlin's equations and the coefficient of determination (r^2) was measured. Goodness-of-fit was also evaluated using the model selection criterion (MSC) as shown in following equation.

$$MSC = \ln \left\{ \frac{\sum_{i=1}^{n} w_i \cdot \left(y_{i_{obs}} - \bar{y}_{obs}\right)^2}{\sum_{i=1}^{n} w_i \cdot \left(y_{i_{obs}} - y_{i_{pre}}\right)^2} \right\} - \frac{2p}{n}$$

where w_i is the weighting factor, which is usually equal to 1 for fitting dissolution data, $y_{i_{obs}}$ is the ith observed y value, $y_{i_{pre}}$ is the *i*th predicted y value, $\bar{y}_{osb}$ is the mean of all observed y-data points, p is the number of parameters in the model, and n is the number of data points.

3.2.4.2. Antimicrobial activities

The test was conducted according to the antimicrobial activity determination as mentioned above (3.1.3.5. Antimicrobial activities).

3.2.5. Characterization of drug-loaded ISM precipitates

The methodologies for characterizing drug-loaded ISMs have been outlined. These methodologies hold significant importance within the context of this research.

3.2.5.1. Time lapse morphology by SEM

The observations gleaned from this technique contribute to the refinement of ISM formulations to ensure their structural integrity and drug release characteristics endure throughout their intended applications. In order to observe the systems' morphology following the drug release test, the dried-ISM were prepared using a freeze dryer (FreeZone 2.5 liter plus benchtop freeze dry system, Labconco, Missouri, USA) and kept them in a desiccator for one week to avoid the melting and collapse of their structures. Determination of topography was undertaken by scanning electron microscopy (SEM) according to the above mentioned (3.1.4.2. Topography by scanning electron microscope (SEM)).

3.2.5.2. X-ray imaging and X-ray tomographic microscopy

The dried-ISMs were prepared utilizing a freeze dryer (FreeZone 2.5 liter plus benchtop freeze dry system, Labconco, Missouri, USA). Subsequently, they were placed within a desiccator for a period of one week. This step was taken to prevent any potential melting or collapse of their structures. The prepared dried-ISMs were investigated at the X-ray tomographic microscopy (XTM) beamline, Synchrotron Light Research Institute (SLRI), NakhonRatchasima, Thailand. Synchrotron radiation X-rays were generated through a 2.2-T multipole wiggler at the Siam Photon Source, operating at 1.2 GV with a current of 150 mA. All SRXTM experiments were conducted utilizing a filtered polychromatic X-ray beam, operating at a mean energy of 12.5 kV. The distance from the source to the sample was maintained at 34 m. The X-ray projections of the samples were acquired via a detection system comprising a 200 µm thick YAG:Ce scintillator (Crytur, Czech Republic), a lens-coupled X-ray microscope (Optique Peter, France), and an sCMOS camera (pco. edge 5.5, 2560×2160 pixels, 16 bits). This setup enabled the precise acquisition of X-ray projections for the subsequent analysis. The tomographic scans were obtained with an isotropic voxel size of 0.72 µm. Subsequent to data acquisition, the X-ray projections underwent normalization through the application of a flat-field correction algorithm. The reconstructed tomographic data was then processed utilizing the Octopus reconstruction software. The 3D representation of the tomographic volumes of the composite films, along with the subsequent segmentation analysis, was conducted using the Drishti software (171). This approach facilitated the generation of comprehensive insights from the acquired tomographic data.

3.2.5.3. *In vitro* degradability study

The *in vitro* degradability study assumes a pivotal role in the evaluation of ISM transformation during drug release. Samples were collected after the release studies and these ISM remnants were dried in a hot air oven with temperature adjusted to 65 °C. After that, the sample was weighted on analytical balance (CP224S, Sartorius, Germany) for recording the remained weight. The percentage of weight loss of each time point was calculated as follows in equation:

$$\% \text{ weight loss} = \frac{\text{Initial weight } (g) - \text{weight in each time } (g)}{\text{initial weight } (g)} \times 100$$

3.3. UV-Vis imaging

Agarose gel (0.6%, w/v) was prepared by dissolving 0.6 percent agarose in PBS (pH 6.8) and poured to a demountable cuvette quartz cell ($10.0 \times 40.0 \times 0.2$ mm^3 (W $\times$ L $\times$ H)) (Starna Scientific Ltd., Hainault, Essex, UK) and this cell was closed. After waiting for 2 h at room temperature for gelation, gel was cut into a direct smooth edge (17 mm away from one edge of the cuvette cell) and removed it. PBS was replaced into the void from removed gel and the cell was closed. The cuvette cell with PBS as reference solution was placed on the cartridge above CMOS chip of D200 ActiPix UV-vis imaging Systems (Paraytec Ltd, York House, York, UK). The light source

was provided by a pulsed Xenon lamp and LEDs lamp, equipped with a band-pass filter for wavelengths of 214 nm, 280 nm, and 525 nm. After calibration and setting the reference with PBS, a sample was replaced the previous PBS and the quartz cell was returned to the cartridge. Moreover, to observe the effect of drug concentration, 0.1% (w/w) Lv was incorporated into the zein solutions in both solvents. The data was recorded, and the signal was transferred to absorbance map by Actipix D200 Acquisition program (Paraytec Ltd, York House, York, UK). The images were taken with 3 frames per minute (file subsample=50) for 12 h in the darkness chamber. Images captured were analyzed and interpreted in intensity mode via the SDI Data Analysis software (version 2.0., Paraytec Ltd, York House, York, UK) and displayed in representative absorbance maps with different colors in each area.
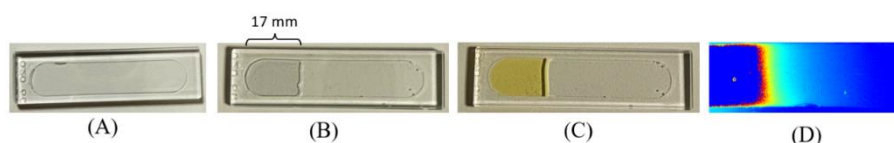
Figure 12. Schematic representation of the demountable cuvette quartz cell setup for UV-vis imaging: (A) Demountable cuvette quartz cell filled with 0.6% agarose gel, (B) Gel removed and replaced with PBS and sample, (C) Sample in contact with agarose gel inside the cuvette, (D) Absorbance map of recorded images analyzed using SDI Data Analysis software.

3.4. Statistical analysis

Statistical analysis of the data was undertaken using the "Statistical Package for Social Sciences" (SPSS 4.0.1., SPSS Inc. Ltd., UK). The statistical significance for the measurement is examined and considered at $p < 0.05$ and 0.01 using one-way analysis of variance (ANOVA) followed by an LSD post-hoc test.

3.5. Numerical methods

This section emphasized the significance of gaining a deep understanding of the drug release mechanisms within zein-based ISMs when dissolved in DMSO and GF. To address this, a numerical simulation, relying on a mathematical model and experimental data, was employed to predict the drug release patterns. This simulation involved discretizing the derivative using a finite differences method, particularly referencing the forward difference formula of order $O(h)$ and the central difference formula of order $O(h^4)$, as discussed in the relevant section. The numerical method was implemented using Octave software (GNU Octave software version 8.2.0 (2023)) (172). To facilitate the simulations, a comprehensive list of model parameters and their corresponding values were provided. These parameter values were derived from solving the ordinary differential equations inherent in the model simulations, with parameters falling within predefined ranges. Additionally, supplementary parameters linked to drug release from the ISM were estimated based on the mechanistic model. This approach enabled a thorough exploration of drug release behavior from zein-based ISMs, shedding light on their underlying mechanisms and serving as a valuable tool for modeling and simulation, incorporating experimental data.

CHAPTER 4

RESULTS AND DISCUSSION

Eudragit® L ISM for periodontitis treatment using MP as a solvent

4.1. Drug-free Eudragit®-based ISM

4.1.1. Physical appearance, viscosity and rheology, injectability, contact angle, and mechanical properties

Investigating the physical attributes of drug-free ISM formulations, it is evident that the clear solutions were attained after varying in L and S concentrations, except for SM20 and SM25, as demonstrated in Figure 13A and Figure 13B. The turbidity observed in SM20 and SM25 suggested a solubility constraint for Eudragit® S in MP, particularly at concentrations exceeding 15%. Furthermore, highly concentrated Eudragit® L solutions exhibited a subtle yellowish color. The viscosity values for LM5, LM10, LM15, LM20, SM5, and SM10 formulations were recorded as 183.54 ± 2.00 cP, 820.02 ± 31.36 cP, 5292.68 ± 222.78 cP, 26214.29 ± 874.33 cP, 171.24 ± 3.16 cP, and 1884.15 ± 134.47 cP, respectively. The augmentation of Eudragit® concentration resulted in elevated apparent viscosity within the ISM formulations (depicted in Figure 14A). Notably, Eudragit® L ISM exhibited significantly lower viscosity compared to Eudragit® S ISM ($p < 0.05$). Eudragit® S formulations featuring polymer concentrations beyond 10% were excluded from viscosity measurement due to excessive viscosity, rendering accurate measurement unfeasible. Considering the predominant influence of substance-solvent interaction over substance-substance interaction, an effective medium for solute solubilization should effectively mitigate mixture viscosity (173).

Examining the rheological characteristics of the formulated ISM, Figure 14B presents a visual representation. For the majority of formulations, a linear relationship between shear stress and shear rate was observed, suggesting a Newtonian flow behavior. This observation corroborates earlier studies on the Newtonian behavior of Eudragit® RS-based ISM, thus reaffirming the Newtonian properties of the ISM, as evidenced by these findings (174). The enhanced formation of a 3D network within Eudragit® molecules can lead to a substantial increase in the viscosity of these formulations (175, 176). Nevertheless, the SM10 curve exhibited a decrease in shear stress value, indicating a pseudoplastic flow behavior. Alterations in the number of molecular entanglements can influence the rheology and structural characteristics of polymer systems with entangled configurations (177). The suitability of their Newtonian and pseudoplastic flow properties for injectable dosage forms is noteworthy. This is because the fluid can be injected through a needle after applying a compression force to the syringe plunger, allowing a physician or dentist to expel the

fluid through the stainless steel needle (176). An Eudragit® L solution dissolved in MP displayed lower viscosity and adhered to Newtonian flow characteristics. This renders such solutions more suitable for injection administration compared to Eudragit® S solutions.

The administration of ISM should be straightforward and devoid of discomfort when employing the suitable needle and syringe. Localized ISMs intended for periodontitis treatment are specifically devised for delivery into periodontal pockets through injections. Therefore, the formulated fluid should be easily expelled from the needle, minimizing patient discomfort during the process (176). Therefore, it becomes imperative to assess injectability, which pertains to the force necessary to expel the product through the needle. The maximum force for injectability was determined for M, LM5, LM10, LM15, LM20, LM25, SM5, SM10, and SM15 formulations, yielding values of 1.02 ± 0.04 N, 1.24 ± 0.07 N, 1.79 ± 0.05 N, 2.33 ± 0.02 N, 10.66 ± 0.30 N, 30.87 ± 1.68 N, 0.94 ± 0.02 N, 1.71 ± 0.01 N, and 27.74 ± 1.04 N, respectively. The low values of force and work of expulsion indicate the ease of injectability. Figure 14C illustrates the force and work derived from the injectability assessment of the test solutions. These values exhibited an increase with Eudragit® concentration, in accordance with their apparent viscosity as explained earlier. The work of expulsion for SM10 and SM15 formulations were 20.22 ± 0.55 mJ and 305.05 ± 24.98 mJ, respectively.

Significant discrepancies were evident in formulations comprising over 10% of these polymers, particularly for Eudragit® S solution. This indicates that higher force and energy were needed to expel the formulation from the needle, resulting in conspicuous high-force values. These outcomes underscore the substantial influence of the type and concentration of Eudragit® on the requisite injection force and energy. Nevertheless, the results underscored that the majority of ISM formulations demanded a relatively low injection force, typically under 50 N. In practical terms, the cumulative expulsive work needed to inject each solution remained below 50 N·mm, suggesting compliance with the injection criterion (49, 178). The addition of peppermint oil and polyethylene glycol (PEG) 1500 improved the injection performance of both drug-free and DH-loaded Eudragit® RS-based ISM formulations (179, 180). In comparison, the hydrophobic nature of peppermint oil resulted in easier injection compared to PEG 1500 as additives in the context of ISM formulations (179, 180). The lubricating effect of incorporating oil on the injection ease of *in situ* forming systems has been previously mentioned (181, 182). For instance, the force and work of injectability of the rosin-based ISM formulations demonstrated a notable reduction after the incorporation of lime peel oil. This reduction can be attributed to the lubricating nature of the oil (183). However, the ease of injection of Eudragit® L was primarily correlated with its lower viscosity. The configuration of polymeric molecules in solutions varies based on their affinity with the solvents used, leading to different chain configurations (184).

The contact angle can indicate the wettability or spreadability of a liquid on a given surface. MP exhibited the lowest contact angle on the glass slide (5.08 ± 1.05 degrees), as depicted in Figure 14D. The contact angles on the glass slide for LM5, LM10, and LM15 were 21.46 ± 0.75 degrees, 34.70 ± 0.10 degrees, and 46.27 ± 0.72 degrees, respectively. The increase in contact angle on the three surfaces was observed with the polymer concentration dependence of Eudragit® solutions, attributed to the higher viscosity that hinders the spreadability of sample droplets on these surfaces (174). The agarose model, designed to mimic the periodontal environment, was utilized to replicate the periodontal pocket. This model facilitated the continuous provision of a small amount of simulated saliva fluid. Importantly, it was observed that the selection of the release medium, whether water, phosphate buffer, or horse serum, did not significantly impact phase separation, water uptake rates, or the matrix's morphology (185). In this model, PBS was employed instead of saliva fluid in order to minimize the number of variables.

The surface of an agarose gel, composed of PBS at pH 6.8, was fabricated to simulate environment similar to that found within the periodontal pocket. Especially, the contact angle of Eudragit®-based ISMs was significantly elevated in comparison to the contact angle of the solvent upon this agarose surface. For instance, in the case of LM10, the contact angle was recorded as 36.97 ± 0.22 degrees, for LM15 it was 50.98 ± 0.58 degrees, and for LM20 it was 67.98 ± 3.18 degrees. This increase in contact angle was particularly conspicuous when compared to the contact angle on a glass slide. This phenomenon signifies an *in-situ* transformation from a solution state to a gel or solid-like Eudragit® matrix. This transformation is prompted by a solvent exchange mechanism between the MP present in the formulation and the aqueous solution within the prepared agarose gels (181-183). The spreadability of the formulations was reduced due to the formation of Eudragit® matrices through solvent exchange (14). The high viscosity of SM10 might impede solvent removal, and its contact angle on the agarose gel was smaller than on the glass slide. Despite having a contact angle greater than 90 degrees, their values were still less than 90 degrees, which signifies satisfactory wettability on the test surfaces (186, 187).

Generally, the resulting ISM matrix, following solvent removal, is expected to effectively fit within the periodontal pocket, withstand the movement of the jaw, and maintain its structural integrity (188, 189). Figure 14E and Figure 14F illustrate the mechanical attributes, showcased as hardness and the "F remaining/F max deformation" ratio. This ratio serves as an assessment of the specimen's elasticity versus plasticity. A heightened value signifies pronounced elasticity, whereas a diminished value implies augmented plasticity (190). These mechanical properties, particularly the adhesive characteristics of the transformed Eudragit® ISM matrices, were assessed to ascertain the potential for preventing undesired displacement of this dosage form from the periodontal pocket (187, 191).

The incorporation of Eudragits® led to an increase in the hardness of the resulting matrix (LM10: 3.15 ± 0.08 N, LM15: 4.03 ± 0.19 N, LM20: 7.70 ± 0.45 N)

due to the higher polymer mass present in the matrix. In comparison, the hardness and the ratio of remaining force (F remaining) to maximum deformation (F max deformation) of Eudragit® L-based ISMs were significantly higher than those of Eudragit® S-based ISMs at the same concentration ($p < 0.05$). The ratio value of the matrix was conspicuously below one, indicating a behavior close to plastic deformation. This signifies that the system's structure was relatively unchanging during the holding time, which could be advantageous in terms of adapting to dynamic changes in the size and shape of the periodontal pocket over time (190). This finding aligns with the observations made in a previously reported matrix from bleached shellac-based ISMs. That matrix also exhibited characteristics indicative of plastic deformation, suggesting its ability to adapt its geometry to dynamic changes (189). All Eudragit®-based ISMs exhibited adhesive strength properties when subjected to the texture analyzer probe. Furthermore, all the matrices obtained during the experiment remained securely attached to the agarose basement throughout the texture analyzer probe pullback.
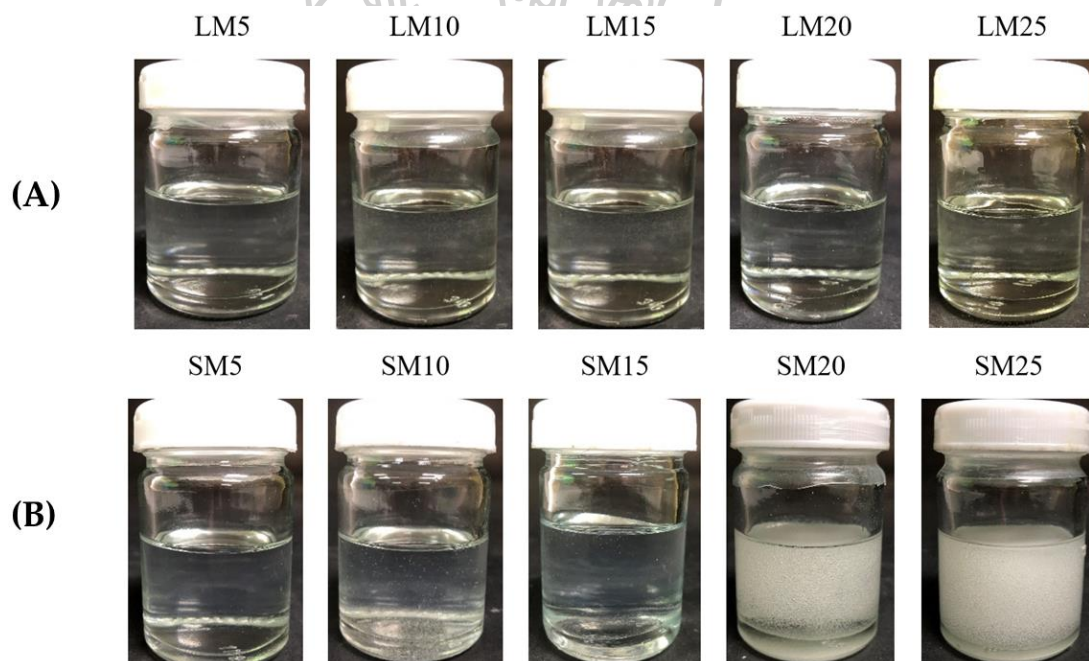
Figure 13. Visual characteristics of ISMs based on Eudragit® L (A) and Eudragit® S (B) with varying polymer concentrations.
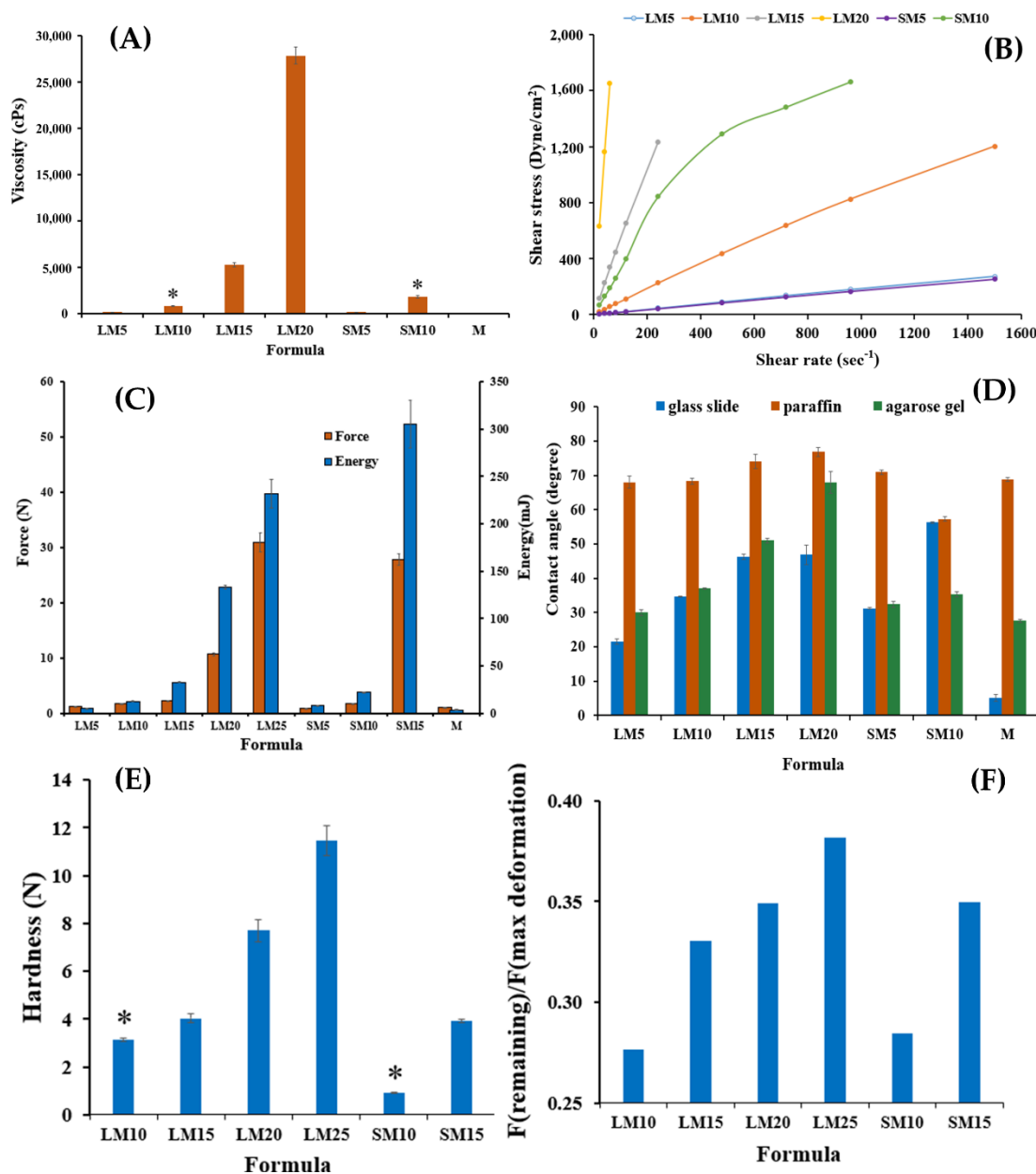
Figure 14. Viscosity (A); the correlation between shear stress and shear rates (B); injection force and energy derived from the injectability test (C); contact angle measurements on distinct surfaces (D); as well as hardness (E) and adhesiveness (F) attributes determined through mechanical testing of Eudragit® L and Eudragit® S-based ISM formulations at 25 °C. The presented data are reflective of triplicate measurements. The asterisk (*) denotes statistically significant disparities ($p < 0.05$).

4.1.2. Matrix formation of Eudragit®-based ISMs

The process of phase transformation for all selected clear Eudragit®-based solutions, transitioning from a gel-like state to an opaque matrix-like state over time, is illustrated in Figure 15A and Figure 15C. The presence of higher concentrations of these polymers led to the formation of a cloudier matrix due to the phase separation of Eudragit®. Notably, formulations LM25 and SM15 encountered greater challenges in terms of injection through the needle and were more prone to sticking within the needles. This can be attributed to their higher viscosity. Consequently, they underwent a swift transition into an opaque matrix state, settling at the base of the PBS in the glass tube. As the formulation came into contact with PBS at pH 6.8, a gradual solvent removal process occurred. Initially, the outer layer transformed into an opaque skin, while the inner matrix phase continued its evolution into an opaque solid polymeric matrix over time (176). Consequently, a higher inclusion of matrix-forming agents expedited the phase transformation of ISMs. In contrast, ISMs containing EC, bleached shellac, and Eudragit® RS in quantities less than 10%, 20%, and 30% w/w, respectively, did not exhibit complete matrix formation. This is attributed to the insufficient polymeric mass present in these formulations, hindering the continuous process of matrix formation (21, 192-194). Figure 15B and Figure 15D depict a cross-sectional view of the matrix formation process observed under a stereoscope using an agarose well as a simulation of the periodontal pocket. As a result of the phase separation of Eudragit®, an opaque layer formed at the periphery of the agarose gel, gradually extending inward into the formulation. In the cases of LM15 and SM10, the matrix formation proceeded slowly due to their dense matrix, which potentially acted as a barrier and hindered solvent exchange. At the interface, a compact network of Eudragit® matrices developed, and this process decelerated over time. This decrease in rate was attributed to the high tortuosity and low porosity of the earlier matrix, which impeded the diffusion of solvent and water (145). However, the elevated polymer content within LM20, LM25, and SM15 formulations exhibited a favorable influence on the growth of the Eudragit® matrix. The process underlying Eudragit® matrix formation can be comprehended as a solvent removal mechanism. In this context, the phase separation of dissolved Eudragit® was distinctly observed, leading to the development of an insoluble solid matrix (194). Due to their lower viscosity, ease of injection, and intriguing matrix formation characteristics, Eudragit® L-based formulations containing 10%, 15%, and 20% were chosen. These selected formulations were intended for loading Lv and for subsequent investigation as ISMs within a periodontal pocket delivery system.
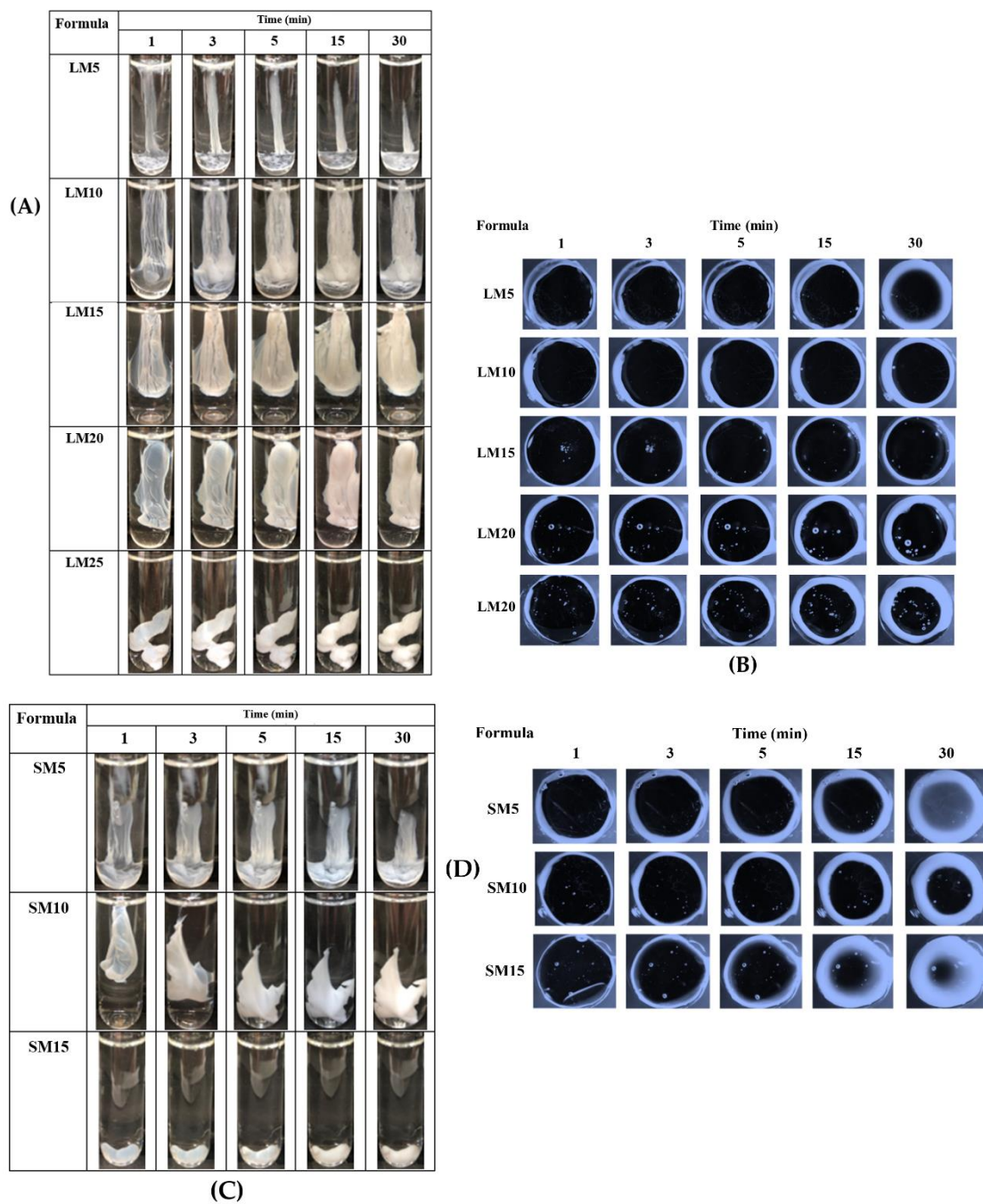
Figure 15. Matrix formation upon injection into PBS (A) and agarose well (B) for Eudragit® L-based ISM formulations, and matrix formation upon injection into PBS (C) and agarose well (D) for Eudragit® S-based ISM formulations.

4.2. Lv-loaded Eudragit®-based ISM

4.2.1. Physical appearance, viscosity and rheology, injectability, contact angle, and mechanical properties

The formulations based on 10%, 15%, and 20% Eudragit® L were successfully prepared. The resulting solutions exhibited a slight yellowish tint, as illustrated in Figure 16. The introduction of the drug led to a decrease in viscosity; however, higher concentrations of Eudragit® L led to an increase in viscosity (depicted in Figure 17A). The presence of the hydrophilic drug compound could hinder the uncoiling of Eudragit® molecules, leading to a reduction in overall viscosity. Figure 17B shows that all formulations exhibited a Newtonian flow pattern. Notably, the viscosity of LLM15 was measured at 3674.54 ± 188.03 cPs, maintaining its Newtonian flow behavior. This flow characteristic is deemed suitable for injectable dosage forms and remains acceptable post-injection (176). The force and work required for injection increased proportionally with higher concentrations of Eudragit® L, as illustrated in Figure 17C. For instance, the force needed to inject LLM15 was measured at 21.08 ± 1.38 mj. The trend in contact angle values closely resembled that of the drug-free Eudragit®-based ISM formulations. This indicated that the elevated viscosity of the systems resulting from the addition of Eudragit® L led to higher contact angle values by hindering the spreadability of the droplet. Similar observations of higher contact angles for solutions containing substances like lauric acid and borneol dissolved in DMSO have been previously reported, and this phenomenon is attributed to their increased concentration and viscosity (174, 195). The rise in contact angle observed on the agarose gel surface can be attributed to the transformation of Eudragit® L into a semi-solid state. This phase-inversion is subsequently followed by a solvent removal process that results in reduced droplet spreading (196). The contact angle values of these ISMs were all below 90 degrees, indicating their good wettability on the test surfaces (187). In practical terms, spreadability is crucial to ensure adequate adhesiveness, which in turn prevents the undesired dislodgment of the transformed ISM from the periodontal pocket (187, 191).

LLM10   LLM15   LLM20
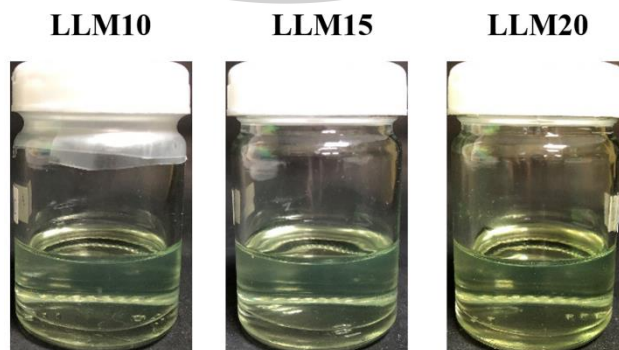
Figure 16. Physical appearance of Lv-loaded Eudragit® L-based ISMs comprising different concentrations of polymer

Investigating the mechanical characteristics of Eudragit® L-based drug-loaded ISMs (Figure 17E and Figure 17F), it is observed that elevating the concentration of Eudragit® L leads to increased hardness in the resulting drug-loaded matrix. Furthermore, the ratio of F remaining/F max deformation was below one, indicating behavior akin to plastic deformation. This mechanical response suggests the ability of these formulations to adapt their geometry within the periodontal pocket, as previously discussed (190). The hardness of the resulting LLM15 matrix measured 3.38 ± 0.23 N. Noticeably, some studies have indicated that the inclusion of volatile oils can enhance the adhesion of rosin ISGs (197). The rosin ISG containing 10% cinnamon oil displayed stronger adhesion properties compared to the formulation with 10% lime peel oil added. However, formulations without the oil additives showed similar adhesion values (183). Thus, the nature of the additive had a distinct influence on the adhesion properties of the ISM system.
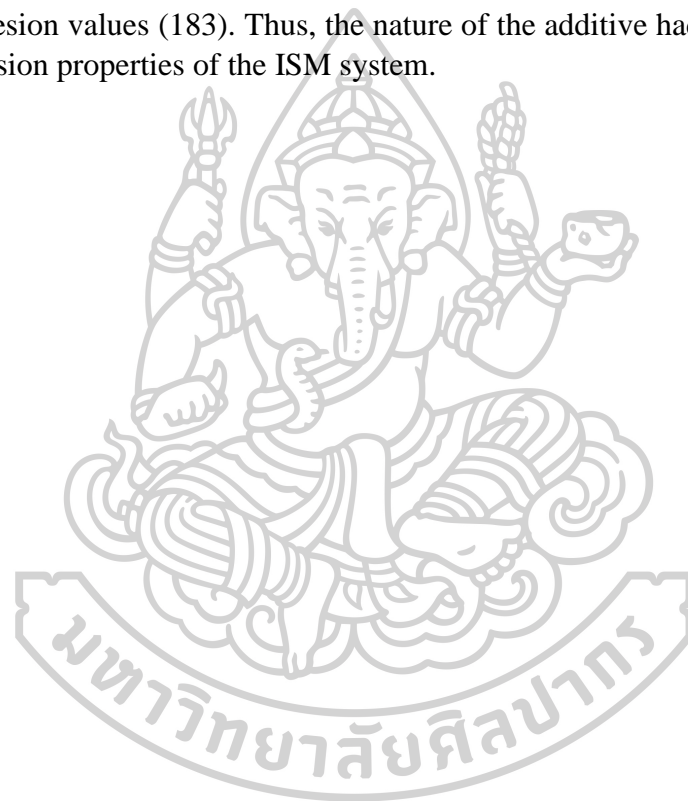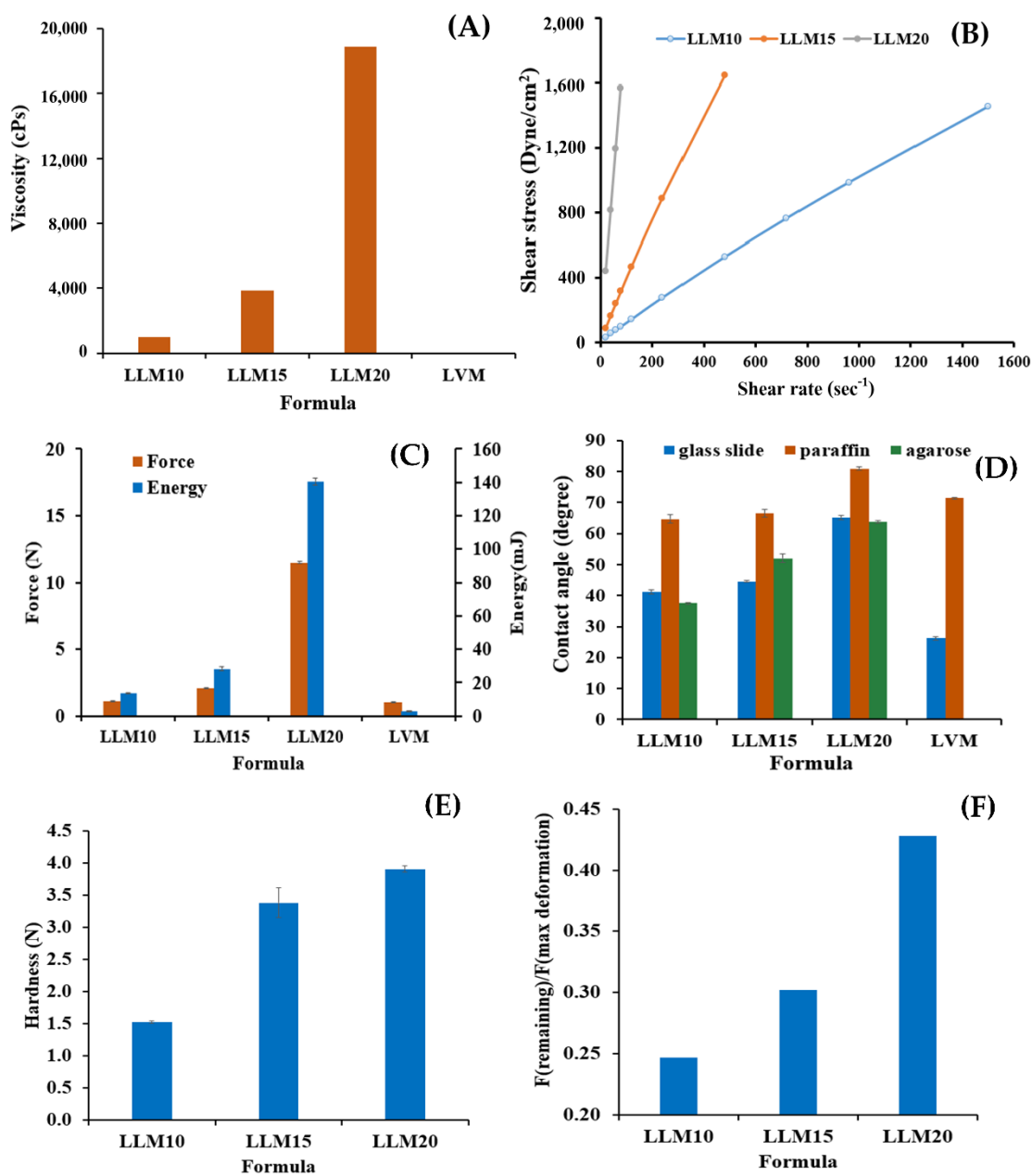
Figure 17. Viscosity (a); shear stress-shear rate relationship (b); injection force and energy from injectability testing (c); contact angle on diverse surfaces (d); hardness (e); and adhesiveness (f) properties were assessed for the Lv-loaded Eudragit® L-based ISM formulations at 25 °C. The data were gathered in triplicate.

4.2.2. Matrix formation of Lv-loaded Eudragit®-based ISM

Exploring the impact of higher concentration Eudragit® L solutions and extended exposure time to PBS on drug-loaded formulations, it becomes apparent that a more extensive cloudy matrix formation occurred, as illustrated in Figure 18A. This phase separation of Eudragit® L can be attributed to its lower solubility in PBS compared to MP. Normally, when the solvent is highly miscible with the aqueous environment, it leads to rapid inward movement of the aqueous phase and outward movement of the solvent phase, followed by a self-forming process of the aqueous-insoluble matrix material (189, 198).

The cross-sectional view of matrix formation in Figure 18B reveals that the slower matrix formation observed in LLM15 is consistent with LM15 (as shown in Figure 15B). This can be attributed to their dense matrix structure, which acts as a barrier, hindering matrix growth and retarding solvent exchange (145). Furthermore, LLM20 exhibited an even cloudier matrix formation. Interestingly, the addition of the drug did not influence the gel or matrix formation process. Similarly, the incorporation of 1% vancomycin HCl had minimal effect on the rate of matrix formation in the borneol-ISG system (174). These test results provided confirmation that the injected drug-loaded Eudragit® L-based ISM had the ability to transition from a solution to an opaque matrix almost immediately. The *in-situ* process of Eudragit® L-based ISM occurred upon contact with simulated periodontal fluid, during which MP diffused outward from the formulation while water entered. This led to the solidification of the initially cloudy Eudragit® L matrix, transforming it into a solid-like matrix over time. The phenomenon of matrix formation induced by solvent exchange has been documented previously in rosin-based ISG formulations (181).
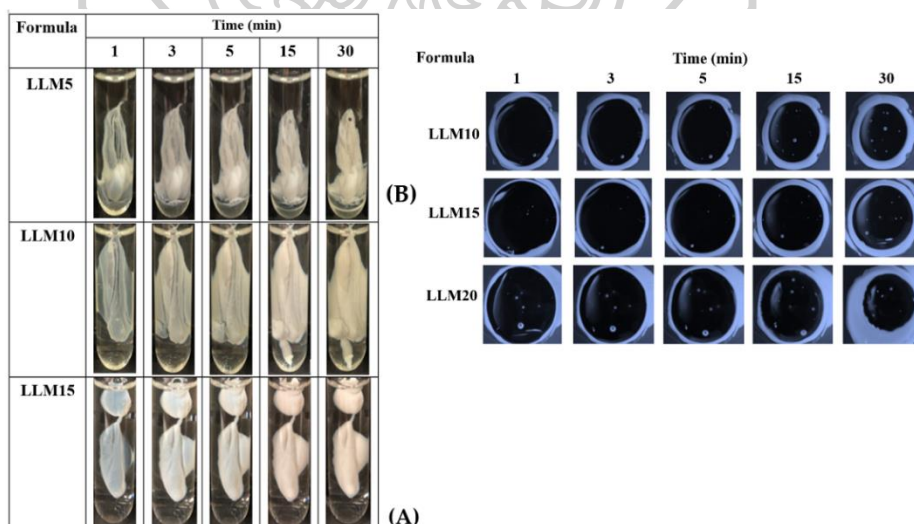
Figure 18. Matrix formation subsequent to injection into PBS (A) and agarose well (B) of Lv-loaded Eudragit® L-based ISM.

4.2.3. Microscopic interface interaction

In the depicted images found in Figure 19 and 20, the movement of fluorescent colors observed at the interface between the agarose gel and the formulation or solvent under a fluorescent microscope. To exemplify this phenomenon, LM10 was utilized as a model formulation in this study, given its lower polymer content that did not interfere with the fluorescence emitted by the dyes during the transformation into a gel or matrix-like structure. In Figure 19, the color movement is depicted from Eudragit® L-based ISM formulations or MP containing SF or NR (right side) to the non-colored agarose gel (left side). The white line demarcates the interface between the right component and the left agarose gel phase. Remarkably, SF is an orange-red, odorless powder that is highly soluble in water and only sparingly soluble in alcohol (199). In practical terms, SF absorbs blue light most effectively within the wavelength range of 465 to 490 nm. This absorption leads to fluorescence emission at yellow-green wavelengths, typically falling between 520 and 530 nm (200). In a neutral to alkaline solution, it displays a vivid yellow-green fluorescence when exposed to ultraviolet light (200). In the SF-loaded LM10 formulation, the SF did not manifest its characteristic green color within MP. However, a distinct dark green band was discernible at the interface, indicating some degree of SF diffusion into this region (Figure 8). Nevertheless, the formation of the Eudragit® L matrix hindered the extensive diffusion of SF into the agarose gel, thus preventing the full expression of its green color. Additionally, the limited movement of water from the agarose gel was inadequate to induce the robust emission of SF as a vibrant green hue in the formulation. In contrast, NR, a hydrophobic probe, exhibits pronounced fluorescence (201). NR's fluorescence becomes evident in organic solvents and it primarily dissolves in hydrophobic substances like lipids; however, its fluorescence is suppressed in water (202). The NR-loaded LM10 formulation initially exhibited a red color due to the emission of NR that was dispersed into the agarose gel. This emission might have been caused by the diffusion of NR along with MP. Subsequently, the NR was absorbed onto the Eudragit® L matrix. However, as water mixed and diluted within the agarose gel, the solubility of NR decreased, causing it to diffuse back into the formulation. This resulted in the fading of the red color in the agarose side and a darker red color in the formulation as more time passed. At 1 minute, a white band representing the formed Eudragit® L matrix appeared at the interface, similar to the test with SF-loaded LM10. The higher intensity of fluorescence colors at equilibrium made it difficult to observe the expansion of this matrix band. However, it appeared to effectively restrict the diffusion of SF and NR into the agarose gel. Rapid diffusion of the green-colored SF from MP into the agarose was evident. While SF did not exhibit its color in MP, it rapidly assumed a green color upon dissolution in a water phase. This abrupt color change was due to the rapid migration of water from the agarose (left side) into the SF-loaded MP, which was faster than its migration into SF-loaded LM10. Similarly, in the case of NR-loaded systems, the swift influx of water into the NR-loaded MP led to a rapid reduction in NR solubility, resulting in the absence of its color. However, NR-loaded

LM10 continued to display a red color since the influx of water was slower, allowing NR to maintain its emission color within the remaining MP.

Formula	Time (min)					
	1	2	3	4	5	6
SF-loaded LM10						
NR-loaded LM10						
SF-loaded monopropyl-ene glycol						
NR-loaded monopropyl-ene glycol						
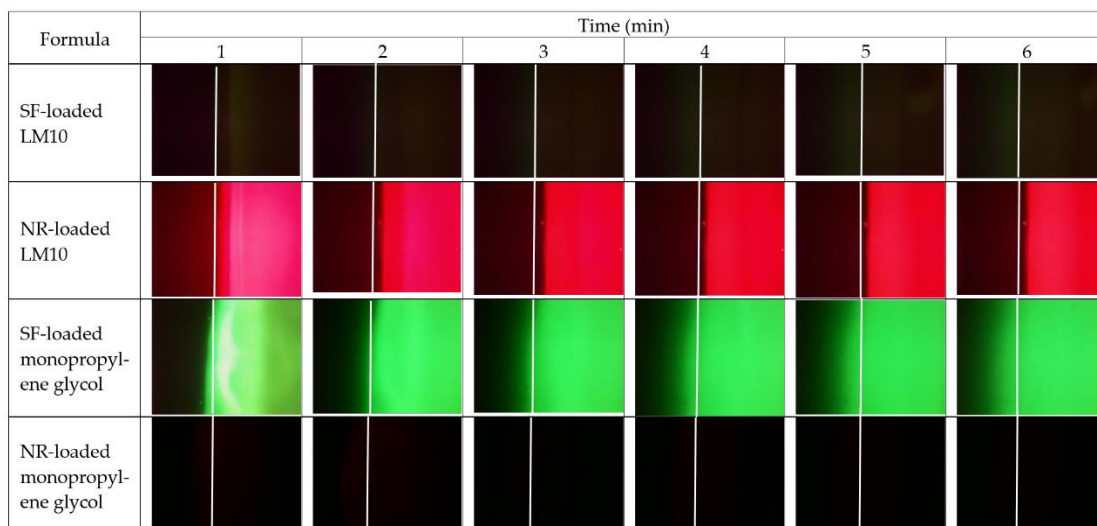
Figure 19. The interface interaction between uncolored agarose gel (on the left side) and Eudragit® L-based ISM formulation or MP containing SF or NR (on the right side) was observed at various time intervals using an inverted fluorescent microscope, magnified at 400×.

The microscopic interface interaction was also assessed using SF-loaded agarose gel, as depicted in Figure 20. The white line designates the initial interface between the two phases. The expansion of an opaque band became apparent after the SF-loaded agarose gel (left side) came into contact with LM10 (right side). This band confirmed the formation of a matrix at the interface, and it gradually extended inward into the formulation over time, consistent with the observations from the cross-section view of matrix formation mentioned earlier. These images further illustrated that SF in the formulation or solvent did not exhibit its characteristic bright green color. In the case of NR-loaded LM10, the initial Eudragit® L matrix appeared as a yellow band, encompassing some NR that formed a narrow orange band near the agarose gel. As time progressed, NR diffused backward with the solvent, accumulating on the formulation side and presenting its red color more prominently. As mentioned earlier, the NR absorbed onto the Eudragit® L matrix was capable of diffusing backward into the formulation, resulting in the fading of the red color on the agarose side and a deeper red color in the formulation. When SF-loaded agarose gel came into contact with NR-loaded MP, a noticeable green color emerged, and the distinct red color was absent. Initially, the red color from NR appeared on the left side of the agarose due to the initial diffusion of the solvent. However, this solvent became diluted after rapid mixing with water from the agarose gel. Once adequately diluted, NR in the formulation became insoluble and could not manifest its color. The Eudragit® L matrix of NR-loaded LM10 effectively hindered the movement of water into the formulation, allowing the solubility of NR to be maintained in the solvent, thereby

exhibiting its red color. The swift movement of SF, facilitated by sufficient water from the agarose, into the MP resulted in a brighter green color in this solvent over time. The dark band observed could be attributed to the accumulation of MP at the interface along with the solvent front during the contact period, causing SF to not exhibit its bright green color distinctly. Thus, the utilization of fluorescence probes like SF and NR can provide valuable insights into the movement of solvents and the formation of the ISM matrix.

Formula	Time (min)					
	1	2	3	4	5	6
LM10						
NR-loaded LM10						
NR-loaded monopropyl-ene glycol						
Monopro-pylene gly-col						
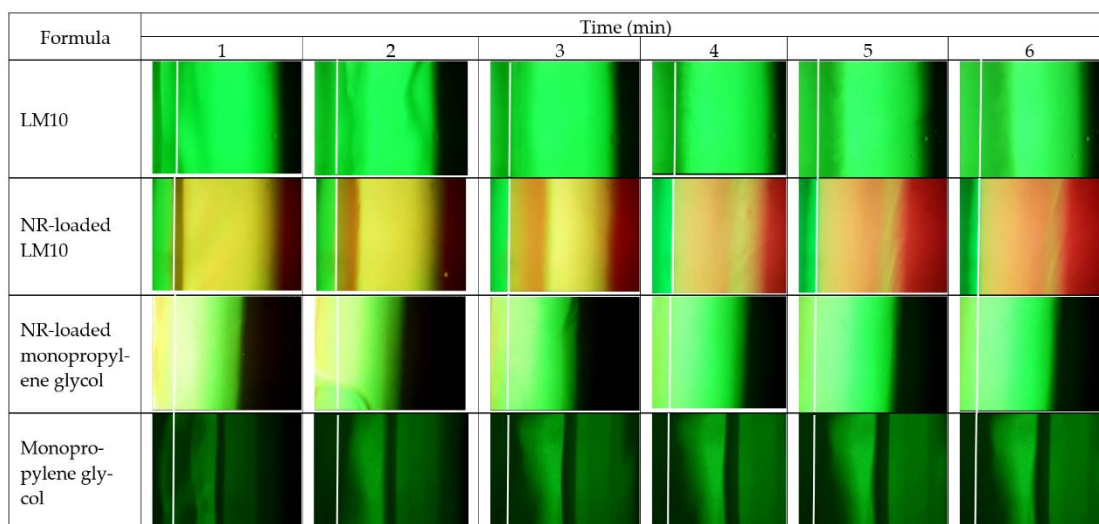
Figure 20. The interaction at the interface between sodium fluorescence-loaded agarose gel (on the left side) and Eudragit® L-based ISM formulation, as well as MP with or without NR (on the right side), was observed at various time intervals using an inverted fluorescent microscope at a magnification of 400×.

4.2.4. Drug content and release of Lv-loaded Eudragit®-based ISMs

The *in vitro* drug release study was carried out in PBS at pH 6.8, aiming to replicate the conditions within the periodontal environment. The initial drug content of the samples, namely LVM, LLM10, LLM15, and LLM20, were measured as 102.52 ± 1.74, 100.85 ± 0.94, 98.77 ± 1.02, and 101.04 ± 0.86, respectively. Prior to conducting the *in vitro* drug release test, the formulations underwent drug content determination using the cup method, which was chosen to mimic the conditions akin to those within the periodontal pocket (183, 197). This method has been previously employed by researchers to investigate the drug release behavior of *in situ* forming drug delivery systems (174, 192, 193). Figure 21 illustrates the release profiles of Lv from Eudragit® L-based ISMs and the control group (LVM). Remarkably, the control group (LVM) with no polymer exhibited a rapid release of Lv, releasing the entire drug within a single day.

Sustained drug release was achieved with the three developed Eudragit® L-based ISMs. Among them, LLM20 exhibited a more efficient and prolonged drug release profile compared to LLM15 and LLM10. These formulations displayed an initial burst of drug release within the first day, followed by a gradual and sustained

release over the course of 1 to 14 days. The outward diffusion of MP into the release medium facilitated a phase inversion process and the formation of a porous rubbery matrix structure. These changes were primarily due to the initial burst release of drugs deposited on the surface layer of the matrix. It's worth noting that the use of hydrophobic solvents like triacetin and ethyl benzoate for dissolving PLGA in ISG resulted in slower gelation and significantly reduced burst drug release, as compared to the observed behavior in this study (117). The initial rapid drug release observed in this formulation has the potential to rapidly achieve a high drug concentration at a therapeutic level above the MIC for effective periodontitis treatment. This is followed by a sustained release phase that helps maintain the drug level at the target site over an extended period. A comparable behavior was observed in a study involving a combination of thermosensitive poloxamer 407 and chitosan gel, where an initial burst release resulted in the release of approximately 60-70% of Lv within a span of 6-7 h (133). The thermosensitive gel, formulated with 0.6% w/v gellan gum and 14% w/v pluronic F127, was able to extend the release of Lv for a duration of 3-4 h (203). Hence, these hydrophilic polymeric gels were not able to sufficiently extend the release of the drug. DH released from 15%, 25%, 30%, and 35% w/w Eudragit® RS-loaded ISGs at 91%, 79%, 71%, and 68% over a 54-h (2.25 days) period, respectively. This behavior can be attributed to the swellable, water-insoluble nature of Eudragit® RS polymer, which forms various loose, swollen membrane structures in aqueous environments, impacting the drug release (21). The commercial product used for treating periodontitis, like Atridox®, employs 5% or 10% DH as the antibacterial agent, loaded into a 33.03% PLA solution. This formulation ensures sustained drug release for a minimum of 7 days (204, 205). In this study, the Lv-loaded Eudragit® L-based ISM formulations demonstrated the capability to regulate drug release for a duration of two weeks, utilizing a lower polymer concentration compared to Atridox®. These developed ISMs offer a promising alternative as a sustainable local drug delivery system for the periodontal pocket, contributing to enhanced patient compliance owing to reduced frequency of drug administration (190, 206). Furthermore, based on the literature review, the MIC of Lv against *S. aureus*, *E. coli*, and *P. gingivalis* was reported as 0.12 µg/mL (167), ≤0.12 µg/mL (168), and 8 µg/mL (207), respectively. Through calculations involving 0.4 grams of the formulation, the prepared cups were then submerged in 50 mL of PBS. The concentration of the complete drug release from this study was 43.75 µg/mL (representing 100% release). As a result, with an 18.29% drug release or after approximately 4 h, all formulations could reach the MIC of Lv against *P. gingivalis* and the other tested microbe.
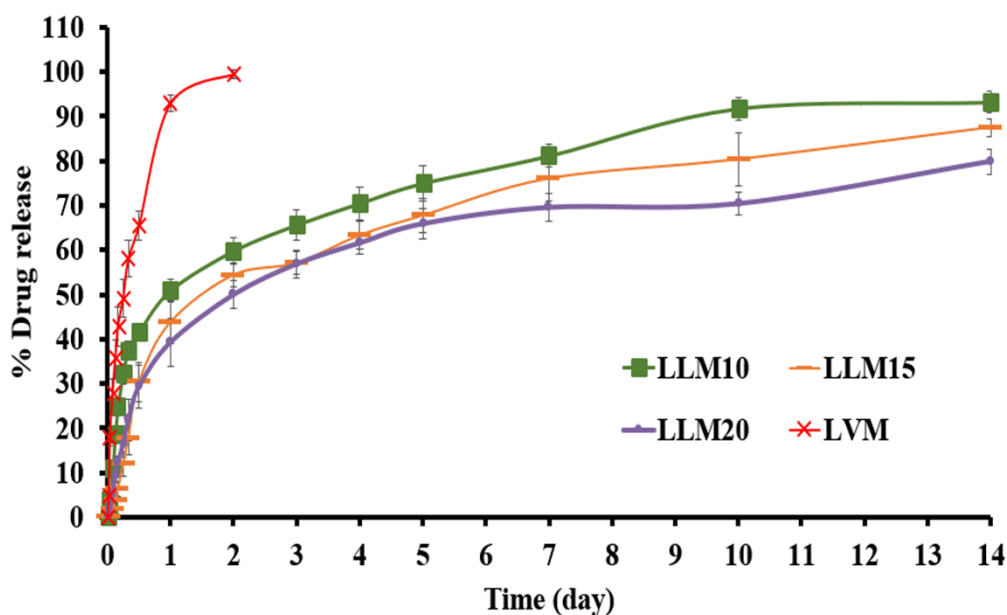
Figure 21. Release of the drug from Lv-loaded Eudragit® L-based ISM formulations (n = 3) (mean ± S.D).

The estimated parameters obtained from fitting the release profiles to various equations such as zero order, first order, Higuchi's, and power law equations, along with the corresponding regression coefficient (r^2) values and MSC, are presented in Table 5. All the release profiles exhibited compatibility with the Korsmeyer-Peppas equation, showing distinctively high r^2 and MSC values. The constant 'k' encompasses structural and geometric characteristics of the device, while 'n' represents the release exponent indicating the mechanism of drug release. In the case of LVM, the drug released fitted well with a first-order equation (with r^2 and MSC values of 0.9744 and 3.3211, respectively), suggesting a behavior dependent on the drug concentration gradient or a fraction of remaining drug in the solution. For the drug release profile of Lv-loaded Eudragit® L-based ISMs, the r^2 and MSC values, along with the diffusion exponent value 'n' (around 0.45), indicated a strong adherence to Higuchi's equation. This finding implied that their drug release kinetics followed Fickian diffusion. It's worth noting that although their release profiles aligned well with Higuchi's equation, the k value in the Higuchi equation decreased significantly with increasing polymer concentration. This decrease was attributed to the denser Eudragit® L matrix retarding the diffusion of the drug into the release medium. Similar observations of hydrophilic drug release from other polymer or fatty acid-based ISGs also largely aligned with Higuchi's equation, reflecting Fickian diffusion kinetics (184, 208).

Table 5. Regression coefficient (r²) value, MSC, and diffusion exponent value (n) extracted from the drug release profile of Lv-loaded Eudragit® L-based ISM formulations fitted using various mathematical equations.

Formula	Zero Order		First Order		Higuchi's		Korsmeyer-PEPPAS				
	r²	MSC	r²	MSC	r²	MSC	r²	MSC	k ± SD	n ± SD	Release Mechanism
LLM10	0.8048	1.3742	0.8683	1.9759	0.9058	2.5144	0.9770	3.5961	3.344 ± 1.837	0.444 ± 0.050	Fickian diffusion
LLM15	0.7118	0.9164	0.8872	2.0854	0.8945	2.0844	0.9503	2.6867	2.603 ± 0.666	0.367 ± 0.028	Fickian diffusion
LLM20	0.7941	1.2387	0.9090	2.3402	0.9188	2.3419	0.9320	2.3732	1.856 ± 0.819	0.444 ± 0.055	Fickian diffusion

4.2.5. Scanning electron microscopy (SEM)

Within the visual representations in Figure 22, SEM images provide insights into the surface and cross-sectional topographies of dried remnants from drug-free Eudragit® L-based ISMs (LM10, LM15, and LM20). Importantly, a prominent scaffold-like topography is observed in both the surface and cross-sectional views for LM10. This characteristic appearance of a scaffold, featuring polymeric fibrous networks, confirmed the effective promotion of polymer separation facilitated by solvent exchange. In contrast, higher polymer loading led to a denser surface, while larger fibrous structures were observed in the cross-sectional aspect. This structure exhibited numerous spherical polymer particles interconnected to form a continuous fibrous network. The size of internal voids within the structure decreased with an increase in polymer concentration. Especially, this topographical pattern resembled that of the dried remnants from Eudragit® RS-based ISGs, as reported previously (21, 179, 180). Eudragit® L exhibits solubility within the pH range of 5.5 to 6.0, making it suitable for delivering medication to the ileum. On the other hand, Eudragit® S offers release within the pH range of 7.0, allowing for medication delivery to the large intestine (52). SEM images of the developed ISMs, captured after the release study, revealed the presence of pores within the inner matrix. The density of these pores varied based on the polymer content. This observation suggests that the drug diffusion, along with solvent from the matrix or *in situ* forming scaffold, contributed to the formation of both pores and a scaffold-like structure within the ISGs, allowing for drug release into the surrounding medium (209). The porosity and connectivity of pores were shown to reflect the path of solvent migration, leading to the formation of the Eudragit® scaffold and subsequent drug release. However, the dissolution of Eudragit® L in pH 6.8 PBS could occur steadily, influenced by the polymer content. Higher polymer content resulted in a more compact structure and reduced matrix dissolution.

An SEM image of Lv powder displayed rod-shaped crystalline particles (Figure 23A). SEM images of the surface and cross-section topographies of remnants from Lv-loaded 10%, 15%, and 20% Eudragit® L-based ISMs after 7 days of drug release were shown in Figure 23B. The absence of drug crystals in the remnants suggested that a small amount of drug might have dispersed at a molecular level within the polymer matrix, and some dispersed drugs had already dissolved from the

matrix. The increased concentration of Eudragit® L notably led to denser surface and inner topographies in the resulting polymer matrix. LLM20 demonstrated more effective drug release prolongation than LLM15 and LLM10 due to its denser topographic matrix with higher polymer content. Comparatively, the porosity of drug-loaded ISM remnants was noticeably lower than that of drug-free ISM remnants. The inclusion of the hydrophilic drug altered the formulation's polarity and potentially facilitated solvent exchange, leading to an accelerated phase separation of the polymer, resulting in smaller fibrous formations. Furthermore, as mentioned in Section 4.2.1, the presence of Lv decreased the viscosity of the prepared ISMs. The nucleation and growth mechanism of the polymer in the dilute phase played a role in the phase separation process, while the spinodal de-mixing occurring during the membrane formation process contributed to the development of interconnectivity between the membranes (210). Alterations in solution viscosity induced by the inclusion of a hydrophilic drug have the potential to influence the rate of phase separation. Consequently, this can lead to variations in matrix morphology, similar to the effects observed with the addition of polyvinyl pyrrolidone (PVP) when producing polyethersulfone hollow fiber membranes (211). The morphology of this membrane was examined in relation to the viscosity of the spinning solution. The inclusion of PVP resulted in a reduction in solution viscosity, facilitating rapid precipitation and leading to the creation of a distinct pore structure reminiscent of finger-like formations within the membrane (211, 212).

As depicted in Figure 23B, the decrease in viscosity resulting from drug loading, as discussed in Section *4.2.1*. Physical appearance, viscosity and rheology, injectability, contact angle, and mechanical properties, could accelerate the phase separation of Eudragit® L from the solution, resulting in a less pronounced pore structure and a diminished finger-like appearance in the remnants of drug-loaded ISMs. Previous studies have indicated that higher polymeric concentrations contribute to the gel's resistance against the influx of water and the efflux of solvent, primarily due to the formation of a less porous structure (213). Consequently, these SEM images underscore the observed slowdown in drug release from Eudragit® L matrices, as discussed earlier in Section *4.2.4.* Drug content and release of Lv-loaded Eudragit®-based ISMs. The morphology displayed by these remnants clearly highlights the unique porous structure, providing evidence of solvent exchange as a governing mechanism that regulates drug release from Eudragit® L-based ISM matrices.
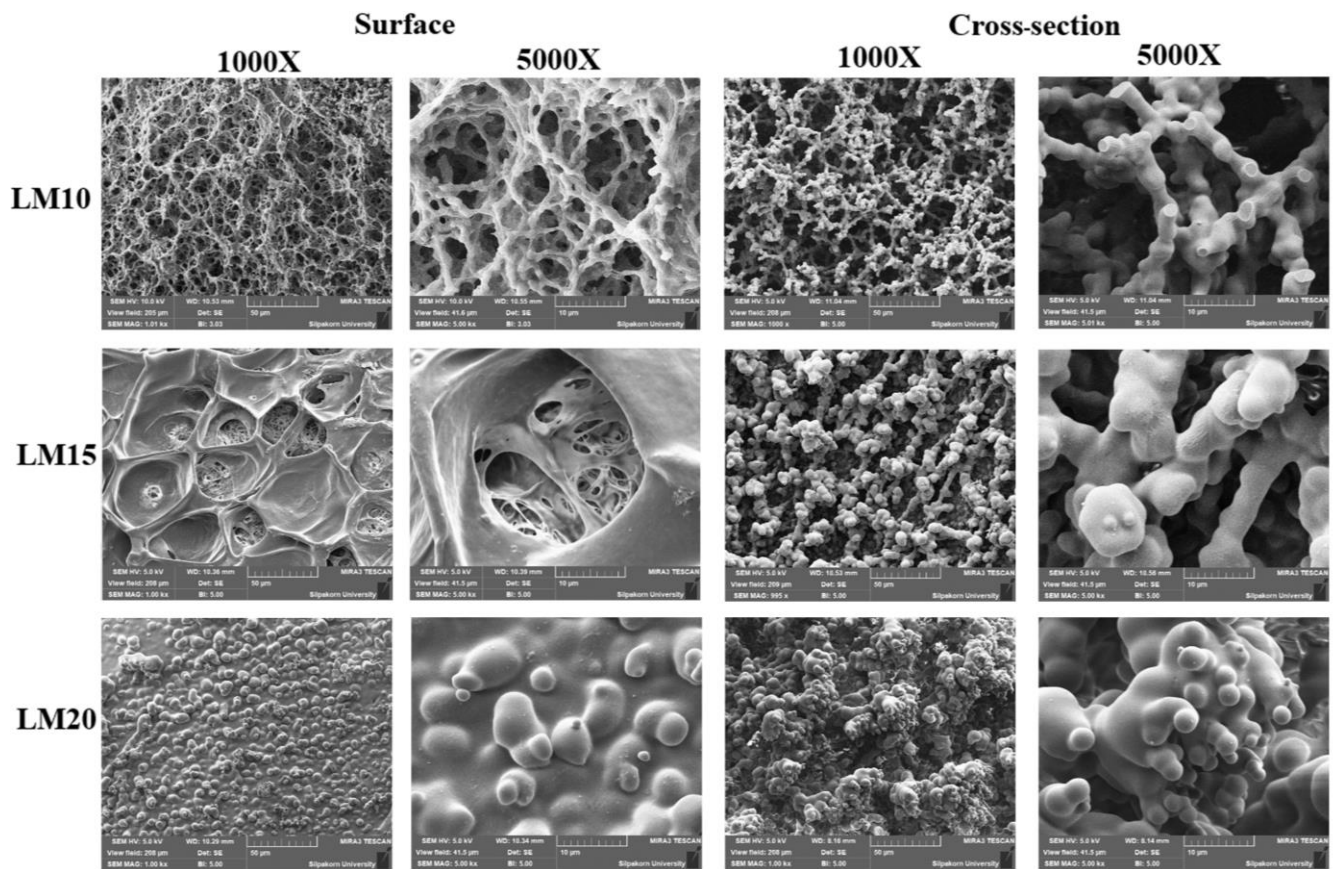
Figure 22. Scanning electron microscopy (SEM) images depicting the surface and cross-section of freeze-dried remnants from Eudragit® L-based ISM formulations subsequent to a 7-day release test, captured at magnifications of 1000× and 5000×.

(A)

Sample	Magnification	
	200X	**500X**
Lv		

(B)

	Surface		Cross-section	
	1000X	**5000X**	**1000X**	**5000X**
LLM10				
LLM15				
LLM20				
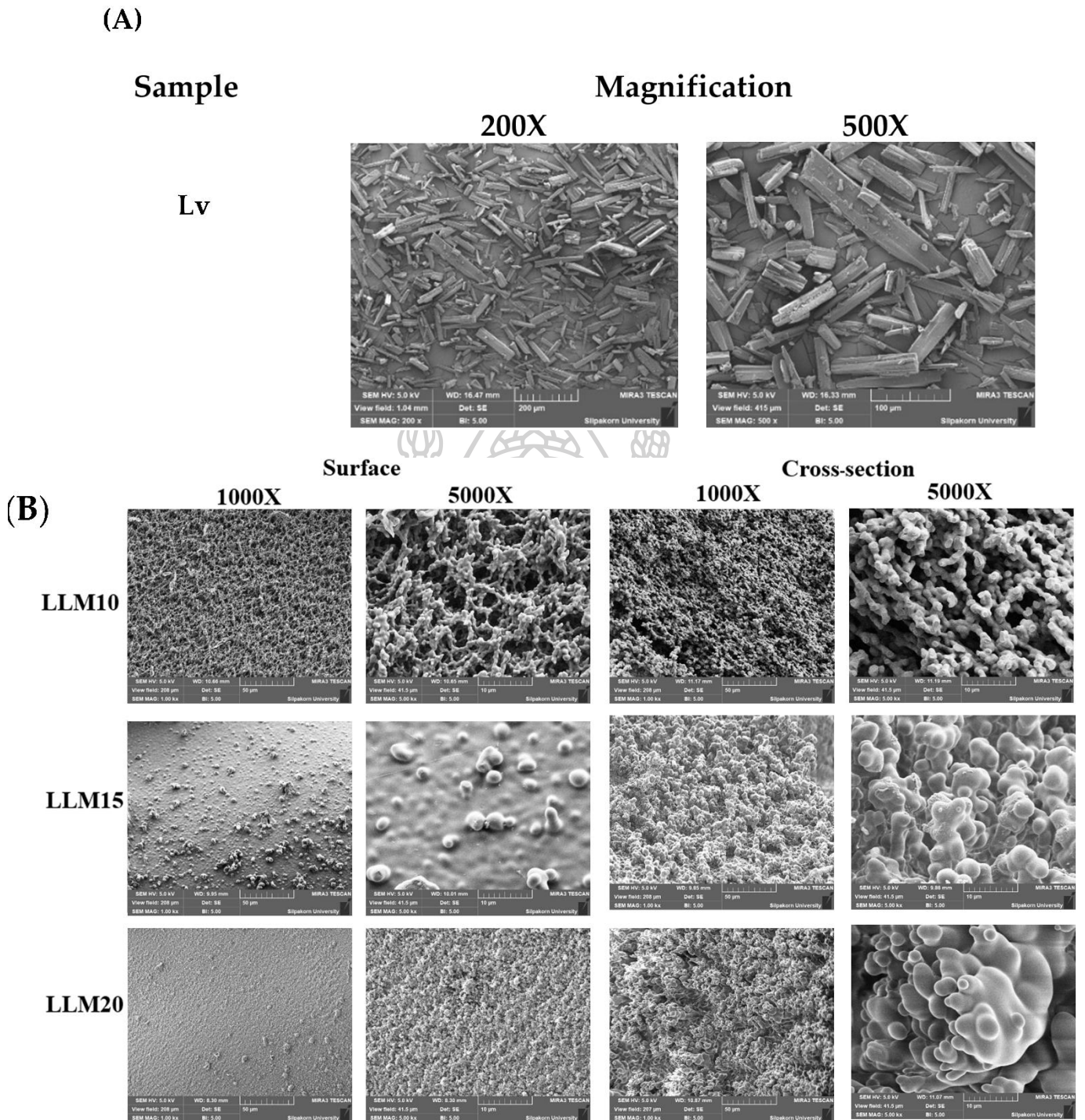
Figure 23. SEM images showcasing Lv powder (A); along with the surface and cross-section of freeze-dried remnants derived from Lv-loaded Eudragit® L-based ISM formulations, magnified at 1000× and 5000× (B).

4.2.6. *In vitro* degradation

The *in vitro* degradation behavior, expressed as the percentage of mass loss for the three drug-loaded formulations, is presented in Table 6. The mass loss observed in our study is primarily attributed to the diffusion of the drug and MP, along with the dissolution of Eudragit® L through interaction with the release medium. The degradation process of drug delivery systems can be characterized by changes in the weight or molecular weight of their constituents, such as polymers (214). The Table 6 highlights that ISM formulations with higher concentrations of Eudragit® L exhibited lower percentage mass loss. Evidently, the three ISMs displayed significantly different values on days 1 and 3 ($p < 0.05$), with LLM10 showing significantly higher mass loss compared to LLM20 on days 5 and 7 ($p < 0.05$). The immersion of these ISMs in the release medium triggered the formation of a porous matrix structure through solvent exchange. Consequently, the primary mass loss from the ISMs stemmed from the diffusion of MP and the drug release, both of which were influenced by the porosity and tortuosity of the Eudragit® L matrices, as discussed in the preceding SEM section. It is important to note that the degradation of polymeric structures like Eudragit® L does not result from enzyme or acidic conditions. Thus, the predominant mass loss observed in this study was attributed to solvent leakage from the matrix depot and gradual dissolution of Eudragit® L. The complete mass loss was achieved at 14 days, as indicated in Table 6, confirming the gradual nature of Eudragit® L dissolution. The higher concentration of the matrix-forming agent led to a denser matrix structure with higher tortuosity, impeding the diffusion of MP and drug molecules into the external medium. Consequently, this phenomenon contributed to reduce *in vitro* degradation and prolonged drug release.

The steep slope observed in the early hours of the drug release profile likely resulted from the rapid release of the drug initially loaded onto or near the surface of the Eudragit® L matrix. This was followed by sustained release of the drug distributed within the inner polymeric matrix. In a separate study, a composite material composed of polyurethane and Eudragit® L as nanofibers, fabricated using the electrospinning technique, demonstrated favorable mechanical properties and *in vitro* cell biocompatibility. These findings suggest that the material holds promise for applications involving drug-eluting stent covers (53). The integration of DNA plasmid for gene delivery and low molecular weight heparin delivery into nanoparticles crafted from this polymer ensemble has received clinical approval in the United States of America, Japan, and Europe. Importantly, these nanoparticles exhibit minimal toxicity (215). Eudragit® L 100 is a methacrylic acid and methyl methacrylate-based anionic copolymer (52). Its intended site for drug release is the jejunum, and it undergoes dissolution at a pH level exceeding 6 (52). Eudragit® L is a pH-dependent polymer that gradually and consistently dissolves at a pH level higher than 6. The degradation rate is influenced by the quantity of polymer present. Lower polymer content accelerates both the rate and extent of degradation. This outcome suggests the potential utility of this system in the development of drug delivery systems for

periodontal pockets. The inherent *in vitro* degradation over time emphasizes its applicability for such purposes.

Table 6. Mass loss observed in the in vitro degradation test of Lv-loaded Eudragit® L-based ISM formulations. The superscripts (a-d) in the column indicate significant distinctions among the tested formulations (p < 0.05).

Formula	Weight Loss (%)				
	Day 1	Day 3	Day 5	Day 7	Day 14
LLM10	85.39 ± 0.32 [a]	91.96 ± 0.98 [b]	94.53 ± 1.46 [c]	94.96 ± 1.21 [d]	100.00 ± 0.00
LLM15	80.22 ± 2.90 [a]	86.95 ± 1.97 [b]	87.91 ± 0.54	92.57 ± 1.92	100.00 ± 0.00
LLM20	72.81 ± 1.85 [a]	82.02 ± 1.4 [b]	85.95 ± 1.98 [c]	90.21 ± 1.80 [d]	100.00 ± 0.00

4.2.7. X-ray computed microtomography (µCT)

µCT is employed for the internal visualization of scanned solid objects, facilitating the acquisition of 3D geometrical details and properties. This technique relies on the concept that internal characteristics of a solid object exhibit density and/or atomic composition variations (216). Its application encompasses the *in vitro* measurement of implant porosity and pore size (217). Figure 24 depicts the µCT images obtained from a synchrotron light source, showcasing the remnants of LLM15 and LLM20. However, the relatively delicate LLM10 was excluded from the assessment, as it couldn't maintain its features over an extended duration under synchrotron light examination. The 3D volume and cross-sectional views with voids within the LLM15 and LLM20 remnants are presented. Remarkably, the LLM20 remnant exhibits a less pronounced void structure compared to that of LLM15. Due to the pronounced contrast predominantly between solid phases and air, this method is suitable for quantifying the porosity of the studied object (216).

Furthermore, the concurrent analysis of the 3D structures revealed that the percentage of porosity (%porosity) in LLM20 was lower than that in LLM15. This observation corresponded with the *in vitro* release behavior and the surface characteristics observed through SEM imaging. Consequently, the presented µCT data served as supportive evidence. It's worth noting that µCT imaging has previously been utilized for assessing the longitudinal degradation quantification and intra-articular biocompatibility of a hydrogel based on an acyl-capped triblock copolymer, poly[E-caprolactone-co-lactide)-b-poly(ethylene glycol]-b-poly[E-caprolactone-co-lactide] (218).
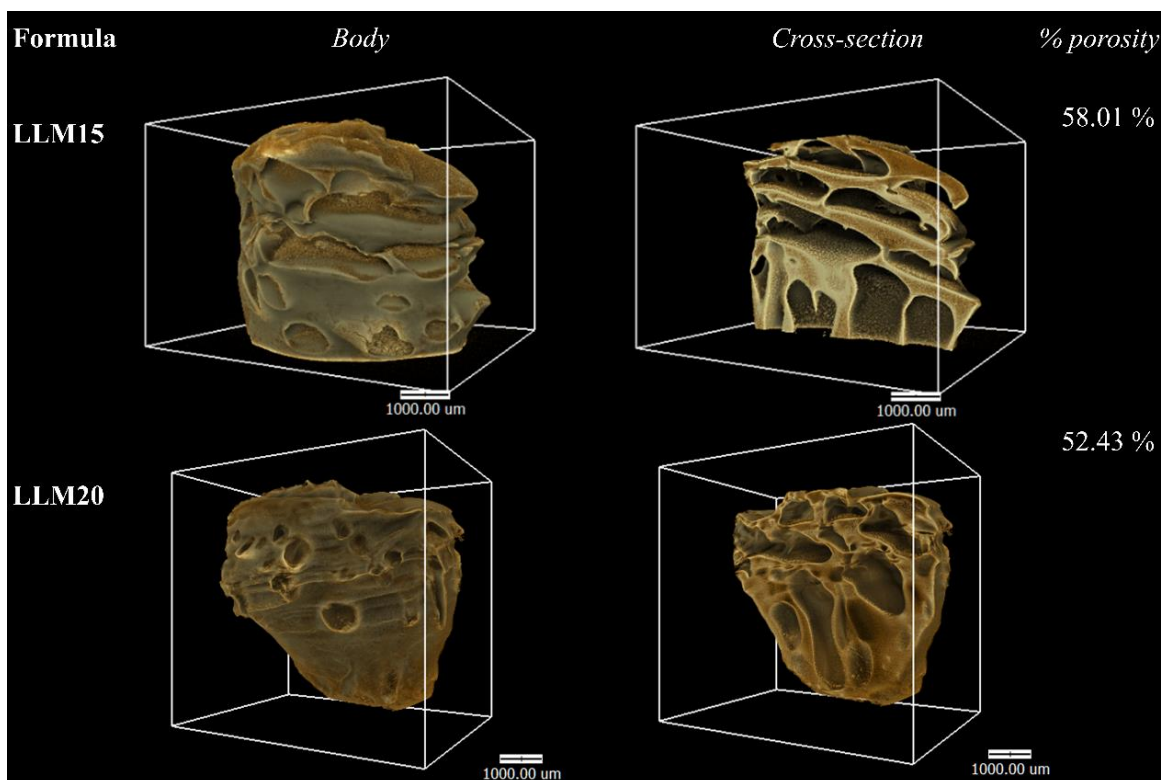
Figure 24. X-ray tomography image and percentage porosity determination using X-ray tomography, performed on the freeze-dried residual material subsequent to a 7-day drug release test of Lv-loaded Eudragit® L-based ISM formulations.

4.2.8. Antimicrobial activities

The inhibition zone diameter of solvents, drug-free, and Lv-loaded Eudragit® L ISMs against various microbial strains, including *S. aureus* (ATCC 6538, 6532, and 25923), MRSA (ATCC 4430), *E. coli* ATCC 8739, *C. albicans* ATCC 10231, *P. gingivalis* ATCC 33277, and *A. actinomycetemcomitans* ATCC 29522, has been determined through antimicrobial activities testing via the cup agar diffusion method, and the results are summarized in Table 7. These tested bacterial and fungal species are commonly associated with periodontitis disease. Particularly, the principal obligates anaerobic pathogen bacteria linked to adult periodontitis have been identified as *P. gingivalis* and *A. actinomycetemcomitans (219, 220)*. Nonetheless, further research is warranted to discern the precise functions that each of these species assumes, both independently and in combination with other species, in the progression of periodontal degradation. Occasional isolation of *S. aureus* from periodontal pockets of individuals with aggressive periodontitis has been observed, and *E. coli* has at times been identified as a microorganism in patients with periodontitis (35). Unlike many other types of infections, all the microorganisms believed to contribute to periodontal disease are naturally present in the oral

microbiota. One specific example is *C. albicans*, which is associated with cases of stubborn refractory periodontitis (221).

The findings of this study indicate that MP exhibited a minor inhibitory effect on the growth of all tested microorganisms, as outlined in Table 7. Previously, it has been reported to possess antimicrobial efficacy against three organisms: *S. mutans*, *E. faecalis*, and *E. coli*. Importantly, the bactericidal activity was observed at concentrations of 50%, 25%, and 50%, respectively (222). Typically, organic solvents like MP possess the potential to disrupt lipids present in microbial cell walls. Consequently, they can hinder microbe growth. In the case of the drug-free Eudragit® L-based ISM, its capacity to inhibit microbe growth was comparatively lower than that of its solvent, and this inhibition exhibited a dependence on polymer concentration. This effect can be attributed to the higher viscosity and more substantial matrix formation, which notably impeded the movement of MP from the ISM into the inoculated agar media. As a result, higher polymer concentrations led to diminished antimicrobial activity. This observation was confirmed by the fact that LM15 and LM20 exhibited no antimicrobial activity against *S. aureus* 25923, whereas the solvent and LM10 demonstrated an inhibition zone. This role of the polymer in retarding solvent diffusion and impacting antimicrobial activities has been previously documented in drug-free borneol-based ISGs (174).

Table 7. The clear zone diameter of MP, drug-free, and Lv-loaded Eudragit® L-based ISM formulations were measured against various strains, including *S. aureus* (ATCC 6538, 6532, and 25923), MRSA (ATCC 4430), *E. coli* ATCC 8739, *C. albicans* ATCC 10231, *P. gingivalis* ATCC 33277, and *A. actinomycetemcomitans* ATCC 29522 (n = 3).

Formula	Clear Zone Diameter (mm.) Mean ± S.D.							
	S. aureus ATCC 6538	*S. aureus* ATCC 4430	*S. aureus* ATCC 6532	*S. aureus* ATCC 25923	*E. coli* ATCC 8739	*C. albicans* ATCC 10231	*P. gingivalis* ATCC 33277	*A. actinomycetemcomitans* ATCC 29522
MP	12.7 ± 0.5	13.0 ± 0.8	12.3 ± 0.5	10.3 ± 0.5	14.7 ± 0.5	18.7 ± 1.2	17.0 ± 2.2	26.3 ± 0.5
LM10	11.7 ± 0.5	10.7 ± 0.5	11.7 ± 0.5	9.8 ± 0.2	12.0 ± 0.8	16.7 ± 0.5	12.0 ± 0.8	23.7 ± 0.5
LM15	10.5 ± 0.4	10.7 ± 0.5	10.7 ± 0.5	-	12.0 ± 1.4	16.0 ± 0.8	15.0 ± 1.4	23.3 ± 0.5
LM20	10.3 ± 1.2	9.7 ± 0.5	11.3 ± 1.2	-	12.7 ± 1.2	15.0 ± 0.8	13.3 ± 1.2	22.3 ± 0.5
LVM	26.3 ± 0.9 [a]	25.3 ± 0.9 [b]	26.0 ± 0.8 [c]	25.3 ± 0.5 [d]	25.3 ± 0.9 [e]	20.0 ± 1.6 [f]	26.0 ± 0.8 [g]	>40
LLM10	26.7 ± 0.5	23.3 ± 0.5	23.3 ± 1.2	23.3 ± 0.5	23.3 ± 0.9	15.3 ± 2.1	25.3 ± 1.2	>40
LLM15	25.3 ± 0.5	22.7 ± 0.5 [b]	21.7 ± 0.5 [c]	22.7 ± 1.2 [d]	22.3 ± 0.5 [e]	16.0 ± 0.8 [f]	23.3 ± 1.2	>40
LLM20	24.3 ± 0.5 [a]	21.3 ± 0.9 [b]	20.3 ± 0.5 [c]	20.7 ± 0.5 [d]	22.0 ± 0.8 [e]	14.7 ± 0.9 [f]	21.3 ± 0.5 [g]	>40

The superscripts (a-g) within the column indicate notable differences among the examined formulations, with statistical significance at $p < 0.05$.

Due to the lack of a polymeric matrix and free drug spreading, the LVM solution served as the control group, exhibiting the largest inhibition zone diameter. This zone was larger than that of the drug-free formulations ($p < 0.05$) against nearly all of the tested microorganisms (Table 7). Evidently, all drug-loaded ISMs exhibited significantly larger inhibition diameters than the free-drug-loaded ISMs ($p < 0.05$), confirming their antimicrobial activity against all microorganisms, with the exception of *C. albicans*. It's worth mentioning that Lv lacks activity against fungi (132). Consequently, LLM10, LLM15, and LLM20 exhibited no significant differences in the clear zone when compared to LM10-20. This observation implies that the antifungal activity against *C. albicans* primarily stemmed from the solvent, as their clear zones closely resembled that of the solvent. Furthermore, there was a discernible trend of decreasing inhibition clear zone diameter corresponding to higher Eudragit® L concentrations, indicating a retardation of drug diffusion into the inoculated media. These findings align with the viscosity of ISMs and their drug-release behaviors.

Additionally, all developed drug-loaded ISMs were capable of inhibiting *S. aureus* 25923. Thus, the Eudragit® L matrices, after undergoing phase transformation, delayed drug movement by sustaining drug release and consequently reducing the inhibition zone diameter. Noticeably, some ISMs loaded with higher polymer concentrations, such as LLM15 and LLM20, displayed significantly smaller inhibition zone diameters than LVM ($p < 0.05$), as demonstrated in Table 7. Analogous findings have been previously reported for matrices resulting from ISM phase transitions, which were fabricated using diverse matrix-forming agents in *in situ* forming systems. These matrix-forming agents include borneol (174), natural resins (181, 186, 223), cholesterol (224), polymers (182, 225), and saturated fatty acids (208).

The inhibition zone diameter of drug-loaded formulations against *A. actinomycetemcomitans* ATCC 29522 exceeded 40 mm, which prevented a direct comparison of efficacy between the formulations. Nevertheless, this outcome underscored the potent inhibitory activity of these formulations against this pathogen. Thus, the effective Lv ISM presents an appealing localized dosage form for controlled drug release in the treatment of periodontitis. Notably, the use of medicated ISM has demonstrated improved clinical outcomes compared to scaling and root planning alone. This could be attributed to the presence of MP, which possesses antimicrobial properties and also serves as a suitable vehicle for delivering the drug into the periodontal pocket. Among the formulations, LLM15 displayed favorable characteristics such as appropriate viscosity, acceptable injectability, and retained scaffold structure, as confirmed by μCT imaging and SEM. Furthermore, this ISM exhibited sustained drug release above the MIC against key pathogens like *P. gingivalis*. Thus, LLM15 stands out as a promising ISM formulation for periodontitis treatment. Importantly, both Eudragit® L and MP are recognized for their safety and non-toxic nature. While existing safety data and applications suggest their suitability for injectable dosage forms, further clinical experimentation is necessary to determine the safety and therapeutic efficacy of the developed LLM15 ISM.

4.3. Summary

The investigation employed MP as a solvent for dissolving both Eudragit® L and Eudragit® S, alongside Lv, to create solvent removal phase-inversion-based ISM. Among these options, the Eudragit® L-based formulation in MP was selected for drug incorporation and subsequent exploration as an ISM for a periodontal pocket delivery system. This decision was based on the favorable physical attributes of this formulation, including lower viscosity and ease of injection, in addition to its matrix-forming capability. The phase transition process involved the transformation of the initially cloudy Eudragit® L matrix solution into a solid-like matrix subsequent to exposure of the ISM to the aqueous environment of PBS and agarose gel. This transition was driven by the gradual diffusion of MP from the ISM into water, leading to the solidification of the matrix over a specific time frame. An interface interaction study was conducted to provide insights into the movement of the solvent and the formation of the ISM matrix, facilitated by tracking the behavior of fluorescence dyes. All of the developed Lv-loaded Eudragit® L-based ISMs exhibited the capability of sustaining drug release over a duration of two weeks, following the principles of Fickian drug diffusion kinetics. The amounts of released drug surpassed the MIC required to inhibit the growth of the tested microorganisms. SEM and µCT images unveiled the development of scaffold-like structures within the ISMs. These structures displayed a denser topographic pattern and reduced porosity, These structures displayed a denser topographic pattern and reduced porosity, attributes attributed to higher polymer content, which in turn resulted in diminished levels of *in vitro* degradation. Among the formulations, LLM15 demonstrated several desirable characteristics, including appropriate viscosity, Newtonian flow behavior, effective matrix formation, and injectability. Furthermore, it exhibited extended drug release over a period of 14 days and robust antimicrobial activity against a range of microorganisms, such as *S. aureus* (ATCC 6538, 6532, and 25923), MRSA (ATCC 4430), *E. coli* ATCC 8739, *C. albicans* ATCC 10231, *P. gingivalis* ATCC 33277, and *A. actinomycetemcomitans* ATCC 29522. Consequently, LLM15 holds significant promise as an ISM formulation for the treatment of periodontitis. While both MP and Eudragit® L possess established safety profiles in various medical applications, the newly developed LLM15 ISM warrants further clinical experimentation to assess its safety and therapeutic effectiveness when used in combination.

Moxifloxacin HCl-loaded nitrocellulose ISM for periodontal pocket delivery

4.4. Nitrocellulose-based ISM

4.4.1. Physical appearance, viscosity and rheology and injectability

Nc readily dissolves in NMP and DMSO, whereas its solubility in GF is comparatively lower than in Py. Figure 25 illustrates the visual appearance of 15% w/w Nc solutions and 0.5% w/w Mx-loaded 15% w/w Nc solutions in different solvents. All solutions exhibited clarity. Solutions prepared in Py, DMSO, and GF displayed a slight yellowish coloration. The flow characteristics of the solutions varied based on the solvent used, which corresponded directly to the obtained viscosity results.
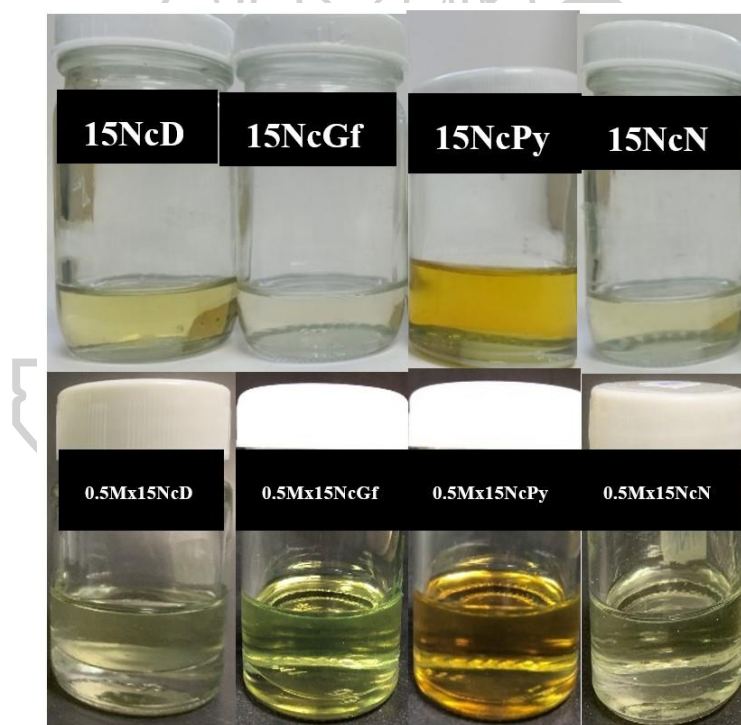
Figure 25. Visual comparison of 15% w/w Nc solutions and 0.5% w/w Mx-loaded 15% w/w Nc solutions in different solvents.
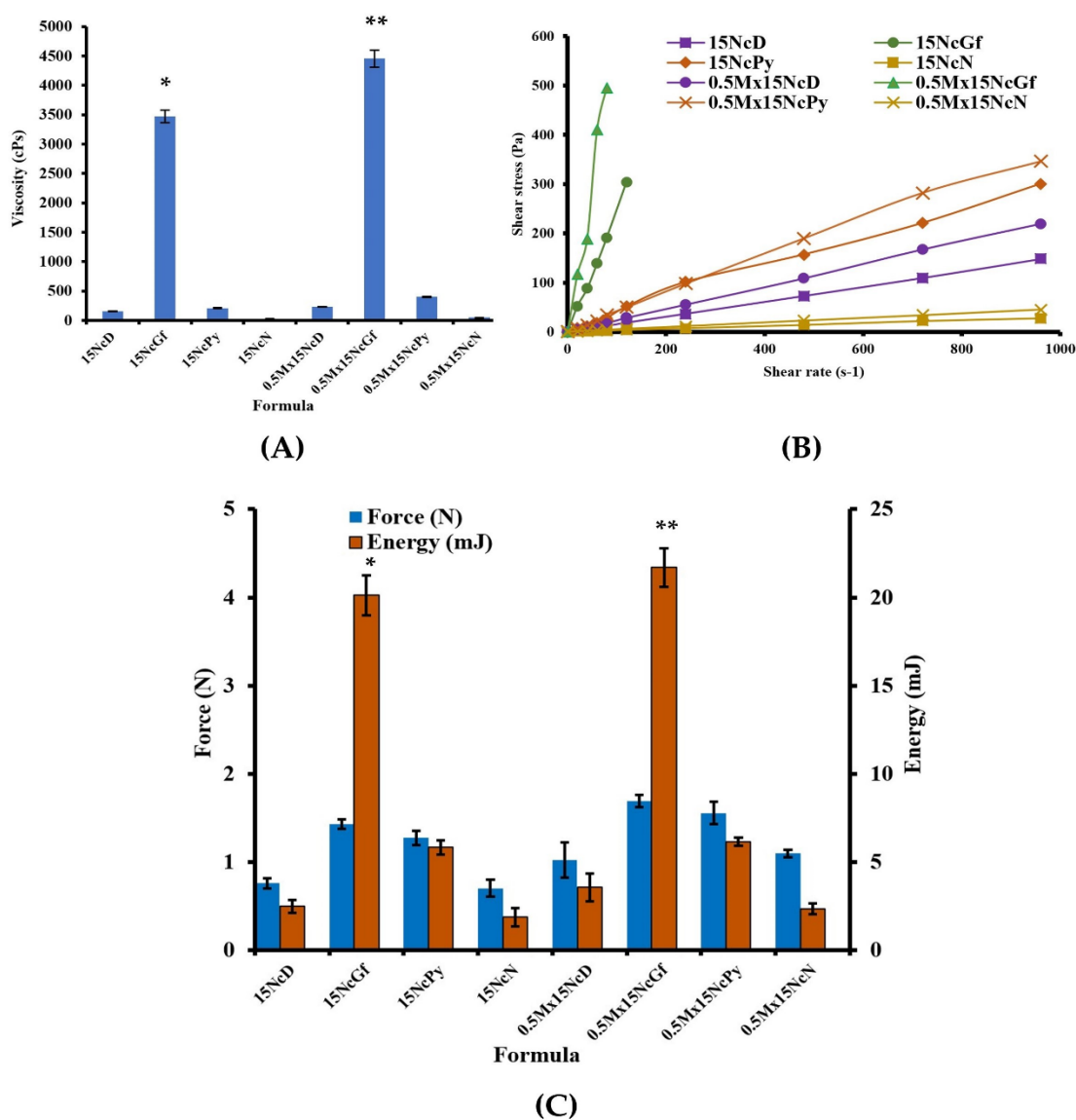
Figure 26. A) Viscosity measurements of drug-free and Mx-incorporated Nc-based ISMs. B) Shear stress and shear rate relationship of the tested formulations. C) Injection force and energy results from the injectability test for drug-free and Mx-incorporated Nc-based ISMs. The symbols * and ** indicate significant differences ($p < 0.01$) among the tested formulations.

The viscosity effects of various solvents on Nc solutions and Mx-loaded Nc solutions are depicted in Figure 26A. NMP usage as the solvent led to lower viscosity in both solutions compared to DMSO, Py, and GF. Remarkably, employing GF as the solvent for drug-free and drug-loaded Nc solutions resulted in significantly higher viscosity ($p < 0.01$). The viscosities measured for DMSO, GF, Py, and NMP were 4.52 ± 0.01, 17.20 ± 0.20, 13.76 ± 0.20, and 4.88 ± 0.20 cPs, respectively. Thus, the choice of solvent played a role in determining the viscosity of the prepared ISMs.

Typically, a solvent with strong affinity for dissolving a compound can reduce the solution's viscosity due to dominant substance-solvent interaction over substance-substance interaction (226). The addition of Mx clearly increased the viscosity of all ISM solutions, attributed to the substitution of solvent with dissolved drug molecules.

All these solutions exhibited Newtonian flow behavior, displaying a linear relationship between shear stress and shear rate, as depicted in Figure 26B. The extent of 3D network formation within the Nc molecule directly correlated with a substantial increase in the viscosity of these formulations. The Newtonian flow characteristics make these formulations suitable for injection dosage forms, as medical professionals can administer them through a needle by exerting force on a syringe plunger to expel the formulation via the stainless-steel needle (176). When examining the outcomes at a polymer concentration of 15% w/w, the shear stress and viscosity of the Nc solution in NMP were comparable to those of EC and exceeded the values of Eudragit® RS and bleached shellac ISGs in NMP, in line with prior findings (227).

The injectability of the fluid through a syringe and needle, quantified by the force and energy required, is depicted in Figure 26C. The selection of solvent notably influenced the maximum force and energy necessary for injection. All formulations were considered suitable for use as injectable dosage forms, as the applied force remained below 50 N (228). Evidently, the maximum force and energy needed for injecting drug-free and drug-incorporated Nc solutions in GF were significantly higher ($p < 0.01$) compared to those dissolved in Py, DMSO, and NMP. This observation is consistent with previous findings that indicated higher values for zein ISM in GF compared to DMSO (229). The energy required for injecting these Nc ISM solutions was lower compared to that required for polymeric ISGs containing 15% w/w bleached shellac (11.73 mJ) and 15% w/w Eudragit® RS (8.04 mJ) (227). The maximum injection force for all the ISMs studied in this research remained below 5 N, signifying comfortable injection and meeting the criteria for minimal discomfort at the injection site (176). Consequently, all the formulated drug-free and Mx-incorporated Nc-based ISMs were determined to be appropriate for utilization as injectable drug delivery systems, providing convenient administration and ensuring patient comfort and compliance (176).

4.4.2. Water tolerance

The initial phase separation of hydrophobic polymers like Nc within ISMs through solvent removal phase-inversion with water becomes apparent through the observed turbidity during titration with distilled water (198, 208). The capacity of ISMs to tolerate water without undergoing phase separation, referred to as water tolerance, can be assessed based on the cloud point or the minimal percentage of water required. Lower water tolerance indicates a higher susceptibility to phase separation upon exposure to water or a reduced ability of the ISM to withstand water. Figure 27 illustrates the water tolerances of drug-free ISMs. Conspicuously, Nc ISMs

dissolved in DMSO exhibited significantly lower water tolerance ($p < 0.05$) compared to those in NMP and Py. The drug-loaded formulations 0.5Mx15NcGf, 0.5Mx15NcPy, 0.5Mx15NcD, and 0.5Mx15NcN had % water amounts inducing phase separation recorded as 12.50 ± 0.72, 15.44 ± 0.89, 10.14 ± 1.06, and $11.73 \pm 0.74\%$, respectively. However, these values did not exhibit a significant difference compared to NMP, although there was a tendency for them to be lower. In DMSO systems, fatty-acid-based ISGs required less water to reach the endpoint compared to systems utilizing NMP as a solvent. This disparity is attributed to DMSO's greater water miscibility resulting from its higher polarity (189). The enhanced polarity of water in comparison to the solvent present in ISMs contributed to the accelerated phase separation of fatty acids from DMSO. As the aqueous phase infiltrated the ISM system and heightened its polarity, the dissolved fatty acids, including Nc, were no longer capable of maintaining their state within the system, resulting in the formation of a cloudy mass. This decrease in water tolerance due to higher concentrations of matrix-forming agents has been documented in studies involving ibuprofen-based ISGs (230) and fatty-acid-based ISGs (198, 208). In comparison, all Nc ISMs displayed greater susceptibility to water-induced phase separation than ibuprofen-based ISGs. This difference stemmed from the fact that the Nc macromolecule was more prone to separation from the solvent in the presence of a non-solvent, unlike smaller molecules. Given the small volume of this injectable delivery system, it could potentially come into contact with crevicular fluid within the periodontal pocket, triggering phase separation. Prominently, the water tolerances of the ISMs were confined to levels below 18% w/w (Figure 27), indicating that the system could swiftly approach its saturation point due to the escalating hydrophilicity of the system and the limited aqueous solubility of Nc.
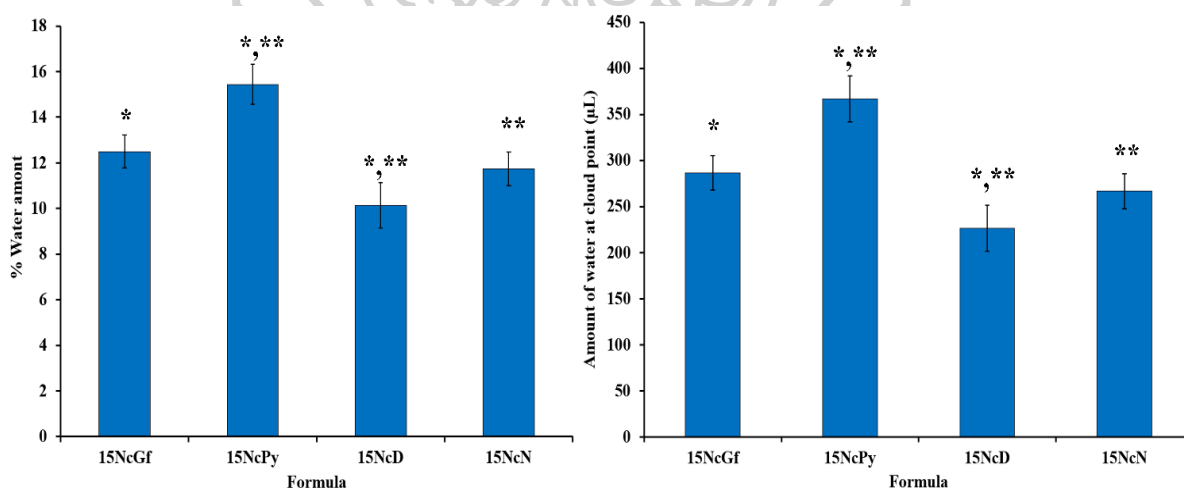
Figure 27. Percentage of water amount and amount of water at cloud point of drug-free and Mx-incorporated Nc-based solutions after titration with deionized water at a temperature of 25 °C (n = 3). The symbols * and ** indicate significant differences ($p < 0.05$) among the tested formulations.

4.4.3. Matrix formation of Mx-loaded Nc-based ISM

Upon injection into PBS in a test tube and agarose wells, the prepared Nc-based ISMs transitioned from a solution into an opaque mass, forming a distinct ring, as depicted in Figure 28. This opaqueness signified the phase inversion of Nc upon encountering water in both PBS and agarose. Comparable observations of such solid-like opaque formations have been documented for ISGs based on natural resins (183, 223) and bleached shellac (194, 227) when exposed to aqueous environments, attributed to their swift phase transformations (230). Importantly, the selection of solvent exerted an influence on the behavior of matrix formation. The Nc present in DMSO formulations underwent a notably swift transformation. This can be attributed to DMSO's higher polarity and water miscibility compared to other solvents, which facilitated rapid water diffusion and induced solvent exchange (189). Moreover, as previously discussed, Nc's heightened sensitivity to water expedited this phase separation process. The relatively rapid transformation of all Nc-ISMs during injection renders them more practically suitable for treating periodontitis. This attribute enhances patient compliance and reduces the risk of formulation leakage from the periodontal pocket (231). However, it remains essential to ensure their capability for controlled drug release and effective antimicrobial activity, particularly against periodontitis-causing pathogens.
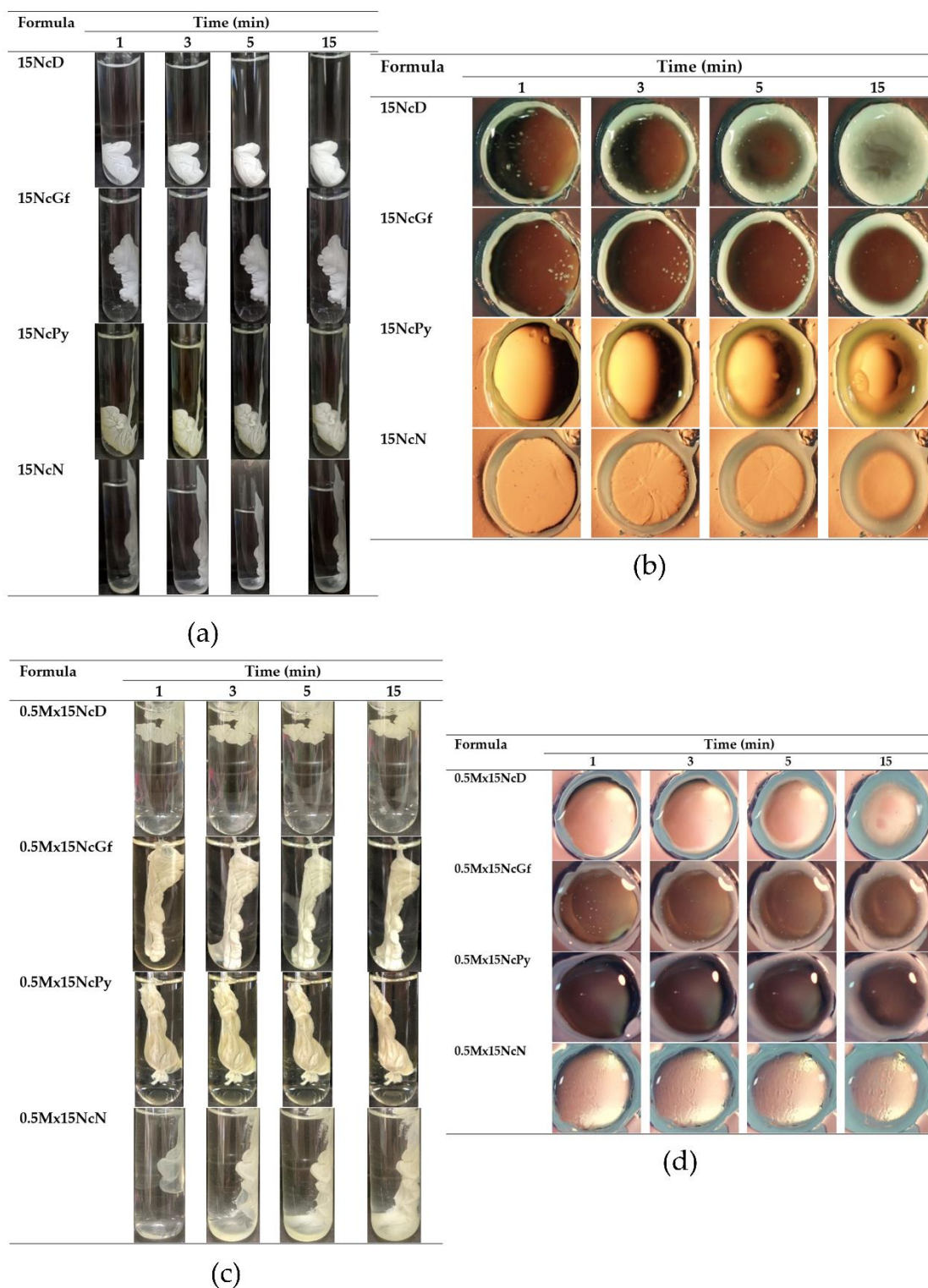
Figure 28. Matrix formation upon injecting formulations into pH 6.8 phosphate buffer (a) and after contact with agarose gel (b) of drug-free Nc-based ISM formulations, and gel formation after injection of the formulations into the phosphate buffer pH 6.8 (c) and after contact with agarose gel (d) of Mx-loaded Nc-based ISMs with different time intervals under a stereomicroscope.

4.4.4. Drug content and release of Mx-loaded Nc-based ISMs

The drug content in samples of Mx dissolved in different solvents, including 0.5MxN, 0.5MxPy, 0.5MxGf, and 0.5MxD, was determined to be 98.27 ± 1.01%, 97.61 ± 0.33%, 99.05 ± 1.06%, and 100.71 ± 0.83%, respectively. Meanwhile, the drug content in drug-incorporated ISMs, namely 0.5Mx15NcN, 0.5Mx15NcPy, 0.5Mx15NcGf, and 0.5Mx15NcD, was measured at 96.46 ± 0.86%, 98.11 ± 0.82%, 97.43 ± 1.27%, and 96.45 ± 0.52%, respectively. The release of Mx from solutions without Nc addition exhibited a rapid release pattern, reaching a plateau within 3 h (Figure 29). In contrast, a slower drug release was observed for all Mx-loaded Nc-based ISMs, with a notable reduction in burst drug release due to the incorporation of Nc. These drug-incorporated Nc-based ISMs showcased a gradual release of Mx during the initial phase of the release profiles. Interestingly, 0.5Mx15NcPy displayed a steeper release at a later stage, indicating a more pronounced and unobstructed release behavior compared to other ISMs. This behavior aligns with the increased pore formation observed in the SEM analysis for 0.5Mx15NcPy. In comparison, the 15% bleached-shellac-based ISG exhibited sustained drug release of approximately 70% over 54 h, emphasizing the pivotal role of polymer concentration in controlling the drug release mechanism (227). The addition of water-soluble additives has been explored as a means to influence the drug release profile. For instance, the incorporation of PEG 1500 has been shown to decrease burst release and enhance sustained release in an Eudragit® RS ISG (180). The incorporation of easily water-soluble compounds can facilitate drug release by promoting high porosity, which in turn leads to increased erosion and subsequent drug release. Commercial products like Atridox® containing DH, utilizing PLA as a polymeric material, have successfully controlled drug release for a period of 1 to 2 weeks (232).

The fitting of drug release profiles, as presented in Table 8, suggests that all ISMs primarily undergo diffusion-controlled drug release, aligning well with Higuchi's equation. Additionally, the estimated "n" values from the Korsmeyer-Peppas equation closely correspond to Fickian diffusion mechanisms. This implies that Mx diffuses through the Nc mass subsequent to its phase inversion into a matrix state. As the solvent content within the ISM diminishes over time, the matrix gradually transforms into a more solid-like matrix. The relatively sharper drug release observed in the initial phase could be attributed to drug diffusion through the matrix state, followed by a slower release through the more solid matrix in the later phase of the release profile. A similar release pattern has been observed for substances like DH and vancomycin HCl released from natural-resin-based ISGs (183, 223). It's important to note that the drug release process is irreversible, as the transformed Nc mass cannot dissolve back into the release medium.
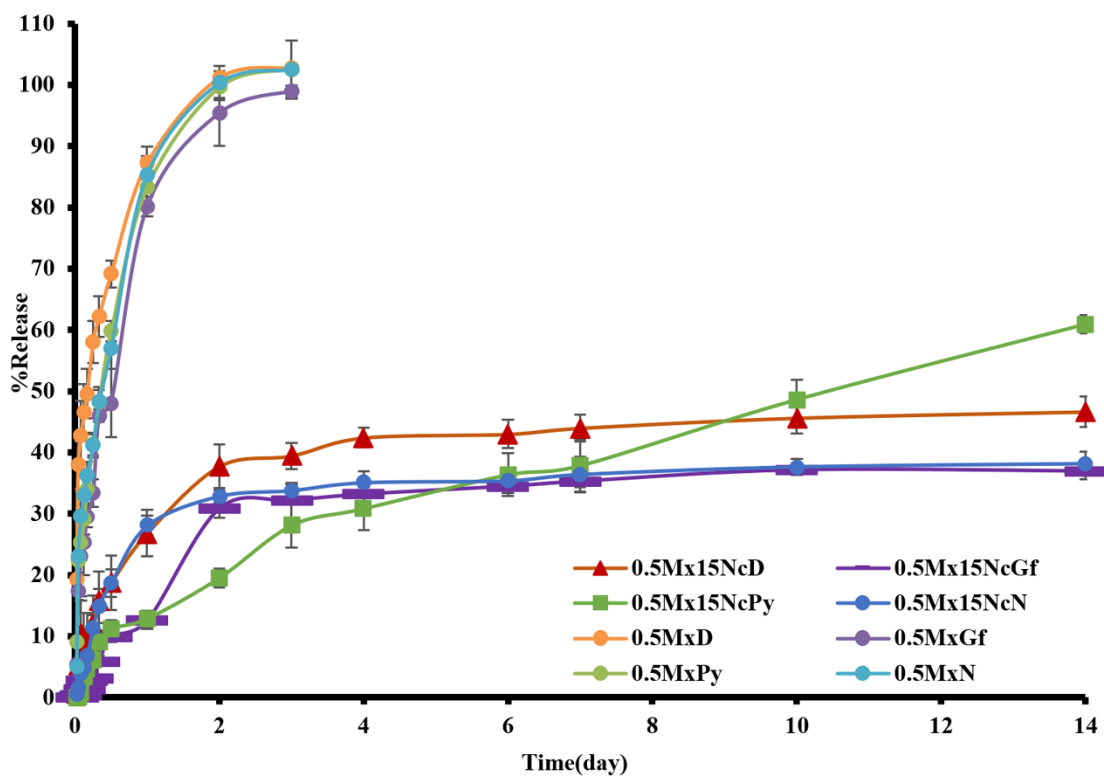
Figure 29. Mx release from Nc-based ISM formulations using the cup method (n = 3).

Table 8. Regression coefficient (r²) and diffusion exponent (n) values derived from drug release profiles of Mx-incorporated Nc-based ISMs fitted to various mathematical equations.

Formula	Zero Order	First Order	Higuchi's	Korsmeyer-Peppas		
	r^2	r^2	r^2	r^2	n	Release Mechanism
0.5Mx15NcD	0.6475	0.4541	0.8074	0.9155	0.298 ± 0.057	Fickian diffusion
0.5Mx15NcGf	0.7150	0.6826	0.8765	0.7805	0.278 ± 0.012	Fickian diffusion
0.5Mx15NcPy	0.9086	0.8892	0.9786	0.9705	0.458 ± 0.047	Fickian diffusion
0.5Mx15NcN	0.5725	0.3375	0.7547	0.8492	0.247 ± 0.053	Fickian diffusion

4.4.5. Scanning electron microscopy (SEM)

The SEM images displayed in Figure 30 offer a visual representation of the surface topography of Mx-loaded Nc-based ISMs formulated using various solvents. These images clearly demonstrate the substantial variation in morphology among these ISMs based on the solvent employed. The choice of solvent notably impacted the surface topography, as depicted in Figure 30a. Specifically, the remnant of 0.5Mx15NcD, following a two-week drug release period, displayed a relatively smooth surface with no apparent pores. Conversely, the remnants of 0.5Mx15NcN and 0.5Mx15NcGf exhibited distinctive rough and undulating surfaces adorned with various open pores. Among them, the surface of 0.5Mx15NcN exhibited a more uniformly distributed arrangement of open pores in comparison to 0.5Mx15NcGf. Importantly, the remnant surface of 0.5Mx15NcPy displayed larger open pores. Cross-sectional views of these ISMs displayed an interconnected porous structure, as depicted in Figure 30b. The presence of a more porous structure on the surface remnants was associated with the heightened drug release observed in 0.5Mx15NcGf, as mentioned earlier. No residual Mx crystals were visible in the remnants, indicating that the drug release had nearly reached completion. Upon contact of the ISM with an aqueous solution, solvent diffusion into the aqueous phase occurred at varying rates due to solvent exchange. This subsequent phase separation of Nc resulted in the immediate formation of a sponge-like structure with a porous surface (229).

In contrast, the topography of the Nc sponge showcased a more uniform and interconnected cellular structure compared to the zein sponge-like ISM remnant discussed in earlier studies (229). The existence of pores within the sponge structure acted as conduits for the release of drug molecules from the internal matrix. The generation of these pores in ISMs is commonly influenced by the speed of solvent exchange (223, 229). Research conducted on propolis and benzoin-based ISGs has indicated that a slower rate of matrix formation leads to increased drug release. Additionally, benzoin-based ISGs possessing hydrophobic traits are better suited for controlling drug release (223). Hence, the properties related to matrix formation and the speed of solvent exchange play a pivotal role in influencing drug release patterns and the sponge-like surface structure of ISM matrices.

Upon interaction with an aqueous phase or bodily fluids, ISMs undergo a phase inversion process within Nc solutions. This process results in the polymer separating into a matrix state and subsequently forming a solid matrix-like structure. A parallel can be drawn between this process and the critical physicochemical parameters that govern drug release modulation in PLGA *in situ* implants, as elaborated by Parent et al. (233). The components utilized in ISGs can also be adapted for creating in *situ* forming scaffolds, a technique often employed in tissue engineering endeavors (233, 234). Examination of the remnants through microphotographs following the release test highlights the existence of pores within the matrix, underscoring the pivotal role of solvent exchange in regulating drug release from Nc-based ISM matrices.
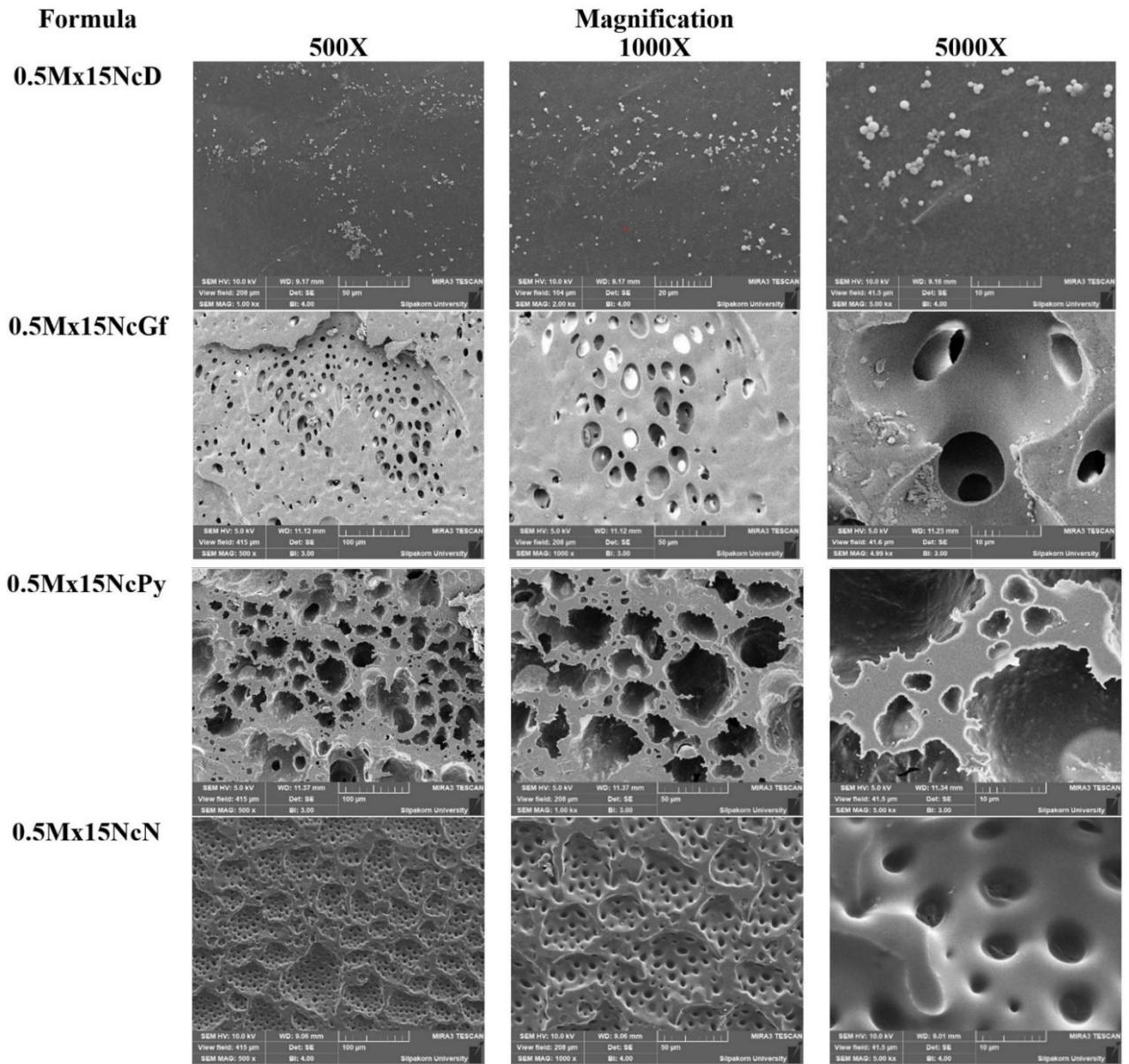
Formula	Magnification		
	500X	1000X	5000X

0.5Mx15NcD

0.5Mx15NcGf

0.5Mx15NcPy

0.5Mx15NcN

(a)

Figure 30. SEM images depicting surface (a) and cross-section (b) views of freeze-dried Mx-loaded Nc-based ISMs captured at varying magnifications (500x, 1000x, and 5000x).

Formula	500X	Magnification 1000X	5000X
0.5Mx15NcD			
0.5Mx15NcGf			
0.5Mx15NcPy			
0.5Mx15NcN			
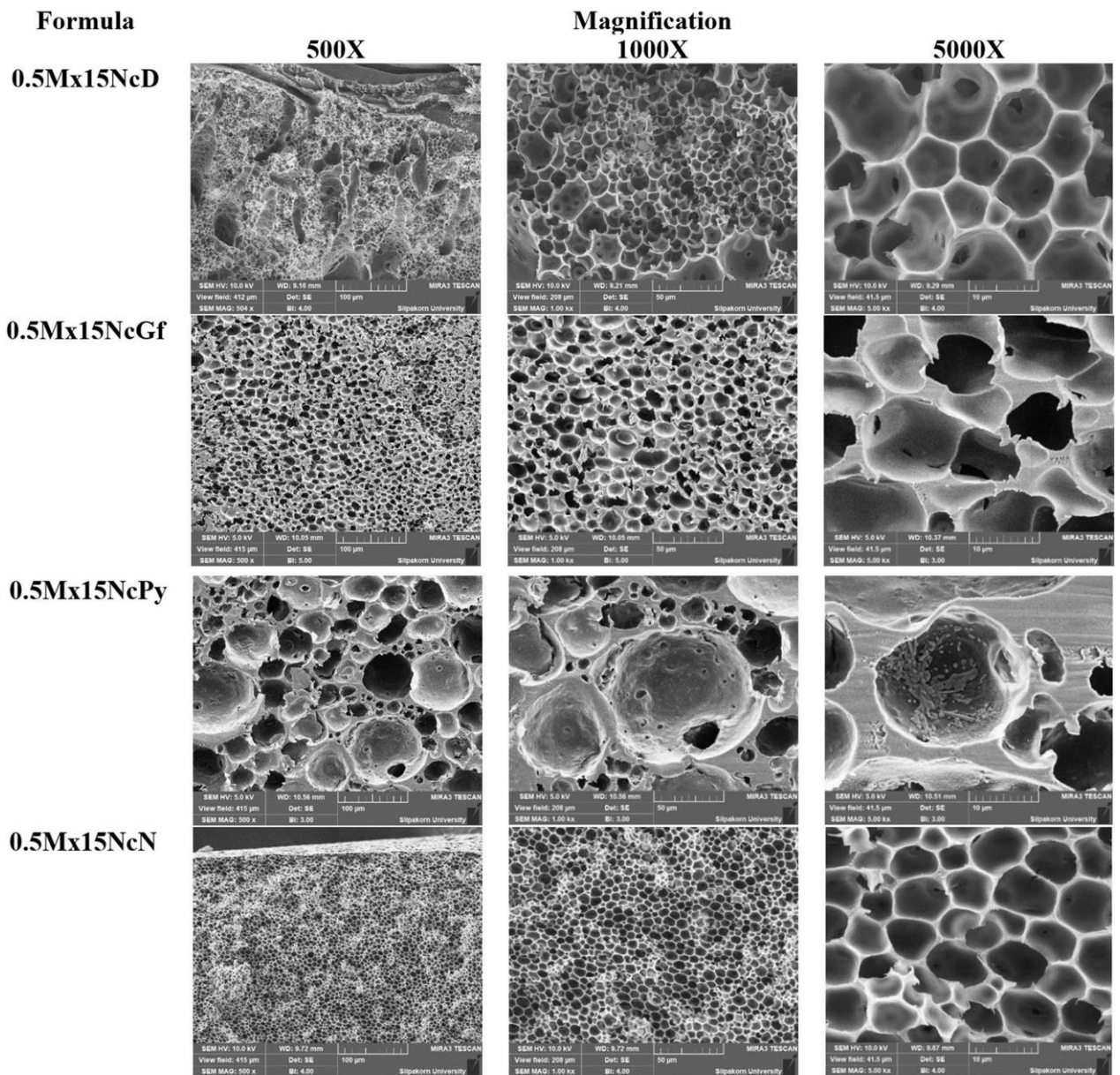
(b)

Figure 30. SEM images depicting surface (a) and cross-section (b) views of freeze-dried Mx-loaded Nc-based ISMs captured at varying magnifications (500x, 1000x, and 5000x) (continued).

4.4.6. *In vitro* degradation

The primary objective of this study was to explore the *in vitro* degradation patterns of the Nc-incorporated ISMs by quantifying the mass loss. The percentage of *in vitro* degradation for these ISMs during a one-week period is graphically illustrated in Figure 31, and the corresponding values for $\%w_{ex}$ (weight loss due to extractables) and $\%w_{obt}$ (weight loss due to biodegradation) are calculated and detailed in Table 9. To evaluate *in vitro* degradation, the ISMs were subjected to incubation within a release medium at a specific pH, which is a commonly employed approach for degradation assessment (235). A rapid initial decrease in mass was observed across all ISMs within the first day, highlighting the diffusion of both Mx and the solvent into the release medium through solvent exchange. As the steady state of solvent and drug release was achieved, the overall mass loss of the ISMs progressively escalated, eventually reaching a plateau. This behavior was significantly influenced by water absorption. Among the ISMs evaluated, 0.5Mx15NcPy exhibited a slightly reduced percentage of degradation in comparison to the other formulations. This trend corresponded to its lower drug release during the initial phase.

The degradation parameters $\%w_{ex}$ and $\%w_{obt}$ have been previously utilized to evaluate the *in vitro* degradation of ISMs based on Eudragit® polymers for controlled periodontal drug delivery (236). $\%w_{ex}$ reflects the degradation considering that the formed matrix remained intact and the solvent was completely removed, inclusive of the weight of the released drug. Conversely, $\%w_{obt}$ accounts for the degradation of the formed matrix and is anticipated to be lower than $\%w_{ex}$. A higher $\%w_{obt}$ compared to $\%w_{ex}$ signifies incomplete solvent exchange, indicating that the system required a longer duration to achieve complete solvent exchange. In this study, the $\%w_{obt}$ values of all ISMs at the concluding time point were found to be lower than $\%w_{ex}$, signifying the degradation of the formed matrix in all ISMs. The gradual erosion of the Nc matrix from the scaffold could occur over the course of time in the release medium, providing additional evidence for the degradation of the formed matrix. These findings underscore the potential of this system for effective drug delivery within periodontal pockets.

The degradation rate and extent of degradation are often influenced by the polymer content. In the case of these ISMs, the relatively lower polymer content contributed to a higher degradation rate and a more significant amount of degradation. In contrast, commercial products like Atridox® utilize a higher polymer content (37.5% PLA in NMP) to achieve controlled drug release (232). The observed % degradation in this study was affected by factors such as the solubility of the drug, the composition of the solid matrix, and the miscibility of the solvent. Nc, known for its non-toxic properties, has been explored in diverse applications such as immobilizing nucleic acids and proteins in blotting techniques, as well as in wound-healing bandages (99, 101, 103). Therefore, Nc demonstrates promising potential as a valuable polymer for serving as the primary constituent in ISMs designed for the treatment of periodontitis.
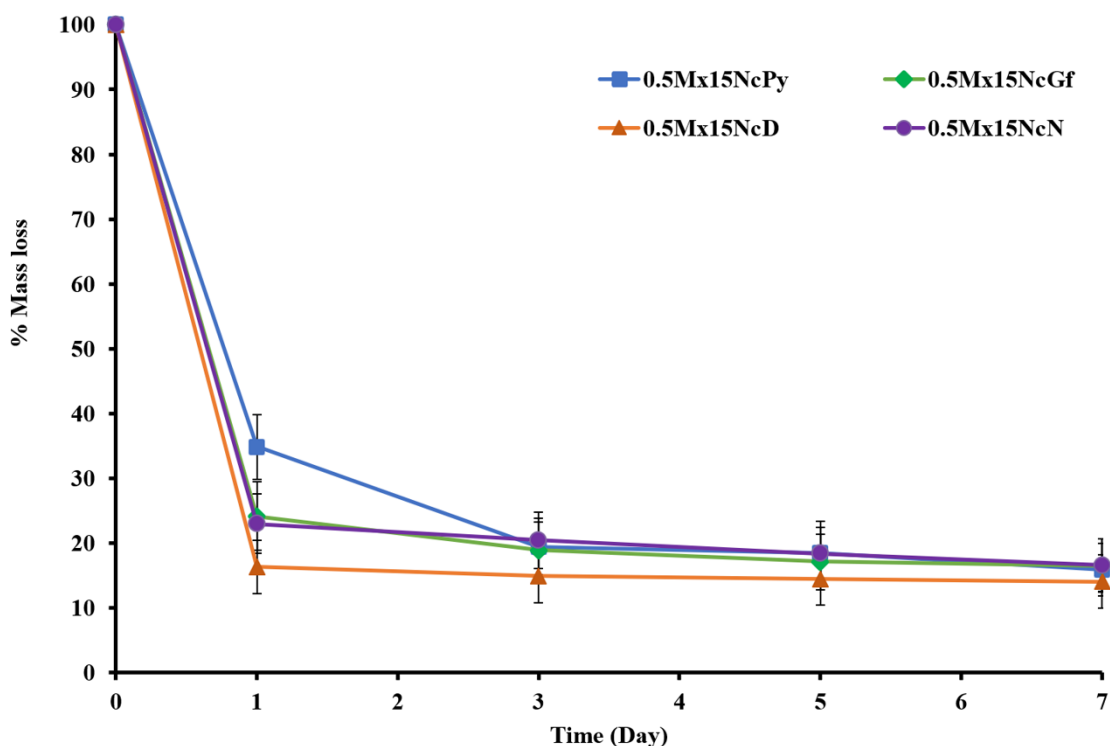
Figure 31. Percentage of mass loss observed in Mx-loaded Nc-based ISMs (n = 3).

Table 9. Degradation parameters for Mx-incorporated Nc-based ISMs.

Day	% Obtained Remaining Weight (%w_{obt})				% Experimental Remaining Weight (%w_{ex})			
	0.5Mx15NcD	0.5Mx15NcGf	0.5Mx15NcPy	0.5Mx15NcN	0.5Mx15NcD	0.5Mx15NcGf	0.5Mx15NcPy	0.5Mx15NcN
1	14.2	21.7	26.9	17.5	21.6	27.2	33.7	28.7
3	13.6	18.2	17.6	16.8	15.2	23.4	29.2	22.4
5	13.8	16.3 *	17.0	15.4	13.4	20.5	25.1	20.7
7	12.5	14.6 *	16.2	15.2	13.1	19.6	22.6	20.9

* Denotes a significant difference (p < 0.05) among the analyzed formulations.

4.4.7. X-ray computed microtomography (μCT)

X-ray computed tomography (μCT) is a non-destructive imaging technique that offers three-dimensional insights into the internal features and characteristics of objects (237). In this research, synchrotron-based X-ray tomographic images of the remnants from Mx-loaded Nc-based ISMs are showcased in Figure 32. The images portray the three-dimensional volume of the remnants on the left, while the cross-sectional views on the right unveil the presence of internal pores within the remnants, providing valuable data about their porosity. The application of X-ray tomographic imaging in this study brings several advantages over traditional SEM. While SEM delivers detailed information about specific regions, X-ray tomography permits a holistic examination of the entire remnant structure. The X-ray tomography images

not only validated the sponge-like surface topography of the remnants but also offered insights into their internal structures that might not be fully captured by SEM.

The remnant of 0.5Mx15NcN exhibited a higher porosity compared to 0.5Mx15NcD, 0.5Mx15NcPy, and 0.5Mx15NcGf, as indicated in Figure 32. This disparity in porosity could be attributed to structural alterations that took place during the freeze-drying process. The remnants displayed features resembling macrovoids or finger-like structures, resembling the architecture of an asymmetric membrane with a thin upper skin layer supported by a sublayer of finger-like projections. This finger-like structure formation typically involves two sequential processes: pore initiation and subsequent growth (238). During the liquid-liquid phase separation process of the Nc-based solution, the emergence of Nc-rich and Nc-lean phases triggers the inception of nuclei that contribute to the formation of finger-like structures. These nuclei primarily develop beneath the upper layer and their growth is contingent upon the condition of the solution at the interface of the phase separation (239). The spontaneous generation of scaffold-like structures is a distinctive trait of injectable *in situ* forming systems for bioactive compound delivery. Consequently, X-ray tomographic imaging proves to be an invaluable technique for examining and visualizing the three-dimensional shapes and porosity attributes of these systems. It offers significant insights into the inner structure and porosity of the remnants, thereby assisting in comprehending and characterizing the Nc-based ISMs.
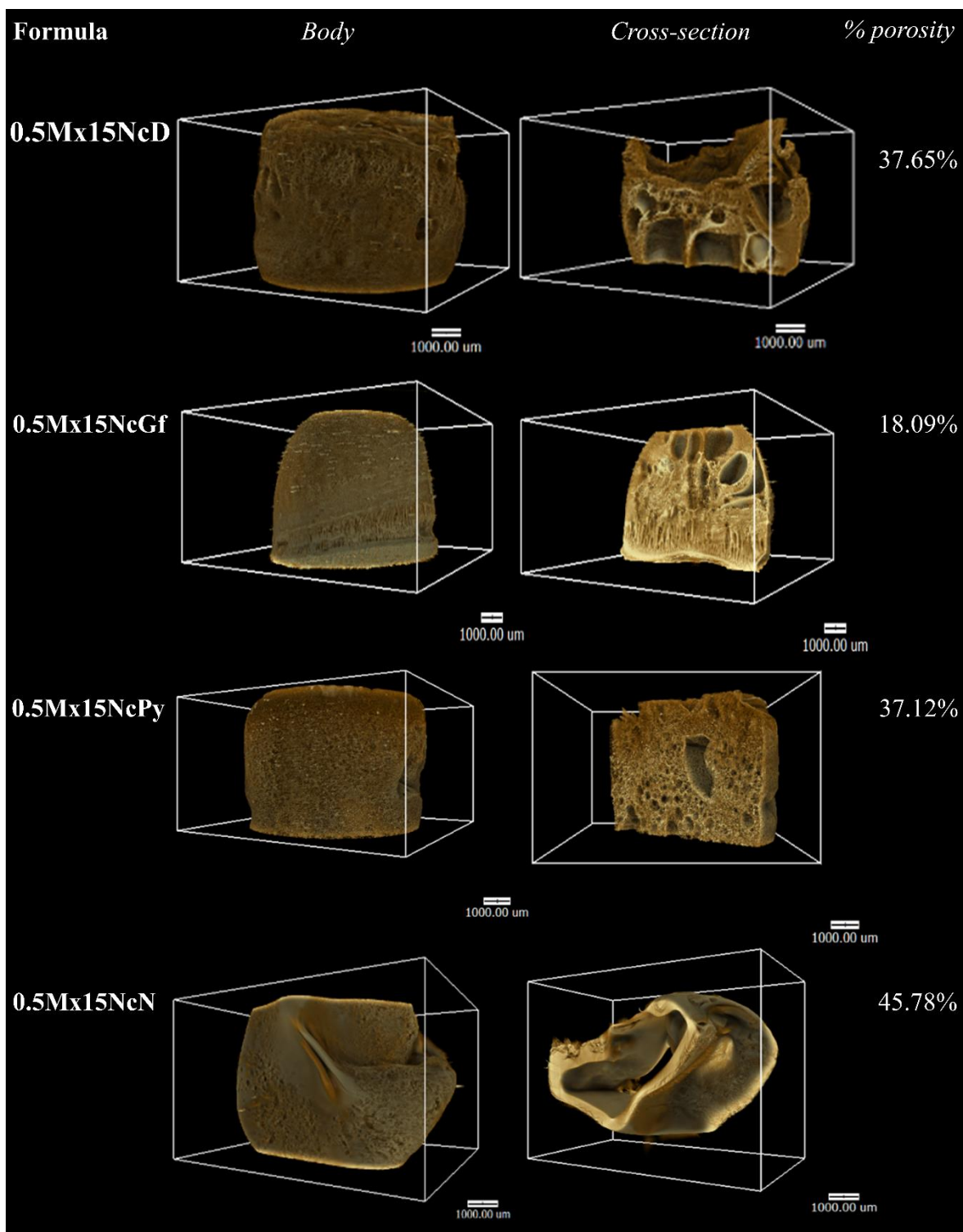
Figure 32. X-ray tomography image and percentage porosity via X-ray tomography of freeze-dried Mx-incorporated Nc-based ISMs.

4.4.8. Antimicrobial activities

A comprehensive overview of the zone of inhibition (ZOI) diameters for solvents, Nc solutions, drug-free Nc ISMs, and Mx-loaded Nc ISMs when tested against a range of microbial strains, including *S. aureus* ATCC 6538, *S. aureus* ATCC 43300 (MRSA), *S. aureus* ATCC 6532, *S. aureus* ATCC 25923, *A. actinomycetemcomitans* ATCC 29522, and *P. gingivalis* ATCC 33277, is provided in Table 10. Illustrative images from the antimicrobial tests against *S. aureus* ATCC 4430 (MRSA), *P. gingivalis* ATCC 33277, and *A. actinomycetemcomitans* ATCC 29522 are depicted in Figure 33. These microorganisms are relevant to periodontitis, with *P. gingivalis* and *A. actinomycetemcomitans* being particularly associated with the disease. *S. aureus* is known to be present in periodontitis (240) and its biofilm-forming ability can lead to antibiotic resistance challenges (241, 242). The organic solvents NMP, DMSO, Py, and GF are commonly employed in the production of depot dosage forms owing to their established safety profiles and minimal toxicity (85, 110, 118, 243). Among the tested solvents, Py exhibited stronger antimicrobial activity against the tested microbes in comparison to NMP. Meanwhile, GF and DMSO demonstrated comparatively lower activities than Py and NMP, as detailed in Table 10. These solvents possess the capability to dissolve lipid components present in bacterial cell envelopes, thereby interfering with nutrient transport processes within the bacteria. As a result, these solvents are well-suited for integration into ISMs, functioning as delivery systems for antimicrobial agents in the treatment of infectious diseases. By leveraging their ability to enhance penetration and permeability through cell membranes, they can augment the overall effectiveness of antimicrobial treatments (107, 244, 245).

Upon incorporating the Nc polymer into the solvent systems, a noticeable reduction in the ZOI was observed for all solvents, as detailed in Table 10. This decrease in ZOI can be attributed to the heightened viscosity introduced by the presence of Nc, coupled with the absence of inherent antibacterial properties within Nc. In numerous instances, the drug-free Nc-based ISMs displayed significantly narrower ZOIs in comparison to their corresponding solvents (p < 0.05). The integration of the Nc network, once dissolved within the ISMs, effectively hindered solvent diffusion, resulting in escalated environmental viscosity and subsequently leading to the reduction in ZOI.

However, the incorporation of the antibacterial drug Mx notably augmented the antibacterial effectiveness of both the polymer-free ISMs and the Nc-based ISMs. The presence of Nc substantially decreased the ZOI values for nearly all the prepared ISMs (p < 0.05). Despite this reduction, a substantial and significant ZOI remained evident against all the tested microbial strains. This underscores the efficacy of Mx, a fourth-generation fluoroquinolone antibiotic, in inhibiting the growth of the tested bacteria. While bacteria are linked to periodontal disease, successful treatment also involves shielding against inflammation and oxidative stress. Consequently, the incorporation of antimicrobials, antioxidants, and anti-inflammatory agents alongside osteogenic active components into drug delivery systems has emerged as an intriguing

avenue (246, 247). Furthermore, it is important to explore the potential for optimization in the development of ISMs through the utilization of design of experiments (DOE) (248). Nowadays, a multitude of cutting-edge technologies, including foam engineering (249), metal-doped graphene models (250), metal-coupled fullerene synthesis (251), and nanocages, hold promise for advancing drug delivery systems like ISMs. These innovations warrant exploration to potentially enhance their utility as intelligent and targeted drug delivery approaches (252). Interest in engineered metal-organic frameworks (MOFs) with controlled sizes for biomedical applications has grown significantly in recent decades (253-255). The tunable porosity, chemical composition, size, shape, and surface functionalization capabilities of MOFs make them increasingly attractive for drug delivery purposes; therefore, the application of MOFs as drug delivery features for ISMs should be of interest for further investigations.
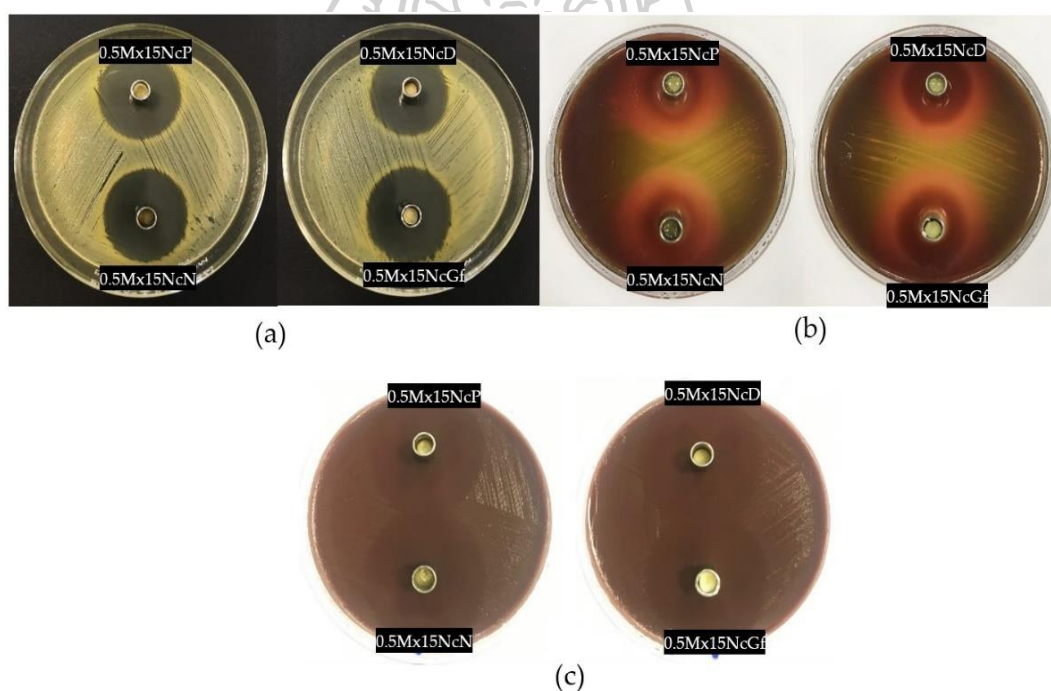
Figure 33. Photographs depicting the inhibition zones of 0.5Mx15NcP (upper-left cup), 0.5Mx15NcD (upper-right cup), 0.5Mx15NcN (lower-left cup), and 0.5Mx15NcGf (lower-right cup) ISM formulations against *S. aureus* 43300 (MRSA) (a), *P. gingivalis* (b), and *A. actinomycetemcomitans* (c) (n = 3).

Table 10. Inhibition zone diameters of solvents, drug solutions, drug-free Nc-based ISMs, and Mx-incorporated Nc-based ISM formulations against different strains of *S. aureus*, *P. gingivalis*, and *A. actinomycetemcomitans* (n = 3).

Formula	Inhibition Zone $\pm$ S.D. (mm)					
	S. aureus 6538	*S. aureus* 43300 (MRSA)	*S. aureus* 6532	*S. aureus* 25923	*P. gingivalis* ATCC 33277	*A. actinomycetemco mitans* ATCC 29522
NMP	15.0 ± 0.8	15.7 ± 0.5	14.0 ± 0.8	13.7 ± 0.5	15.7 ± 0.5	42.0 ± 1.6
2-PYR	17.7 ± 0.5	18.7 ± 0.9	16.7 ± 1.2	15.7 ± 0.5	20.7 ± 0.9	42.3 ± 0.5
DMSO	11.3 ± 0.5	12.0 ± 0.0	10.0 ± 0.8	9.7 ± 0.5	17.3 ± 0.5	26.3 ± 0.9
Glycerol formal	11.3 ± 0.5	11.3 ± 0.5	11.0 ± 0.8	13.3 ± 0.5	16.0 ± 0.8	32.0 ± 0.8
15NcN	11.3 ± 0.5 *	13.7 ± 1.2	14.0 ± 1.6	11.7 ± 1.2	12.0 ± 0.8	34.7 ± 0.9 *
15NcPy	12.0 ± 0.8 *	15.7 ± 1.2 *	13.7 ± 1.2	12.7 ± 0.5 *	13.7 ± 1.7 *	34.7 ± 1.2 *
15NcD	9.7 ± 0.5	10.0 ± 0.8	10.3 ± 0.5	- *	14.3 ± 1.2	21.3 ± 0.5 *
15NcGf	- *	12.0 ± 0.8	12.7 ± 1.2	10.0 ± 0.0	15.0 ± 0.8	29.7 ± 1.2 *
0.5MxN	32.0 ± 0.8	31.3 ± 0.5	33.0 ± 0.8	30.3 ± 0.5	29.0 ± 2.4	44.3 ± 0.5
0.5MxPy	33.3 ± 0.5	32.3 ± 0.5	33.3 ± 0.9	32.7 ± 0.5	25.7 ± 0.9	45.0 ± 0.8
0.5MxG	37.7 ± 1.2	37.0 ± 0.8	38.0 ± 0.8	35.3 ± 0.5	34.7 ± 0.5	45.0 ± 0.8
0.5MxD	37.7 ± 0.5	37.7 ± 0.5	37.7 ± 0.9	35.3 ± 0.9	32.7 ± 0.9	45.7 ± 0.9
0.5Mx15NcN	28.7 ± 0.5 **	29.7 ± 1.2	30.0 ± 1.6	27.0 ± 0.8 **	25.7 ± 0.9	39.7 ± 0.5 **
0.5Mx15NcPy	26.7 ± 0.5 **	28.3 ± 0.5 **	28.0 ± 0.8**	27.0 ± 0.0 **	27.0 ± 0.8	40.7 ± 0.5 **
0.5Mx15NcGf	32.7 ± 0.5 **	31.0 ± 0.0 **	32.7 ± 0.5	30.0 ± 0.0 **	26.7 ± 0.5 **	41.0 ± 0.8
0.5Mx15NcD	33.7 ± 0.5 **	31.7 ± 0.5 **	34.0 ± 0.8**	29.3 ± 1.2 **	27.3 ± 0.9 **	43.3 ± 0.5 **

"-" = no inhibition zone; the asterisk "" indicates a significantly ($p < 0.05$) lesser inhibition zone diameter than that obtained using the pure solvent; the asterisks "**" indicate a significantly lesser inhibition zone diameter than that obtained using the drug-loaded solvent; established by using one-way ANOVA followed by an LSD post-hoc test.*

4.5 Summary

The study examined the impact of different solvents, such as NMP, DMSO, Py, and GF, on the physical and chemical characteristics as well as the bioactivity of Mx-incorporated Nc-based ISMs designed for delivering drugs to periodontal pockets. Among the investigated parameters, the viscosity and the force necessary for injecting drug-free and Nc-containing ISMs were notably elevated when GF was employed as the solvent, in comparison to Py, DMSO, and NMP. All the tested formulations demonstrated a Newtonian flow behavior, and they underwent a transition from a liquid solution to a matrix-like state over time when exposed to an aqueous environment. This transformation led to the formation of a more solid-like matrix structure. Despite this transformation, the injection force required for these ISMs remained low, indicating their ease of administration and high level of acceptability. This characteristic ensures convenient delivery and patient compliance. Among the solvents studied, the Nc-based ISMs prepared in DMSO displayed a higher sensitivity to water, leading to a more rapid matrix transformation. However, all the Nc-based ISMs exhibited water sensitivity and underwent a phase transition from a clear solution to an opaque matrix upon exposure to water. This behavior highlights their potential as *in situ* forming dosage forms triggered by aqueous environments. The incorporation of Nc into the ISMs contributed to prolonged drug release, with the Nc

matrix effectively controlling the release of Mx for up to two weeks in simulated crevicular fluid. Additionally, the initial burst release of the drug was mitigated by the presence of Nc in the ISM matrix. SEM and X-ray imaging demonstrated that the choice of solvent influenced the formation of distinct sponge-like 3D structures and porosity within the dried Nc scaffold. This phenomenon was attributed to the process of solvent exchange occurring with the release medium, alongside the simultaneous outward diffusion of the solvent. As a result, the primary mass loss during drug release could be attributed to these mechanisms. Incorporating Nc into the ISMs had the effect of mitigating both solvent and drug diffusions, which consequently led to a reduction in the diameter of the zone of bacterial growth inhibition. This outcome indicated that Nc had a substantial impact on modulating the release behavior and antimicrobial activity of the ISMs. Nonetheless, the developed Mx-incorporated Nc-based ISMs proved to be highly effective in inhibiting the growth of various strains of *S. aureus*, including MRSA, as well as the two pathogens associated with periodontitis, namely *A. actinomycetemcomitans and P. gingivalis*. This success underscores the potential of the localized delivery of Mx via the fabricated Nc-based ISMs. These ISMs, formulated using DMSO and NMP as solvents, which undergo a transformation into matrices upon exposure to aqueous conditions, act as carriers for Mx-incorporated Nc matrices and subsequent matrices. This strategy enables sustained drug release while maintaining efficient antibacterial activity. Nevertheless, further investigations through clinical experiments are imperative to evaluate the efficacy and safety of these Mx-incorporated aqueous-induced Nc-based ISMs comprehensively.

Levofloxacin HCl-loaded zein ISM for periodontitis treatment

4.6. Zein-based ISM

4.6.1. Viscosity and rheological behavior

The impact of varying zein concentrations on the apparent viscosity of ISM formulations is portrayed in Figure 34a. As the zein concentration rises, there is a concurrent increase in the apparent viscosity of the ISM formulations. The viscosities for Lv20ZD, Lv25ZD, Lv20ZG, and Lv25ZG were 376.37 ± 1.90, 759.09 ± 2.32, 1353.85 ± 14.37, and 7694 ± 6.08 cP, respectively. Additionally, employing DMSO as a solvent resulted in lower viscosity due to its lower viscosity and zein's more soluble nature compared to GF. Generally, using a suitable solvent for dissolving a substance can decrease the viscosity of the mixture by favoring substance-solvent interactions over substance-substance interactions (226, 256-258). The presence of dissolved zein led to an increase in viscosity in the formulations due to its large protein structure in the solution (259). While zein is generally insoluble in water, it behaves as a globular protein in nonaqueous solutions, demonstrating conformational characteristics similar to those of more conventionally behaving globular proteins (260). The intrinsic viscosity of bleached shellac dissolved in NMP was found to be higher compared to its dissolution in DMSO and PYR. This suggests that NMP is an effective solvent for dissolving shellac (226, 256). Polymers exhibit varying chain configurations in different dispersing fluids due to their distinct affinities with solvents (256). The interaction between polymers and solvents is particularly pronounced in dilute polymeric solutions, leading to increased viscosity as solvent power increases. Conversely, at higher polymer concentrations, poor solvents exhibit higher viscosity compared to good solvents (257).

Nevertheless, the viscosity of zein ISM systems increased when the drug was incorporated due to a lower solvent content in the system (258, 260-262). This leads to an increase in viscosity within these systems. Previously, various polymers like EC, bleached shellac, Eudragit® RS, PLA, and PLGA have been explored as matrix-forming agents in ISG systems. However, these materials often result in high-viscosity ISGs with compromised injectability (194, 262). As an illustration, ISGs based on 25-35% (w/w) PLA and PLGA exhibit viscosities ranging from approximately 44,200 to 204,400 cPs (262). Hence, the zein-based ISM demonstrated lower viscosity. However, viscosity also impacts the diffusion of substances within the solidifying matrix. Higher viscosity typically hinders water penetration and drug diffusion, leading to reduced initial burst drug release and delayed polymer degradation.

The rheological characteristics of the prepared ISM formulations are depicted in Figure 34b. All the formulations displayed a linear correlation between shear stress and shear rate. The shift of the curve towards higher shear stress values was attributed

to the more condensed zein structure within the formulations. As a result, the prepared formulations demonstrated a Newtonian flow pattern. These findings were consistent with a previous study reporting Newtonian flow behavior in polymer solutions (263). Furthermore, the increased formation of a three-dimensional network within the zein molecules corresponded to a significant elevation in the viscosity of these formulations (260, 261). Given their Newtonian flow behavior, these formulations have been deemed suitable for injection-based dosage forms. This is particularly relevant in medical and dental applications, as injections through needles are feasible, with the force applied to the syringe plunger effectively expelling the formulation through the stainless steel needle (176).
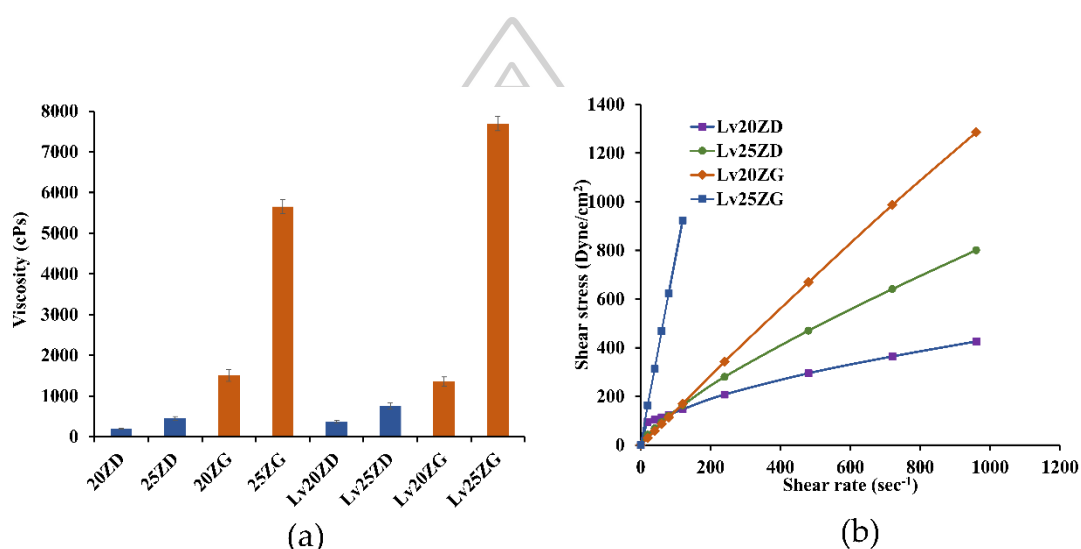
Figure 34. Viscosity (a) and shear stress-shear rate relationship (b) of zein-loaded ISM formulations at 25 °C. The data is presented in triplicate.

4.6.2. Injectability

In the context of dosage form design, ISMs are intended for precise administration through targeted injections into the human body. Thus, the formulation needs to be in a fluid state to ensure painless and efficient injection (264). Moreover, the use of a higher force of expulsion indicates reduced injectability. The force and energy required for injection, obtained from the injectability assessment of the formulated preparations, are presented in Table 11. Evidently, ZG25 and LvZG25 formulations necessitated greater force and energy for injection compared to the other formulations (p-value < 0.05), particularly zein in DMSO-based formulations. Additionally, with an increase in zein concentration from 20% w/w to 25% w/w in both DMSO and GF formulations, the work needed to expel the formulation through the needles also demonstrated a significant increase (p < 0.05), aligning with the observed viscosity outcomes (265). This highlights the significant influence of solvent type and zein concentration on the required force and energy for injection. Nevertheless, the findings indicated that most ISM formulations demanded a relatively lower injection force (<5 N). Especially, despite the higher force of

injectability associated with the ISM system prepared using GF as a solvent compared to other formulations, it could still be comfortably administered through the employed needle. Interestingly, despite the higher viscosity attributed to the polymeric nature of zein-based ISM systems, their expulsion work was evidently lower than that of bleached shellac, EC, and Eudragit® RS ISG systems (194, 258). Practically, the complete expulsion of each solution required less than 50 N.mm, underscoring their suitability within the acceptable injection criteria (228).

Table 11. Injectability characteristics of zein-loaded ISM formulations (n = 3).

Formula	Injectability Force	Work of injectability (N.mm)
20ZD	1.02 ± 0.08	7.51 ± 0.15^c
25ZD	1.19 ± 0.05	$9.13 \pm 0.21^{c, e}$
20ZG	1.07 ± 0.10^a	13.75 ± 0.95^f
25ZG	3.02 ± 0.04^a	42.31 ± 1.23^f
Lv20ZD	1.00 ± 0.04	$7.09 \pm 0.17^{\,d}$
Lv25ZD	1.14 ± 0.03	$12.34 \pm 0.21^{d, e}$
Lv20ZG	1.15 ± 0.06^b	15.20 ± 0.40^g
Lv25ZG	3.07 ± 0.13^b	44.75 ± 1.14^g

The superscripts (a–g) in the column represent a significant difference within the tested formulations (p < 0.05).

4.6.3. Matrix formation

Upon injection of the formulation into PBS at pH 6.8, a process of solvent removal phase-inversion ensued. Consequently, the outer portion of all formulations swiftly formed an opaque skin, while the matrix transitioned into a pale-yellow solid mass, as depicted in Figure 35. Typically, the expedited phase separation rate of the ISM was attributed to the presence of a higher concentration of loaded polymer (258). Upon contact with the PBS solution, formulations containing higher zein concentrations (20% and 25%) underwent an instantaneous transformation into a matrix state, descending to the bottom of the PBS. With an increase in zein content, the matrix appeared cloudier, resembling a solid-like matrix. The observation of a solid-like opaque appearance was reminiscent of what is seen in PLGA-based ISGs after exposure to an aqueous phase, attributed to the polymeric phase inversion process (266). Furthermore, the choice of solvent (GF and DMSO) also influenced the initiation of matrix formation (208). Zein-based formulations dissolved in DMSO exhibited a faster transformation into a gel matrix compared to those in GF formulations. This disparity is attributed to DMSO's higher polarity and greater miscibility with water, which promotes faster water diffusion and facilitates solvent elimination. Viscosity also played a role in the matrix formation of the ISM system. Specifically, ZG's higher viscosity in comparison to ZD resulted in reduced water diffusion within the system. Consequently, the rapid phase inversion of ZD,

transitioning from a solution to a matrix-like state, was apparent due to its lower viscosity facilitating solvent exchange (124). Nonetheless, all zein-based ISMs exhibited a swift and full transformation within just 30 minutes. This rapid transformation during the injection process enhances the practicality of periodontitis treatment, boosts patient compliance, and prevents any inadvertent formula leakage from the periodontal pocket (231).
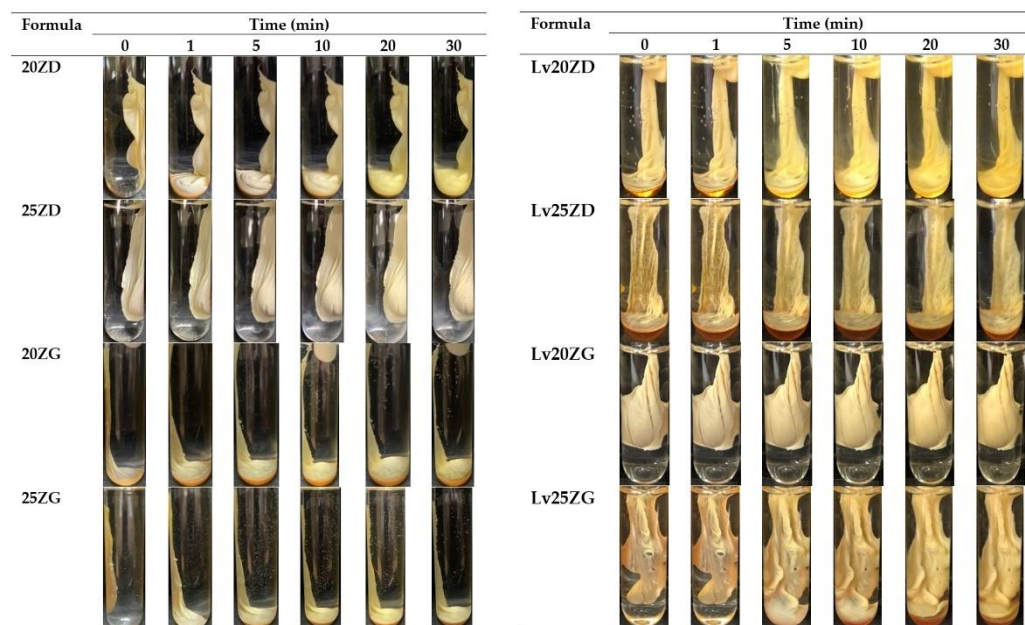
Figure 35. Matrix formation of drug-free and Lv-loaded zein-based ISM formulations upon injection into phosphate buffer at pH 6.8.

Additionally, the investigation into the transformation of these zein-based ISMs within agarose agar yielded insights into the matrix formation process. A thinner opaque layer emerged over time, marking the transformation at the interface of the contact surface (depicted in Figure 36). The phase transition of zein-based ISMs initiated the development of an outer matrix layer initially, with the polymer interior gradually evolving into a stable matrix. In all formulations, a matrix layer formed within the first minute upon contact with the aqueous phase of the agarose gel. Subsequently, Lv20ZD and Lv25ZD formulations displayed complete opaque matrix formation within 25 minutes. Due to its lower viscosity, DMSO effectively facilitated the matrix formation of the zein-based ISMs compared to GF, as the rate of solvent exchange played a crucial role in driving the matrix formation process (181, 182). The sequence of solvent viscosity followed the pattern: GF > triacetin > PYR > isopropyl myristate > NMP> DMSO [53]. Notably, ISM systems dissolved in DMSO exhibited swift matrix formation due to the solvent's relatively high polarity. This polarity facilitated rapid diffusion of DMSO into water, expediting solvent removal and thereby promoting the matrix formation process (226, 267). Comparatively, the dense

matrix obtained from drug-free and Lv-loaded 25% zein ISMs seemed to act as a barrier that slowed down the process of solvent exchange, thereby hindering the complete formation of an opaque matrix. The more porous gel-like matrices of drug-free and Lv-loaded 25% zein ISMs almost entirely filled the agarose well, as depicted in Figure 36. The incorporation of Lv appeared to enhance the zein matrix formation. Consequently, the presence of dissolved Lv contributed to the acceleration of matrix formation in the exchange region due to its hydrophilic nature. Additionally, for periodontitis treatment, a 5% DH ISG transformed into a matrix by utilizing a 30% w/w Eudragit® RS matrix-forming agent (194), whereas, a concentration of 0.75% vancomycin HCl facilitated the process of gel formation in saturated fatty acid-based ISG, which is intended for patients with joint infections following total knee arthroplasty (208). The efficient transformation indicated the high permeability of the formed matrices to aqueous substances. A small volume of less than 50 µL of ISM loaded with antibacterial agents could be easily injected into the periodontal pocket for the treatment of periodontitis (34, 231). Therefore, the crevicular fluid could interact with this substantial surface area relative to the ISM's mass, prompting a phase transition within the zein matrix that governs the modulation of drug release.
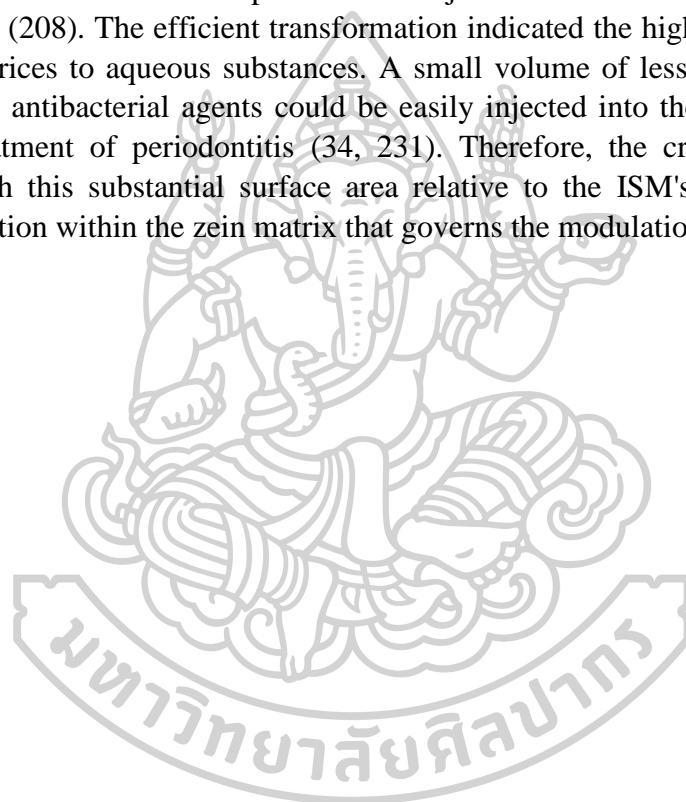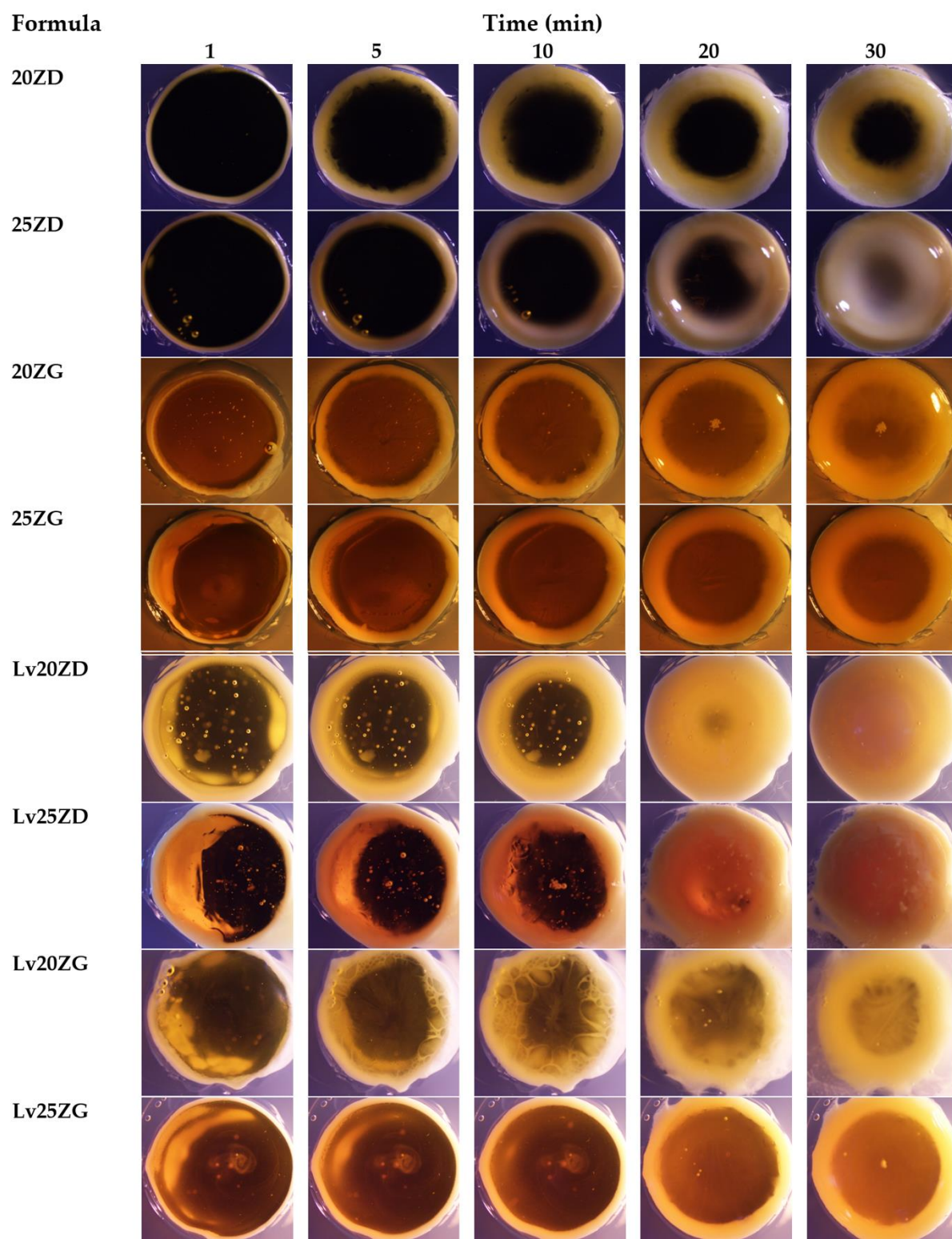
Figure 36. Matrix formation of drug-free and Lv-loaded zein-based ISM formulations upon contact with agarose gel at various time intervals, visualized under a stereomicroscope, magnified at 12×.

4.6.4. Drug content and release of Lv-loaded zein-based ISMs

The Lv content percentages in the LvD, LvG, Lv20ZD, Lv25ZD, Lv20ZG, and Lv25ZG formulations were found to be $100.08 \pm 0.74\%$, $97.41 \pm 0.16\%$, $102.62 \pm 0.82\%$, $101.46 \pm 0.88\%$, $98.46 \pm 0.82\%$, and $99.11 \pm 1.06\%$, respectively. These formulations were prepared through a simple mixing process, resulting in Lv content close to 100%. Subsequently, the drug-loaded zein ISMs underwent *in vitro* cumulative drug release assessment using the cup method, designed to replicate the conditions within a periodontal pocket (183, 194). Indeed, several researchers have utilized the cup method to investigate the drug release characteristics of *in situ* forming drug delivery systems. In this context, the cup method has been applied to study the sustained release of DH from various ISGs, including those formulated with EC, beta-cyclodextrin, and PLGA (49, 148, 193). The control groups, represented by LvD and LvG, exhibited complete drug release at 28 h and 36 h, respectively. In contrast, the zein-based ISMs demonstrated a gradual release of Lv over a span of 7 days when exposed to a PBS pH 6.8 solution (Figure 37). Remarkably, formulations with higher concentrations of zein loading exhibited extended Lv release profiles. Additionally, the utilization of GF as a solvent led to a slower release of the drug from the ISMs. This phenomenon can be attributed to the denser matrices created by the high-loading polymers, effectively sustaining the release of the drug. These matrices acted as barriers, impeding the removal of solvent and diffusion of the drug, which in turn contributed to the prolonged release pattern (193). In addition, the less viscous DMSO series ISM exhibited enhanced water entry and a consequent faster release of Lv into the medium compared to the GF series ISMs.

The use of GF as a solvent along with a 25% zein concentration notably prolonged the release of Lv, as depicted in Figure 37. This observation underscores the effective role of zein as the matrix-forming agent within the ISM, efficiently regulating the drug release process. Atridox®, a commercial product utilizing DH-loaded into a 33.03% PLA solution, was able to sustain drug release for a period of 7 days (205, 268). Periodontitis is commonly treated by dentists through the cleaning of the periodontal pocket using an irrigating solution. This is often followed by flushing the pocket with an irrigating solution, such as chlorhexidine mouthwash, aimed at reducing the presence of plaque bacteria. Subsequently, the pocket may be treated with a sustained-release antibacterial dosage form for extended antibacterial action (44). Therefore, the Lv-loaded zein-based ISM formulation from this study effectively achieved a controlled release of the drug over a period of 7 days. As a result, these zein-based ISMs demonstrated their ability to provide sustained release of Lv in the affected pocket area, which can contribute to improved patient compliance due to the reduced need for frequent drug administration (269).
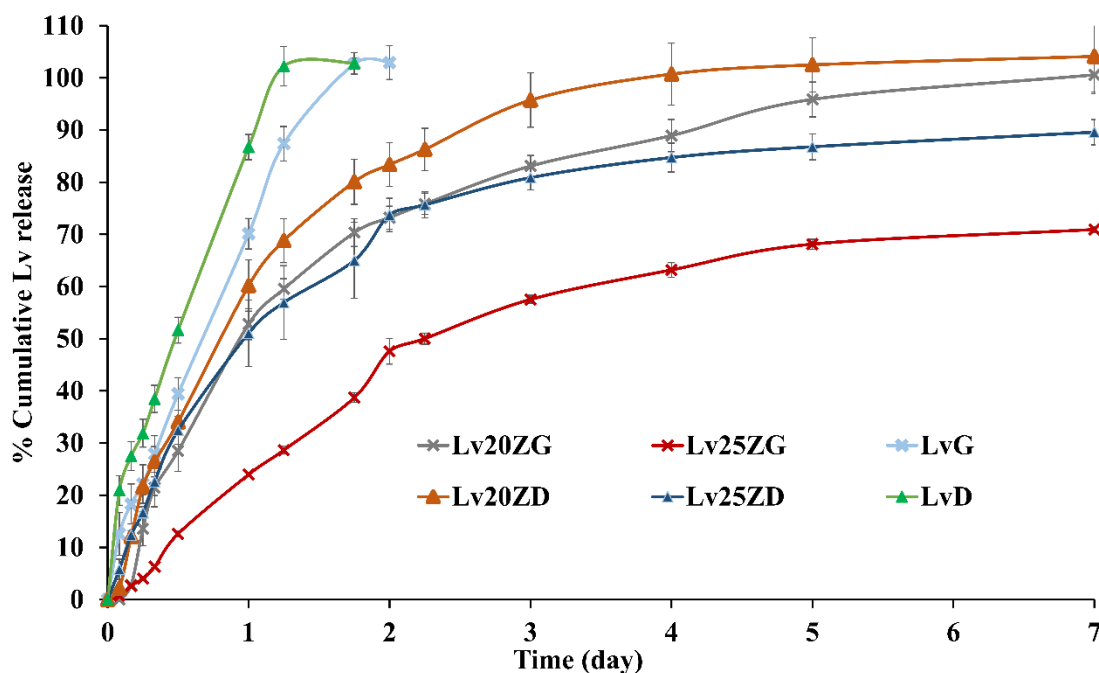
Figure 37. Lv release from zein-based ISM formulations via the cup method (n = 3).

In the context of non-swellable cylindrical matrices, the Korsmeyer-Peppas equation assigns values of 0.45 and 1.0 to Fickian and case-II transport mechanisms, respectively (156). When the calculated n value falls between 0.45 and 1.0, the release behavior is classified as non-Fickian (156, 270). A value of n = 1 corresponds to a zero-order release pattern (270, 271). Table 12 presents the regression coefficient (r^2) values and diffusion exponent (n) values resulting from fitting the drug release profile of Lv-loaded zein-based ISMs to various mathematical equations. Among these equations, the first-order kinetic model emerged as the most suitable, suggesting that the drug release is influenced by the fraction of remaining drug within the matrix. Consequently, the release of Lv is primarily governed by the diffusion of the surrounding medium into the composite zein matrix. Conversely, when considering drug release from ISMs formed using other matrix-forming agents derived from polymers or fatty acids, the majority of cases conformed well to Higuchi's equation, indicating a Fickian diffusion mechanism for drug release (208). In contrast, the release behavior of DH from formulations containing 5-15% w/w EC, 15-25% w/w bleached shellac, and 15-30% w/w Eudragit® RS, as assessed using the cup method, exhibited a strong conformity to the first-order model. This suggests that the drug release from these formulations is characterized by a fraction of the remaining drug within the matrix being released over time (194). The treatment of periodontal diseases with metronidazole-loaded polycaprolactone/alginic acid-based polymeric films exhibited a release pattern characterized by an initial rapid drug release followed by a slower and more gradual release phase.

This release pattern was accurately described by fitting the experimental data to the first-order kinetic model, indicating that the drug release is determined by a fraction of the remaining drug within the matrix being progressively released over the

course of time (272). Anomalous or non-Fickian diffusion becomes predominant when the rates of liquid diffusion and polymer relaxation are similar during immersion in the release medium (273). Fickian diffusion occurs when the rate of liquid diffusion is slower than the relaxation rate of the polymeric chains. On the other hand, case II transport becomes dominant when the relaxation process is significantly slower than the diffusion process (273). In general, hydrophilic drugs tend to release more rapidly than hydrophobic drugs, especially during the initial stages when the ISM is still undergoing solidification. This often leads to a burst release of the drug (274). However, these zein-based ISMs managed to achieve a gradual drug release without experiencing a burst release. The progressive formation of a viscous zein matrix over time, prior to complete transformation into zein matrices, effectively slowed down the initial drug diffusion.

Table 12. Regression coefficient (r²) value and diffusion exponent value (n) extracted from drug release profiles of Lv-loaded zein-based ISMs fitted to various mathematical equations.

Formula	Zero	First order	Higuchi's		Korsmeyer-Peppas	
	r^2	r^2	r^2	r^2	n	Release mechanism
LvD	0.9437	0. 9693	0. 9730	0. 9809	0.599 ± 0.055	non-Fickian diffusion
LvG	0.9712	0. 9336	0. 9175	0. 9774	0.797 ± 0.054	non-Fickian diffusion
Lv20ZD	0. 8449	0. 9930	0. 9578	0. 9597	0.530 ± 0.015	non-Fickian diffusion
Lv25ZD	0. 7644	0. 9774	0. 9228	0. 9542	0.387 ± 0.020	non-Fickian diffusion
Lv20ZG	0. 8345	0. 9855	0. 9345	0. 9451	0.574 ± 0.045	non-Fickian diffusion
Lv25ZG	0. 7944	0. 9622	0. 9408	0. 9418	0.477 ± 0.010	non-Fickian diffusion

4.6.5. Scanning electron microscopy (SEM)

The SEM images displayed the surface and cross-sectional features of Lv-loaded 20% and 25% zein-based ISM remnants post drug release (Figure 38). The images revealed the presence of crystalline Lv particles with varying sizes. The concentration of zein played a significant role in determining both the surface and inner topographies, particularly the interconnected porous structure of the ISM. Apparently, Lv20ZD exhibited a more pronounced porous scaffold structure, which correlated with its higher drug release, as previously discussed. When the Lv20ZD solutions were introduced into the buffer release medium, the less viscous DMSO-based formulation swiftly diffused into the aqueous phase through solvent removal phase-inversion leading to the simultaneous formation of a porous structure characterized by a sponge-like topography and a porous surface (181).

The pore sizes of the structure exhibited a reduction as the zein content increased. This feature was consistent with the *in vitro* matrix formation process, wherein matrices became more solid and opaque with higher concentrations of zein (Figure 35). These pores acted as primary conduits for the release of Lv molecules from the internal zein gel or matrix into the surrounding release medium. The dense

matrix topography was evident both on the surface and in cross-sectional views, particularly pronounced in Lv25ZD, contributing to a more effective retardation of drug release. The higher-loaded zein formulation, Lv25ZD, displayed a greater agglomeration of zein fibers (Figure 38). This phenomenon can be attributed to the characteristic behavior of zein as a globular protein in nonaqueous solutions, exhibiting conformational traits akin to those of more typical globular proteins (260). Furthermore, ISMs with higher viscosity tend to absorb less water, leading to a slower diffusion of solvent and resulting in a smoother surface texture (233, 263), and aligns with this study.

However, the SEM image of two ISMs using GF as a solvent showed a distinct morphology, lacking the interconnected porous structure as depicted in Figure 38. There were no residual Lv crystals visible in the remnants, indicating nearly complete drug release. However, some crystals were observed in the inner part of the zein matrix of Lv25ZG. Both formulations exhibited a combination of dense and porous structures. The transformed zein matrices in Lv25ZG were thicker and denser compared to the aforementioned ISMs. The lower porosity of Lv25ZG contributed to a slower drug release rate than the Lv20ZG matrix.

The formation of pores in the ISM is influenced by the rate of solvent exchange in determining the structural characteristics of the matrix and, consequently, the release of the incorporated drug. Solvent exchange is influenced by factors such as the zein concentration and the choice of solvent. Higher zein concentration or the use of a viscous solvent hindered water entry and solvent leaching, resulting in a less interconnected porous structure (213). This characteristic highlights the delayed drug release from the zein ISM. The microphotographs of the remnants after the release test depicted the formation of pores within the matrix, confirming the role of solvent exchange in regulating drug release from the zein ISM matrices.

.

	Surface	**Cross-section**
LvZD20		
LvZD25		
LvZG20		
LvZG25		
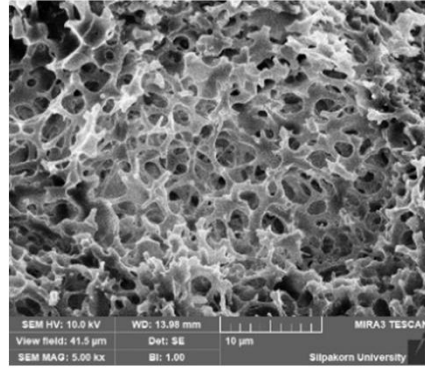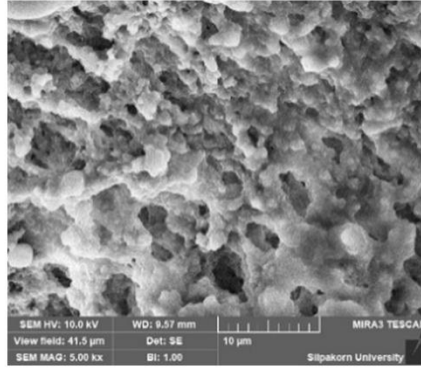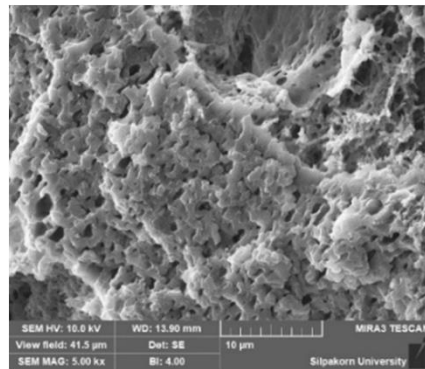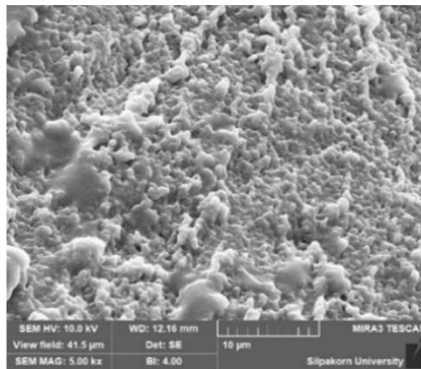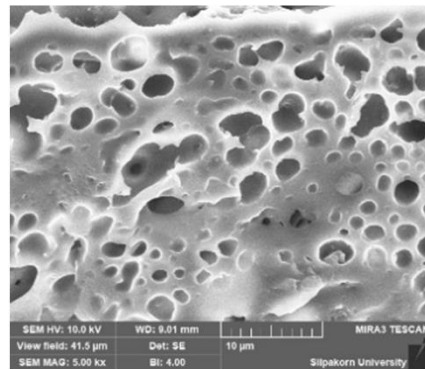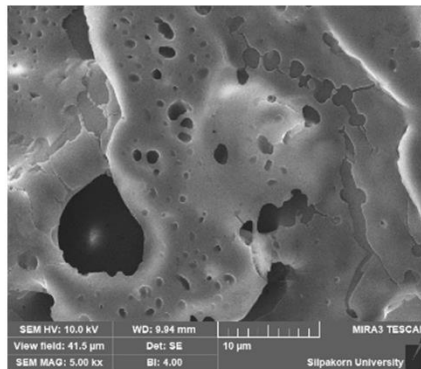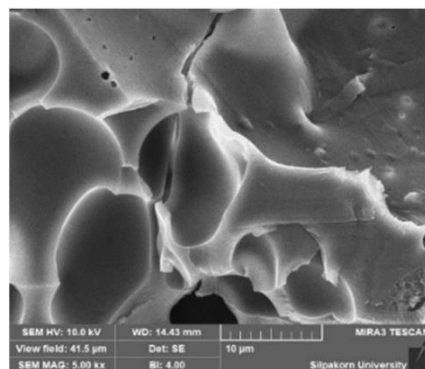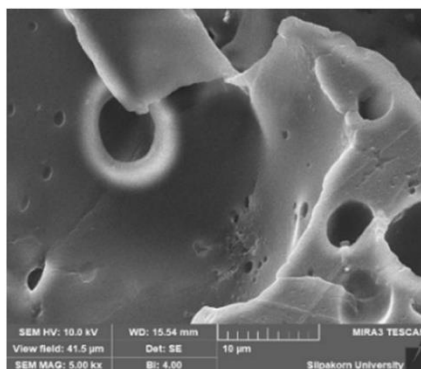
Figure 38. SEM images of freeze-dried Lv-loaded zein-based ISMs at a magnification of 5000×

4.6.6. X-ray computed microtomography (µCT)

X-ray tomographic imaging is a non-destructive method used to visualize internal structures of solid objects and gather digital data about their 3D shapes and characteristics. This technique can be applied using synchrotron sources and various available contrast modes for imaging (275). X-ray tomographic images captured using a synchrotron light source depict the remnants of Lv-loaded zein-based ISMs in Figure 39. The skin-like appearance is particularly prominent in the Lv25ZD remnant, leading to a more pronounced retardation of drug release compared to Lv20ZD. Noticeably, the Lv25ZD remnant exhibited a lower percentage of porosity than Lv20ZD. Furthermore, the 3D analysis revealed that both Lv20ZD and Lv25ZD had higher percentages of porosity compared to Lv20ZG and Lv25ZG, respectively. This observation suggests that GF solvent might have a slightly negative impact on porosity compared to DMSO.

Additionally, both Lv25ZD and Lv25ZG showed decreased porosity, indicating that higher zein incorporation results in a denser matrix, thus prolonging drug release, as previously discussed. The X-ray tomographic images corroborate the topography findings from SEM and drug release behavior. Furthermore, the lower porosity values observed in the more zein-incorporated ISMs highlight the formation of denser matrices and extended drug release. Thus, X-ray tomography provides supportive evidence for explaining topographical characteristics observed through SEM and drug release behavior. Moreover, the porosity and pore connectivity play a crucial role in facilitating solvent removal and drug diffusion in ISM that transform into scaffolds. Numerous studies have demonstrated the utility of injectable biomaterial dosage forms that form scaffolds *in situ* for localized or systemic drug delivery systems (181, 182, 233, 276). X-ray tomographic imaging proves to be a valuable technique for examining the 3D geometries and porosity features of ISM systems.
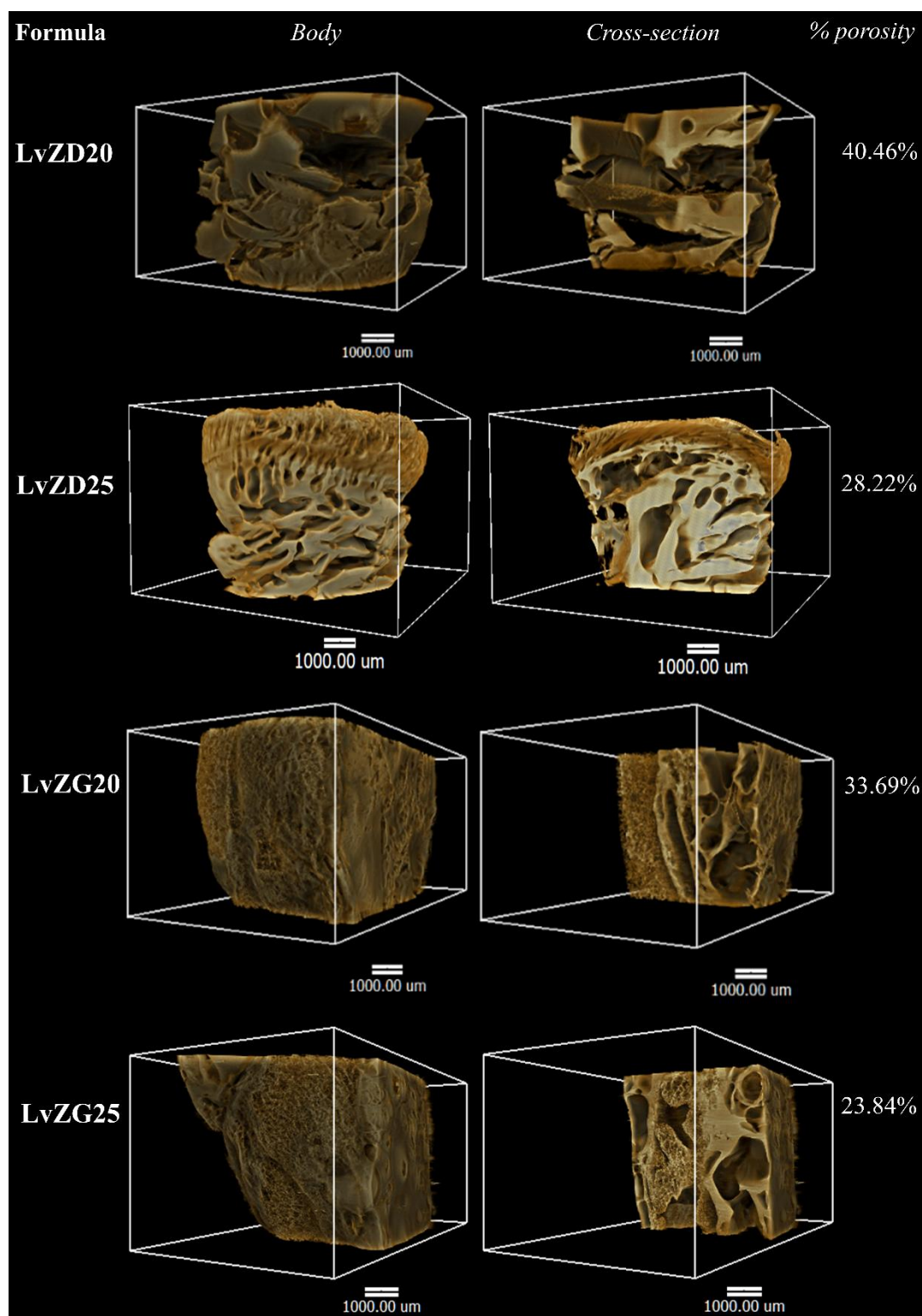
Figure 39. X-ray tomography image and percentage porosity (% porosity) determination using X-ray tomography of the freeze-dried Lv-loaded zein-based ISMs.

4.6.7. Antimicrobial activities

The results presented in Figure 40 illustrate the inhibition zones of solvents, drug-free, and Lv-loaded zein ISMs against various microbial strains, including *S. aureus* (ATCC 6538), *E. coli* ATCC 8739, *C. albicans* ATCC 10231, and *P. gingivalis* ATCC 33277, as observed in the antimicrobial test. The corresponding inhibition diameters for these strains are detailed in Table 13. Notably, these microbe species are closely linked to periodontitis disease, with a specific emphasis on pathogens such as *P. gingivalis* ATCC 33277. DMSO and GF are employed as organic solvents in the formulation of depot dosage forms due to their proven safety profiles and low toxicity. DMSO, in particular, serves as a vehicle for developing injectable subcutaneous implants (277, 278). The LD50 values for intravenous and subcutaneous injections of DMSO in rats are 5.3 g/kg and 12 g/kg, respectively (279). Furthermore, it can serve as a solvent to dissolve the polymer used in the formulation of *in situ* forming implants (280).

GF is recognized as a parenteral solvent capable of dissolving a broad spectrum of aqueous-insoluble compounds (7, 244). It has been utilized as a co-solvent in veterinary formulations to create highly viscous systems aimed at controlling drug release. Additionally, it has found application as an injectable solvent for *in situ*-forming implant systems (7, 87). Furthermore, GF has found utility as a solvent in other applications. For instance, it was utilized as the solvent for subcutaneous injections of ivermectin in young pigs (281). Additionally, it played a role in enhancing the pharmacokinetics of a pyrethroid insecticide, deltamethrin, when administered as an injected suspension, leading to a prolonged half-life and a slower clearance rate (282). Importantly, the LD100 (lethal dose for 100% of subjects) of GF through intravenous injection in mice has been determined to be 3 g/kg (244, 283). Safety data are available for various medical applications of DMSO, GF, and zein; however, the formulations developed in this study need further investigation through clinical experiments to ensure their safety. It is noteworthy that GF exhibited more potent antimicrobial activity compared to DMSO, particularly against *C. albicans*, though not as effective against *P. gingivalis*, as indicated in Table 13. Despite GF having higher viscosity than DMSO, it displayed more efficient inhibition of microbial growth. Organic solvents like DMSO and GF have the potential to solubilize lipids present in microbial cell walls, thereby inhibiting their growth.

The zein-based ISM without Lv exhibited smaller inhibition zone diameters compared to its respective solvent, particularly the 25ZD formulation. This could be attributed to the increased viscosity resulting from the addition of zein, which could impede the outward diffusion of solvent from the ISMs into the inoculated media. The Lv solutions used as the control group displayed significant inhibition zone diameters, except for *C. albicans*. Inhibition against *C. albicans* appeared to be primarily due to the solvent, especially GF, rather than the drug compound itself, as the clear zones were smaller than those of the solvents. In contrast, the Lv-zein-based ISM showed significantly smaller inhibition zone diameters for *S. aureus*, *E. coli*, and *P. gingivalis*

compared to the Lv solutions used as the control group. The incorporation of zein slowed down drug diffusion, leading to smaller inhibition clear zones, particularly with increasing zein concentration. This observation was consistent with the drug release behavior of Lv from the prepared ISMs, as previously discussed. In addition, Lv25ZD did not exhibit an inhibition zone against *C. albicans*. The reduced amount of DMSO in combination with the viscous formulation appears to have hindered its antifungal activity. Actually, a smaller clear zone was observed as zein loading increased. This observation suggests that the zein matrices, subsequent to undergoing phase transformation, played a role in slowing down the diffusion of the drug outward, which in turn led to a prolonged drug release profile. Additionally, this modulation of drug diffusion resulted in a decrease in the diameter of the inhibition zone, indicating a correlation between drug release kinetics and the observed antimicrobial activity. Similar trends have been previously noted in the context of *in situ*-forming systems that utilize diverse matrix-forming agents, such as PLGA (148), natural resins (181, 182), polymers (193, 194), and saturated fatty acids (193). The exact roles and contributions of various types and species of microbes in the initial stages of periodontal breakdown, whether acting individually or in concert, are still not fully understood. Unlike more widespread major infections, all the microorganisms implicated in periodontal disease are part of the natural oral flora. Typically, *C. albicans* has been identified as a cause of persistent and challenging refractory periodontitis (284). Additionally, *S. aureus* has been found in the periodontal pockets of patients with aggressive periodontitis, while *E. coli* has been recognized as a common microorganism in individuals with periodontitis (35). These findings emphasize the complex and localized nature of periodontal disease, with indigenous oral microorganisms potentially playing pivotal roles in its development and progression. Consequently, an effective ISM designed to inhibit the various pathogens associated with periodontitis in a controlled and targeted drug-release manner has become a compelling localized treatment option. Practically, the medicated ISM has demonstrated superior clinical outcomes when compared to conventional scaling and root planing procedures alone. This enhanced efficacy can potentially be attributed to the inclusion of GF, which serves not only as an effective treatment agent for periodontitis but also as a suitable vehicle for delivering the drug into the periodontal pocket.

Existing commercial products like Atridox®, Atrisorb-D®, and FreeFlow™ offer ISGs for periodontitis treatment, but they often incorporate costly matrix-forming agents. Therefore, the exploration of alternative materials, such as zein as a matrix-forming agent, holds promise for the development of novel ISMs. Take Atridox® as an example-a subgingival controlled-release product that involves a two-syringe mixing system. The first syringe contains a flowable polymeric formulation comprising PLA dissolved in an organic solvent. Upon mixing, the second pre-filled syringe contains DH powder. This approach with pre-filled syringes enhances drug stability. Furthermore, the use of Lv-incorporated zein-based ISMs, which undergo solvent removal and phase inversion without an aqueous phase or heating, presents a

potential strategy to prevent drug degradation. In summary, the development of innovative ISMs holds promise for improved localized treatment of periodontitis, offering efficient drug delivery and potentially overcoming some limitations of existing commercial products.

Lv is a third-generation fluoroquinolone antibiotic known for its broad-spectrum activity. Lv functions by diffusing through the bacterial cell wall and inhibiting enzymes such as DNA gyrase and topoisomerase IV, which are crucial for DNA replication (124, 126). Lv has been shown to exhibit varying MIC against different microbial strains. Specifically, its MIC against *S. aureus*, *E. coli*, and *P. gingivalis* has been reported as 0.12 µg/mL (167), ≤ 0.12 µg/mL (168), and 8 µg/mL (169), respectively. In this study, the total concentration of Lv released was 43.75 µg/mL (100% release). Consequently, formulations, except for Lv25ZG, achieved approximately 18.29% drug release, which is equivalent to achieving the MIC of Lv against *P. gingivalis* after around 6 h. These results demonstrate that Lv20ZG and Lv20ZD formulations achieved controlled drug release over a span of 7 days while effectively maintaining antimicrobial activity against all tested microbes. Nonetheless, X-ray imaging indicated that the matrix structure of Lv20ZD was incomplete. As a result, Lv20ZG stands out as a more promising ISM formulation for periodontitis treatment, with the added advantage of releasing Lv concentrations above the MIC for pathogens like *P. gingivalis*. In practical terms, local drug delivery strategies aim to concentrate a high dose of the drug precisely at the target site for optimal therapeutic effects. In the case of Lv, its hydrophilic nature and controlled release from the zein-based solvent removal phase inversion ISM allow for efficient diffusion into the agar medium, which contains lower water content compared to the release medium. This controlled diffusion effectively inhibits the antimicrobial activities of the released Lv, as illustrated in Table 13.
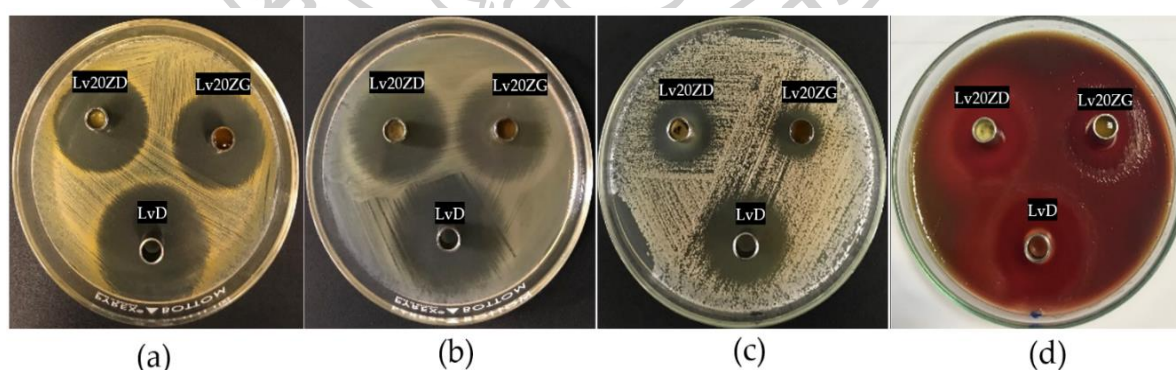
Figure 40. Photographs of inhibition zones for Lv20ZD (upper-left corner cup) and Lv20ZG (upper-right corner cup) ISM formulations against *S. aureus* (a), *E. coli* (b), *C. albicans* (c), and *P. gingivalis* (d), and the control group (LvD) at the bottom cup.

Table 13. Inhibition zone dimensions for DMSO, GF, and zein-based ISM formulations loaded with Lv against *S. aureus*, *E. coli*, *C. albicans*, and *P. gingivalis* (n = 3).

Formula	Inhibition Zone $\pm$ S.D. (mm)			
	S. aureus ATCC *6538*	*E. coli* ATCC *8739*	*C. albicans* ATCC *10231*	*P. gingivalis* ATCC *33277*
DMSO	12.3 ± 0.5[a]	16.0 ± 0.8[a]	25.7 ± 1.2[a]	17.3 ± 0.5[a]
GF	15.7 ± 1.2[c]	16.3 ± 0.5[c]	31.3 ± 1.2[c]	13.3 ± 0.5[c]
20ZD	11.3 ± 0.5	14.0 ± 0.0	13.7 ± 2.1	16.0 ± 0.8
25ZD	-	-	10.3 ± 0.5[a]	-
20ZG	12.7 ± 0.9[c]	15.0 ± 0.8	14.0 ± 1.4[c]	14.0 ± 0.8
25ZG	-	-	14.7 ± 0.9[c]	-
LvD	37.7 ± 0.5[a, b]	38.3 ± 1.2[a, b]	19.7 ± 1.7[a]	39.7 ± 1.7[a, b]
LvG	37.0 ± 0.8[c, d]	35.7 ± 0.5[c, d]	27.3 ± 0.9[d]	33.7 ± 0.5[c, d]
Lv20ZD	34.3 ± 0.5[b]	32.0 ± 0.8[b]	16.7 ± 2.1	35.3 ± 1.2[b]
Lv25ZD	34.3 ± 0.5[b]	31.3 ± 0.5[b]	-	29.0 ± 0.8[b]
Lv20ZG	34.3 ± 0.5[d]	30.7 ± 0.5[d]	17.0 ± 1.4[d]	29.3 ± 1.7[d]
Lv25ZG	32.3 ± 0.5[d]	29.7 ± 0.5[d]	12.0 ± 1.6[d]	26.0 ± 0.8[d]

"- "= No inhibition zone; the superscripts a–d indicate a significant difference ($p < 0.05$) using one-way ANOVA followed by an LSD post-hoc test.

4.7. Summary

The successful development of the solvent removal phase inversion zein-based ISM formulation was achieved using DMSO and GF as solvents. The viscosity and required injection force for the zein ISM prepared with GF were notably higher compared to those prepared with DMSO. Additionally, the matrix formation process was slower in the case of GF. Higher zein loading resulted in a more prolonged release of Lv. The use of GF as a solvent led to the formation of a denser matrix in the ISM, which in turn contributed to a more extended drug release profile. SEM and X-ray imaging unveiled distinct surface topographies and 3D structures of the dried ISM samples. The percentage of porosity exhibited a correlation with their phase transformation behavior and drug release profiles. The incorporation of zein in the formulation led to a retardation of drug diffusion, resulting in smaller inhibition clear zones, which was consistent with the drug release behavior observed. The concentration of drug release from all formulations surpassed the MIC values required against pathogenic microbes, and they exhibited controlled drug release for a duration of 7 days. Among these formulations, Lv20ZG demonstrated suitable viscosity, Newtonian flow characteristics, acceptable matrix formation, and injectability. Furthermore, it sustained Lv release for the entire 7-day period, effectively inhibiting the growth of *S. aureus*, *E. coli*, *C. albicans*, and *P. gingivalis*. Consequently, Lv20ZG emerges as a promising ISM formulation for the treatment of periodontitis. While zein and GF have established safety profiles in various medical applications, further clinical experiments are essential to confirm the safety of this developed ISM formulation.

A numerical mechanistic modeling of drug release from solvent-removal zein-based *in situ* matrix formulations.

4.8 Model development

Following the introduction of ISM formulations composed of solvent, polymer, and drug into an aqueous environment, the initiation of phase inversion within ISMs becomes apparent. This process triggers the rapid formation of a fragile shell, composed of a polymer matrix, which envelops a consistent empty area. This shell encapsulates an internal core comprising the implant solution, retaining its state without undergoing phase inversion. Consequently, this leads to the initial onset of drug release. A visual depiction of this phenomenon is provided in Figure 41. The movement of the solvent and drug occurs outward, from the interior to the exterior, facilitated by their passage through the porous matrix. Concurrently, water diffuses inward, from the external environment to the internal void fraction. Upon reaching a certain threshold, the polymer precipitates at the interface between the array and the solution, thereby promoting an enhanced development of the polymer matrix. As time elapses, the volume of the matrix phase progressively increases, causing the inner phase to expand due to the diffusion of water. Eventually, complete polymer precipitation takes place, resulting in the creation of a matrix that envelops an inner region saturated with water (148).

4.8.1 Characteristics of depot formation

Drawing from prior research, a mathematical framework has been utilized to portray the intricate dynamics of mass concentration concerning solvent, polymer, drug, and water within the matrix precipitation and phase inversion process (163, 164). The release model pertinent to Lv-loaded zein ISM postulates a system of spherical symmetry encompassing three distinct phases: the internal liquid phase (1), the solid polymer matrix phase (2), and the external bath solution phase (3), as elucidated in Figure 41.
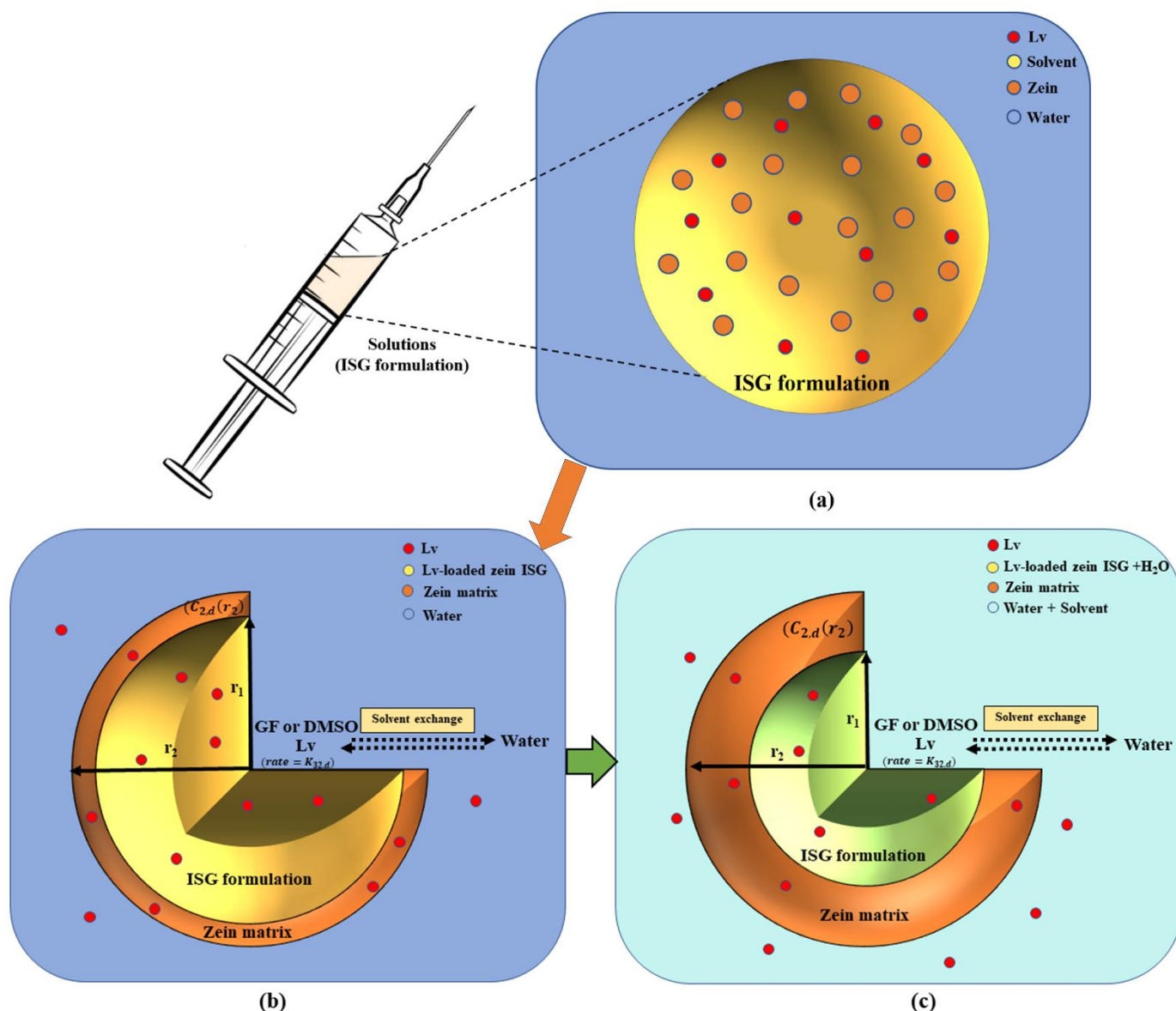
Figure 41. The schematic representation provides an overview of the rational design strategy and the sequential steps involved in the creation of solvent-removal zein-based ISM: Prior to injection, an ISM is composed of a solution comprising polymers, organic solvents, and drugs (a). Upon ISM formulation injection, the phase-inversion process initiates by solvent removal, the polymer intentionally designed to be insoluble in water (b), undergoes solidification and transforms into a solid-like matrix (c). A The schematic of the Lv-loaded zein ISM release model illustrates an axially symmetric model geometry with three different phases: the inner non-phase inverted interior phase ($r < r_1$), the polymer matrix phase ($r_1 < r < r_2$), and the bath solution phase. The diagram includes $C_{2,k}$, which represents the drug concentration at the edge of the matrix phase, and $K_{32,k}$, which represents the drug permeability coefficient between the polymer matrix and the exterior phase.

4.8.2 Model of transport processes and matrix development

Interior phase

The concentration of the drug within the internal depot phase experiences alterations influenced by both radial distance and time. This behavior is governed by the following diffusion equation:

$$\frac{\partial C_{1,k}}{\partial t} = \frac{D_{1,k}}{r^2} \frac{\partial}{\partial r}\left[r^2 \frac{\partial C_{1,k}}{\partial r}\right]. \tag{1}$$

where $C_{1,k}$ represents the drug concentration at the interior phase, r is the radial distance, t is time and $D_{1,k}$ denotes the diffusivity of drug k through the interior phase.

The spherical symmetry of the system enables the description of conditions at the center in the subsequent manner:

$$r = 0 : \frac{\partial C_{1,k}}{\partial t} = 0 \tag{2}$$

The drug concentrations and transport rates at the interface between the interior phase and the matrix's void space exhibit continuity. As a result,

$$r = r_1(t): C_{1,k} = C_{2,k} ; \quad D_{1,k} \frac{\partial C_{1,k}}{\partial r} = \varepsilon D_{2,k} \frac{\partial C_{2,k}}{\partial r} . \tag{3}$$

Where $C_{2,k}$ signifies the drug concentration within the matrix phase, $D_{2,k}$ represents the diffusion coefficient of species k, and ε corresponds to the void fraction, denoting the ratio of free space to the total space within the matrix.

Matrix phase

The drug is enclosed within the void space of the matrix phase. Consequently, due to diffusion taking place within this void space, the concentrations of species display variations both in terms of radial distance and time, as outlined below:

$$\frac{\partial C_{2,k}}{\partial t} = \frac{D_{2,k}}{r^2} \frac{\partial}{\partial r}\left[r^2 \frac{\partial C_{2,k}}{\partial r}\right] \tag{4}$$

where $D_{2,k}$ represents the drug's diffusion coefficient. In the initial stage, within the void space of the thin matrix shell, the alterations in drug concentrations are presumed to exhibit a linear correlation concerning radial position. Thus

$$t = t_0 : C_{2,k}(r,t_0) = \left[C_{3,k}(t_0) - C_{1,k}(t_0)\right]\left[\frac{r - r_1(t_0)}{r_2(t_0) - r_1(t_0)}\right] + C_{1,k}(t_0). \tag{5}$$

At the external interface, denoted as $r_2(t)$, the rate of species transfer occurring between the polymer matrix and the surrounding external phase is equivalently matched to the rate of species diffusion transpiring within the confines of the polymer matrix.

Exterior phase

In the external phase, the water concentration ($C_{3,\text{w}}$) and phase volume (V_3) remain constant due to the surplus water present in the external environment. The rate of mass alteration for both solvent and drug species in the external phase is equivalent to the rate of species transport occurring between the polymer matrix and the external phase. Hence,

$$V_3 \frac{\mathrm{d}}{\mathrm{d}t} C_{3,k} = K_{32,k} (C_{2,k}(r_2) - C_{3,k}),$$

$$\frac{\mathrm{d}}{\mathrm{d}t} C_{3,k} + \frac{K_{32,k}}{V_3} C_{3,k} = \frac{K_{32,k}}{V_3} C_{2,k}(r_2). \tag{6}$$

The integrating factor of Equation (6) is:

$$\mu(t) = e^{\int \frac{K_{32,k}}{V_3} dt} = e^{\frac{K_{32,k}}{V_3}t}.$$

Applying the integrating factor to Equation (6) we have

$$\frac{K_{32,k}}{V_3} C_{2,k}(r_2)\, e^{\frac{K_{32,k}}{V_3}t} = e^{\frac{K_{32,k}}{V_3}t} \frac{\mathrm{d}}{\mathrm{d}t} C_{3,k} + \frac{K_{32,k}}{V_3} e^{\frac{K_{32,k}}{V_3}t} C_{3,k} = \frac{\mathrm{d}}{\mathrm{d}t} \left[e^{\frac{K_{32,k}}{V_3}t} C_{3,k} \right]. \tag{7}$$

Rearranging Equation (7) and subsequently integrating, we acquire:

$$\int d\left[e^{\frac{K_{32,k}}{V_3}t} C_{3,k} \right] = \frac{K_{32,k}}{V_3} C_{2,k}(r_2) \int e^{\frac{K_{32,k}}{V_3}t} dt,$$

$$e^{\frac{K_{32,k}}{V_3}t} C_{3,k} = C_{2,k}(r_2) e^{\frac{K_{32,k}}{V_3}t} + cont,$$

$$C_{3,k} = C_{2,k}(r_2) + cont. \times e^{\frac{-K_{32,k}}{V_3}t},$$

where cont. represents the integration constant.

By applying the initial condition of the drug concentrations at time:

$$t = t_0 : \left(C_{3,k}(t_0) = 0 \right)$$

Specifically:

$$C_{2,k}(r_2) + cont. \times e^{\frac{-K_{32,k}}{V_3}t_0} = C_{3,k}(t_0) = 0$$

resultant expression is as follows:

$$cont. = -C_{2,k}(r_2)e^{\frac{K_{32,k}}{V_3}t_0}.$$

Therefore, the particular solution of Equation (6) can be expressed as follows:

$$C_{3,k}(t) = C_{2,k}(r_2) - C_{2,k}(r_2)e^{\frac{K_{32,k}}{V_3}t_0} \times e^{\frac{-K_{32,k}}{V_3}t} = C_{2,k}(r_2)[1 - e^{\frac{K_{32,k}}{V_3}(t_0-t)}]. \qquad (8)$$

The drug concentrations exhibit gradual augmentation and converge towards the value of $C_{2,k}(r_2)$ at a rate of $\frac{K_{32,k}}{V_3}$. This segment seeks to ascertain the rate $\frac{K_{32,k}}{V_3}$ as well as the value of $C_{2,k}(r_2)$ when the drug concentration $C_{3,k}(t)$ is provided at a given time. However, the nonlinearity exhibited by the function on the right-hand side of Equation (8) presents challenges for inversion. In such instances, a numerical technique can be employed for solving the ordinary differential equation (ODE) (285). For the sake of convenience, the subsequent notations are introduced:

$$y(t) = C_{3,k}(t), \quad a = \frac{K_{32,k}}{V_3} \quad and \quad b = \frac{K_{32,k}}{V_3}C_{2,k}(r_2).$$

Equation (6) can be reformulated as follows:

$$\frac{dy}{dt} + ay = b. \qquad (9)$$

The differentiation process can be discretized through the utilization of a finite differences approach. This procedure can be executed by consulting the pertinent section expounding the forward difference formula of order $O(h)$ and the central difference formula of order $O(h^4)$ (286). The ensuing subsection delineates the discretization methodology enacted for the computation of the parameters 'a' and 'b'.

4.8.2.1. Forward difference formula of order O(h)

For $i = 1, 2, 3, ..., n$, where $y(t_i) = y_i$ and $h = t_{i+1} - t_i$, in accordance with Equation (9), the application of the forward difference formula results in:

$$\frac{y_{i+1} - y_i}{h} + ay_i = b. \qquad (10)$$

After rearranging Equation (10), the resulting equation is:

$$y_{i+1} + (ah - 1)y_i = hb$$

$$(1 - ah)y_i + hb = y_{i+1} \quad \text{for} \quad i = 1, 2, 3, ..., n. \qquad (11)$$

Expanding Equation (11) for $i = 1, 2, 3, ..., n-1$ yields:

$$(1-ah)y_1 + hb = y_2$$
$$(1-ah)y_2 + hb = y_3$$
$$(1-ah)y_3 + hb = y_4$$
$$\vdots$$
$$(1-ah)y_{n-1} + hb = y_n$$

$$\Rightarrow \quad \begin{bmatrix} y_1 & 1 \\ y_2 & 1 \\ y_3 & 1 \\ \vdots & \vdots \\ y_{n-1} & 1 \end{bmatrix} \begin{bmatrix} 1-ah \\ hb \end{bmatrix} = \begin{bmatrix} y_2 \\ y_3 \\ y_4 \\ \vdots \\ y_n \end{bmatrix} \tag{12}$$

Define

$$A = \begin{bmatrix} y_1 & 1 \\ y_2 & 1 \\ y_3 & 1 \\ \vdots & \vdots \\ y_{n-1} & 1 \end{bmatrix}, \quad d = \begin{bmatrix} y_2 \\ y_3 \\ y_4 \\ \vdots \\ y_n \end{bmatrix} \quad and \quad x = \begin{bmatrix} 1-ah \\ hb \end{bmatrix}.$$

Now the matrix-vector form is represented as

$$Ax = d. \tag{13}$$

The absence of an inverse for the non-square matrix A with dimensions (n-1, 2) precludes direct inversion. Nonetheless, the solution x to Equation (13) remains attainable through the utilization of the normal equation:

$$A^T A x = A^T d \tag{14}$$

where A^T is a transpose of A.

The solution $x = [x_1 \quad x_2]^T$ can be obtained as $x = (A^T A)^{-1} A^T d$

4.8.2.2. Central difference formula of order O(h^4)

Continuing in a similar manner as elucidated earlier, when utilizing the central difference formula to approximate the derivative in Equation (9), a linear system is derived:

$$\frac{-y_{i+2} + 8y_{i+1} - 8y_{i-1} + y_{i-2}}{12h} + ay_i = b. \tag{15}$$

Rearranging Equation (15), we obtain

$$12hay_i - 12hb = y_{i+2} - 8y_{i+1} + 8y_{i-1} - y_{i-2} \tag{16}$$

for $i = 3, 4, 5, \dots, n-2$.

Defined $\Delta_i = y_{i+2} - 8y_{i+1} + 8y_{i-1} - y_{i-2}$, the matrix-vector representation of Equation (16) is

$$(1-ah)y_1 + hb = y_2$$
$$(1-ah)y_2 + hb = y_3$$
$$(1-ah)y_3 + hb = y_4$$
$$\vdots$$
$$(1-ah)y_n + hb = y_{n+1}$$

$$\Rightarrow \quad \begin{bmatrix} y_3 & -1 \\ y_4 & -1 \\ y_5 & -1 \\ \vdots & \vdots \\ y_{n-2} & -1 \end{bmatrix} \begin{bmatrix} 12ah \\ 12hb \end{bmatrix} = \begin{bmatrix} \Delta_3 \\ \Delta_4 \\ \Delta_5 \\ \vdots \\ \Delta_{n-2} \end{bmatrix}. \quad (17)$$

Define

$$A = \begin{bmatrix} y_3 & -1 \\ y_4 & -1 \\ y_5 & -1 \\ \vdots & \vdots \\ y_{n-2} & -1 \end{bmatrix}, \quad d = \begin{bmatrix} \Delta_3 \\ \Delta_4 \\ \Delta_5 \\ \vdots \\ \Delta_{n-2} \end{bmatrix} \quad and \quad x = \begin{bmatrix} 12ah \\ 12hb \end{bmatrix}.$$

A solution $[x_1 \quad x_2]^T$ of Equation (17) is $x = (A^T A)^{-1} A^T d$.

Regarding both the forward difference formula of order O(h) and the central difference formula of order O(h^4), it is important to observe that:

$$a = \frac{K_{32,k}}{V_3}, b = \frac{K_{32,k}}{V_3} C_{2,k}(r_2) \quad and \quad \frac{b}{a} = C_{2,k}(r_2)$$

Using the derived solution, the parameters $C_{2,k}(r_2)$ and $\frac{K_{32,k}}{V_3}$ can be calculated when the drug concentration $C_{3,k}(t)$ at a given time is given.

4.8.3 Modelling of *in vitro* drug release profile using mathematic methods based on rate of species transport from the polymer matrix and exterior phase on drug release patterns of drug-loaded ISM.

To examine the correlation between the drug concentration $C_{2,k}(r_2)$ at the edge of the matrix phase and the transport rate $\frac{K_{32,k}}{V_3}$ of drug between the polymer matrix and the exterior phase in relation to drug release patterns, the drug release data, represented as the concentration of drug in the aqueous medium at time $(C_{3,k}(t))$ is used to substitute in Equation (12) and Equation (17). Then, the parameters $C_{2,k}$ and $K_{32,k}$ are calculated by using numerical method as discussed above. The scripts for the forward difference formula employed in this study are given below.

```
load info.dat
t = info(:,1);
n = length(t);
y = info(:,2);
plot(t,y,'*r','linewidth',2)
h = t(2)-t(1);
E = ones(n-1,1);
A = [y(1:end-1) E];
b = y(2:end);
x = inv(A'*A)*A'*b;
sol_a = (1-x(1))/h
sol_b = x(2)/h
sol_c = sol_b/sol_a
t0 = 0;
time = t0:0.5:7;
y_app = sol_c*(1-exp(sol_a*(t0-time)));
err = norm(y-y_app)/norm(y)
hold on
plot(time,y_app,'--k','linewidth',2)
set(gca,'fontsize',30)
xlabel('{\bf Time (day)}')
legend('Experimental data','Simulation','location','SouthEast')
ylabel('{\bf C_{3,k}(t)}')
```

In addition, the scripts for model method by using the central difference formula of order $O(h^4)$ to approximate the derivative are given below.

```
load info.dat
t = info(:,1);
n = length(t);
y = info(:,2);
plot(t,y,'*r','linewidth',2)
h = t(2)-t(1);
E = - ones(n-4,1);
A = [y(3:end-2) E];
for i = 1:n-4
b(i,1) = -y(i)+8*y(i+1)-8*y(i+3)+y(i+4);
end
x = inv(A'*A)*A'*b;
sol_a = x(1)/(12*h)
sol_b = x(2)/(12*h)
sol_c = sol_b/sol_a
t0 = 0;
time = t0:0.5:7;
y_app = sol_c*(1-exp(sol_a*(t0-time)));
err = norm(y-y_app)/norm(y)
hold on
plot(time,y_app,':g','linewidth',2)
set(gca,'fontsize',30)
xlabel('{\bf Time (day)}')
legend('Experimental data','Simulation','location','SouthEast')
ylabel('{\bf C_{3,k}(t)}')
```

The effect of matrix forming agents on drug release behavior could be discussed via calculated rate of species transport the polymer matrix and exterior phase parameters.

4.8.4 Investigation of drug release profile variations

This subsection is dedicated to simulating the drug release profile by manipulating the rate of drug transport from the polymer matrix to the exterior phase $K_{32,k}$ and the drug concentration at the edge of the matrix phase $C_{2,k}$.

A comprehensive compilation of model parameters along with their corresponding values for simulation purposes is presented in Table 14. The parameter values were determined through the solution of the ordinary differential equation in the model simulations, utilizing the parameter range outlined in Table 14. Furthermore, supplementary parameters related to drug release from ISM were estimated based on this mechanistic model. These additional parameters encompass the rate of drug transport from the polymer matrix to the exterior phase ($K_{32,k}$) and the drug concentration at the edge of the matrix phase ($C_{2,k}$), as elaborated in Equation (8)

$$C_{3,k}(t) = C_{2,k}(r_2)[1 - e^{\frac{K_{32,k}}{V_3}(t_0 - t)}]$$

By employing the rate of drug transport and the drug concentration at the edge of the matrix phase as specified in Table 14, the following scripts facilitate the generation of the drug release profile:

```
V = 80;
t = 0:0.5:7;
k = 0:1:80;
c2= 0:10:100;
[T,C2] = meshgrid(t,c2);
Z = C2.*(1-exp((k(61)/V).*(-T)))
surf(T,C2,Z)
set(gca,'fontsize',30)
xlabel('{\bf Time (day)}  ','fontsize',30)
ylabel('{\bf C_{2,k}}','fontsize',30)
zlabel('{\bf C_{3,k}}','fontsize',30)
save data.dat Z -ascii
load data.dat
```

```
V = 80;
t = 0:0.5:7;
k = 0:10:80;
c2= 0:10:100;
[T,K] = meshgrid(t,k);
Z = c2(11).*(1-exp((K/V).*(-T)));
surf(T,K,Z)
set(gca,'fontsize',30)
xlabel('{\bf Time (day)}','fontsize',30)
ylabel('{\bfk_{32d}}','fontsize',30)
zlabel('{\bfC_{3,k}}','fontsize',30)
```

4.9. Simulation of *in vitro* drug release profile

The primary focus of this study revolves around the mathematical modeling of drug release from drug-loaded zein ISMs using the cup method, aiming to replicate the environment of a periodontal pocket (185). Earlier investigators utilized this approach to examine the drug release characteristics of *in situ* forming drug delivery systems (165, 183, 192). To comprehensively assess the drug release characteristics of *in situ* forming systems, the critical influence of zein concentration and solvent selection was considered. Figure 42 presents observed drug release profiles from four distinct Lv-loaded formulations: 20% zein in DMSO (LvZD20), 25% zein in DMSO (LvZD25), 20% zein in GF (LvZG20), and 25% zein in GF (LvZG25). The observed drug release from the ISM is presented in Figure 42, displaying the percentage of drug amount released (% relative to 40 mg) over time (days). The drug release data from experimental observations over 12 h to 7 days were compared with the simulation results obtained using numerical differentiation methods: forward difference formula of order $O(h)$ and central difference formula of order $O(h^4)$. These comparisons are shown in Figure 42 (a, b, c, d) and Figure 42 (e, f, g, h), respectively.

Upon analysis, it was observed that the simulation results for LvZD20 and LvZD25 closely aligned with the experimental data, as evident in Figure 42 (c, d, g, h). Conversely, the simulation outcomes employing order $O(h)$ for LvZG20 and LvZG25 demonstrated superior agreement with the experimental data when compared to the simulations utilizing order $O(h^4)$. In a parallel manner, researchers developed a mechanistic model to evaluate and predict drug release kinetics from millirods (155). Their model provides invaluable insights into the intricate nature of drug-loaded millirod systems, unveiling the mechanisms that enable a rigorous quantification of the processes governing drug release from a polymer matrix.

In Table 14, it was observed that LvZD20 and LvZG20 exhibited nearly 100% Lv content, with $C_{2,k}(r_2)$ (maximum drug concentration at the edge of the matrix phase) ranging from 98.35% to 105.50%. Conversely, LvZD25 and LvZG25 displayed Lv content around 70% and 90% respectively, with $C_{2,k}(r_2)$ values ranging from 71.58% to 88.97%. As the concentration of zein increased, there was a decrease in the rate of LV release, which was further prolonged by the inclusion of GF. The denser matrices formed by high-loading polymers effectively extended the duration of ISM drug release by establishing a robust barrier against solvent removal and drug diffusion (193, 287). Additionally, the values of $K_{32,k}$ (rate of drug transport from the polymer matrix to exterior phase) for LvZD20 and LVZD25 ranged from 32.55 to 50.23 (day^{-1}), while in LvZG20 and LvZG25, they ranged from 51.57 to 64.76 (day^{-1}), This implies that LvZD demonstrated a higher rate of drug transport from the zein matrix to the exterior phase compared to LvZG (288). The ISM composed of the less viscous DMSO series exhibited enhanced water penetration, facilitating accelerated drug release into the medium compared to the GF series ISM (229). The viscous zein matrix formation over time effectively delayed initial drug diffusion before transforming into zein matrices (289).

Furthermore, the parameter values from Table 14 were utilized to estimate the drug release equation, as presented in Equation (8), and the results are shown in Table 15. The simulation of drug transport using this model allowed for a reasonable approximation of drug release from Lv-loaded zein ISMs filled in the periodontal pocket.

In addition to providing Lv transport parameters, this work represents a methodological improvement with potential future applications. The numerical differentiation methods have presented a versatile approach. Specifically, the forward difference formula of order O(h) and the central difference formula of order O(h^4) offer distinct advantages over analytical solutions. These methods are particularly beneficial when dealing with arbitrary geometries or functions that pose challenges for analytical expression. These developments could potentially offer advantages in upcoming investigations and efforts to enhance drug delivery techniques.

Table 14. Estimated drug release parameters by numerical differentiation: forward difference formula approximates of order O(h) and central difference formula of order O(h^4).

Formula	Numerical methods	$K_{32,k}$ (day^{-1}) (Rate of drug transport from the polymer matrix to exterior phase)	$C_{2,k}(r_2)$ (%) (Drug concentration at the edge of the matrix phase)
Lv20ZD	O(h)	56.65	103.50
	O(h^4)	52.91	105.50
Lv25ZD	O(h)	51.57	88.97
	O(h^4)	64.76	88.60
Lv20ZG	O(h)	47.58	98.35
	O(h^4)	32.55	104.50
Lv25ZG	O(h)	34.47	74.01
	O(h^4)	50.23	71.58

Table 15. Estimated drug release equation by numerical differentiation: forward difference formula of order O(h) and central difference formula of order O(h^4), where $C_{3,k}(t)$ represents the total quantity of drug released at a specified time (t) (day).

Formula	Forward difference formula O(h)	Rel. Err. O(h)	Central difference formula O(h^4)	Rel. Err. O(h^4)
Lv20ZD	$C_{3,k}(t) = 103.5[1 - e^{0.7081(-t)}]$	1.34	$C_{3,k}(t) = 105.5[1 - e^{0.6614(-t)}]$	1.36
Lv25ZD	$C_{3,k}(t) = 88.97[1 - e^{0.6446(-t)}]$	1.38	$C_{3,k}(t) = 88.6[1 - e^{0.8095(-t)}]$	1.29
Lv20ZG	$C_{3,k}(t) = 98.35[1 - e^{0.5948(-t)}]$	1.40	$C_{3,k}(t) = 104.5[1 - e^{0.4069(-t)}]$	1.55
Lv25ZG	$C_{3,k}(t) = 74.01[1 - e^{0.4309(-t)}]$	1.52	$C_{3,k}(t) = 71.58[1 - e^{0.6279(-t)}]$	1.37
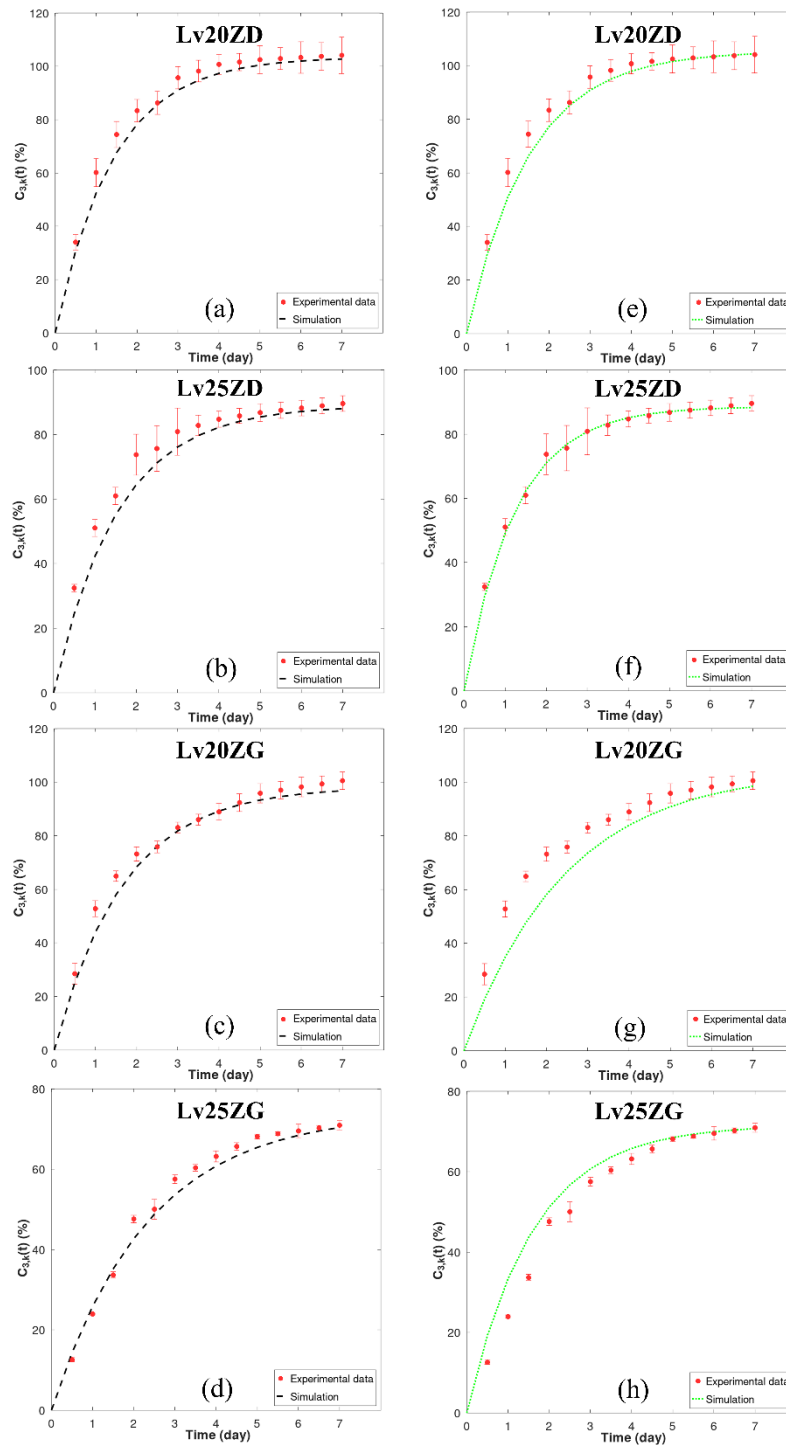
Figure 42. Model fit to experimental Lv-release data of zein-loaded ISM formulations by numerical differentiation: forward difference formula of order O(h) (a, b, c, d) and central difference formula of order O(h^4) (e, f, g, h). The y-axis ($C_{3,k}$) represents the % cumulative of Lv released over time. The corresponding relative errors for (a)-(d) for O(h) were found to be between 1.34 and 1.52 The corresponding relative errors for (e)-(h) for O(h^4) were found to be between 1.29 and 1.55, respectively.

4.10. Simulation of drug release pattern by varying the rate of drug transport from polymer matrix to exterior phase ($K_{32,k}$) and drug release profile by varying the maximum drug concentration at the edge of the matrix phase $C_{2,k}(r_2)$

As illustrated, this model effectively traced the changes in drug concentrations within zein-based ISM system over time. This stands in contrast to previously established mathematical models that characterize controlled drug release from matrix systems (290-292). Upon collecting experimental data, the model output was fitted with the experimental data to acquire optimal parameter estimates listed in Table 14. The parameter values were obtained by solving the ordinary differential equation of the model simulations within the specified parameter range. These parameters encompass the rate of drug transport from the polymer matrix to the external phase ($K_{32,k}$). Specifically, $K_{32,k}$ values as indicated at 30 (day^{-1}) and 65 (day^{-1}). Additionally, the maximum drug concentration at the edge of the matrix phase $C_{2,k}(r_2)$ was considered, with $C_{2,k}$ values of 70% and 105%. These parameters, crucial for drug release from the ISM, were determined using the mechanistic model described in Equation (8). The model predictions for drug release from zein-based ISM formulations were assessed for different $C_{2,k}(r_2)$ values, specifically considering $K_{32,k}$ values of 30 (day^{-1}) and 65 (day^{-1}). These predictions are visualized in Figure 43 (a, b) and Figure 43 (c, d) respectively.

Although the general initial trends remained consistent with these alterations, it was observed that implants with lower $K_{32,k}$ values (Figure 43a and 43b) displayed a comparatively slower initial release rate compared to those with higher $K_{32,k}$ values (Figure 42c and 42d). However, upon reaching a stable steady state in the release of both the solvent and the drug (293), the Lv content in the formulations approached levels close to $C_{2,k}(r_2)$ by the 7th day. Furthermore, the selection of the range of drug transport rates, which spans from 32.55 (day^{-1}) to 64.76 (day^{-1}), was based on the order O(h^4) from Table 14, allowing for a more accurate estimation." For LvZG20 and LvZG25, the rates of drug transport were 32.55 and 50.23 (day^{-1}), respectively. Conspicuously, it showed the reduced rates of drug transport at lower concentrations. Additionally, the formation of zein at higher polymer concentrations can be attributed to enhanced molecular chain entanglement, which in turn inhibited the breakup of the polymer jet, leading to sustained release of the loaded drug (65, 294). This observation echoes the earlier finding where the lower molecular weight PLGA implants exhibited a slower initial release rate than the higher molecular weight PLGA implants, with the former demonstrating degradative release at an earlier stage (160). This approach was mirrored in our selection of ISM formulations, where diverse concentrations of zein were utilized. This deliberate selection aligns with earlier research highlighting the efficacy of varying the concentration of zein in formulations to control the release of low molecular weight drugs (158).

The findings from Table 14 indicate that both LvZD20 and LvZG20 formulations displayed $C_{2,k}(r_2)$ values around 100-105%, while LvZD25 and LvZG25 formulations exhibited $C_{2,k}(r_2)$ values of approximately 70-90%. The model's estimations of drug release from zein-based ISM formulations were examined for different $K_{32,k}$ values, specifically with regard to $C_{2,k}(r_2)$ values of 70% and 105%. These estimations are visualized in Figure 44 (a, b) and Figure 44 (c, d), respectively.

The outcomes emphasize the significance of altering $K_{32,k}$ value. Lower $K_{32,k}$ values were correlated with a comparatively slower initial release rate compared to formulations featuring higher $K_{32,k}$ values. However, during the steady-state phase, the cumulative Lv content gradually approached and eventually reached levels near $C_{2,k}(r_2)$ %. It is noteworthy that formulations with $K_{32,k}$ values ranging from 10 to 40 (day^{-1}) not achieve the $C_{2,k}(r_2)$% within the span of 7 days. Nonetheless, it is evident that these formulations exhibit a tendency to approach the specified threshold, although they require an extended duration to achieve complete release. The concentration of zein significantly impacted the surface and internal topographies, particularly the interconnected porous structure of the ISM (65). Furthermore, in our previous work, as the amount of zein increased, the pore sizes within the structure notably diminished. These pores served as primary conduits for the release of Lv molecules from the inner zein gel or matrix into the surrounding release medium (229). This outcome was particularly evident (here or in previous work (229)), indicating that higher zein concentrations were more effective in retarding the drug release.
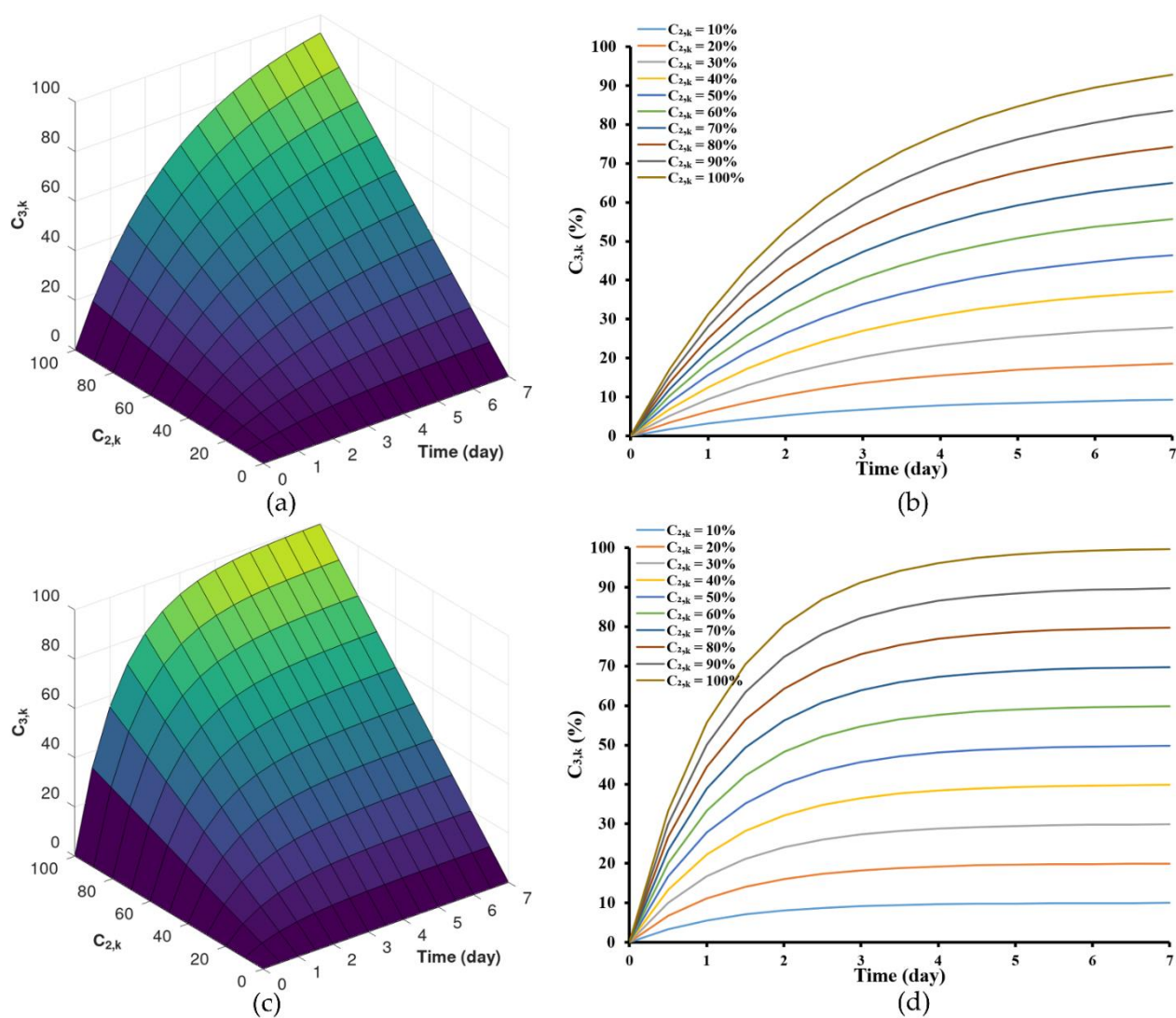
Figure 43. Model predictions of drug release from zein-based ISM formulations for different concentration of drug in the interior at the interface between the interior phase and void space of the matrix, $K_{32,k} = 30$ (day^{-1}) (a, b) and $K_{32,k} = 65$ (day^{-1}) (c, d)
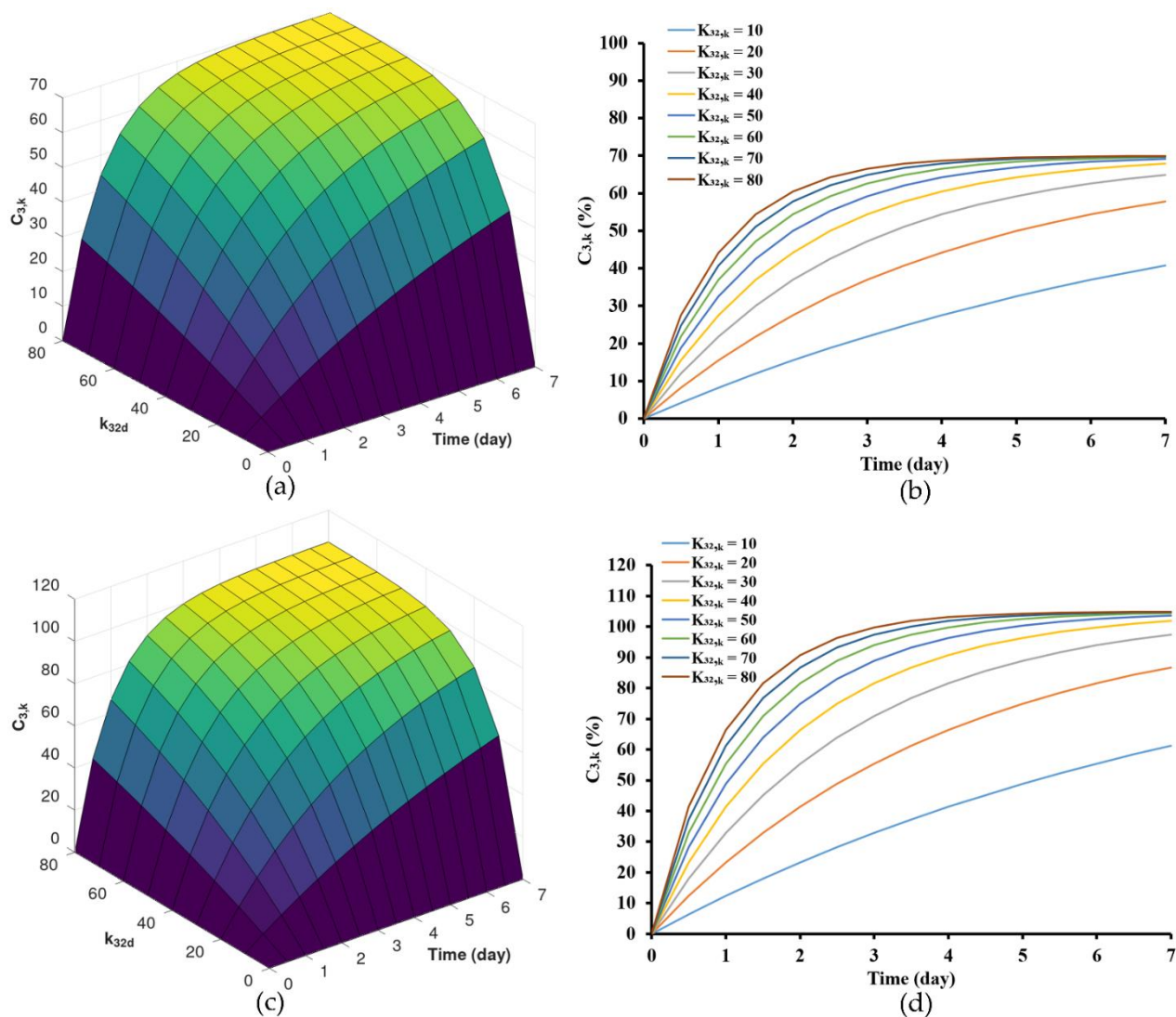
Figure 44. Model predictions of drug release from zein-based ISM formulations for different drug permeability coefficient, $C_{2,k}(r_2) = 70$ % (a, b) and $C_{2,k}(r_2) = 105$ % (c, d)

4.11. The behavior of Lv diffusion, solvent diffusion and matrix formation using UV-vis imagine.

In the typical process, solvent exchange occurred upon the ISMs contact with an aqueous solvent (7). This initial mechanism within the ISM led to matrix formation and subsequently controlled the drug release. To visualize the mechanisms of the solvent (DMSO and GF), drug (Lv), and matrix-forming component (zein) interactions, an agarose gel system was employed, multiple techniques can be utilized, including UV-vis imaging, staining, or fluorescent labeling (295-297), could be utilized for visualizing these interactions within the matrix, UV-vis imaging stands out due to its advantages. Staining techniques, while valuable in certain cases, come with limitations compared to UV-vis imaging. UV-vis imaging offers real-time visualization and quantitative analysis of drug release, ensuring a more accurate and comprehensive tracking of drug behavior within the matrix. Therefore, considering the specific research goals, UV-vis imaging was selected as the more robust method for tracking drug release in this study (148). The wavelength of 214 nm was selected to monitor the solvents, while a wavelength of 280 nm was chosen to monitor the drug diffusion. Additionally, a wavelength of 525 nm was employed to observe the formation of the solid-like matrix derived from zein, in line with previous studies (150, 296, 298). The selection of these wavelengths was motivated by the chromophores of the various components. To this end, GF does not posses a viable chromophore, the apparent change in absorbance was probably reflecting a change in refractive index. A recognised challenge of UV-vis spectrophoptometry and therefore of UV-vis imaging is the lack of selectivity as considered below.

Once in contact with aqueous phase from agarose, the ISM prompts diffusion of its solvent (and drug) into the agarose gel, the transport gradually slows down over time as the concentration gradient becomes less steep. The absorbance profile of the solvent on the agarose gel was visualized through color mapping and is displayed in Figure 45A and Figure 46A. The color-coded map depicts solvent absorbances across the agarose gel. Red indicates high concentration, while blue marks near-zero absorbance areas. At the outset, solvent diffusion exhibited its highest rate, gradually diminishing over time. The result might appear similar for both DMSO and ZG20 because, after more than 3 h, formulations containing zein and DMSO exhibited a behavior where the DMSO solvent could permeate the matrix, similar to what was observed with DMSO alone. Therefore, while we did not quantify the concentration, the behavior of DMSO and ZG20 in terms of solvent permeation exhibited similarities beyond a certain timeframe. Indeed, during the initial phase, the matrix formation should occur abruptly, leading to a partial obstruction of solvent diffusion. This obstruction subsequently results in a slowdown of the solvent exchange process (65, 193, 299). GF displayed minimal, if any, noticeable absorbance shifts. (Figure 46A), signifying the inadequacy of the 214 nm wavelength for detecting GF. Additionally, it was observed that zein did absorb light at 214 nm (300), as seen in Figure 46A. Over time, the matrix derived from 20ZG exhibited a gradual increase in thickness and

firmness. Similarly, in formulations incorporating Lv, the absorbance of Lv at 214 nm was notable (301).

The wavelength of 280 nm was chosen for Lv in this study due to its close alignment with the peak absorbance on the Lv spectrum (302). Figure 45B and Figure 46B depict the diffusion behavior of Lv through the agarose gel. In Figure 45B at t = 0 h, the coloration that appears as blue corresponds to low absorbance values. However, it is important to consider the potential impact of DMSO interference, which arises from the absorption of DMSO within the spectral range of 289-303 nm (303). At t = 3 h in Figure 46B, detection of GF was not possible at 280 nm. As depicted in Figure 45b, the vibrant shades of yellow and red (represented using false coloring) in the images correspond to both dissolved drug and drug that has precipitatedas previously explained in comprehensive detail (304). Subsequent to ISM's contact with the agarose gel, Lv diffusion occurred concurrently with an increasing distance within the matrix over time. This behavior is attributed to the solubility of the drug in the zein, solvent and its concentration, which could result in either drug dissolution or dispersion within the *in situ* forming implant (233). Depending on these factors, different behaviors have been observed and described. For instance, the impact of low drug loading on the release of in *situ* implants has been explored in various studies. Wang et al. (305) investigated the effect of ketoprofen loading from 4 to 10% m/m (PLGA 70:30, 35% m/m in NMP) and concluded that it had no significant impact on *in vitro* drug release. In the case of zein ISM using both DMSO and GF as solvents, it is noteworthy that formulations loaded with 1% Lv, surpassing the 0.1% Lv concentration, exhibited a gradual decline in concentration with increasing distance from the interface. This behavior is attributed to the influence of ingredient concentration on the absorbance profile (306), might be influenced by zein's impact on Lv absorbance. This suggests a possible artifact from UV imaging, demanding further investigation for a complete understanding.

In visible imaging at 525 nm, as observed in Figure 45C and Figure 46C, the transformation of zein in DMSO into a matrix appeared to occur more rapidly as compared to GF containing formulations. Additionally, the type of solvent (GF and DMSO) influenced the initiation of matrix formation (293). DMSO, due to its greater polarity and water miscibility in contrast to GF, exerted a stronger effect on the rate and morphology of zein matrix formation , subsequently impacting solvent exchange and controlled drug release rates. The absence of pores within the matrix played a crucial role in determining the drug retention capacity (307). A well-structured and robust matrix often led to the development of a thick matrix. When a drug was loaded into such a rigid matrix, it became entrapped, resulting in a gradual release over time. Conversely, a less dense matrix could weaken matrix formation and fail to effectively control drug release (229, 263). This outcome reaffirms the previous findings, demonstrating that the utilization of GF as a solvent substantially led to a slower release of Lv compared to DMSO as the solvent (229).
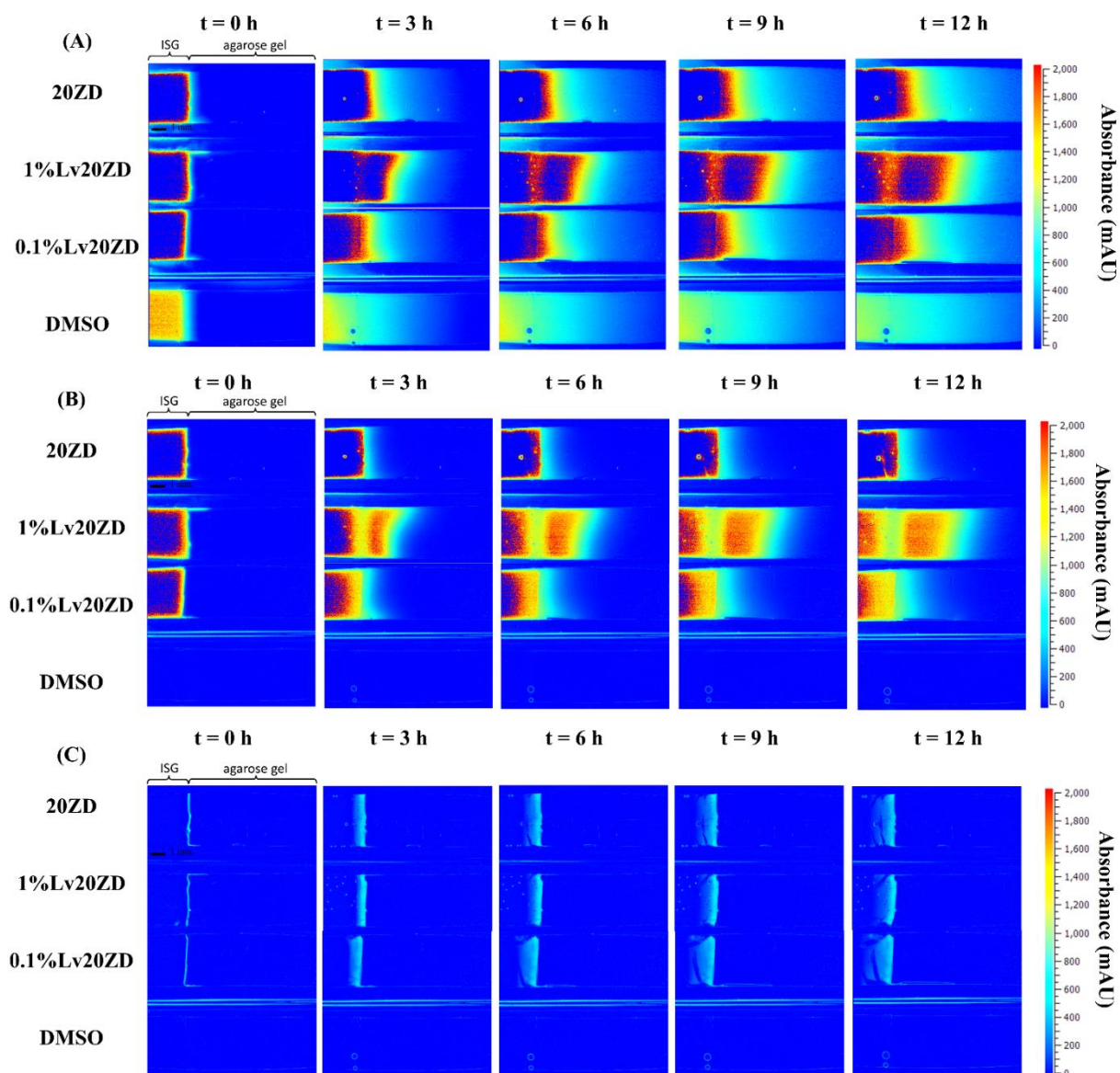
Figure 45. Representative absorbance maps of 20ZD, 1%Lv20ZD, 0.1%Lv20ZD and DMSO observed by UV imaging at 214 nm (A), 280 nm (B), and visible imaging at 525 nm (C) in 0.6% (w/v) agarose gel at selected time points.
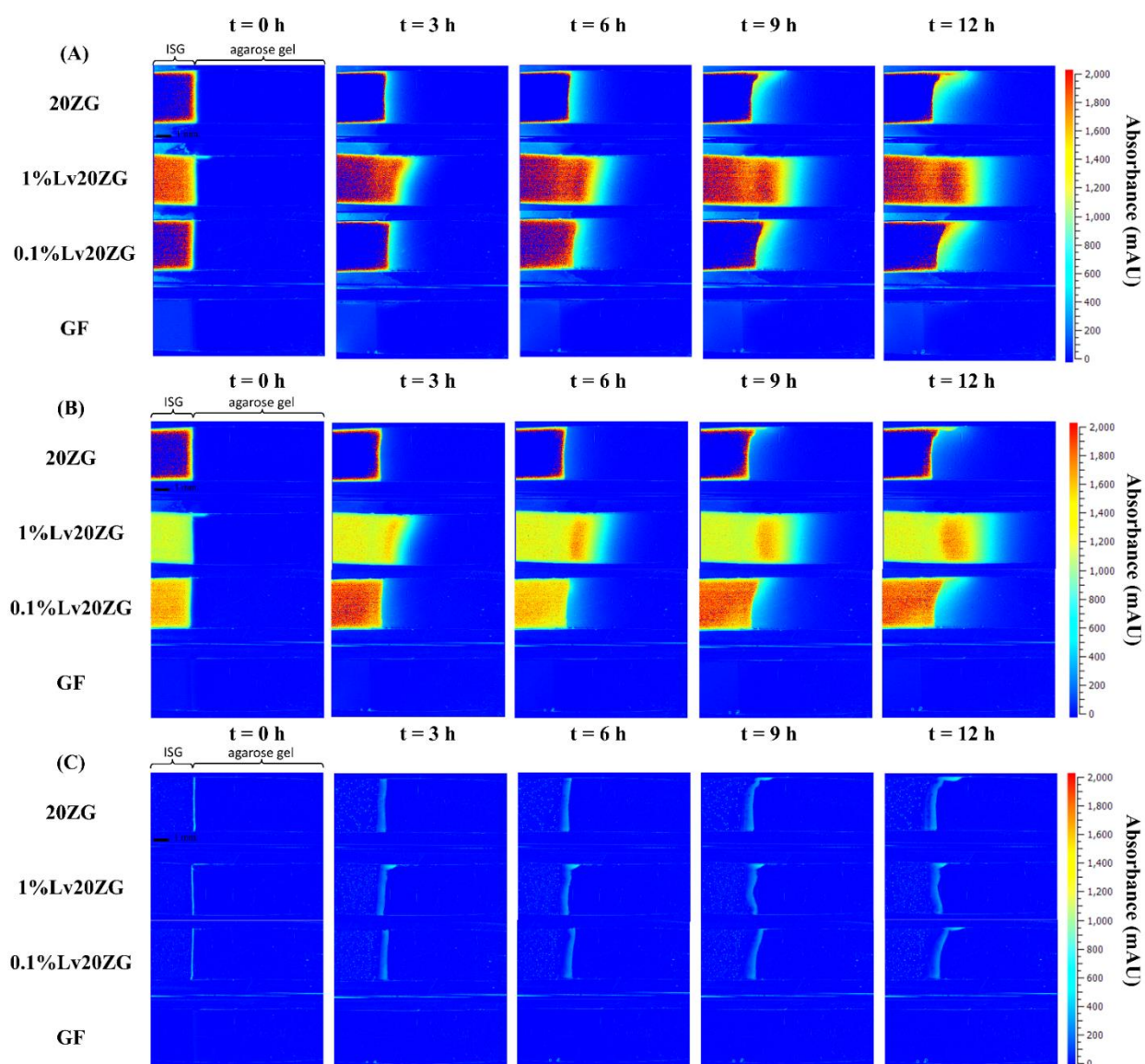
Figure 46. Representative absorbance maps of 20ZG, 1%Lv20ZG, 0.1%Lv20ZG and GF observed by UV-vis imaging at 214 nm (A), 280 nm (B), and visible imaging at 525 nm (C) in 0.6% (w/v) agarose gel at selected time points.

4.12. Summary

This study was primarily focused on the mathematical modeling of drug release from zein-based ISMs. The experimental drug release data were compared with simulation results obtained using numerical differentiation methods. LvZD20 and LvZD25 formulations closely matched the experimental data, and LvZG20 and LvZG25 formulations better aligned with experimental data when employing the forward difference formula of order $O(h)$ rather than $O(h^4)$. Parameters derived from numerical differentiation were utilized to estimate the drug release equation (Equation 8), providing insights into the transport of Lv. The innovation of this study lies in the adaptable numerical differentiation methods capable of handling intricate geometries or functions. The findings revealed that higher zein concentrations resulted in prolonged drug release, facilitated by denser matrices in formulations with high polymer loadings. Additionally, the values of $K_{32,k}$ indicated that LvZD formulations exhibited a faster drug transport rate from the polymer matrix to the external phase compared to LvZG formulations. UV-vis imaging conducted at 214 nm, 280 nm, and 525 nm visualized the processes of solvent, drug, and zein matrix formation. The choice of DMSO or GF solvent influenced matrix formation rates, impacting solvent exchange and drug release. Distinctively, GF led to a slower release compared to DMSO. These findings contribute to a deeper comprehension of controlled drug release from matrix systems and offer methodological advancements for future research in drug delivery.

CHAPTER 5

Conclusion

In conclusion, this thesis embarks on a comprehensive journey through the realm of ISM formulations, illuminating their profound potential as advanced drug delivery systems, particularly in the context of localized therapies for periodontal pocket treatment. This exploration unfolds in four distinct parts, each interwoven to reveal a multi-dimensional understanding of ISMs. Initially, the choice of MP as a solvent for Eudragit® L-based ISMs demonstrates its pivotal role in crafting formulations tailored for periodontitis management, marked by optimal physical attributes, controlled drug delivery capabilities, and a transition from a cloudy gel solution to a solid matrix in the presence of aqueous environments. Fluorescence dye tracking adds depth to our understanding. Moreover, delves into the diverse impact of solvents on Mx-incorporated Nc-based ISMs, designed for targeted drug delivery to periodontal pockets. This exploration unravels the intricate interplay of various solvents, influencing viscosity, injection force, matrix formation, and water sensitivity, ultimately leading to Newtonian flow behavior and efficient matrix formation upon contact with water. The versatility of these formulations ensures patient compliance, while the antimicrobial effectiveness against various strains, including MRSA, underlines their potential. Nevertheless, introduces a zein-based ISM formulation, where DMSO and GF solvents leave their indelible mark, significantly impacting viscosity, injection force, and drug release profiles. GF's contribution, leading to extended drug release, is showcased through SEM and X-ray imaging, unveiling distinct topographic patterns and porosity. Zein's incorporation fine-tunes drug diffusion, enhancing its efficacy. The fourth facet delves into mathematical modeling, offering insights into drug release kinetics and transport mechanisms, complemented by UV-vis imaging that sheds light on solvent, drug, and matrix formation. Solvent choice emerges as a pivotal factor shaping matrix formation rates and drug release profiles. In concert, these four facets of the thesis paint a holistic picture of ISM formulations' potential for controlled drug delivery in periodontal pocket treatment. By melding innovative approaches like UV-vis imaging and mathematical modeling, this research pushes the boundaries of our understanding of formulation attributes, release kinetics, and therapeutic outcomes. The discoveries underscore the promise of these advanced drug delivery systems, underscoring the imperative need for rigorous clinical trials to gauge their safety and efficacy in real-world scenarios. Moving forward, this body of work paves the way for the development of tailored and effective drug delivery strategies that address a wide range of therapeutic needs beyond periodontal care.

Suggestion

This study serves as a first steps exploration into the potential of utilizing these polymers, particularly Nc, as matrix-forming agents in solvent removal phase-inversion-based ISM systems. To advance our understanding, further research is recommended. Conducting comparative drug release studies with existing commercial ISM formulations would provide valuable insights into the performance of the developed formulations. Optimizing the concentration of Nc within the ISM systems would be beneficial to achieve optimal physicochemical properties. Additionally, other relevant experiments should be pursued to enhance our comprehension of these systems, including more comprehensive numerical simulations to refine and validate the mathematical models used. Considering the importance of safety, it's advisable to conduct cytotoxicity studies on various cell lines. Moreover, moving towards *in vivo* studies involving animal models is crucial for assessing cytotoxicity and the pharmaceutical efficacy of the ISM systems in treating periodontitis. These comprehensive investigations would contribute to the safe and effective utilization of these ISM formulations in pharmaceutical applications, ultimately enhancing their potential impact in clinical practice.
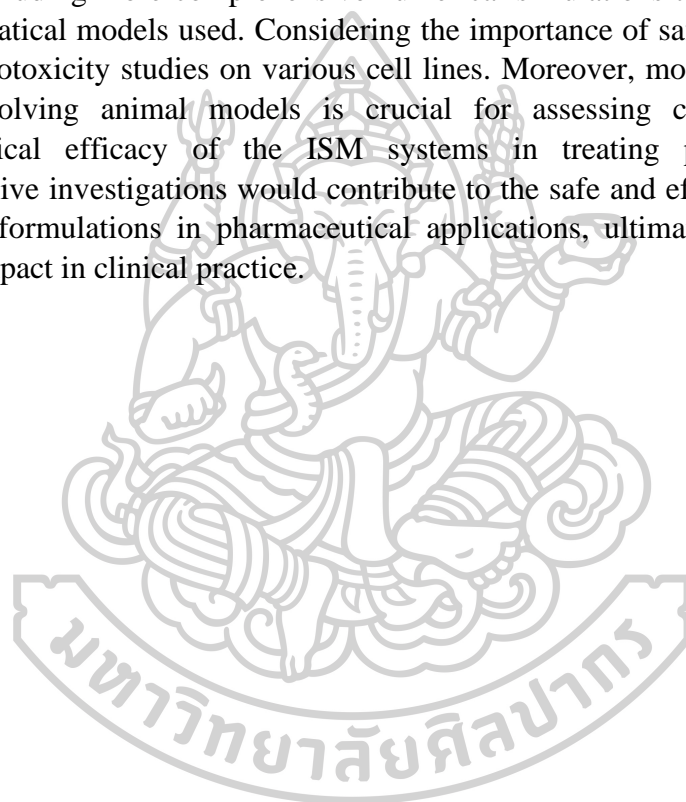
REFERENCES

1. Elstad NL, Fowers KD. OncoGel (ReGel/paclitaxel)--clinical applications for a novel paclitaxel delivery system. Adv Drug Deliv Rev. 2009;61(10):785-94. doi:10.1016/j.addr.2009.04.010.

2. Cleland JL, Daugherty A, Mrsny R. Emerging protein delivery methods. Curr Opin Biotechnol. 2001;12(2):212-9. doi:10.1016/s0958-1669(00)00202-0.

3. Dong WY, Körber M, López Esguerra V, Bodmeier R. Stability of poly(D,L-lactide-co-glycolide) and leuprolide acetate in *in-situ* forming drug delivery systems. J Control Release. 2006;115(2):158-67. doi:10.1016/j.jconrel.2006.07.013.

4. Hatefi A, Amsden B. Biodegradable injectable *in situ* forming drug delivery systems. J Control Release. 2002;80(1-3):9-28. doi:10.1016/s0168-3659(02)00008-1.

5. Chitkara D, Shikanov A, Kumar N, Domb AJ. Biodegradable injectable *in situ* depot-forming drug delivery systems. Macromol Biosci. 2006;6(12):977-90. doi:10.1002/mabi.200600129.

6. Kanwar N, Sinha VR. In Situ Forming Depot as Sustained-Release Drug Delivery Systems. Crit Rev Ther Drug Carrier Syst. 2019;36(2):93-136. doi:10.1615/CritRevTherDrugCarrierSyst.2018025013.

7. Thakur RRS, McMillan HL, Jones DS. Solvent induced phase inversion-based *in situ* forming controlled release drug delivery implants. J Control Release. 2014;176:8-23. doi:https://doi.org/10.1016/j.jconrel.2013.12.020.

8. Karp F, Turino LN, Helbling IM, Islan GA, Luna JA, Estenoz DA. *In situ* formed implants, based on PLGA and Eudragit blends, for novel florfenicol controlled release formulations. J Pharm Sci. 2021;110(3):1270-8. doi:10.1016/j.xphs.2020.11.006.

9. Ganguly S, Dash AK. A novel *in situ* gel for sustained drug delivery and targeting. Int J Pharm. 2004;276(1-2):83-92. doi:10.1016/j.ijpharm.2004.02.014.

10. Raman C, McHugh AJ. A model for drug release from fast phase inverting injectable solutions. J Control Release. 2005;102(1):145-57. doi:10.1016/j.jconrel.2004.09.022.

11. Graham PD, Brodbeck KJ, McHugh AJ. Phase inversion dynamics of PLGA solutions related to drug delivery. J Control Release. 1999;58(2):233-45. doi:10.1016/s0168-3659(98)00158-8.

12. McHugh AJ. The role of polymer membrane formation in sustained release drug delivery systems. J Control Release. 2005;109(1-3):211-21. doi:10.1016/j.jconrel.2005.09.038.

13. Kranz H, Bodmeier R. A novel *in situ* forming drug delivery system for controlled parenteral drug delivery. Int J Pharm. 2007;332(1-2):107-14. doi:10.1016/j.ijpharm.2006.09.033.

14. Phaechamud T, Chanyaboonsub N, Setthajindalert O. Doxycycline hyclate-loaded bleached shellac *in situ* forming microparticle for intraperiodontal pocket local delivery. Eur J Pharm Sci. 2016;93:360-70. doi:10.1016/j.ejps.2016.08.034.

15. Kranz H, Yilmaz E, Brazeau GA, Bodmeier R. *In vitro* and *in vivo* drug release from a novel *in situ* forming drug delivery system. Pharm Res. 2008;25(6):1347-54. doi:10.1007/s11095-007-9478-y.

16. Kranz H, Bodmeier R. Structure formation and characterization of injectable drug loaded biodegradable devices: *in situ* implants versus *in situ* microparticles. Eur J Pharm Sci. 2008;34(2-3):164-72. doi:10.1016/j.ejps.2008.03.004.

17. Dunn RL, English JP, Cowsar DR, Vanderbilt DP, Biodegradable in-situ forming implants and methods of producing the same. US patent US 4938763 A. 1999 1997-11-07.

18. Sartor O. Eligard: leuprolide acetate in a novel sustained-release delivery system. Urology. 2003;61(2 Suppl 1):25-31. doi:10.1016/s0090-4295(02)02396-8.

19. Stoller NH, Johnson LR, Trapnell S, Harrold CQ, Garrett S. The pharmacokinetic profile of a biodegradable controlled-release delivery system containing doxycycline compared to systemically delivered doxycycline in gingival crevicular fluid, saliva, and serum. J Periodontol. 1998;69(10):1085-91. doi:10.1902/jop.1998.69.10.1085.

20. Garrett S, Johnson L, Drisko CH, Adams DF, Bandt C, Beiswanger B, et al. Two multi-center studies evaluating locally delivered doxycycline hyclate, placebo control, oral hygiene, and scaling and root planing in the treatment of periodontitis. J Periodontol. 1999;70(5):490-503. doi:10.1902/jop.1999.70.5.490.

21. Phaechamud T, Jantadee T, Mahadlek J, Charoensuksai P, Pichayakorn W. Characterization of antimicrobial agent loaded eudragit RS solvent exchange-induced *in situ* forming gels for periodontitis treatment. AAPS PharmSciTech. 2017;18(2):494-508. doi:10.1208/s12249-016-0534-y.

22. Antunes JL, Toporcov TN, Bastos JL, Frazão P, Narvai PC, Peres MA. Oral health in the agenda of priorities in public health. Rev Saude Publica. 2016;50:57. doi:10.1590/s1518-8787.2016050007093.

23. Griffin SO, Barker LK, Griffin PM, Cleveland JL, Kohn W. Oral health needs among adults in the United States with chronic diseases. J Am Dent Assoc. 2009;140(10):1266-74. doi:10.14219/jada.archive.2009.0050.

24. Fiorillo L. Oral health: the first step to well-being. Medicina. 2019;55(10). doi:10.3390/medicina55100676.

25. Nazir MA. Prevalence of periodontal disease, its association with systemic diseases and prevention. Int J Health Sci (Qassim). 2017;11(2):72-80.

26. Nazir M, Al-Ansari A, Al-Khalifa K, Alhareky M, Gaffar B, Almas K. Global prevalence of periodontal disease and lack of its surveillance. Sci World J. 2020;2020:2146160. doi:10.1155/2020/2146160.

27. สำนักงานทันตสาธารณสุข. รายงานผลการสำรวจสภาวะสุขภาพช่องปากแห่งชาติ ครั้งที่ 8 ประเทศไทย พ.ศ. 2560. 2018:19-20.

28. Janket SJ, Baird AE, Chuang SK, Jones JA. Meta-analysis of periodontal disease and risk of coronary heart disease and stroke. Oral Surg Oral Med Oral Pathol Oral Radiol Endod. 2003;95(5):559-69. doi:10.1067/moe.2003.107.

29. Kinane DF, Stathopoulou PG, Papapanou PN. Periodontal diseases. Nat Rev Dis Primers. 2017;3:17038. doi:10.1038/nrdp.2017.38.

30. Özdoğan AI, İlarslan YD, Kösemehmetoğlu K, Akca G, Kutlu HB, Comerdov E, et al. *In vivo* evaluation of chitosan based local delivery systems for atorvastatin in treatment of periodontitis. Int J Pharm. 2018;550(1-2):470-6. doi:10.1016/j.ijpharm.2018.08.058.

31. Najeeb S, Zafar MS, Khurshid Z, Zohaib S, Madathil SA, Mali M, et al. Efficacy of metformin in the management of periodontitis: A systematic review and meta-

analysis. Saudi Pharm J. 2018;26(5):634-42. doi:https://doi.org/10.1016/j.jsps.2018.02.029.

32. Patil V, Mali R, Mali A. Systemic anti-microbial agents used in periodontal therapy. J Indian Soc Periodontol. 2013;17(2):162-8. doi:10.4103/0972-124X.113063.

33. Slots J. Selection of antimicrobial agents in periodontal therapy. J Periodontal Res. 2002;37(5):389-98. doi:10.1034/j.1600-0765.2002.00004.x.

34. Vyas SP, Sihorkar V, Mishra V. Controlled and targeted drug delivery strategies towards intraperiodontal pocket diseases. J Clin Pharm Ther. 2000;25(1):21-42. doi:10.1046/j.1365-2710.2000.00261.x.

35. Yacoubi DA, Bouziane D, Leila M, Bensoltane A. Microbiological study of periodontitis in the west of Algeria. World J Medical Sci. 2010;5 (1):07-12.

36. Fritschi BZ, Albert-Kiszely A, Persson GR. *Staphylococcus aureus* and other bacteria in untreated periodontitis. J Dent Res. 2008;87(6):589-93. doi:10.1177/154405910808700605.

37. Baliga S, Muglikar S, Kale R. Salivary pH: A diagnostic biomarker. J Indian Soc Periodontol. 2013;17(4):461-5. doi:10.4103/0972-124x.118317.

38. Genco RJ. Antibiotics in the treatment of human periodontal diseases. J Periodontol. 1981;52(9):545-58. doi:10.1902/jop.1981.52.9.545.

39. Sanz I, Alonso B, Carasol M, Herrera D, Sanz M. Nonsurgical treatment of periodontitis. J Evid Based Dent Pract. 2012;12(3 Suppl):76-86. doi:10.1016/s1532-3382(12)70019-2.

40. Pitcher GR, Newman HN, Strahan JD. Access to subgingival plaque by disclosing agents using mouthrinsing and direct irrigation. J Clin Periodontol. 1980;7(4):300-8. doi:10.1111/j.1600-051x.1980.tb01972.x.

41. Slots J, Rams TE. Antibiotics in periodontal therapy: advantages and disadvantages. J Clin Periodontol. 1990;17(7 (Pt 2)):479-93. doi:10.1111/j.1365-2710.1992.tb01220.x.

42. Zilberman M, Elsner JJ. Antibiotic-eluting medical devices for various applications. J Control Release. 2008;130(3):202-15. doi:10.1016/j.jconrel.2008.05.020.

43. Rams TE, Degener JE, van Winkelhoff AJ. Antibiotic resistance in human chronic periodontitis microbiota. J Periodontol. 2014;85(1):160-9. doi:10.1902/jop.2013.130142.

44. H R R, Dhamecha D, Jagwani S, Rao M, Jadhav K, Shaikh S, et al. Local drug delivery systems in the management of periodontitis: A scientific review. J Control Release. 2019;307. doi:10.1016/j.jconrel.2019.06.038.

45. Ghavami-Lahiji M, Shafiei F, Najafi F, Erfan M. Drug-loaded polymeric films as a promising tool for the treatment of periodontitis. J Drug Deliv Sci Technol. 2019;52:122-9. doi:https://doi.org/10.1016/j.jddst.2019.04.034.

46. Mummolo S, Severino M, Campanella V, Barlattani A, Jr., Quinzi V, Marchetti E. Chlorhexidine gel used as antiseptic in periodontal pockets. J Biol Regul Homeost Agents. 2019;33(3 Suppl. 1):83-8. Dental supplement.

47. Moran J, Addy M, Wade W, Newcombe R. The use of antimicrobial acrylic strips in the nonsurgical management of chronic periodontitis. Clin Mater. 1990;6(2):123-35. doi:10.1016/0267-6605(90)90003-e.

48. Swain GP, Patel S, Gandhi J, Shah P. Development of Moxifloxacin

Hydrochloride loaded *in-situ* gel for the treatment of periodontitis: *In-vitro* drug release study and antibacterial activity. J Oral Biol Craniofac Res. 2019;9(3):190-200. doi:10.1016/j.jobcr.2019.04.001.

49. Rein SMT, Lwin WW, Tuntarawongsa S, Phaechamud T. Meloxicam-loaded solvent exchange-induced *in situ* forming beta-cyclodextrin gel and microparticle for periodontal pocket delivery. Mater Sci Eng C. 2020;117:111275. doi:https://doi.org/10.1016/j.msec.2020.111275.

50. Scaling and root planing for gum disease - American Dental Association [Internet]. Mouthhealthy.org. [cited 28 January 2022].

51. Widjaja M, Gan J, Talpaneni JS, Tjandrawinata RR. Determination of Eudragit® L100 in an enteric-coated tablet formulation using size-exclusion chromatography with charged-aerosol detection. Sci Pharm. 2018;86(3):38. doi:10.3390/scipharm86030038.

52. Patra CN, Priya R, Swain S, Kumar Jena G, Panigrahi KC, Ghose D. Pharmaceutical significance of Eudragit: A review. Future J Pharm Sci. 2017;3(1):33-45. doi:https://doi.org/10.1016/j.fjps.2017.02.001.

53. Aguilar LE, Unnithan AR, Amarjargal A, Tiwari AP, Hong ST, Park CH, et al. Electrospun polyurethane/Eudragit® L100-55 composite mats for the pH dependent release of paclitaxel on duodenal stent cover application. Int J Pharm. 2015;478(1):1-8. doi:10.1016/j.ijpharm.2014.10.057.

54. Malipeddi VR, Awasthi R, Ghisleni DD, de Souza Braga M, Kikuchi IS, de Jesus Andreoli Pinto T, et al. Preparation and characterization of metoprolol tartrate containing matrix type transdermal drug delivery system. Drug Deliv Transl Res. 2017;7(1):66-76. doi:10.1007/s13346-016-0334-7.

55. Sareen R, Nath K, Jain N, Dhar KL. Curcumin loaded microsponges for colon targeting in inflammatory bowel disease: fabrication, optimization, and *in vitro* and pharmacodynamic evaluation. Biomed Res Int. 2014;2014:340701. doi:10.1155/2014/340701.

56. Li P, Yang Z, Wang Y, Peng Z, Li S, Kong L, et al. Microencapsulation of coupled folate and chitosan nanoparticles for targeted delivery of combination drugs to colon. J Microencapsul. 2015;32(1):40-5. doi:10.3109/02652048.2014.944947.

57. Hosny KM, Ahmed OAA, Al-Abdali RT. Enteric-coated alendronate sodium nanoliposomes: a novel formula to overcome barriers for the treatment of osteoporosis. Expert Opin Drug Deliv. 2013;10(6):741-6. doi:10.1517/17425247.2013.799136.

58. Wilson B, Babubhai PP, Sajeev MS, Jenita JL, Priyadarshini SRB. Sustained release enteric coated tablets of pantoprazole: Formulation, *in vitro* and *in vivo* evaluation. Acta Pharmaceutica. 2013;63(1):131-40. doi:doi:10.2478/acph-2013-0002.

59. Mahadlek J, Tuntarawongsa S, Senarat S, Phaechamud T. *In situ* solvent removal-based Eudragit®L/dimethyl sulfoxide forming gel for periodontal pocket drug delivery. Mater Today: Proc. 2022;52:2394-99. doi:https://doi.org/10.1016/j.matpr.2021.10.248.

60. Shukla R, Cheryan M. Zein: the industrial protein from corn. Ind Crops Prod. 2001;13(3):171-92. doi:https://doi.org/10.1016/S0926-6690(00)00064-9.

61. Wang SZ, Esen A. Primary structure of a proline-rich zein and its cDNA. Plant

Physiol. 1986;81(1):70-4. doi:10.1104/pp.81.1.70.

62. Lawton JW. Zein: A history of processing and use. Cereal Chem. 2002;79(1):1-18. doi:https://doi.org/10.1094/CCHEM.2002.79.1.1.

63. Wang Y, Padua GW. Nanoscale characterization of zein self-assembly. Langmuir. 2012;28(5):2429-35. doi:10.1021/la204204j.

64. Madeka H, Kokini JL. Effect of glass transition and cross-linking on rheological properties of zein: Development of a preliminary state diagram. Cereal Chemistry. 1996;73(4):433-8.

65. Paliwal R, Palakurthi S. Zein in controlled drug delivery and tissue engineering. J Control Release. 2014;189:108-22. doi:10.1016/j.jconrel.2014.06.036.

66. Ravindran Girija A, Sivakumar B, Brahatheeswaran D, Fukuda T, Yoshida Y, Maekawa T, et al. Biocompatible fluorescent zein nanoparticles for simultaneous bioimaging and drug delivery application. Adv Nat Sci: NanosciNanotechnol. 2012;3. doi:10.1088/2043-6262/3/2/025006.

67. Argos P, Pedersen K, Marks MD, Larkins BA. A structural model for maize zein proteins. J Biol Chem. 1982;257(17):9984-90.

68. Esen A. A proposed nomenclature for the alcohol-soluble proteins (zeins) of maize (Zea mays L.). J Cereal Sci. 1987;5(2):117-28. doi:https://doi.org/10.1016/S0733-5210(87)80015-2.

69. Bagga S, Adams HP, Rodriguez FD, Kemp JD, Sengupta-Gopalan C. Coexpression of the maize delta-zein and beta-zein genes results in stable accumulation of delta-zein in endoplasmic reticulum-derived protein bodies formed by beta-zein. Plant Cell. 1997;9(9):1683-96. doi:10.1105/tpc.9.9.1683.

70. Meyer N, Rivera LR, Ellis T, Qi J, Ryan MP, Boccaccini AR. Bioactive and antibacterial coatings based on zein/bioactive glass composites by electrophoretic deposition. Coatings. 2018;8(1):27. doi:10.3390/coatings8010027.

71. Podaralla S, Perumal O. Influence of formulation factors on the preparation of zein nanoparticles. AAPS PharmSciTech. 2012;13(3):919-27. doi:10.1208/s12249-012-9816-1.

72. Kale AV, Cheryan M. Rapid analysis of xanthophylls in ethanol extracts of corn by HPLC. J Liq Chromatogr Relat. 2007;30(8):1093-104. doi:10.1080/10826070601128469.

73. Weissmueller NT, Lu HD, Hurley A, Prud'homme RK. Nanocarriers from GRAS zein proteins to encapsulate hydrophobic actives. Biomacromolecules. 2016;17(11):3828-37. doi:10.1021/acs.biomac.6b01440.

74. Wu Y, Luo Y, Wang Q. Antioxidant and antimicrobial properties of essential oils encapsulated in zein nanoparticles prepared by liquid–liquid dispersion method. LWT. 2012;48(2):283-90. doi:https://doi.org/10.1016/j.lwt.2012.03.027.

75. Brahatheeswaran D, Mathew A, Aswathy RG, Nagaoka Y, Venugopal K, Yoshida Y, et al. Hybrid fluorescent curcumin loaded zein electrospun nanofibrous scaffold for biomedical applications. Biomed Mater. 2012;7(4):045001. doi:10.1088/1748-6041/7/4/045001.

76. Podaralla S, Averineni R, Alqahtani M, Perumal O. Synthesis of novel biodegradable methoxy poly(ethylene glycol)-zein micelles for effective delivery of curcumin. Mol Pharm. 2012;9(9):2778-86. doi:10.1021/mp2006455.

77. Gong SJ, Sun SX, Sun QS, Wang JY, Liu XM, Liu GY. Tablets based on compressed zein microspheres for sustained oral administration: design,

pharmacokinetics, and clinical study. J Biomater Appl. 2011;26(2):195-208. doi:10.1177/0885328210363504.

78. Lin T, Lu C, Zhu L, Lu T. The biodegradation of zein *in vitro* and *in vivo* and its application in implants. AAPS PharmSciTech. 2011;12(1):172-6. doi:10.1208/s12249-010-9565-y.

79. Corradini E, Curti PS, Meniqueti AB, Martins AF, Rubira AF, Muniz EC. Recent advances in food-packing, pharmaceutical and biomedical applications of zein and zein-based materials. Int J Mol Sci. 2014;15(12):22438-70. doi:10.3390/ijms151222438.

80. Sun Q-S, Dong J, Lin Z-X, Yang B, Wang J-Y. Comparison of cytocompatibility of zein film with other biomaterials and its degradability *in vitro*. Biopolymers. 2005;78(5):268-74. doi:https://doi.org/10.1002/bip.20298.

81. Wang HJ, Gong SJ, Lin ZX, Fu JX, Xue ST, Huang JC, et al. *In vivo* biocompatibility and mechanical properties of porous zein scaffolds. Biomaterials. 2007;28(27):3952-64. doi:10.1016/j.biomaterials.2007.05.017.

82. Xiao D, Davidson PM, Zhong Q. Spray-dried zein capsules with coencapsulated nisin and thymol as antimicrobial delivery system for enhanced antilisterial properties. J Agric Food Chem. 2011;59(13):7393-404. doi:10.1021/jf200774v.

83. Wongsasulak S, Puttipaiboon N, Yoovidhya T. Fabrication, gastromucoadhesivity, swelling, and degradation of zein-chitosan composite ultrafine fibers. J Food Sci. 2013;78(6):N926-35. doi:10.1111/1750-3841.12126.

84. Berardi A, Abdel Rahim S, Bisharat L, Cespi M. Swelling of zein matrix tablets benchmarked against HPMC and ethylcellulose: challenging the matrix performance by the addition of co-excipients. Pharmaceutics. 2019;11(10):513. doi:10.3390/pharmaceutics11100513.

85. Gao Z, Ding P, Zhang L, Shi J, Yuan S, Wei J, et al. Study of a pingyangmycin delivery system: Zein/Zein-SAIB *in situ* gels. Int J Pharm. 2007;328(1):57-64. doi:10.1016/j.ijpharm.2006.07.048.

86. Cao X, Geng J, Su S-W, Zhang L-n, Xu Q, Zhang L, et al. Doxorubicin-loaded zein *in situ* gel for interstitial chemotherapy. Chem Pharm Bull. 2012;60:1227-33. doi:10.1016/j.apsb.2012.09.001.

87. Li M, Tang Z, Zhang D, Sun H, Liu H, Zhang Y, et al. Doxorubicin-loaded polysaccharide nanoparticles suppress the growth of murine colorectal carcinoma and inhibit the metastasis of murine mammary carcinoma in rodent models. Biomaterials. 2015;51:161-72. doi:10.1016/j.biomaterials.2015.02.002.

88. Yan-Zhi X, Jing-Jing W, Chen YP, Liu J, Li N, Yang FY. The use of zein and Shuanghuangbu for periodontal tissue engineering. Int J Oral Sci. 2010;2(3):142-8. doi:10.4248/ijos10056.

89. Sousa FFO, Luzardo-Álvarez A, Pérez-Estévéz A, Seoane-Prado R, Blanco-Méndez J. Sponges containing tetracycline loaded-PLGA-zein microparticles as a periodontal controlled release device. J Drug Deliv Sci Technol. 2020;59:101858. doi:https://doi.org/10.1016/j.jddst.2020.101858.

90. Zhang Y, Cui L, Li F, Shi N, Li C, Yu X, et al. Design, fabrication and biomedical applications of zein-based nano/micro-carrier systems. Int J Pharm. 2016;513(1):191-210. doi:https://doi.org/10.1016/j.ijpharm.2016.09.023.

91. Quinn MJ. Chapter 11 - Wildlife toxicity assessment for nitrocellulose. In: Williams MA, Reddy G, Quinn MJ, Johnson MS, editors. Wildlife toxicity

assessments for chemicals of military concern: Elsevier; 2015. p. 217-26.

92. Liu J. Nitrate esters chemistry and technology: Springer; 2019. 469-76 p.

93. Fernandez de la Ossa MA, López-López M, Torre M, García-Ruiz C. Analytical techniques in the study of highly-nitrated nitrocellulose. TrAC - Trends Anal Chem. 2011;30:1740-55. doi:10.1016/j.trac.2011.06.014.

94. Cellulosics DW. "Walsroder® Nitrocellulose essential for an extra-special finish," 1998. p. 31.

95. Fernandez de la Ossa MA, Torre M, García-Ruiz C. Nitrocellulose in propellants: characteristics and thermal properties. In: Wythers MC, editor. Vol. 7: Hauppauge: Nova Science Publishers; 2012. p. 201-20.

96. He Y, He Y, Liu J, Li P, Chen M, Wei R, et al. Experimental study on the thermal decomposition and combustion characteristics of nitrocellulose with different alcohol humectants. J Hazard Mater. 2017;340:202-12. doi:https://doi.org/10.1016/j.jhazmat.2017.06.029.

97. Saunders CW, Taylor LT. A review of the synthesis, chemistry and analysis of nitrocellulose. Journal of Energetic Materials. 1990;8(3):149-203. doi:10.1080/07370659008012572.

98. Samuel J, Edwards P. Solvent-based inkjet inks. The chemistry of inkjet inks: World Scientific; 2009. p. 141-59.

99. Sun S, Feng S, Ji C, Shi M, He X, Xu F, et al. Microstructural effects on permeability of Nitrocellulose membranes for biomedical applications. J Membr Sci. 2020;595:117502. doi:https://doi.org/10.1016/j.memsci.2019.117502.

100. Fernández JG, Almeida CA, Fernández-Baldo MA, Felici E, Raba J, Sanz MI. Development of nitrocellulose membrane filters impregnated with different biosynthesized silver nanoparticles applied to water purification. Talanta. 2016;146:237-43. doi:https://doi.org/10.1016/j.talanta.2015.08.060.

101. Fridley GE, Holstein CA, Oza SB, Yager P. The evolution of nitrocellulose as a material for bioassays. MRS Bulletin. 2013;38(4):326-30. doi:10.1557/mrs.2013.60.

102. Kim BB, Im WJ, Byun JY, Kim HM, Kim M-G, Shin Y-B. Label-free CRP detection using optical biosensor with one-step immobilization of antibody on nitrocellulose membrane. Sens Actuators B Chem. 2014;190:243-8. doi:https://doi.org/10.1016/j.snb.2013.08.078.

103. Mu X, Yu H, Zhang C, Chen X, Cheng Z, Bai R, et al. Nano-porous nitrocellulose liquid bandage modulates cell and cytokine response and accelerates cutaneous wound healing in a mouse model. Carbohydr Polym. 2016;136:618-29. doi:10.1016/j.carbpol.2015.08.070.

104. Wang L, Wang A, Zhao X, Liu X, Wang D, Sun F, et al. Design of a long-term antipsychotic *in situ* forming implant and its release control method and mechanism. Int J Pharm. 2012;427(2):284-92. doi:10.1016/j.ijpharm.2012.02.015.

105. Brodbeck KJ, DesNoyer JR, McHugh AJ. Phase inversion dynamics of PLGA solutions related to drug delivery. Part II. The role of solution thermodynamics and bath-side mass transfer. J Control Release. 1999;62(3):333-44. doi:10.1016/s0168-3659(99)00159-5.

106. Brodbeck Kevin J, Gaynor-Duarte Ann T, Shen Theodore T-I, inventors; ALZA CORP, assignee. Gel Composition And Methods. US patent US 6130200 A. 2000

1997/12/18.

107. Jouyban A, Fakhree MA, Shayanfar A. Review of pharmaceutical applications of N-methyl-2-pyrrolidone. J Pharm Pharm Sci. 2010;13(4):524-35. doi:10.18433/j3p306.

108. Agrawal AG, Kumar A, Gide PS. Toxicity study of a self-nanoemulsifying drug delivery system containing N-methyl pyrrolidone. Drug Res (Stuttg). 2015;65(8):446-8. doi:10.1055/s-0034-1389985.

109. National Center for Biotechnology Information. "PubChem Compound Summary for CID 13387, 1-Methyl-2-pyrrolidinone" PubChem. 2022.

110. Yu ZW, Quinn PJ. Dimethyl sulphoxide: a review of its applications in cell biology. Biosci Rep. 1994;14(6):259-81. doi:10.1007/bf01199051.

111. National Center for Biotechnology Information. PubChem Compound Summary for CID 679, Dimethyl sulfoxide. . 2022.

112. Bagheri A, Abolhasani A, Moghadasi AR, Nazari-Moghaddam AA, Alavi SA. Study of surface tension and surface properties of binary systems of DMSO with long chain alcohols at various temperatures. J Chem Thermodyn. 2013;63:108-15. doi:10.1016/j.jct.2013.04.009.

113. Mehtälä P, Pashley DH, Tjäderhane L. Effect of dimethyl sulfoxide on dentin collagen. Dent Mater J. 2017;33(8):915-22. doi:https://doi.org/10.1016/j.dental.2017.04.018.

114. Jacob SW, Wood DC. Dimethyl sulfoxide (DMSO). Toxicology, pharmacology, and clinical experience. Am J Surg. 1967;114(3):414-26. doi:10.1016/0002-9610(67)90166-3.

115. Dmitriev YV, Minasian SM, Demchenko EA, Galagudza MM. Cardioprotective properties of dimethyl sulfoxide during global ischemia-reperfusion of isolated rat heart. Bull Exp Biol Med. 2012;154(1):47-50. doi:10.1007/s10517-012-1872-8.

116. Harreus AL, Backes R, Eichler J-O, Feuerhake R, Jäkel C, Mahn U, et al. 2-Pyrrolidone. Ullmann's Encyclopedia of Industrial Chemistry2011.

117. Ahmed T. Review: approaches to develop PLGA based *in situ* gelling system with low initial burst. Pak J Pharm Sci. 2015;28(2):657-65.

118. Lewis RJ. Sax's dangerous properties of industrial materials. 9th ed. Volumes 1-3. New York, NY: Van Nostrand Reinhold,. 1996:2844.

119. Agostini E, Winter G, Engert J. Water-based preparation of spider silk films as drug delivery matrices. J Control Release. 2015;213:134-41. doi:10.1016/j.jconrel.2015.06.025.

120. Center for the Evaluation of Risks to Human Reproduction, NTP-CERHR Expert Panel report on the reproductive and developmental toxicity of propylene glycol. Reprod Toxicol. 2004;18(4):533-79. doi:https://doi.org/10.1016/j.reprotox.2004.01.004.

121. FDA. Generally recognized as safe; 1982. 21 CFR 184.1666.

122. Mahmoud DB, Shukr MH, ElMeshad AN. Gastroretentive cosolvent-based *in situ* gel as a promising approach for simultaneous extended delivery and enhanced bioavailability of mitiglinide calcium. J Pharm Sci. 2019;108(2):897-906. doi:https://doi.org/10.1016/j.xphs.2018.09.020.

123. Souza de Araujo GR, de Oliveira Porfírio L, Santos Silva LA, Gomes Santana D, Ferreira Barbosa P, Pereira dos Santos C, et al. *In situ* microemulsion-gel

obtained from bioadhesive hydroxypropyl methylcellulose films for transdermal administration of zidovudine. Colloids Surf B. 2020;188:110739. doi:https://doi.org/10.1016/j.colsurfb.2019.110739.

124. Langtry HD, Lamb HM. Levofloxacin. Its use in infections of the respiratory tract, skin, soft tissues and urinary tract. Drugs. 1998;56(3):487-515. doi:10.2165/00003495-199856030-00013.

125. Levofloxacin. LiverTox: Clinical and research information on drug-induced liver injury. Bethesda (MD): NIDDK; 2012.

126. Davis R, Bryson HM. Levofloxacin. A review of its antibacterial activity, pharmacokinetics and therapeutic efficacy. Drugs. 1994;47(4):677-700. doi:10.2165/00003495-199447040-00008.

127. Anderson VR, Perry CM. Levofloxacin : a review of its use as a high-dose, short-course treatment for bacterial infection. Drugs. 2008;68(4):535-65. doi:10.2165/00003495-200868040-00011.

128. Tözüm TF, Yildirim A, Cağlayan F, Dinçel A, Bozkurt A. Serum and gingival crevicular fluid levels of ciprofloxacin in patients with periodontitis. J Am Dent Assoc. 2004;135(12):1728-32. doi:10.14219/jada.archive.2004.0127.

129. Kleinfelder JW, Mueller RF, Lange DE. Fluoroquinolones in the treatment of Actinobacillus actinomycetemcomitans-associated periodontitis. J Periodontol. 2000;71(2):202-8. doi:10.1902/jop.2000.71.2.202.

130. Stein GE, Goldstein EJ. Review of the *in vitro* activity and potential clinical efficacy of levofloxacin in the treatment of anaerobic infections. Anaerobe. 2003;9(2):75-81. doi:10.1016/s1075-9964(03)00056-8.

131. Aksoy F, Dogan R, Ozturan O, Altuntas E, Yener FG, Topcu G, et al. Effect of a combination of mometasone furoate, levofloxacin, and retinyl palmitate with an *in situ* gel-forming nasal delivery system on nasal mucosa damage repair in an experimental rabbit model. Biomed Pharmacother. 2017;96:603-11. doi:https://doi.org/10.1016/j.biopha.2017.10.023.

132. Bansal M, Mittal N, Yadav SK, Khan G, Mishra B, Nath G. Clinical evaluation of thermoresponsive and mucoadhesive Chitosan *in situ* gel containing Levofloxacin and Metronidazole in the treatment of periodontal pockets – A split-mouth, clinical study. J Pierre Fauchard Acad. 2016;30(1):6-14. doi:https://doi.org/10.1016/j.jpfa.2016.10.003.

133. Bansal M, Mittal N, Yadav SK, Khan G, Gupta P, Mishra B, et al. Periodontal thermoresponsive, mucoadhesive dual antimicrobial loaded *in-situ* gel for the treatment of periodontal disease: Preparation, *in-vitro* characterization and antimicrobial study. J Oral Biol Craniofac Res. 2018;8(2):126-33. doi:10.1016/j.jobcr.2017.12.005.

134. Mah FS. Fourth-generation fluoroquinolones: new topical agents in the war on ocular bacterial infections. Curr Opin Ophthalmol. 2004;15(4):316-20. doi:10.1097/00055735-200408000-00007.

135. Stein GE, Goldstein EJC. Fluoroquinolones and anaerobes. Clin Infect Dis. 2006;42(11):1598-607. doi:10.1086/503907.

136. Guo Q, Aly A, Schein O, Trexler MM, Elisseeff JH. Moxifloxacin *in situ* gelling microparticles-bioadhesive delivery system. Results Pharma Sci. 2012;2:66-71. doi:10.1016/j.rinphs.2012.09.002.

137. Mandal S, Thimmasetty MK, Prabhushankar G, Geetha M. Formulation and

evaluation of an *in situ* gel-forming ophthalmic formulation of moxifloxacin hydrochloride. Int J Pharm Investig. 2012;2(2):78-82. doi:10.4103/2230-973x.100042.

138. Kraisit P, Sarisuta N. Development of triamcinolone acetonide-loaded nanostructured lipid carriers (NLCs) for buccal drug delivery using the Box-Behnken Design. Molecules. 2018;23(4):982. doi:10.3390/molecules23040982.

139. Canette A, Briandet R. Microscopy: Confocal laser scanning microscopy. In: Encyclopedia of food microbiology. 2014. p. 676–83.

140. Subongkot T, Ngawhirunpat T. Development of a novel microemulsion for oral absorption enhancement of all-trans retinoic acid. Int J Nanomedicine. 2017;12:5585-99. doi:10.2147/IJN.S142503.

141. Greenspan P, Mayer EP, Fowler SD. Nile red: a selective fluorescent stain for intracellular lipid droplets. J Cell Biol. 1985;100(3):965-73. doi:10.1083/jcb.100.3.965.

142. Gessner T, Mayer U. Triarylmethane and diarylmethane dyes. Ullmann's encyclopedia of industrial chemistry. 2000.

143. Vincent SJ. Contact Lens Practice, Third Edition Nathan Efron (Editor) Elsevier, Edinburgh, UK, 2018, 471 pages, RRP $220. Clinical and Experimental Optometry. 2017;100(5):143-55. doi:https://doi.org/10.1111/cxo.12580.

144. Olubiyi OI, Lu F-K, Calligaris D, Jolesz FA, Agar NY. Chapter 17 - Advances in molecular imaging for surgery. In: Golby AJ, editor. Image-Guided Neurosurgery. Boston: Academic Press; 2015. p. 407-39.

145. Kolawole OM, Cook MT. *In situ* gelling drug delivery systems for topical drug delivery. Eur J Pharm Biopharm. 2023;184:36-49. doi:https://doi.org/10.1016/j.ejpb.2023.01.007.

146. Sun Y, Jensen H, Petersen NJ, Larsen SW, Østergaard J. Concomitant monitoring of implant formation and drug release of *in situ* forming poly (lactide-co-glycolide acid) implants in a hydrogel matrix mimicking the subcutis using UV-vis imaging. J Pharm Biomed Anal. 2018;150:95-106. doi:10.1016/j.jpba.2017.11.065.

147. Mészáros LA, Galata DL, Madarász L, Köte Á, Csorba K, Dávid ÁZ, et al. Digital UV/VIS imaging: A rapid PAT tool for crushing strength, drug content and particle size distribution determination in tablets. Int J Pharm. 2020;578:119174. doi:https://doi.org/10.1016/j.ijpharm.2020.119174.

148. Li Z, Mu H, Weng Larsen S, Jensen H, Østergaard J. An *in vitro* gel-based system for characterizing and predicting the long-term performance of PLGA *in situ* forming implants. Int J Pharm. 2021;609:121183. doi:https://doi.org/10.1016/j.ijpharm.2021.121183.

149. Mészáros LA, Farkas A, Madarász L, Bicsár R, Galata DL, Nagy B, et al. UV/VIS imaging-based PAT tool for drug particle size inspection in intact tablets supported by pattern recognition neural networks. Int J Pharm. 2022;620:121773. doi:10.1016/j.ijpharm.2022.121773.

150. Li Z, Mu H, Larsen SW, Jensen H, Østergaard J. Initial leuprolide acetate release from poly(d,l-lactide-co-glycolide) *in situ* forming implants as studied by ultraviolet-visible imaging. Mol Pharm. 2020;17(12):4522-32. doi:10.1021/acs.molpharmaceut.0c00625.

151. Krupka TM, Weinberg BD, Wu H, Ziats NP, Exner AA. Effect of intratumoral

injection of carboplatin combined with pluronic P85 or L61 on experimental colorectal carcinoma in rats. Exp Biol Med (Maywood). 2007;232(7):950-7.

152. MicroMath. MicroMath scientist handbook Rev. 7EEF;: MicroMath: Salt Lake City; 1995.

153. Costa P, Sousa Lobo JM. Modeling and comparison of dissolution profiles. Eur J Pharm Sci. 2001;13(2):123-33. doi:https://doi.org/10.1016/S0928-0987(01)00095-1.

154. Krupka TM, Weinberg BD, Ziats NP, Haaga JR, Exner AA. Injectable polymer depot combined with radiofrequency ablation for treatment of experimental carcinoma in rat. Invest Radiol. 2006;41(12):890-7. doi:10.1097/01.rli.0000246102.56801.2f.

155. Wang F, Saidel GM, Gao J. A mechanistic model of controlled drug release from polymer millirods: effects of excipients and complex binding. J Control Release. 2007;119(1):111-20. doi:10.1016/j.jconrel.2007.01.019.

156. Ritger PL, Peppas NA. A simple equation for description of solute release I. Fickian and non-fickian release from non-swellable devices in the form of slabs, spheres, cylinders or discs. J Control Release. 1987;5(1):23-36. doi:https://doi.org/10.1016/0168-3659(87)90034-4.

157. Blanco E, Bey EA, Dong Y, Weinberg BD, Sutton DM, Boothman DA, et al. Beta-lapachone-containing PEG-PLA polymer micelles as novel nanotherapeutics against NQO1-overexpressing tumor cells. J Control Release. 2007;122(3):365-74. doi:10.1016/j.jconrel.2007.04.014.

158. Solorio L, Babin BM, Patel RB, Mach J, Azar N, Exner AA. Noninvasive characterization of *in situ* forming implants using diagnostic ultrasound. J Control Release. 2010;143(2):183-90. doi:10.1016/j.jconrel.2010.01.001.

159. Kempe S, Metz H, Pereira PG, Mäder K. Non-invasive *in vivo* evaluation of *in situ* forming PLGA implants by benchtop magnetic resonance imaging (BT-MRI) and EPR spectroscopy. Eur J Pharm Biopharm. 2010;74(1):102-8. doi:10.1016/j.ejpb.2009.06.008.

160. Patel RB, Carlson AN, Solorio L, Exner AA. Characterization of formulation parameters affecting low molecular weight drug release from *in situ* forming drug delivery systems. J Biomed Mater Res A. 2010;94(2):476-84. doi:10.1002/jbm.a.32724.

161. Ravivarapu HB, Moyer KL, Dunn RL. Parameters affecting the efficacy of a sustained release polymeric implant of leuprolide. Int J Pharm. 2000;194(2):181-91. doi:10.1016/s0378-5173(99)00371-3.

162. Helbling IM, Luna JA, Cabrera MI. Mathematical modeling of drug delivery from torus-shaped single-layer devices. J Control Release. 2011;149(3):258-63. doi:https://doi.org/10.1016/j.jconrel.2010.10.018.

163. Weinberg BD, Patel RB, Wu H, Blanco E, Barnett CC, Exner AA, et al. Model simulation and experimental validation of intratumoral chemotherapy using multiple polymer implants. Med Biol Eng Comput. 2008;46(10):1039-49. doi:10.1007/s11517-008-0354-7.

164. Patel RB, Exner AA. Development of a novel combined experimental and modeling approach to characterize *in situ* forming implants for intratumoral drug delivery [dissertation]. Ohio (U.S.A.): Case Western Reserve University; 2011.

165. Lertsuphotvanit N, Tuntarawongsa S, Chantadee T, Phaechamud T. Phase

inversion-based doxycycline hyclate-incorporated borneol *in situ* gel for periodontitis treatment. Gels. 2023;9(7):557. doi:10.3390/gels9070557.

166. Sato Y, Oba T, Watanabe N, Danjo K. Development of formulation device for periodontal disease. Drug Dev Ind Pharm. 2012;38(1):32-9. doi:10.3109/03639045.2011.589852.

167. Speck S, Wenke C, Feßler AT, Kacza J, Geber F, Scholtzek AD, et al. Borderline resistance to oxacillin in *Staphylococcus aureus* after treatment with sub-lethal sodium hypochlorite concentrations. Heliyon. 2020;6(6):e04070. doi:https://doi.org/10.1016/j.heliyon.2020.e04070.

168. Rattanaumpawan P, Nachamkin I, Bilker WB, Roy JA, Metlay JP, Zaoutis TE, et al. High fluoroquinolone MIC is associated with fluoroquinolone treatment failure in urinary tract infections caused by fluoroquinolone susceptible Escherichia coli. Ann Clin Microbiol Antimicrob. 2017;16(1):25. doi:10.1186/s12941-017-0202-4.

169. Koeth LM, Good CE, Appelbaum PC, Goldstein EJ, Rodloff AC, Claros M, et al. Surveillance of susceptibility patterns in 1297 European and US anaerobic and capnophilic isolates to co-amoxiclav and five other antimicrobial agents. J Antimicrob Chemother. 2004;53(6):1039-44. doi:10.1093/jac/dkh248.

170. Zhang Y, Huo M, Zhou J, Zou A, Li W, Yao C, et al. DDSolver: an add-in program for modeling and comparison of drug dissolution profiles. AAPS PharmSciTech. 2010;12(3):263-71. doi:10.1208/s12248-010-9185-1.

171. Sriphan S, Charoonsuk T, Maluangnont T, Pakawanit P, Rojviriya C, Vittayakorn N. Multifunctional nanomaterials modification of cellulose paper for efficient triboelectric nanogenerators. Adv Mater Technol. 2020;5(5):2000001. doi:https://doi.org/10.1002/admt.202000001.

172. John W. Eaton DB, Søren Hauberg, Rik Wehbring. GNU Octave version 8.2.0 manual: a high-level interactive language for numerical computations. 2023.

173. Fujisawa R, Mizuno M, Katano H, Otabe K, Ozeki N, Tsuji K, et al. Cryopreservation in 95% serum with 5% DMSO maintains colony formation and chondrogenic abilities in human synovial mesenchymal stem cells. BMC Musculoskeletal Disorders. 2019;20(1):316. doi:10.1186/s12891-019-2700-3.

174. Lertsuphotvanit N, Santimaleeworagun W, Narakornwit W, Chuenbarn T, Mahadlek J, Chantadee T, et al. Borneol-based antisolvent-induced *in situ* forming matrix for crevicular pocket delivery of vancomycin hydrochloride. Int J Pharm. 2022;617:121603. doi:https://doi.org/10.1016/j.ijpharm.2022.121603.

175. Dos Santos J, da Silva GS, Velho MC, Beck RCR. Eudragit®: A versatile family of polymers for hot melt extrusion and 3D printing processes in pharmaceutics. Pharmaceutics. 2021;13(9):1424. doi:10.3390/pharmaceutics13091424.

176. Zhang Q, Fassihi MA, Fassihi R. Delivery considerations of highly viscous polymeric fluids mimicking concentrated biopharmaceuticals: Assessment of injectability via measurement of total work done "WT". AAPS PharmSciTech. 2018;19(4):1520-8. doi:10.1208/s12249-018-0963-x.

177. Seo YP, Seo Y. Effect of molecular structure change on the melt rheological properties of a polyamide (Nylon 6). ACS Omega. 2018;3(12):16549-55. doi:10.1021/acsomega.8b02355.

178. Thurein SM, Lertsuphotvanit N, Phaechamud T. Physicochemical properties of β-cyclodextrin solutions and precipitates prepared from injectable vehicles. Asian J

Pharm Sci. 2018;13(5):438-49. doi:10.1016/j.ajps.2018.02.002.

179. Phaechamud T, Mahadlek J, Tuntarawongsa S. Peppermint oil/doxycycline hyclate-loaded Eudragit RS *in situ* forming gel for periodontitis treatment. J Pharm Investig. 2018;48(4):451-64. doi:10.1007/s40005-017-0340-x.

180. Lwin WW, Puyathorn N, Senarat S, Mahadlek J, Phaechamud T. Emerging role of polyethylene glycol on doxycycline hyclate-incorporated Eudragit RS *in situ* forming gel for periodontitis treatment. J Pharm Investig. 2020;50(1):81-94. doi:10.1007/s40005-019-00430-6.

181. Chuenbarn T, Sirirak J, Tuntarawongsa S, Okonogi S, Phaechamud T. Design and comparative evaluation of vancomycin HCl-loaded rosin-based *in situ* forming gel and microparticles. Gels. 2022;8(4). doi:10.3390/gels8040231.

182. Chuenbarn T, Chantadee T, Phaechamud T. Doxycycline hyclate-loaded Eudragit® RS PO *in situ*-forming microparticles for periodontitis treatment. J Drug Deliv Sci Technol. 2022;71:103294. doi:https://doi.org/10.1016/j.jddst.2022.103294.

183. Khaing EM, Mahadlek J, Okonogi S, Phaechamud T. Lime peel oil-incorporated rosin-based antimicrobial *in situ* forming gel. Gels. 2022;8(3):169. doi:10.3390/gels8030169.

184. Phaechamud T, Setthajindalert O. Antimicrobial *in-situ* forming gels based on bleached shellac and different solvents. J Drug Deliv Sci Technol. 2018;46:285-93. doi:https://doi.org/10.1016/j.jddst.2018.05.035.

185. Do MP, Neut C, Metz H, Delcourt E, Siepmann J, Mäder K, et al. Mechanistic analysis of PLGA/HPMC-based *in-situ* forming implants for periodontitis treatment. Eur J Pharm Biopharm. 2015;94:273-83. doi:10.1016/j.ejpb.2015.05.018.

186. Hoang C, Nguyen AK, Nguyen TQ, Fang W, Han B, Hoang BX, et al. Application of dimethyl sulfoxide as a therapeutic agent and drug vehicle for eye diseases. J Ocul Pharmacol Ther. 2021;37(8):441-51. doi:10.1089/jop.2021.0043.

187. Zheng ZJ, Ye H, Guo ZP. Recent progress in designing stable composite lithium anodes with improved wettability. Adv Sci (Weinh). 2020;7(22):2002212. doi:10.1002/advs.202002212.

188. Mei L, Huang X, Xie Y, Chen J, Huang Y, Wang B, et al. An injectable *in situ* gel with cubic and hexagonal nanostructures for local treatment of chronic periodontitis. Drug Deliv. 2017;24(1):1148-58. doi:10.1080/10717544.2017.1359703.

189. Senarat S, Charoenteeraboon J, Praphanwittaya P, Phaechamud T. Phase behavior of doxycycline hyclate-incorporated bleached shellac *in situ* forming gel/microparticle after solvent movement. Key Eng Mater. 2020;859:21-6. doi:10.4028/www.scientific.net/KEM.859.21.

190. Do MP, Neut C, Delcourt E, Seixas Certo T, Siepmann J, Siepmann F. *In situ* forming implants for periodontitis treatment with improved adhesive properties. Eur J Pharm Biopharm. 2014;88(2):342-50. doi:https://doi.org/10.1016/j.ejpb.2014.05.006.

191. Golmaghani-Ebrahimi E, Bagheri A, Fazli M. The influence of temperature on surface concentration and interaction energy between components in binary liquid systems. J Chem Thermodyn. 2020;146:106105. doi:https://doi.org/10.1016/j.jct.2020.106105.

192. Phaechamud T, Mahadlek J, Chuenbarn T. *In situ* forming gel comprising bleached shellac loaded with antimicrobial drugs for periodontitis treatment. Mater Des. 2016;89:294-303. doi:https://doi.org/10.1016/j.matdes.2015.09.138.

193. Phaechamud T, Mahadlek J. Solvent exchange-induced *in situ* forming gel comprising ethyl cellulose-antimicrobial drugs. Int J Pharm. 2015;494(1):381-92. doi:10.1016/j.ijpharm.2015.08.047.

194. Senarat S, Wai Lwin W, Mahadlek J, Phaechamud T. Doxycycline hyclate-loaded *in situ* forming gels composed from bleached shellac, Ethocel, and Eudragit RS for periodontal pocket delivery. Saudi Pharm J. 2021;29(3):252-63. doi:10.1016/j.jsps.2021.01.009.

195. Puyathorn N, Sirirak J, Chantadee T, Phaechamud T. Phase separation and intermolecular binding energy of ibuprofen in some organic solvents. Mater Today: Proc. 2022;65:2303-8. doi:https://doi.org/10.1016/j.matpr.2022.05.030.

196. Ershad AL, Rajabi-Siahboomi A, Missaghi S, Kirby D, Mohammed AR. Multi-analytical framework to assess the *in vitro* swallowability of solid oral dosage forms targeting patient acceptability and adherence. Pharmaceutics. 2021;13(3):411. doi:10.3390/pharmaceutics13030411.

197. Khaing EM, Intaraphairot T, Mahadlek J, Okonogi S, Pichayakorn W, Phaechamud T. Imatinib mesylate-loaded rosin/cinnamon oil-based *in situ* forming gel against colorectal cancer cells. Gels. 2022;8(9):526. doi:10.3390/gels8090526.

198. Chantadee T, Santimaleeworagun W, Phorom Y, Chuenbarn T, Phaechamud T. Vancomycin HCl-loaded lauric acid *in situ*-forming gel with phase inversion for periodontitis treatment. J Drug Deliv Sci Technol. 2020;57:101615. doi:https://doi.org/10.1016/j.jddst.2020.101615.

199. Baddam DO, Ragi SD, Tsang SH, Ngo WK. Ophthalmic Fluorescein Angiography. In: Tsang SH, Quinn PMJ, editors. Retinitis Pigmentosa. New York, NY: Springer US; 2023. p. 153-60.

200. Gusmão MR, Alves TC, Lemes AP, Bettiol GM, Pedroso AdF, Barioni Junior W, et al. Sodium fluorescein as an internal tracer on the location of bovine urine patches in pastures. Grass Forage Sci. 2016;71(2):305-14. doi:https://doi.org/10.1111/gfs.12182.

201. Alemán-Nava GS, Cuellar-Bermudez SP, Cuaresma M, Bosma R, Muylaert K, Ritmann BE, et al. How to use nile red, a selective fluorescent stain for microalgal neutral lipids. J Microbiol Methods. 2016;128:74-9. doi:10.1016/j.mimet.2016.07.011.

202. Martinez V, Henary M. Nile red and nile blue: applications and syntheses of structural analogues. Chemistry – A European Journal. 2016;22(39):13764-82. doi:https://doi.org/10.1002/chem.201601570.

203. Ashish G, Rahul Y, Mukesh R, Prakash M. Formulation and evaluation of *in situ* gel containing ciprofloxacin hydrochloride in the treatment of periodontitis. Asian J Pharm Clin Res. 2017;10:154-9. doi:10.22159/ajpcr.2017.v10i6.17558.

204. Costa JV, Portugal J, Neves CB, Bettencourt AF. Should local drug delivery systems be used in dentistry? Drug Deliv Transl Res. 2022;12(6):1395-407. doi:10.1007/s13346-021-01053-x.

205. Javali MA, Vandana KL. A comparative evaluation of atrigel delivery system (10% doxycycline hyclate) Atridox with scaling and root planing and

combination therapy in treatment of periodontitis: A clinical study. J Indian Soc Periodontol. 2012;16(1):43-8. doi:10.4103/0972-124x.94603.

206. Nair SC, Anoop KR. Intraperiodontal pocket: An ideal route for local antimicrobial drug delivery. J Adv Pharm Technol Res. 2012;3(1):9-15. doi:10.4103/2231-4040.93558.

207. Conrads G, Klomp T, Deng D, Wenzler JS, Braun A, Abdelbary MMH. The antimicrobial susceptibility of P*orphyromonas gingivalis*: genetic repertoire, global phenotype, and review of the literature. Antibiotics (Basel). 2021;10(12):1438. doi:10.3390/antibiotics10121438.

208. Chantadee T, Sawangsri P, Santimaleeworagun W, Phaechamud T. Vancomycin hydrochloride-loaded stearic acid/lauric acid *in situ* forming matrix for antimicrobial inhibition in patients with joint infection after total knee arthroplasty. Mater Sci Eng C Mater Biol Appl. 2020;115:110761. doi:10.1016/j.msec.2020.110761.

209. Poursamar SA, Azami M, Mozafari M. Controllable synthesis and characterization of porous polyvinyl alcohol/hydroxyapatite nanocomposite scaffolds via an in situ colloidal technique. Colloids Surf B Biointerfaces. 2011;84(2):310-6. doi:10.1016/j.colsurfb.2011.01.015.

210. Machado PST, Habert AC, Borges CP. Membrane formation mechanism based on precipitation kinetics and membrane morphology: flat and hollow fiber polysulfone membranes. J Membr Sci. 1999;155(2):171-83. doi:https://doi.org/10.1016/S0376-7388(98)00266-X.

211. Dias RA, Medeiros VdN, Silva BIA, Araújo EM, Lira HdL. Study of the influence of viscosity on the morphology of polyethersulfone hollow fiber membranes/additives. Mater Res. 2019;22:e20180913.

212. Pawar IA, Joshi PJ, Kadam AD, Pande NB, Kamble PH, Hinge SP, et al. Ultrasound-based treatment approaches for intrinsic viscosity reduction of polyvinyl pyrrolidone (PVP). Ultrason Sonochem. 2014;21(3):1108-16. doi:10.1016/j.ultsonch.2013.12.013.

213. Ranch KM, Maulvi FA, Koli AR, Desai DT, Parikh RK, Shah DO. Tailored doxycycline hyclate loaded *in situ* gel for the treatment of periodontitis: optimization, *in vitro* characterization, and antimicrobial studies. AAPS PharmSciTech. 2021;22(3):77. doi:10.1208/s12249-021-01950-x.

214. Tahtat D, Mahlous M, Benamer S, Nacer Khodja A, Larbi Youcef S. Effect of molecular weight on radiation chemical degradation yield of chain scission of γ-irradiated chitosan in solid state and in aqueous solution. Radiat Phys Chem. 2012;81(6):659-65. doi:https://doi.org/10.1016/j.radphyschem.2012.02.036.

215. Chen GL, Cai HY, Chen JP, Li R, Zhong SY, Jia XJ, et al. Chitosan/alginate nanoparticles for the enhanced oral antithrombotic activity of clam heparinoid from the clam *Coelomactra antiquata*. Mar Drugs. 2022;20(2):136. doi:10.3390/md20020136.

216. Zhang P, Lee YI, Zhang J. A review of high-resolution X-ray computed tomography applied to petroleum geology and a case study. Micron. 2019;124:102702. doi:10.1016/j.micron.2019.102702.

217. Liu Y, Xie D, Zhou R, Zhang Y. 3D X-ray micro-computed tomography imaging for the microarchitecture evaluation of porous metallic implants and scaffolds. Micron. 2021;142:102994. doi:10.1016/j.micron.2020.102994.

218. Zhang Z, Ni J, Chen L, Yu L, Xu J, Ding J. Biodegradable and thermoreversible PCLA-PEG-PCLA hydrogel as a barrier for prevention of post-operative adhesion. Biomaterials. 2011;32(21):4725-36. doi:10.1016/j.biomaterials.2011.03.046.

219. Papapanou PN, Susin C. Periodontitis epidemiology: is periodontitis under-recognized, over-diagnosed, or both? Periodontol 2000. 2017;75(1):45-51. doi:10.1111/prd.12200.

220. Sanz M, Ceriello A, Buysschaert M, Chapple I, Demmer RT, Graziani F, et al. Scientific evidence on the links between periodontal diseases and diabetes: Consensus report and guidelines of the joint workshop on periodontal diseases and diabetes by the International diabetes Federation and the European Federation of Periodontology. Diabetes Res Clin Pract. 2018;137:231-41. doi:10.1016/j.diabres.2017.12.001.

221. Rajendiran M, Trivedi HM, Chen D, Gajendrareddy P, Chen L. Recent development of active Ingredients in mouthwashes and toothpastes for periodontal diseases. Molecules. 2021;26(7). doi:10.3390/molecules26072001.

222. Nalawade TM, Bhat K, Sogi SH. Bactericidal activity of propylene glycol, glycerine, polyethylene glycol 400, and polyethylene glycol 1000 against selected microorganisms. J Int Soc Prev Community Dent. 2015;5(2):114-9. doi:10.4103/2231-0762.155736.

223. Khaing EM IT, Santimaleeworagu W, Phorom Y, Chuenbarn T, Phaechamud T. Natural-resin *in-situ*-forming gels: Physicochemical characteristics and bioactivities. Pharm Sci Asia. 2021;48(5):461–70. doi:doi:10.29090/psa.2021.05.20.077

224. Phaechamud T, Setthajindalert O. Cholesterol in situ forming gel loaded with doxycycline hyclate for intra-periodontal pocket delivery. Eur J Pharm Sci. 2017;99:258-65. doi:10.1016/j.ejps.2016.12.023.

225. Siepmann J, Siepmann F. Mathematical modeling of drug dissolution. Int J Pharm. 2013;453(1):12-24. doi:10.1016/j.ijpharm.2013.04.044.

226. Phaechamud T, Praphanwittaya P, Laotaweesub K. Solvent effect on fluid characteristics of doxycycline hyclate-loaded bleached shellac *in situ*-forming gel and -microparticle formulations. J Pharm Investig. 2018;48(3):409-19. doi:10.1007/s40005-017-0338-4.

227. Srichan T, Phaechamud T. Designing solvent exchange-induced *in situ* forming gel from aqueous insoluble polymers as matrix base for periodontitis treatment. AAPS PharmSciTech. 2017;18(1):194-201. doi:10.1208/s12249-016-0507-1.

228. Rungseevijitprapa W, Bodmeier R. Injectability of biodegradable *in situ* forming microparticle systems (ISM). Eur J Pharm Sci. 2009;36(4-5):524-31. doi:10.1016/j.ejps.2008.12.003.

229. Senarat S, Rojviriya C, Puyathorn N, Lertsuphotvanit N, Phaechamud T. Levofloxacin HCl-incorporated zein-based solvent removal phase inversion *in situ* forming gel for periodontitis treatment. Pharmaceutics. 2023;15(4):1199. doi:10.3390/pharmaceutics15041199.

230. Puyathorn N, Senarat S, Lertsuphotvanit N, Phaechamud T. Physicochemical and bioactivity characteristics of doxycycline hyclate-loaded solvent removal-induced ibuprofen-based *in situ* forming gel. Gels. 2023;9(2):128. doi:10.3390/gels9020128.

231. Philippot P, Lenoir N, D'Hoore W, Bercy P. Improving patients' compliance with the treatment of periodontitis: a controlled study of behavioural intervention. J Clin Periodontol. 2005;32(6):653-8. doi:10.1111/j.1600-051X.2005.00732.x.

232. Madan M, Bajaj A, Lewis S, Udupa N, Baig JA. *In situ* forming polymeric drug delivery systems. Indian J Pharm Sci. 2009;71(3):242-51. doi:10.4103/0250-474x.56015.

233. Parent M, Nouvel C, Koerber M, Sapin A, Maincent P, Boudier A. PLGA *in situ* implants formed by phase inversion: critical physicochemical parameters to modulate drug release. J Control Release. 2013;172(1):292-304. doi:10.1016/j.jconrel.2013.08.024.

234. Ibrahim TM, El-Megrab NA, El-Nahas HM. An overview of PLGA in-situ forming implants based on solvent exchange technique: effect of formulation components and characterization. Pharm Dev Technol. 2021;26(7):709-28. doi:10.1080/10837450.2021.1944207.

235. Hadavi E, de Vries RHW, Smink AM, de Haan B, Leijten J, Schwab LW, et al. *In vitro* degradation profiles and *in vivo* biomaterial–tissue interactions of microwell array delivery devices. J Biomed Mater Res Part B Appl Biomater. 2021;109(1):117-27. doi:https://doi.org/10.1002/jbm.b.34686.

236. Senarat S, Pichayakorn W, Phaechamud T, Tuntarawongsa S. Antisolvent Eudragit® polymers based *in situ* forming gel for periodontal controlled drug delivery. J Drug Deliv Sci Technol. 2023;82:104361. doi:https://doi.org/10.1016/j.jddst.2023.104361.

237. Withers PJ, Bouman C, Carmignato S, Cnudde V, Grimaldi D, Hagen CK, et al. X-ray computed tomography. Nat Rev Methods Primers. 2021;1(1):18. doi:10.1038/s43586-021-00015-4.

238. He T. Finger-Like Structure. In: Drioli E, Giorno L, editors. Encyclopedia of Membranes. Berlin, Heidelberg: Springer Berlin Heidelberg; 2015. p. 1-2.

239. Xiao P, Nghiem LD, Yin Y, Li X-M, Zhang M, Chen G, et al. A sacrificial-layer approach to fabricate polysulfone support for forward osmosis thin-film composite membranes with reduced internal concentration polarisation. J Membr Sci. 2015;481:106-14. doi:https://doi.org/10.1016/j.memsci.2015.01.036.

240. Souto R, Andrade A, Uzeda M, Colombo A. Prevalence of "non oral" bacteria in subgingival biofilm of subjects with chronic periodontitis. Braz J Microbiol. 2006;37:208-15. doi:10.1590/S1517-83822006000300002.

241. Carpentier B, Cerf O. Biofilms and their consequences, with particular reference to hygiene in the food industry. J Appl Bacteriol. 1993;75(6):499-511. doi:10.1111/j.1365-2672.1993.tb01587.x.

242. Costerton JW, Lewandowski Z, Caldwell DE, Korber DR, Lappin-Scott HM. Microbial biofilms. Annu Rev Microbiol. 1995;49:711-45. doi:10.1146/annurev.mi.49.100195.003431.

243. Shortt J, Hsu AK, Martin BP, Doggett K, Matthews GM, Doyle MA, et al. The drug vehicle and solvent N-methylpyrrolidone is an immunomodulator and antimyeloma compound. Cell Rep. 2014;7(4):1009-19. doi:10.1016/j.celrep.2014.04.008.

244. Rein SMTI, T.; Santimaleeworagun, W.; Chantadee, T.; Chuenbarn, T.; Phaechamud, T. Fluid properties of solvents and oils used in *in situ* forming microparticles. Thai J Pharm Sci. 2022;46:46-55.

245. Barakat NS. Evaluation of glycofurol-based gel as a new vehicle for topical application of naproxen. AAPS PharmSciTech. 2010;11(3):1138-46. doi:10.1208/s12249-010-9485-x.

246. Lee Y, Gou Y, Pan X, Gu Z, Xie H. Advances of multifunctional hydrogels for periodontal disease. Smart Mater Med. 2023;4:460-7. doi:https://doi.org/10.1016/j.smaim.2023.02.001.

247. Ding Y, Wang Y, Li J, Tang M, Chen H, Wang G, et al. Microemulsion-thermosensitive gel composites as *in situ*-forming drug reservoir for periodontitis tissue repair through alveolar bone and collagen regeneration strategy. Pharm Dev Technol. 2023;28(1):30-9. doi:10.1080/10837450.2022.2161574.

248. Pardeshi S, Mistari H, Jain R, Pardeshi P, Rajput R, Mahajan D, et al. Development and optimization of sustained-release moxifloxacin hydrochloride loaded nanoemulsion for ophthalmic drug delivery: A 3^2 factorial design approach. Micro Nano Syst. 2020;13(3):292-302. doi:10.2174/1876402912999200826111031.

249. Sun N, Yao X, Liu J, Li J, Yang N, Zhao G, et al. Breakup and coalescence mechanism of high-stability bubbles reinforced by dispersed particle gel particles in the pore-throat micromodel. Geoenergy Sci Eng. 2023;223:211513. doi:https://doi.org/10.1016/j.geoen.2023.211513.

250. Esfahani S, Akbari J, Soleimani-Amiri S, Mirzaei M, Ghasemi Gol A. Assessing the drug delivery of ibuprofen by the assistance of metal-doped graphenes: Insights from density functional theory. Diam Relat Mater. 2023;135:109893. doi:https://doi.org/10.1016/j.diamond.2023.109893.

251. Esrafili MD, Kadri M. Efficient delivery of anticancer 5-fluorouracil drug by alkaline earth metal functionalized porphyrin-like porous fullerenes: A DFT study. J Mol Graph Model. 2023;120:108403. doi:https://doi.org/10.1016/j.jmgm.2023.108403.

252. Saadh MJ, Abdullaev SS, Falcon-Roque JM, Cosme-Pecho RD, Castillo-Acobo RY, Obaid M, et al. Sensing functions of oxidized forms of carbon, silicon, and silicon-carbon nanocages towards the amantadine drug: DFT assessments. Diam Relat Mater. 2023;137:110137. doi:https://doi.org/10.1016/j.diamond.2023.110137.

253. He S, Wu L, Li X, Sun H, Xiong T, Liu J, et al. Metal-organic frameworks for advanced drug delivery. Acta Pharm Sin B. 2021;11(8):2362-95. doi:10.1016/j.apsb.2021.03.019.

254. Ashi M, Indrajit R, Sona G. Drug delivery applications of metal-organic frameworks (MOFs). In: Luis Jesús V-G, editor. Drug Carriers. Rijeka: IntechOpen; 2022. p. Ch. 4.

255. Jeyaseelan C, Jain P, Soin D, Gupta D. Metal organic frameworks: an effective application in drug delivery systems. Inorg Nano-Met Chem. 2022;52(12):1463-75. doi:10.1080/24701556.2021.1956966.

256. Tsampanakis I, Orbaek White A. The mechanics of forming ideal polymer-solvent combinations for open-loop chemical recycling of solvents and plastics. Polymers (Basel). 2021;14(1):112. doi:10.3390/polym14010112.

257. Gandhi KS, Williams MC. Solvent effects on the viscosity of moderately concentrated polymer solutions. J Polym Sci, Polym Symp. 1971;35(1):211-34. doi:https://doi.org/10.1002/polc.5070350117.

258. Phaechamud T, Lertsuphotvanit N, Praphanwittaya P. Viscoelastic and thermal properties of doxycycline hyclate-loaded bleached shellac *in situ*-forming gel and –microparticle. J Drug Deliv Sci Technol. 2018;44:448-56. doi:https://doi.org/10.1016/j.jddst.2018.01.021.

259. Tortorella S, Maturi M, Vetri Buratti V, Vozzolo G, Locatelli E, Sambri L, et al. Zein as a versatile biopolymer: different shapes for different biomedical applications. RSC Adv. 2021;11(62):39004-26. doi:10.1039/d1ra07424e.

260. Danzer LA, Ades H, Rees ED. The helical content of zein, a water insoluble protein, in non-aqueous solvents. Biochim Biophys Acta. 1975;386(1):26-31. doi:10.1016/0005-2795(75)90242-1.

261. Kaufman HSF, J.J. Introduction to polymer science and technology. In SPE Textbook; John Wiley & Sons: New York, NY, USA, 1977; pp. 1–268.

262. Gad HA, El-Nabarawi MA, Abd El-Hady SS. Formulation and evaluation of PLA and PLGA *in situ* implants containing secnidazole and/or doxycycline for treatment of periodontitis. AAPS PharmSciTech. 2008;9(3):878-84. doi:10.1208/s12249-008-9126-9.

263. Jagdale PP, Li D, Shao X, Bostwick JB, Xuan X. Fluid rheological effects on the flow of polymer solutions in a contraction-expansion microchannel. Micromachines (Basel). 2020;11(3):278. doi:10.3390/mi11030278.

264. Xiong W, Gao X, Zhao Y, Xu H, Yang X. The dual temperature/pH-sensitive multiphase behavior of poly(N-isopropylacrylamide-co-acrylic acid) microgels for potential application in *in situ* gelling system. Colloids Surf B Biointerfaces. 2011;84(1):103-10. doi:10.1016/j.colsurfb.2010.12.017.

265. Rini CJ, Roberts BC, Vaidyanathan A, Li A, Klug R, Sherman DB, et al. Enabling faster subcutaneous delivery of larger volume, high viscosity fluids. Expert Opin Drug Deliv. 2022;19(9):1165-76. doi:10.1080/17425247.2022.2116425.

266. Ibrahim TM, Eissa RG, El-Megrab NA, El-Nahas HM. Morphological characterization of optimized risperidone-loaded *in-situ* gel forming implants with pharmacokinetic and behavioral assessments in rats. J Drug Deliv Sci Technol. 2021;61:102195. doi:https://doi.org/10.1016/j.jddst.2020.102195.

267. Rarokar NR, Saoji SD, Raut NA, Taksande JB, Khedekar PB, Dave VS. Nanostructured cubosomes in a thermoresponsive depot system: an alternative approach for the controlled delivery of Docetaxel. AAPS PharmSciTech. 2016;17(2):436-45. doi:10.1208/s12249-015-0369-y.

268. Schwach-Abdellaoui K, Vivien-Castioni N, Gurny R. Local delivery of antimicrobial agents for the treatment of periodontal diseases. Eur J Pharm Biopharm. 2000;50(1):83-99. doi:10.1016/s0939-6411(00)00086-2.

269. Kornman KS. Controlled-release local delivery antimicrobials in periodontics: prospects for the future. J Periodontol. 1993;64(8 Suppl):782-91. doi:10.1902/jop.1993.64.8s.782.

270. Siepmann J, Siepmann F. Mathematical modeling of drug delivery. Int J Pharm. 2008;364(2):328-43. doi:10.1016/j.ijpharm.2008.09.004.

271. Shefeeq T, Ahmad N. Mathematical modelling for the diffusional release of a dispersed solute from a cylindrical polymer matrix into finite external volume. Appl Math. 2012;03:34-8. doi:10.4236/am.2012.31006.

272. Shafiei F, Ghavami-Lahiji M, Jafarzadeh Kashi TS, Najafi F. Drug release

kinetics and biological properties of a novel local drug carrier system. Dent Res J (Isfahan). 2021;18:94. doi:10.4103/1735-3327.330875.

273. Perioli L, Ambrogi V, Rubini D, Giovagnoli S, Ricci M, Blasi P, et al. Novel mucoadhesive buccal formulation containing metronidazole for the treatment of periodontal disease. J Control Release. 2004;95(3):521-33. doi:10.1016/j.jconrel.2003.12.018.

274. Joiner JB, Prasher A, Young IC, Kim J, Shrivastava R, Maturavongsadit P, et al. Effects of drug physicochemical properties on *in-situ* forming implant polymer degradation and drug release kinetics. Pharmaceutics. 2022;14(6):1188. doi:10.3390/pharmaceutics14061188.

275. Rawson SD, Maksimcuka J, Withers PJ, Cartmell SH. X-ray computed tomography in life sciences. BMC Biol. 2020;18(1):21. doi:10.1186/s12915-020-0753-2.

276. Rezaei A, Mohammadi MR. *In vitro* study of hydroxyapatite/polycaprolactone (HA/PCL) nanocomposite synthesized by an *in situ* sol-gel process. Mater Sci Eng C Mater Biol Appl. 2013;33(1):390-6. doi:10.1016/j.msec.2012.09.004.

277. Lee DK, Wang DP. Formulation development of allopurinol suppositories and injectables. Drug Dev Ind Pharm. 1999;25(11):1205-8. doi:10.1081/ddc-100102289.

278. Strickley RG. Solubilizing excipients in oral and injectable formulations. Pharm Res. 2004;21(2):201-30. doi:10.1023/b:pham.0000016235.32639.23.

279. Rowe RCS, P.J.; Quinn, M.E. Handbook of Pharmaceutical Excipients, 6th ed.; Pharmaceutical Press: London, UK, 2009.

280. Ahmed TA, Ibrahim HM, Samy AM, Kaseem A, Nutan MT, Hussain MD. Biodegradable injectable *in situ* implants and microparticles for sustained release of montelukast: *in vitro* release, pharmacokinetics, and stability. AAPS PharmSciTech. 2014;15(3):772-80. doi:10.1208/s12249-014-0101-3.

281. Matschke C, Isele U, van Hoogevest P, Fahr A. Sustained-release injectables formed in situ and their potential use for veterinary products. J Control Release. 2002;85(1-3):1-15. doi:10.1016/s0168-3659(02)00266-3.

282. Kim KB, Anand SS, Muralidhara S, Kim HJ, Bruckner JV. Formulation-dependent toxicokinetics explains differences in the GI absorption, bioavailability and acute neurotoxicity of deltamethrin in rats. Toxicology. 2007;234(3):194-202. doi:10.1016/j.tox.2007.02.015.

283. Spiegel AJ, Noseworthy MM. Use of nonaqueous solvents in parenteral products. J Pharm Sci. 1963;52:917-27. doi:10.1002/jps.2600521003.

284. Seymour RA, Heasman PA. Pharmacological control of periodontal disease. II. Antimicrobial agents. J Dent. 1995;23(1):5-14. doi:10.1016/0300-5712(95)90654-z.

285. Bayen AM, Siauw T. Chapter 19 - Ordinary Differential Equations (ODEs). In: Bayen AM, Siauw T, editors. An Introduction to MATLAB® Programming and Numerical Methods for Engineers. Boston: Academic Press; 2015. p. 277-99.

286. Bayen AM, Siauw T. Chapter 17 - Numerical Differentiation. In: Bayen AM, Siauw T, editors. An Introduction to MATLAB® Programming and Numerical Methods for Engineers. Boston: Academic Press; 2015. p. 245-57.

287. Liu H, Venkatraman SS. Cosolvent effects on the drug release and depot swelling in injectable *in situ* depot-forming systems. J Pharm Sci. 2012;101(5):1783-93.

doi:10.1002/jps.23065.

288. Raza A, Hayat U, Zhang X, Wang J-Y. Self-assembled zein organogels as *in situ* forming implant drug delivery system and 3D printing ink. Int J Pharm. 2022;627:122206. doi:https://doi.org/10.1016/j.ijpharm.2022.122206.

289. Raza A, Zhang Y, Hayat U, Liu C, Song JL, Shen N, et al. Injectable zein gel with *in situ* self-assembly as hemostatic material. Biomater Adv. 2023;145:213225. doi:10.1016/j.bioadv.2022.213225.

290. Khachatoorian R, Yen TF. Numerical modeling of *in situ* gelation of biopolymers in porous media. J Pet Sci Eng. 2005;48(3):161-8. doi:https://doi.org/10.1016/j.petrol.2005.06.006.

291. Lucero-Acuña A, Gutiérrez-Valenzuela CA, Esquivel R, Guzmán-Zamudio R. Mathematical modeling and parametrical analysis of the temperature dependency of control drug release from biodegradable nanoparticles. RSC Adv. 2019;9(16):8728-39. doi:10.1039/c9ra00821g.

292. Zhang Q, Fassihi R. Release rate determination from *in situ* gel forming PLGA implant: a novel 'shape-controlled basket in tube' method. J Pharm Pharmacol. 2020;72(8):1038-48. doi:10.1111/jphp.13277.

293. Senarat S, Rojviriya C, Sarunyakasitrin K, Charoentreeraboon J, Pichayakorn W, Phaechamud T. Moxifloxacin HCl-incorporated aqueous-induced nitrocellulose-based *in situ* gel for periodontal pocket delivery. Gels. 2023;9(7):572. doi:10.3390/gels9070572.

294. Li Y, Lim LT, Kakuda Y. Electrospun zein fibers as carriers to stabilize (-)-epigallocatechin gallate. J Food Sci. 2009;74(3):C233-40. doi:10.1111/j.1750-3841.2009.01093.x.

295. Sun Y, Chapman A, Larsen SW, Jensen H, Petersen NJ, Goodall DM, et al. UV-vis imaging of piroxicam supersaturation, precipitation, and dissolution in a flow-through setup. Anal Chem. 2018;90(11):6413-8. doi:10.1021/acs.analchem.8b00587.

296. Brown B, Ward A, Fazili Z, Østergaard J, Asare-Addo K. Application of UV dissolution imaging to pharmaceutical systems. Adv Drug Deliv Rev. 2021;177:113949. doi:10.1016/j.addr.2021.113949.

297. Smolewski P, Bedner E, Gorczyca W, Darzynkiewicz Z. "Liquidless" cell staining by dye diffusion from gels and analysis by laser scanning cytometry: potential application at microgravity conditions in space. Cytometry. 2001;44(4):355-60. doi:10.1002/1097-0320(20010801)44:4<355::aid-cyto1127>3.0.co;2-w.

298. Sun Y, Jensen H, Petersen NJ, Larsen SW, Østergaard J. Phase separation of *in situ* forming poly (lactide-co-glycolide acid) implants investigated using a hydrogel-based subcutaneous tissue surrogate and UV-vis imaging. J Pharm Biomed Anal. 2017;145:682-91. doi:10.1016/j.jpba.2017.07.056.

299. Yu Y, Li S-Y, Xu T-C, Huang G-Q, Xiao J-X. Assembly of zein/propylene glycol alginate nanoparticles in aqueous ethanol and the binding kinetics. Food Hydrocoll. 2023;139:108545. doi:https://doi.org/10.1016/j.foodhyd.2023.108545.

300. Lau ET, Giddings SJ, Mohammed SG, Dubois P, Johnson SK, Stanley RA, et al. Encapsulation of hydrocortisone and mesalazine in zein microparticles. Pharmaceutics. 2013;5(2):277-93. doi:10.3390/pharmaceutics5020277.

301. Mat Amin KA, Gilmore KJ, Matic J, Poon S, Walker MJ, Wilson MR, et al.

Polyelectrolyte complex materials consisting of antibacterial and cell-supporting layers. Macromol Biosci. 2012;12(3):374-82. doi:10.1002/mabi.201100317.

302. Senarat S, Tuntarawongsa S, Lertsuphotvanit N, Rojviriya C, Phaechamud T, Chantadee T. Levofloxacin HCl-loaded Eudragit L-based solvent exchange-induced *in situ* forming gel using monopropylene glycol as a solvent for periodontitis treatment. Gels. 2023;9(7):583. doi:10.3390/gels9070583.

303. Bozic A, Filipović N, Novakovic I, Bjelogrlic S, Nikolic J, Drmanić S, et al. Synthesis, antioxidant and antimicrobial activity of Carbohydrazones. J Serb Chem Soc. 2017;82:45-. doi:10.2298/JSC161220045B.

304. Østergaard J, Wu JX, Naelapää K, Boetker JP, Jensen H, Rantanen J. Simultaneous UV imaging and raman spectroscopy for the measurement of solvent-mediated phase transformations during dissolution testing. J Pharm Sci. 2014;103(4):1149-56. doi:10.1002/jps.23883.

305. Wang SH, Liang ZH, Zeng S. Monitoring release of ketoprofen enantiomers from biodegradable poly(D,L-lactide-co-glycolide) injectable implants. Int J Pharm. 2007;337(1-2):102-8. doi:10.1016/j.ijpharm.2006.12.031.

306. Wang X, Burgess DJ. Drug release from *in situ* forming implants and advances in release testing. Adv Drug Deliv Rev. 2021;178:113912. doi:10.1016/j.addr.2021.113912.

307. Fosca M, Rau JV, Uskoković V. Factors influencing the drug release from calcium phosphate cements. Bioact Mater. 2022;7:341-63. doi:10.1016/j.bioactmat.2021.05.032.

APPENDICES

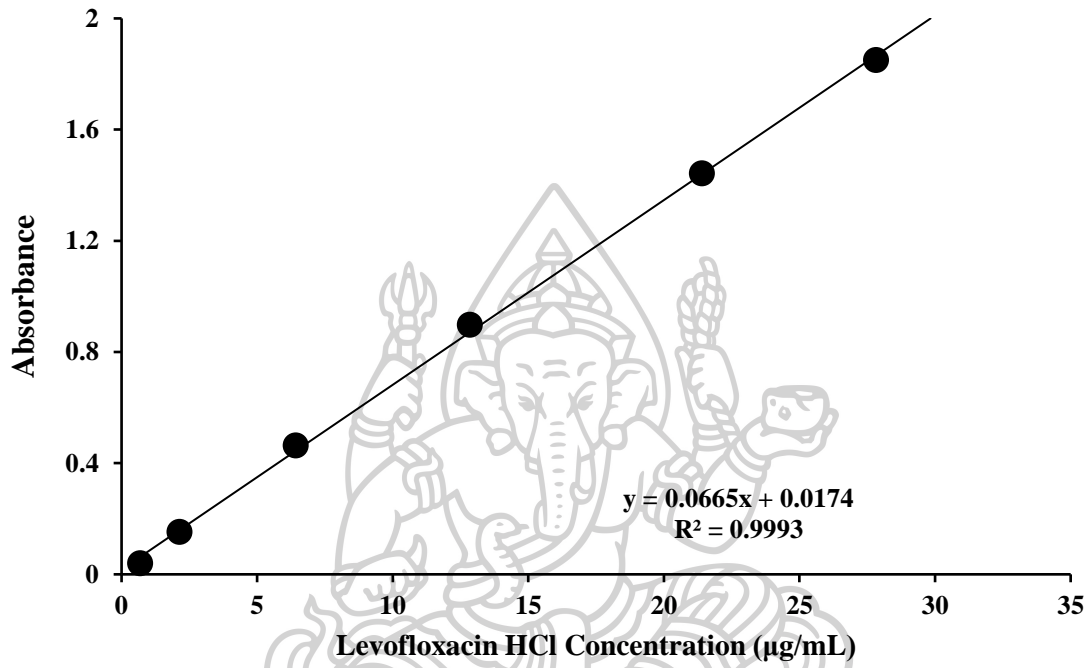**Appendix I: Calibration curve for *in vitro* release study**

Figure 47. Calibration curve of Lv in phosphate buffer pH 6.8 for the in vitro release study (UV-vis at 287 nm)
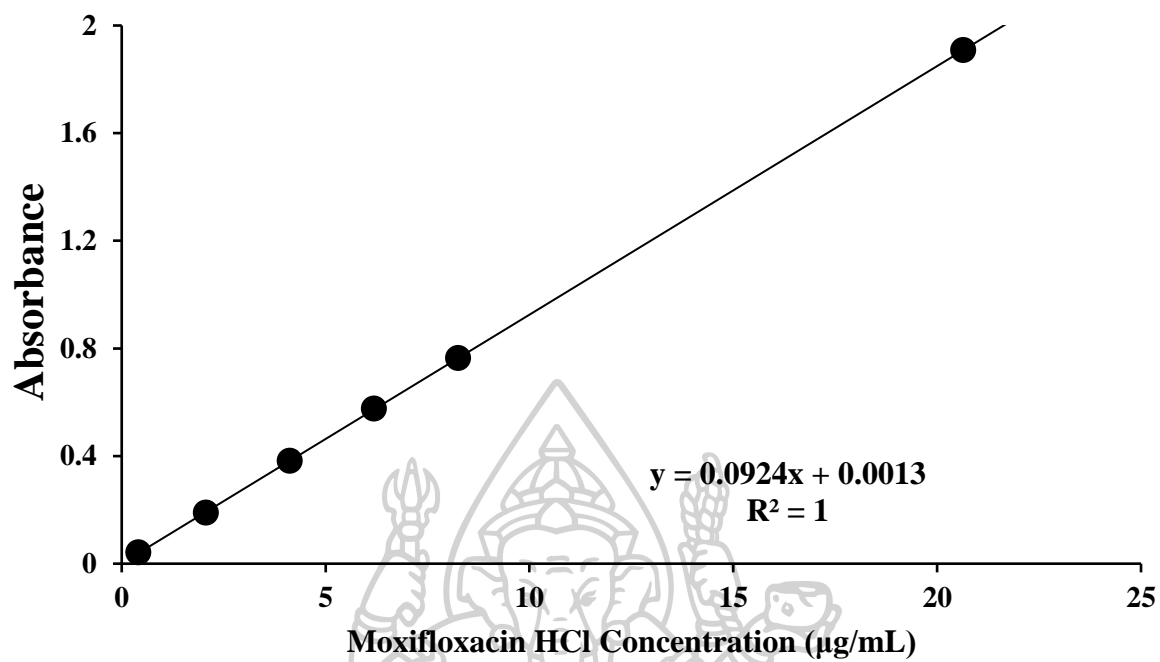
Figure 48. Calibration curve of Mx in phosphate buffer pH 6.8 for the in vitro release study (UV-vis at 288 nm)

VITA

NAME   Setthapong Senarat

INSTITUTIONS   Doctor of Pharmacy (Pharm. D.), Faculty of Pharmacy,
ATTENDED   Silpakorn University, Nakorn Pathom, Thailand
PUBLICATION   Senarat S, Tuntarawongsa S, Lertsuphotvanit N, Rojviriya
C, Phaechamud T, Chantadee T. Levofloxacin HCl-loaded
Eudragit L-based solvent exchange-induced in situ
forming gel using monopropylene glycol as a solvent for
periodontitis treatment. Gels. 2023;9(7):583.
doi:10.3390/gels9070583.

Lertsuphotvanit N, Senarat S, Tuntarawongsa S,
Phaechamud T. Sublimation/evaporation behaviors of
borneol in-situ forming matrix. Mater. Today: Proc
(accepted). 2023.
https://doi.org/10.1016/j.matpr.2023.03.768.

Thammasut W, Intaraphairot T, Chantadee T, Senarat S,
Patomchaiviwat V, Chuenbarn T, et al. Antimicrobial and
antitumoral activities of saturated fatty acid solutions.
Mater. Today: Proc (accepted). 2023
https://doi.org/10.1016/j.matpr.2023.03.769.

Senarat S, Rojviriya C, Puyathorn N, Lertsuphotvanit N,
Phaechamud T. Levofloxacin HCl-incorporated zein-based
solvent removal phase inversion in situ forming gel for
periodontitis treatment. Pharmaceutics 2023;15:1199.
https://doi.org/10.3390/pharmaceutics15041199.

Senarat S, Pichayakorn W, Phaechamud T, Tuntarawongsa
S. Antisolvent Eudragit® polymers based in situ forming
gel for periodontal controlled drug delivery. J Drug Deliv
Sci Technol. 2023;82:104361.
https://doi.org/10.1016/j.jddst.2023.104361.

Puyathorn N, Senarat S, Lertsuphotvanit N, Phaechamud
T. Physicochemical and bioactivity characteristics of
doxycycline hyclate-loaded solvent removal-induced
ibuprofen-based in situ forming gel. Gels. 2023;9(2):128.
doi:10.3390/gels9020128.

Senarat S, Pichayakorn W, Phaechamud T, Tuntarawongsa
S. Antisolvent Eudragit® polymers based in situ forming
gel for periodontal controlled drug delivery. J Drug Deliv
Sci Technol. 2023;82:104361.

https://doi.org/10.1016/j.jddst.2023.104361.

Chaiya P, Senarat S, Phaechamud T, Narakornwit W. In vitro anti-inflammatory activity using thermally inhibiting protein denaturation of egg albumin and antimicrobial activities of some organic solvents. Mater. Today: Proc. 2022;65:2290-5.
https://doi.org/10.1016/j.matpr.2022.04.916.

Senarat S, Phaechamud T, Mahadlek J, Tuntarawongsa S. Fluid properties of various Eudragit® solutions in different solvent systems for periodontal pocket injection Mater Today Proc. 2022;65:2399-406.
https://doi.org/10.1016/j.matpr.2022.05.527.

Mahadlek J, Tuntarawongsa S, Senarat S, Phaechamud T. In situ solvent removal-based Eudragit®L/dimethyl sulfoxide forming gel for periodontal pocket drug delivery. Mater Today Proc. 2022.
doi:10.1016/j.matpr.2021.10.248.

Tuntarawongsa S, Mahadlek J, Senarat S, Phaechamud T. Eudragit® RL in 2-pyrrolidone as antisolvent-based in-situ forming matrix. Mater Today Proc. 2022;52:2534-8.
https://doi.org/10.1016/j.matpr.2021.11.060.

Senarat S, Wai Lwin W, Mahadlek J, Phaechamud T. Doxycycline hyclate-loaded in situ forming gels composed from bleached shellac, Ethocel, and Eudragit RS for periodontal pocket delivery. Saudi Pharm J. 2021;29(3):252-63. doi:10.1016/j.jsps.2021.01.009.

Senarat S, Charoenteeraboon J, Praphanwittaya P, Phaechamud T. Phase behavior of doxycycline hyclate-incorporated bleached shellac in situ forming gel/microparticle after solvent movement. Key Eng Mater. 2020;859:21-6.
doi:10.4028/www.scientific.net/KEM.859.21

Lwin WW, Puyathorn N, Senarat S, Mahadlek J, Phaechamud T. Emerging role of polyethylene glycol on doxycycline hyclate-incorporated Eudragit RS in situ forming gel for periodontitis treatment. J Pharm Investig. 2020;50(1):81-94. doi:10.1007/s40005-019-00430-6.

Phaechamud T, Senarat S, Puyathorn N, Praphanwittaya P. Solvent exchange and drug release characteristics of

doxycycline hyclate-loaded bleached shellac in situ-forming gel and -microparticle. Int J Biol Macromol. 2019;135:1261-72. https://doi.org/10.1016/j.ijbiomac.2018.11.098.

Puyathorn N, Chantadee T, Senarat S, Phaechamud T. Characterization of Lauric Acid Precipitated from Biocompatible Solvents. Key Eng Mater. 2019;819:209-14. https://doi.org/10.4028/www.scientific.net/kem.819.209.

Senarat S, Chantadee T, Santimaleeworagun W, Phorom Y, Phaechamud T. Alpha-Mangostin Phase Inversion Induced In Situ Forming Gel. Key Eng Mater. 2019;819:202-8. https://doi.org/10.4028/www.scientific.net/kem.819.202.

AWARD RECEIVED

Oral presentation award 2023 (together Thawatchai Paecharmard) in the field of lecture, science of chemistry, and pharmaceuticals) for the research work titled "Moxifloxacin HCl-Incorporated Nitrocellulose-Based In Situ Gel for Periodontitis Treatment." Presented at the 34th National Conference and the 1st International Conference on ASEAN Sustainable Development (ICASD 2023) at Thaksin University, July 20-21, 2023, Crystal Hotel, Songkhla Province.

Poster presentation award 2023 (together Cholakarn Fukasem, Nichapat Tuangkraisint, Sunisa Boonchai, Warakorn Thammasutt, Napphapol Puyathorn, Setthapong Senarat, Saran Tuntarawongsa, and Thawatchai Paechamud) Science of Chemistry and Pharmacy for the research work titled "Matrix Formation at the Site of Origin for Encapsulating Levofloxacin Hydrochloride for Periodontitis Treatment Using Myristic Acid as a Matrix-Forming Material." Presented at the 34th National Conference and 1st International Conference on ASEAN Sustainable Development (ICASD 2023) at Thaksin University, July 20-21, 2023, Crystal Hotel, Songkhla Province.

Oral presentation award 2021 (together with Pornsit Chaiya, Setthapong Senarat, Thawatchai Phaechamud, Worrakanya Narakornwit) in title "In vitro anti-inflammatory activity using thermally Inhibiting protein denaturation of egg albumin and antimicrobial activities of some organic solvents" the The 5th International Conference on Applied Physics and Materials

Applications & Applied Magnetism and Ferroelectrics (ICAPMA-JMAG-2021), 1-4 December, 2021, NongNooch Pattaya Garden & Resort, Chonburi, Thailand.

Best poster presentation award for undergraduate students (Gold Medal) 2019 (together with Setthapong Senarat, Takron Chantadee, Wichai Santimaleeworagun, Yaowarak Phorom and Thawatchai Phaechamud) in title "Alpha-mangostin Phase Inversion Induced In Situ Forming Gel" the International Conference and Exhibition on Pharmaceutical Sciences and Technology 2019 (PST2019), 18-19 June, 2019, Ambassador Hotel, Bangkok, Thailand, Bangkok.

First runner up award 2018 of Thailand Innovation Award 18 (together with Siripong Srisukha, Supanat Pongaree, Setthapog Senarat and Wichai Santimaleeworagun) in title In situ forming gel from fatty acid for treatment in patients with osteoarthritis after post-surgery total knee arthroplasty, Innovation Thailand Expo 2018, 4-5 October, 2018, Faculty of Pharmacy, Silpakorn University, Nakhon Pathom, Thailand.

First runner up award 2018 (together with Natchapol Intasorn, Siripong Srisukha, Supanat Pongaree, Setthapog Senarat and Wichai Santimaleeworagun) in title Vancomycin hydrochloride in situ forming gel using stearic acid and lauric acid as matrix former for bacteria inhibition, Senior project award 2018, 30 April – 2 May, 2018, Faculty of Pharmacy, Silpakorn University, Nakhon Pathom, Thailand.

Conferences

Nutdanai Lertsuphotvanit, Setthapong Senarat, Sarun Tuntarawongsa, Thawatchai Phaechamud. Sublimation/evaporation behaviors of borneol in-situ forming matrix. International Conference and Exhibition on Science, Technology and Engineering of Materials (ISTEM2022), (November 29 - December 2, 2022), Nongnooch Garden Pattaya, Chonburi, Thailand. organized by American Ceramic Society: Thailand Chapter (ACerS-Thailand Chapter) committee and Nakhon Pathom Rajabhat University.

Warakon Thammasut, Torsak Intaraphairot, Takron

Chantadee, Setthapong Senarat, Vipaluk Patomchaiviwat, Tiraniti Chuenbarn, Thawatchai Phaechamud. Antimicrobial and antitumoral activities of saturated fatty acid solutions. International Conference and Exhibition on Science, Technology and Engineering of Materials (ISTEM2022), (November 29 - December 2, 2022), Nongnooch Garden Pattaya, Chonburi, Thailand. organized by American Ceramic Society: Thailand Chapter (ACerS-Thailand Chapter) committee and Nakhon Pathom Rajabhat University.

Setthapong Senarata, Tiraniti Cheunbanb, Thawatchai Phaechamuda, Takron Chantadee. Interfacial properties of rosin solution for the development of natural resinbased in situ forming systems (International conference on advanced materials in environment, energy and health applications (AMEEHA 2022), Pathumwan Princess Hotel, Bangkok, Thailand (3-5 August, 2022)). organized by Department of Chemical Engineering, Khon Kaen University, Thailand and Department of Environmental Sciences, JSS Academy of Higher Education and Research, India.

Pornsit Chaiya, Setthapong Senarat, Thawatchai Phaechamud, Worrakanya Narakornwit. 2021. In vitro anti-inflammatory activity using thermally inhibiting protein denaturation of egg albumin and antimicrobial activity of some organic solvents. The Joint International Conference on Applied Physics and Materials Applications & Applied Magnetism and Ferroelectrics (ICAPMA-JMAG-2021)., 1-4 Dec, 2021).

Setthapong Senarat, Thawatchai Phaechamud, Jongjan Mahadlek, Sarun Tuntarawongsa. Fluid properties of various Eudragit® solutions in different solvent systems for periodontal pocket injection. The Joint International Conference on Applied Physics and Materials Applications & Applied Magnetism and Ferroelectrics (ICAPMA-JMAG-2021)., 1-4 Dec, 2021).

Jongjan Mahadlek, Sarun Tuntarawongsa, Setthapong Senarat, Thawatchai Phaechamud. In situ solvent removal-based Eudragit®L/dimethyl sulfoxide forming gel for periodontal pocket drug delivery. (1-2 September, 2021 Research, Invention, and Innovation Congress (RI2C2021) hosted by King Mongkut's University of Technology North Bangkok (KMUTNB), Bangkok, Thailand)

Sarun Tuntarawongsa, Jongjan Mahadlek, Setthapong Senarat, Thawatchai Phaechamud. Eudragit® RL in 2-pyrrolidone as antisolvent-based in-situ forming matrix.. (1-2 September, 2021 Research, Invention, and Innovation Congress (RI2C2021) hosted by King Mongkut's University of Technology North Bangkok (KMUTNB), Bangkok, Thailand)

Wai Wai Lwin, Napaphol Puyathorn, Setthapong Senarat, Jongjan Mahadlek, Thawatchai Phaechamud. Emerging role of polyethylene glycol on doxycycline hyclate-incorporated Eudragit RSin situ forming gel for periodontitis treatment. International Conference on Materials Research and Innovation (ICMARI 2018) 17-21 December, 2018. The emerald hotel, Bangkok, Thailand. p.66.